ABSTRACT

SHEAR STRENGTHENING OF RC BEAMS USING CARBON FIBER REINFORCED POLYMER LAMINATES

by
Zhichao Zhang

Shear failure is catastrophic and occurs usually without advanced warning, thus it is desirable that the beam fails in flexure rather than in shear. Many existing reinforced concrete (RC) members are found to be deficient in shear strength and need to be repaired. Deficiencies occur due to several reasons such as insufficient shear reinforcement or reduction in steel area due to corrosion, increased service load, and construction defects. Externally bonded reinforcement such as Carbon Fiber Reinforced Polymer (CFRP) provides an excellent solution in these situations.

In order to investigate the shear behavior of RC beams with externally bonded CFRP shear reinforcement, experimental programs as well as analytical studies were conducted in this research. The research consists of three parts. They are 1). Regular beams with CFRP shear strengthening; 2). Deep beams with CFRP shear strengthening; and 3). Shear damaged beams with CFRP shear strengthening. CFRP laminates of various types and configurations were applied externally to the beams as shear reinforcement.

During the present experimental investigation, a total of five 4-foot long and six 6-foot long regular RC beams and sixteen 3-foot long deep RC beams were tested to study the behavior of shear strengthening using CFRP system. All beams were loaded by a 220-kip MTS TestStar II testing system. Results of the test demonstrate the feasibility

of using externally applied, epoxy-bonded CFRP system to restore or increase the load-carrying capacity in shear of RC beams. The CFRP system has been found to increase significantly the serviceability, ductility, and ultimate shear strength of a concrete beam. Restoring beam shear strength using CFRP is a highly effective technique.

Based on the experiments and analysis carried out at NJIT and the results from other researchers, new analysis and design methods for both regular and deep RC beams with externally bonded CFRP shear strengthening have also been proposed as well.

SHEAR STRENGTHENING OF RC BEAMS USING CARBON FIBER REINFORCED POLYMER LAMINATES

by

Zhichao Zhang

A Dissertation
Submitted to the Faculty of
New Jersey Institute of Technology
in Partial Fulfillment of the Requirements for the Degree of
Doctor of Philosophy in Civil Engineering

Department of Civil and Environmental Engineering

January 2003

APPROVAL PAGE

SHEAR STRENGTHENING OF RC BEAMS USING CARBON FIBER REINFORCED POLYMER LAMINATES

Zhichao Zhang

Dr. C. T. Thomas Hsu, Dissertation Advisor — Date
Professor of Civil and Environmental Engineering, NJIT

Dr. William R. Spillers, Committee Member — Date
Distinguished Professor of Civil and Environmental Engineering, NJIT

Dr. Jay N. Meegoda, Committee Member — Date
Professor of Civil and Environmental Engineering, NJIT

Professor. Walter Konon, Committee Member — Date
Professor of Civil and Environmental Engineering, NJIT

Dr. Wei Wang, Committee Member — Date
President of UrbanTech Associates.

BIOGRAPHICAL SKETCH

Author: Zhichao Zhang

Degree: Doctor of Philosophy

Date: January 2003

Undergraduate and Graduate Education:

- Doctor of Philosophy in Civil Engineering
  New Jersey Institute of Technology, New Jersey, 2003
- Master of Science in Civil Engineering
  Southwest Jiaotong University, Chengdu, Sichuan, China, 1998
- Bachelor of Science in Civil Engineering
  Shijiazhuang Railway Institute, Shijiazhuang, Hebei, China, 1995

Major: Civil Engineering

Presentations and Publications:

Zhichao Zhang, and Cheng-Tzu Thomas Hsu, "Shear Strengthening of RC Beams Using Carbon Fiber Reinforced Polymer Strips", Proceedings of 15th ASCE Engineering Mechanics Conference, Columbia University, New York City, N. Y., June 2-5, 2002.

Zhichao Zhang, and Cheng-Tzu Thomas Hsu, "Shear behavior of Reinforced Concrete Beams Strengthened by Sika's CFRP Laminates", A final report submitted to Sika Corp., N. J., Technical Report Structural Series No. 2000-1, Department of Civil & Environmental Engineering, NJIT, Newark, N. J., December 2000, 41 pages.

This dissertation is dedicated to my parents.

ACKNOWLEDGMENTS

The work presented in this thesis has been carried out under the direction of my advisor, Professor C. T. Thomas Hsu, to whom I am much indebted for his guidance, constant encouragement and invaluable suggestions throughout the years.

I would like to thank my committee members: Professor William R. Spillers, Professor Jay N. Meegoda, Professor Walter Konon and Dr. Wei Wang for their constructive evaluations and suggestions.

I would also like to thank Sika Corporation for the donation of all CFRP composite materials. Special thanks go to Mr. David White at Sika for his help and expertise on CFRP application.

The financial assistance received from the Department of Civil and Environmental Engineering during my study at NJIT is greatly appreciated.

Special thanks go to Mr. Allyn Luke, Assistant to the Chairman for Laboratories, for his knowledge and assistance on the experiment setup in the Structures Laboratory.

Special thanks also go to Dr. Insang Lee, Mr. Jon Moren, Mr. Julio Zeballos, Mr. Sun Punurai, Mr. Xiaobin Lu, Mr. Voradej Vongvorakarn, and Mr. Jian Chen for their help in mixing and testing of the beams.

Finally, I would like to thank my parents and my cousin for their love, support and understanding throughout my study at NJIT.

TABLE OF CONTENTS

TABLE OF CONTENTS
(Continued)

Chapter **Page**

TABLE OF CONTENTS
(Continued)

Chapter **Page**

TABLE OF CONTENTS
(Continued)

Chapter **Page**

LIST OF TABLES

LIST OF FIGURES

LIST OF FIGURES
(Continued)

LIST OF FIGURES
(Continued)

LIST OF FIGURES
(Continued)

LIST OF FIGURES
(Continued)

LIST OF FIGURES
(Continued)

CHAPTER 1

INTRODUCTION

1.1 General

It is well known now that a significant part of the infrastructure in North America is in urgent need of strengthening and rehabilitation. As documented in the eleventh report of the Secretary of Transportation to the Congress of the United States on "Highway Bridge Replacement and Rehabilitation Program", over one third of the nation's 575,413 inventoried highway bridges are classified as either structurally deficient or functionally obsolete (FHA 1993). According to CERF, Civil Engineering Research Foundation, ASCE (1994), 40% of the nation's bridges are structurally deficient or functionally obsolete, 60% of the nation's pavement requires rehabilitation. The cost of replacing all deficient structures is prohibitive. Limited financial resources and current technology together will not be enough to solve the problem. High-tech solutions must be investigated so innovative use of new technologies and materials can be employed to rebuild the infrastructure.

Historically, concrete members have been repaired by post tensioning or jacketing with new concrete in conjunction with a surface adhesive (Klaiber et al. 1987). Since the mid 1960's, epoxy-bonded steel plates have been used in Europe and South Africa to retrofit flexural members (Dussek 1987). However, steel plates have a durability problem unique to this application, because corrosion may occur along the adhesive interface. This type of corrosion adversely affects the bond at the steel plate/concrete interface and is difficult to monitor during routine inspections. The problem was extremely worse in the United States, where deicing salts were heavily used to enhance winter road safety.

Additionally, special equipment is necessary to install the heavy plates. Engineers have to search for alternative materials.

In past twenty years, a new technique has been developed involving the replacement of steel plates by fiber reinforced polymers (FRP), or simply composites, wrapped or epoxy-bonded to the web or tension side of concrete, in the form of thin laminates or fabric. Fiber reinforced plastic materials have been used successfully in the aerospace and automotive industry for more than three decades. They are generally constructed of high performance fibers such as carbon, aramid, or, glass which are placed in a resin matrix. By selecting among the many available fibers, geometry and polymers, the mechanical and durability properties can be tailored for particular application. This synthetic quality makes FRP a good choice for civil engineering application as well. The FRP offer the engineer an outstanding combination of properties, such as low weight (making them much easier to handle on site), immunity to corrosion, excellent mechanical strength and stiffness, and the ability of formation in very long length, thus eliminating the need for lapping at joints. Although FRP is a relatively expensive material compare to steel, the total rehabilitation project costs is about 20% (Mufti, et al., 1991) lower by using FRP than steel due to the savings in construction expenses. The FRP-strengthening technique has found wide attractiveness and acceptance among researchers and engineers today in many parts of the world.

1.2 Objectives of Proposed Research

In order to take full advantage of the potential ductility of the RC beam, it is desirable that the beam fails in flexure rather than in shear. Shear failure is catastrophic and occurs usually without advanced warning. Many existing RC members are found to be deficient in shear strength and need to be repaired. Deficiencies occur due to several reasons such as insufficient shear reinforcement or reduction in steel area due to corrosion, increased service load, and construction defects. Externally bonded reinforcement such as Carbon Fiber Reinforced Polymer (CFRP) provides an excellent solution in these situations.

However, detailed investigation in shear strengthening using externally bonded CFRP has been limited, and to a certain degree, controversial. The analytical models proposed in the literature sometimes are contradictory. The design approach for such reinforcement is far from complete and straightforward.

To further understand the behavior of shear strengthening of RC beams using externally bonded CFRP laminates as the shear reinforcement, the following objectives of this research have been established:

1. To increase the database of shear strengthening using externally bonded composites.
2. To investigate the shear behavior and modes of failure of RC beams with shear deficiencies after strengthening with CFRP laminates.
3. To study the effect of various CFRP types and shear reinforcement configurations on the shear behavior of the beam.
4. To study the bond mechanism between the CFRP laminates and the concrete surface.

5. To study the shear span to depth ratio (a/d) effect on shear strengthening of deep beams using CFRP laminates.
6. To propose design approaches based on experiments and analytical studies.

1.3 Originality of Proposed Research

Having made the point that the rehabilitation of the infrastructure is an important matter for the United States, the proposed research is expected to generate both the scientific knowledge and the engineering method in the infrastructure field. With the developing analytical model, and the design recommendations for the CFRP strengthened reinforced concrete beams, the proposed research will develop new methods to predict the strength and deformation of the CFRP strengthened concrete structures.

The proposed experiment test will help understand the behavior of CFRP strengthened beams and other structural members; it will also be used to verify the validity of the previous proposed theories. The proposed research will greatly increase the applicability of the strengthening methods with externally epoxy-bonded CFRP strips. It will also broaden the knowledge related to the reinforced concrete structures as well.

The originality of the proposed research can be found in the following aspects:

1. The behavior of RC beams of different lengths in shear strengthening by externally bonded CFRP laminates was investigated. In the proposed research, not only beams with different application methods were studied, but also beams with the same CFRP application but different lengths were investigated as well.

2. A new effective strain model was proposed in the design of the shear strength of RC beams with externally bonded CFRP laminates.
3. Shear strengthening of deep beams using CFRP laminates of various configurations including anchorage effect was studied.
4. The effect of shear span to depth ratio (a/d) was studied in shear strengthening of deep beams using CFRP laminates.
5. Design formulas for shear strengthening of deep beams using CFRP laminates has been proposed and validated.
6. Shear repairing using CFRP laminates for RC beams with previously developed shear cracks was investigated.

1.4 Literature Review

The use of fiber reinforced polymer (FRP) in strengthening reinforced concrete structures has become an increasingly popular retrofit technique. The technique of strengthening reinforced concrete structures by externally bonded FRP laminates was started in 1980's and has since attracted many researchers around the world. It was investigated in the USA (Diab, et al., 1984; Saadatmanesh and Ehsani, 1991, 1997; Chajes, et al., 1994; Nanni, 1995; Hsu, Bian and Jia, 1997; Bian, Hsu and Wang, 1997), Switzerland (Meier, 1987; Meier et al., 1992, Steiner, 1996), Greece (Triantafillou, 1998, 2000), Canada (Eriki et al., 1996; Alexander and Cheng, 1996; Chaallal et al., 1998), Japan and several other European countries.

1.4.1 Shear Strength of RC Beams

The failures in RC beams that commonly referred to as "shear failures" are actually tension failures at the inclined cracks. One of the earliest to recognize this was E. Morsch in Germany in the early 1900s. The formation of inclined cracks is due to the high shear stress on a beam, which is particularly true for beams having only longitudinal reinforcements. The transfer of shear in reinforced concrete beams occurs by a combination of the following mechanisms (Wang and Salmon, 1992):

1. Shear resistance of the uncracked concrete.
2. Aggregate interlock (or interface shear transfer) force, tangentially along a crack and similar to a frictional force due to irregular interlocking of the aggregates along the rough concrete surfaces on each side of the crack.
3. Dowel action, the resistance of the longitudinal reinforcement to a transverse force.
4. Shear reinforcement resistance, from vertical or inclined stirrups.

For rectangular beams without shear reinforcement, it is reported that after an inclined crack has formed, the proportion of the shear transferred by the various mechanisms is as follows: 15 to 25% by dowel action; 20 to 40% by the uncracked concrete compression zone; and 33 to 50% by aggregate interlock or interface shear transfer (Wang and Salmon, 1992).

To provide shear strength by allowing a redistribution of interval forces, the shear reinforcement has three primary functions: (1) to carry part of the shear; (2) to restrict the growth of inclined cracks and thus help maintain aggregate interlock; and (3) to tie the longitudinal reinforcement in place and thereby increase the dowel action.

The traditional ACI approach (ACI Building Code 318-99) to design for shear strength is to consider the total nominal shear strength as the sum of two parts:

$$V_n = V_c + V_s \tag{1.1}$$

Where V_n is the nominal shear strength; V_c is the shear strength of the beam attributable to the concrete; and V_s is the shear strength of the beam attributable to the shear reinforcement.

1. **Strength V_c Attributable to Concrete.** The development of the detailed equation for V_c is based on the test results. ACI-11.3.1 and 11.3.2 permit using either of the following:

   (1) For the simplified method,

   $$V_c = 2\sqrt{f_c'}\, b_w d \tag{1.2}$$

   $$V_c = (0.8 + 100\rho_w)\sqrt{f_c'}\, b_w d \text{, for } \rho_w < 0.012 \tag{1.3}$$

   (2) For more detailed method,

   $$V_c = \left(1.9\sqrt{f_c'} + 2500\rho_w \frac{V_u d}{M_u}\right) b_w d \le 3.5\sqrt{f_c'}\, b_w d \text{ , } \frac{V_u d}{M_u} \le 1.0 \tag{1.4}$$

   In above equations, M_u is the factored moment, V_u is the factored shear force, f_c' is the compressive strength for the concrete, ρ_w is the reinforcement ratio, b_w is web width, and d is the effective depth of the cross section.

2. **Strength V_s Attributable to Shear Reinforcement.** The contribution of shear reinforcement is described as follows:

$$V_s = \frac{A_v f_y}{s}(\sin\alpha + \cos\alpha) \tag{1.5}$$

Where A_v is the area of shear reinforcement, f_y is the yield stress of the reinforcement, s is the spacing of the shear reinforcement, and α is the angle between the orientation of the shear reinforcement and the longitudinal axis of the beam.

1.4.2 Shear Strength of Deep Beams

Classic literature review compiled by Albritton (1965), the Cement and Concrete Association (C&CA) (1969) and Construction Industry Research and Information Association (CIRIA) (1977) show that the early investigations are mostly on the elastic behavior with the beam assumed to be homogeneous, which can be carried out nowadays using the standard finite element method. Reinforcing is placed in regions where tensile stresses are above the estimated strength of the concrete. However, a serious disadvantage of elastic studies is the usual assumption of isotropic materials obeying Hooke's Law, which does not give sufficient guidance for practical design.

It was not until the 1960s that systematic ultimate load tests were carried out by de Paiva and Siess (1965) and Leonhardt and Walther (1966). Leonhardt and Walther (1966) considered two states — the un-cracked and the cracked. They found that the cracking followed the tensile stress trajectories. However, after cracking and stress redistribution, the elastic approach did not adequately describe the stress distributions of deep beams. Actual stresses exceeded theoretical stresses at sections near supports and center of the spans. These tests were a major step forward in deep beam research. They revealed a concern for empirical evidence that emphasized the importance of

experimental knowledge of the actual behavior. The lead provided by these pioneers subsequently followed by many other researchers around the world (reviews by CIRIA, 1977; Chemrouk, 1998).

The solution of the deep beam problem using plasticity concepts was reported by Nielsen (1971) and Braestrup and Nielson (1983). Kong and Robins (1971) reported the inclined web reinforcement was highly effective in shear for deep beams. This was confirmed by Kong and Singh (1972) and Kong et al. (1972) who also proposed a method for comparing quantitatively the effects of different types of web reinforcement (Kong et al., 1972). Kong and Sharp (1973) reported on the strength and failure modes of deep beams with web openings. Robins and Kong (1973) used finite element method to predict the ultimate loads and crack patterns of deep beams. Taner et al. (1977) reported that the finite element gave good results when applied to flanged deep beams. Rogowsky et al. (1986) carried out extensive tests on continuous deep beams. Mau and Hsu (1987) applied softened truss model theory to deep beams and proposed design equations. Kotsovos (1998) studied deep beams in the light of a comprehensive investigation into the fundamental causes of shear failure. Wang, Jiang and Hsu (1993) studied the shear strength of the deep beams and derived equations based on limit analysis theorems and associated flow rule.

The shear provisions of ACI code (ACI Building Code 318-99) classify members with a clear span to depth ratio l_n / d less than 5 as deep beams if they are loaded on the top face and supported on the bottom face. The shear strength of the reinforced deep beams is calculated based on Equation (1.1). On deep beams, shear reinforcement will

usually be the same throughout the span; on a simply supported deep beam, the shear reinforcement is required to be the same throughout the span.

1.4.2.1 Shear Strength of Simply Supported Deep Beams. The nominal shear strength V_n should not exceed the following:

$$V_n = 8\sqrt{f_c'}b_w d \qquad \text{for } l_n / d < 2 \tag{1.6}$$

$$V_n = (2/3)(10 + l_n / d)\sqrt{f_c'}b_w d \qquad \text{for } 2 \le l_n / d < 5 \tag{1.7}$$

Where f_c' is the concrete cylinder compressive strength (lb/in^2), b_w is the beam web width (in.), l_n is the clear span and d is the effective depth (in.)

1. **Strength V_c Attributable to Concrete.** The development of the detailed equation for V_c is based on the test results. ACI-11.8.6 permits using either of the following:

   (1) For the simplified method,

   $$V_c = 2\sqrt{f_c'}b_w d \tag{1.8}$$

   (2) For more detailed method,

   $$V_c = \left(3.5 - 2.5\frac{M_u}{V_u d}\right)\left(1.9\sqrt{f_c'} + 2500\rho_w \frac{V_u d}{M_u}\right)b_w d \tag{1.9}$$

   In above equations, M_u is the factored moment, V_u is the factored shear force, f_c' is the compressive strength for the concrete, ρ_w is the reinforcement ratio, b_w is web width, and d is the effective depth of the cross section. The second term on the right-hand side of Equation (1.9) is the concrete shear strength for normal beams. The first term on the left-

hand side is the multiplier to allow for strength increase in deep beams, subjected to the restrictions that follows:

$$3.5 - 2.5\frac{M_u}{V_u d} \le 2.5 \tag{1.10}$$

$$V_c \le 6\sqrt{f_c'}\, b_w d \tag{1.11}$$

2. Strength V_s Attributable to Shear Reinforcement. The contribution of shear reinforcement is described as followed:

$$V_s = \left[\frac{A_v}{s}\left(\frac{1+l_n/d}{12}\right) + \frac{A_{vh}}{s_2}\left(\frac{11-l_n/d}{12}\right)\right] f_y d \tag{1.12}$$

Where

l_n = clear span

A_v = vertical stirrup area

A_{vh} = longitudinal shear reinforcement area

s = spacing of vertical stirrups

s_2 = vertical spacing of longitudinal shear reinforcement

ACI-11.8.9 and 11.8.10 provide for minimum amounts of shear reinforcement for A_v and A_{vh}.

$$\min A_v = 0.0015 b_w s, \qquad s \le \frac{d}{5} \le 18in. \tag{1.13}$$

$$\min A_{vh} = 0.0025 b_w s_2, \qquad s_2 \le \frac{d}{3} \le 18in. \tag{1.14}$$

1.4.2.2 Shear Strength of Continuous Deep Beams. ACI-11.8.3 indicates that ordinary beam expressions for V_c shall apply to continuous deep beams.

1. **Strength V_c Attributable to Concrete.**

   (1) For the simplified method,

$$V_c = 2\sqrt{f_c'}b_w d \tag{1.15}$$

   (2) For more detailed method,

$$V_c = \left(1.9\sqrt{f_c'} + 2500\rho_w \frac{V_u d}{M_u}\right) b_w d \le 3.5\sqrt{f_c'}b_w d \tag{1.16}$$

2. **Strength V_s Attributable to Shear Reinforcement.** The contribution of shear reinforcement is described as followed:

$$V_s = \frac{A_v f_y d}{s} \tag{1.17}$$

Where the minimum amounts of shear reinforcement, A_v and A_{vh}, are the same for continuous beams as for simply supported beams.

1.4.3 Researches on Shear Strengthening of RC Beams by Externally Bonded FRP Laminates

Strengthening with externally bonded FRP laminates has been shown to be applicable to many kinds of structures. Currently, this method has been applied to strengthen such structures as columns, beams, walls, slabs, etc. The use of external FRP reinforcement may be classified as flexural strengthening, improving the ductility of compression members, and shear strengthening.

A lot of studies have been conducted to explain the behavior of externally bonded FRP laminates used to increase the moment capacity of flexural members. However, not many studies have specifically addressed the shear strengthening. Berset (1992) at the Massachusetts Institute of Technology did the first research on FRP shear strengthening. He tested several RC beams with and without shear reinforcement in the form of GFRP (Glass Fiber Reinforced Polymer) laminates vertically bonded to both sides of the beam in the shear-critical zone. A simple analytical model for the contributions of the external reinforcement in shear was developed. In Berset's model, the FRP shear reinforcement was treated in analogy with steel stirrups. Failure occurs when the FRP laminate reaches the maximum allowable strain, which is determined by experiments.

The second study reported in literature is that of Uji (1992), who tested reinforced concrete beams strengthened in shear with both CFRP fabrics wrapped around the beam and CFRP laminates bonded on vertical sides of the beam (with fibers either vertical or inclined). His model for CFRP's contribution to shear capacity is based on the bonding interfaces between the CFRP laminates and the concrete surface. The average shear stresses during the peeling-off of the fabrics are adopted, which is determined by experiments (about 1.3 MPa). The upper limit to the FRP contribution is given by its tensile strength.

Dolan et al. (1992) tested prestressed concrete beams with externally applied AFRP (Aramid Fiber Reinforced Polymer) and concluded that such reinforcement did quite well for shear strengthening.

Al-Sulaimani et al. (1994) did research on shear strengthening using GFRP (Graphite Fiber Reinforced polymer) laminates in the form of plates. Their model is

based on the assumption that the average shear stresses between the GFRP and the concrete are equal to 0.8 MPa and 1.2 MPa for plates and strips, respectively.

Ohuchi et al. (1994) carried out an extensive series of tests on RC beams strengthened in shear with CFRP wrap. They modeled the CFRP shear contribution in an analogy with steel stirrups, assuming a limiting strain for the external reinforcement equal to either tensile failure strain of CFRP or 2/3 of it, depending on the thickness of the fabrics.

At another research effort, Chajes et al. (1995) did some experiments on RC beams strengthened in shear with different types of FRPs, namely glass, aramid, and carbon. Again, in their work, the shear contribution of FRPs is modeled in analogy with steel stirrups, and a limiting FRP strain is assumed to be equal to 0.005 approximately, according to the experiments.

Malvar et al. (1995) also conducted some research on this topic and found out that CFRP strengthening in shear was a highly effective technique. They also stated that the contribution to shear capacity could be obtained by using the similar analysis for steel stirrups, and the limiting strain was equal to the tensile failure of the CFRP.

Vielhaber and Limberger (1995) reported that on the shear strengthening of large scale reinforced concrete beams with CFRP fabrics and demonstrated through testing that even small amounts of external reinforcement provided considerable safety against brittle shear failure.

Sato et al. (1996) did some research on RC beams strengthened in shear with either CFRP strips or continuous laminates, and described that the observed failure mode

(CFRP debonding) through a simple model to account for partial shear transfer by CFRP debonding.

Based on mostly qualitative arguments, Triantafillou (1998) derived a polynomial function that related the strain in the FRP at shear failure of the member, defined as effective strain, to the axial rigidity of externally bonded strips or sheets.

In a recent study, Khalifa et al. (1998) used a slightly modification of Triantafillou's equation (1998) (calibrated with more test results, including both FRP rupture and debonding) to describe shear failure combined with FRP rupture. Meanwhile, the bond model of Maeda et al. (1997) was used to describe shear failure combined with FRP debonding. The two models were then presented in the ACI shear design format.

CHAPTER 2

EXPERIMENTAL PROGRAM ON SHEAR STRENGTHENING OF REGULAR RC BEAMS USING CARBON FIBER REINFORCED POLYMER LAMINATES

2.1 Test Specimens

2.1.1 Design of Concrete Beams

All the beams to be tested are designed to fail in shear. That means if the beams fail in flexure first, one will be unable to know whether the externally bonded CFRP laminates help or not to carry the shear force, let lone to decide how much contribution it would make to the whole shear resistant of the beam. Thus, the shear force that plain concrete can resist without any shear reinforcement should be the minimum load to determine the flexural reinforcement. At the same time, the flexural reinforcement ratio ρ should be higher than the minimum reinforcement ratio ρ_{min}. Although the higher the flexural reinforcement ratio is, the more unlikely the failure will be in bending. However, the failure of over-reinforced beam always begins with the concrete crushing on the top of the beam, which is brittle and dangerous. Therefore, the flexural reinforcement ratio ρ should also be lower than the maximum reinforcement ratio ρ_{max} as well.

Based on the above reasons, six No. 3 bars were used in the flexural reinforcement. Proper anchorage was provided at the end of the steel bars to prevent pullout failure. Both ends of the steel bars were bent up to a certain length l_{dh}, which is 8.5in. based on the design guidelines.

Since the purpose of this study is to investigate the shear contribution of externally bonded CFRP, no internal steel shear reinforcement should be used in any of

the beams. However, to prevent the local failure at the supports and loading points, five No.2 stirrups were provided at these locations (Figure 2.1).

2.1.2 Cast of Concrete Beams

Eleven RC beams having cross-sectional dimension of 6x9-in. were cast in the wood forms at the concrete laboratory of New Jersey Institute of Technology. Five beams are 4-foot long and other six beams are 6-foot long. Five batches of concrete were used to fabricate the beams and standard 6x12-in. test cylinders. All beams and cylinders were cured in a water bath for at least 28 days before testing. The cylinders were tested at the same time that the beams were tested. Compressive strengths of the cylinders from all batches are given in Table 2.1.

2.1.3 Materials

Four types of materials were used to fabricate these beams, which included concrete mix, steel re-bars, CFRP laminates and Epoxy for CFRP bonding.

- A concrete mix of Type I portland cement and aggregate with maximum size of 3/8 in. was used. The water cement ratio by weight was 0.5.
- No.3 steel re-bars were used as flexural reinforcement. The mean value of the yield stress was 58 ksi from the tests.
- Unidirectional carbon fiber strips from SIKA Corp., which were named Sika®Carbodur® Plates, were used in this research. There were two kinds of strips. One was used where long and continuous strips were needed, which was 50mm wide and 1mm thick; another was used where only short strips were

needed, which was 40mm wide and 1.5mm thick. The representative properties of the strips are given in Table 2.2.

- SikaWrap® Hex, which was a kind of woven composite fabrics, was employed in this study. The representative properties are also given in Table 2.2.
- Sikadur-30, a two-component rubber-toughened cold-curing-construction epoxy was used for bonding the CFRP strips to concrete. The properties are given in Table 2.3.
- Sikadur-330, another epoxy adhesives, was used for bonding the CFRP fabrics to concrete. It was also a two-component epoxy, much thinner compared to Sikadur-30. Its properties are presented in Table 2.3.

Table 2.1 Maximum Compressive Strength of Concrete Cylinders

Concrete Batch	Ultimate Strength f_c' (psi)			
	Cylinder 1	Cylinder 2	Cylinder 3	Average
1	6606	7002	6844	6817
2	6525	6048	N.G.	6287
3	6048	6128	6286	6154
4	6286	6446	6367	6366
5	6207	6127	6207	6180

Table 2.2 Laminate Properties

Property	Sika CarboDur Strips	SikaWrap Hex 230c
Description	E-Glass Fabric (dry-lay-up)	Pultruded Carbon Fiber Laminate
Tensile Strength	406,000psi (2,800 N/mm^2)	139,000psi (960 N/mm^2)
Tensile Modulus	23.9msi (165,000 N/mm^2)	10.60msi (73,100 N/mm^2)
Elongation at Break	1.9%	1.33%
Nominal Thickness	0.047in. (1.2mm)	0.013in. (0.33mm)
Tensile Strength per inch Width	19,082lbs./layer (84.8KN)	1,807lbs./layer (8.0KN)

Table 2.3 Epoxy Properties

Property	SikaDur -30	SikaDur -330
Compressive Strength	>95 N/mm^2	
Adhesive Strength on Steel	>26 N/mm^2	
Adhesive Strength on Concrete	>4 N/mm^2 (concrete failure)	>4 N/mm^2 (concrete failure)
E-modulus	12,800 N/mm^2	
Flexural Modulus		3,800 N/mm^2

2.1.4 Bonding of Composite Materials to Beams

Prior to bonding of CFRP to the beams, both sides of the beams were sandblasted until the layer of laitance was removed. Afterwards, the surface of the beams was cleaned using compressed air to remove any loose particles.

- Bonding of Sika®Carbodur® Plates:

  The strips were cut to the required length and then thoroughly cleaned with acetone as recommended by the manufacturer. Epoxy adhesive Sikadur-30 was

used for bonding of the strips to the concrete. It was hand mixed and applied evenly, approximately 1mm thick, on both CFRP strips and the concrete surface using a spatula. After the strips were put on the designated position, constant pressure was applied on the strip surface by a roller to ensure the perfect bonding between concrete and CFRP strips. The excess epoxy was squeezed out along the edges of the CFRP strips, assuring the complete coverage. The adhesive was cured at room temperature for at least seven days before testing.

- Bonding of SikaWrap® Hex Fabrics:

  There was no special treatment on the fabrics, except blowing away the dust from the surface. Epoxy adhesive Sikadur-330, which was thinner than Sikadur-30, was used for bonding of the fabrics to the concrete. After the epoxy was mixed, it was applied on the concrete surface using the roller. The fabrics were then placed onto both sides of the beam and excess epoxy was wiped off. Another layer of epoxy was put on top of the fabric, evenly spread out using the roller. The adhesive was cured at room temperature for at least seven days before testing.

2.1.5 Beam Configuration

All beam configurations are listed below. As mentioned earlier, there are two sets of beams. They have the same steel reinforcement, CFRP spacing and cross sectional areas but different lengths and number of CFRP strips. For 4-foot long beams, there are six strips on each side; for 6-foot long beams, there are 10 strips on each side.

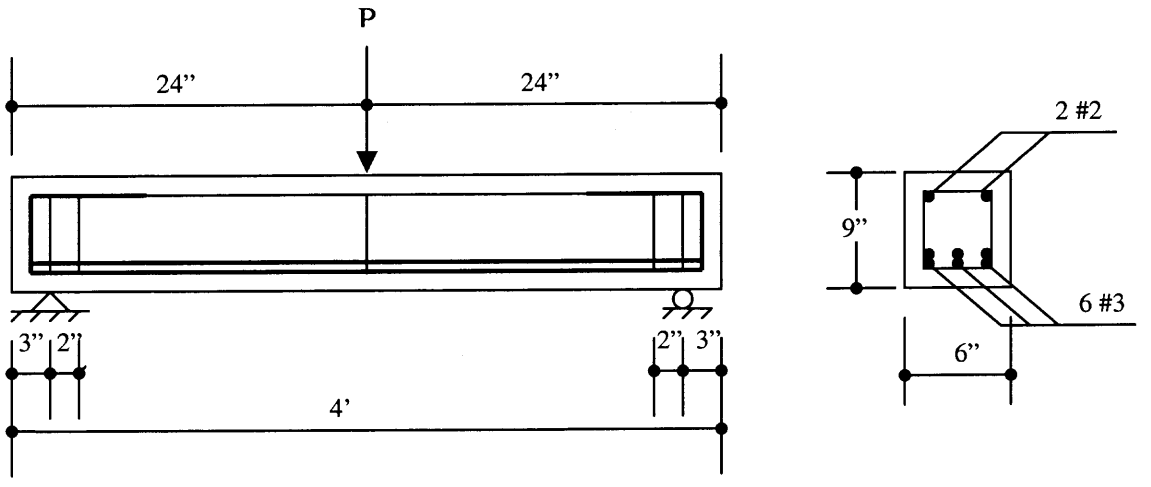

Figure 2.1 Control beam ZC4.

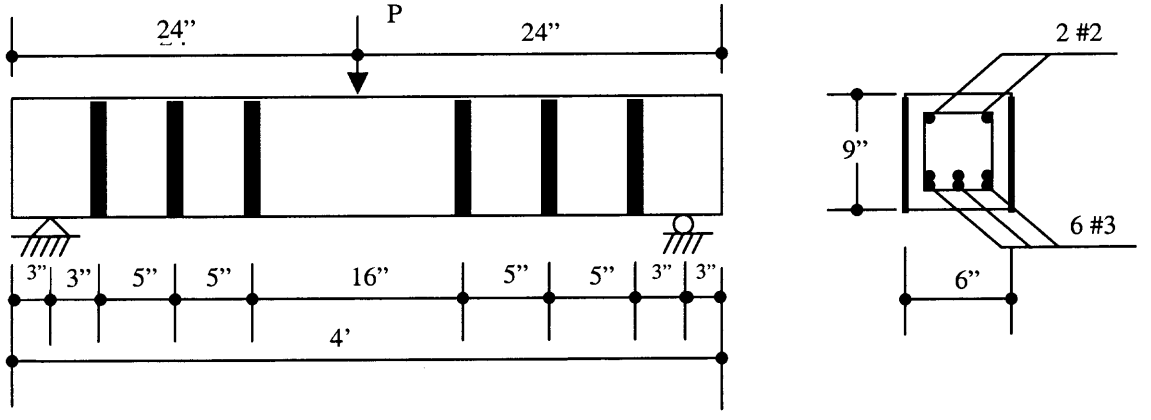

Figure 2.2 Beam Z4-90.

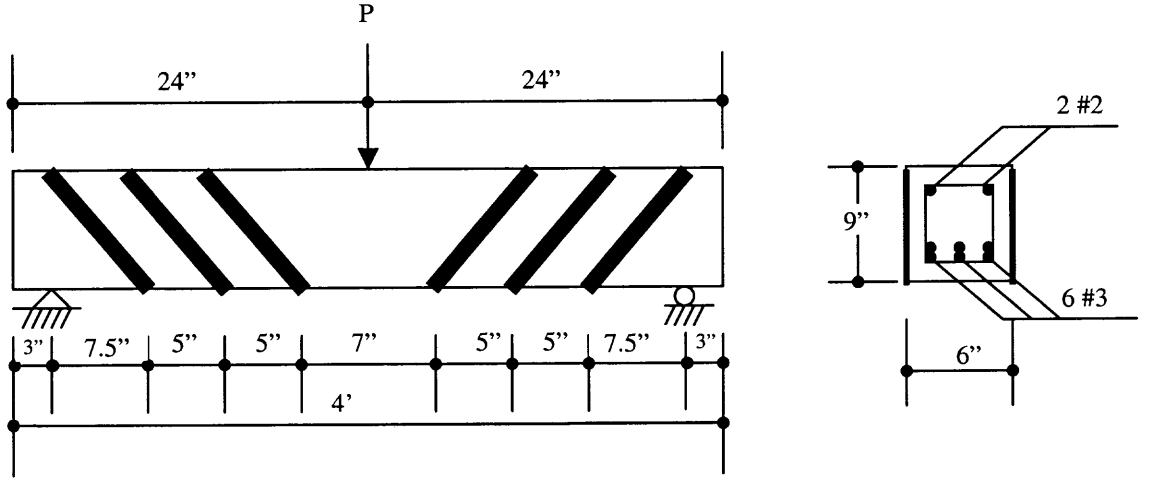

Figure 2.3 Beam Z4-45.

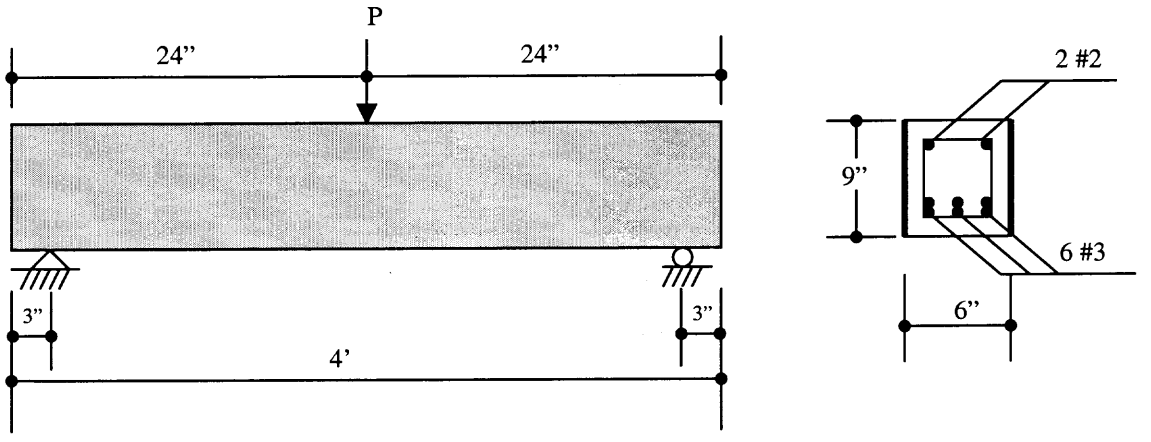

Figure 2.4 Beam Z4-Fab.

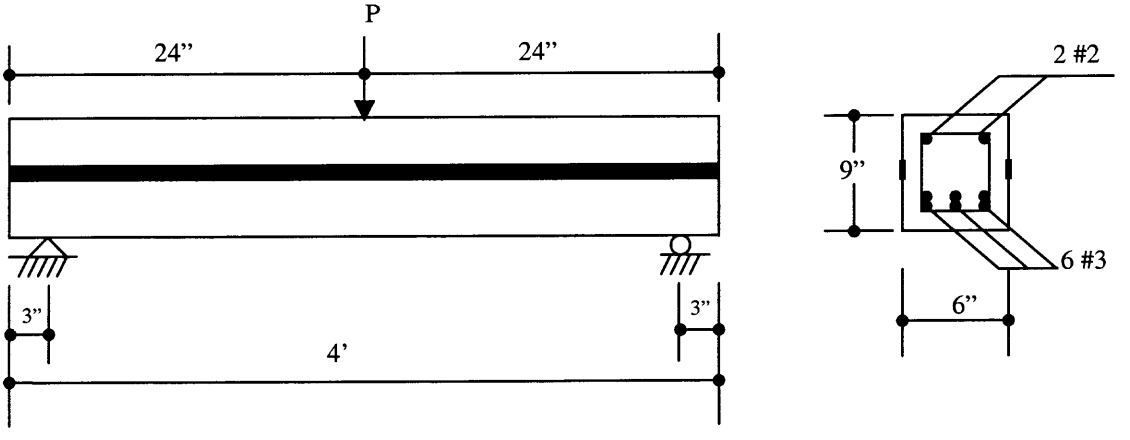

Figure 2.5 Beam Z4-Mid.

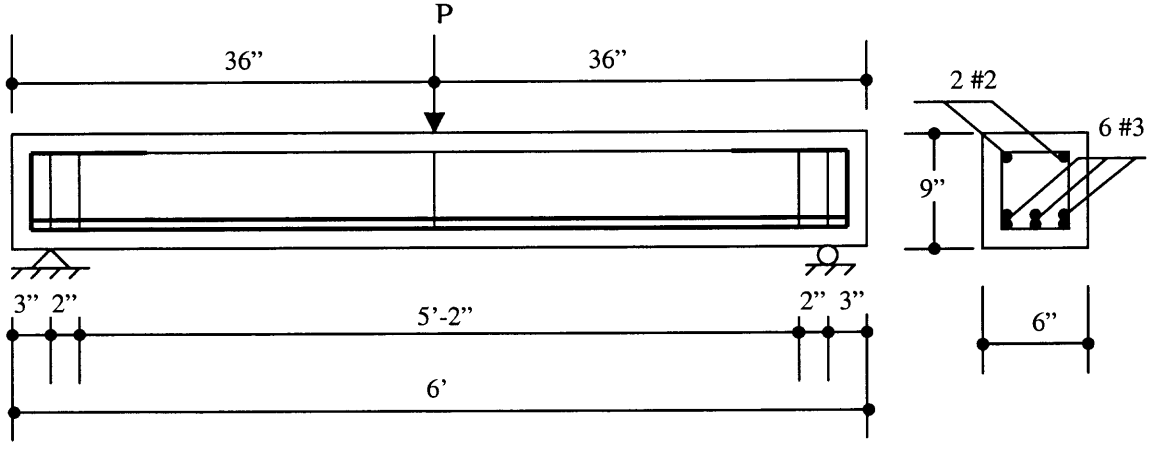

Figure 2.6 Control beam ZC6.

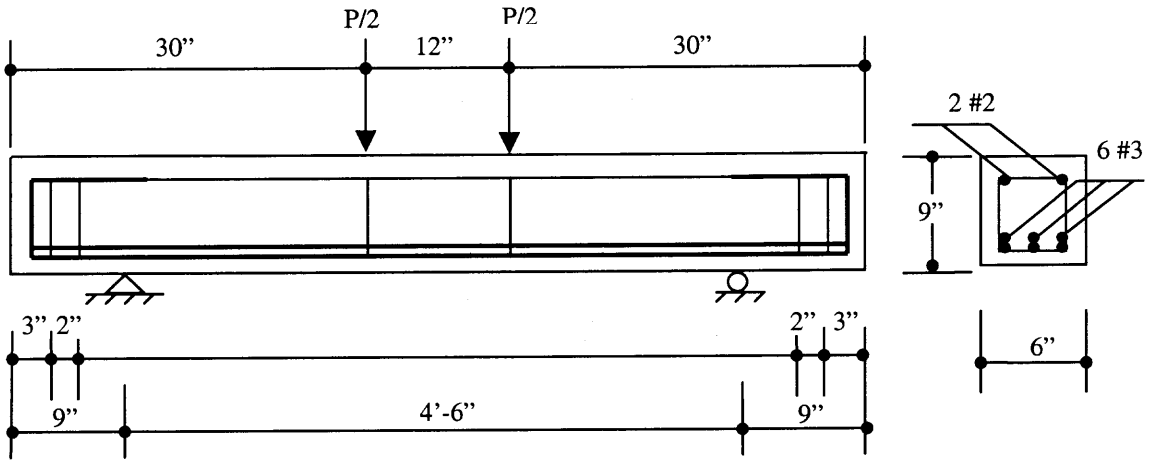

Figure 2.7 Control beam ZC6(2).

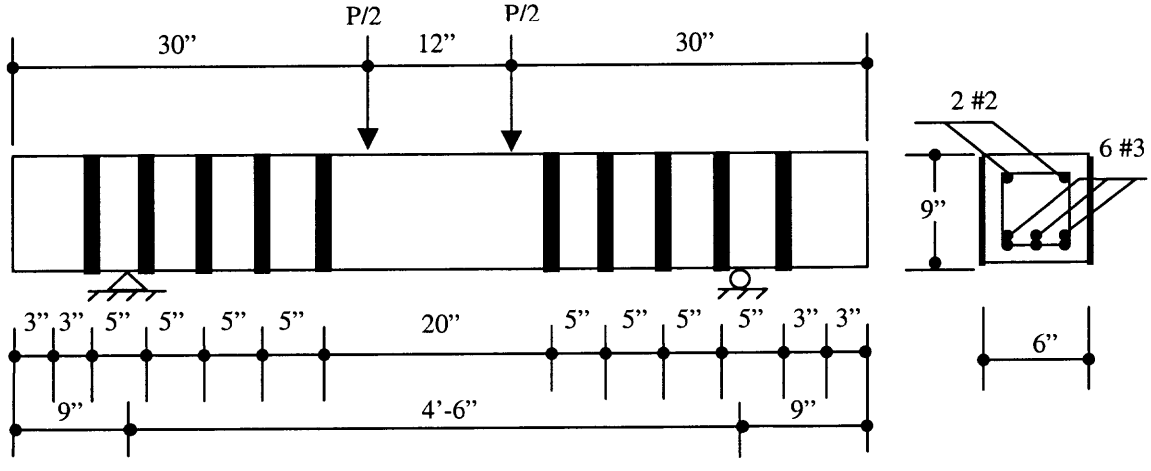

Figure 2.8 Beam Z6-90.

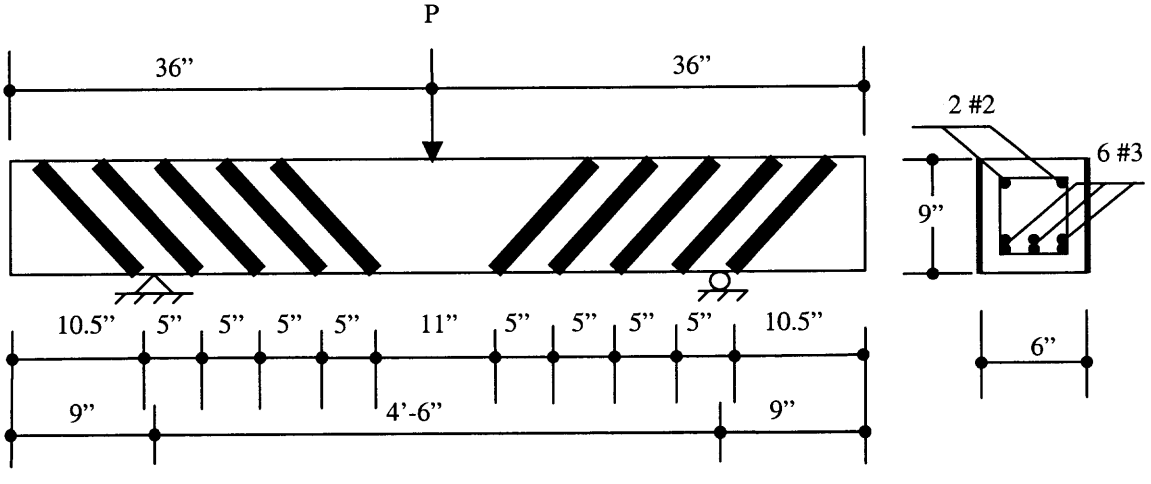

Figure 2.9 Beam Z6-45.

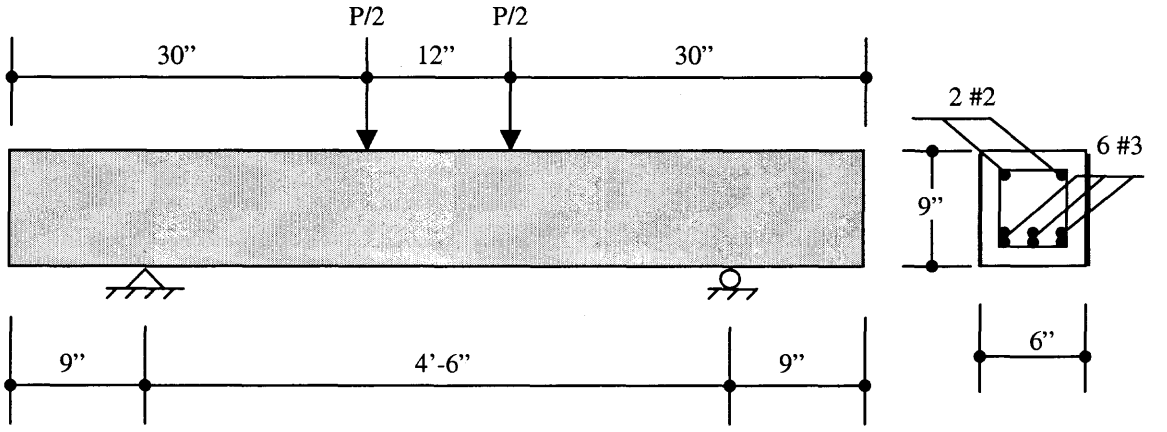

Figure 2.10 Beam Z6-Fab.

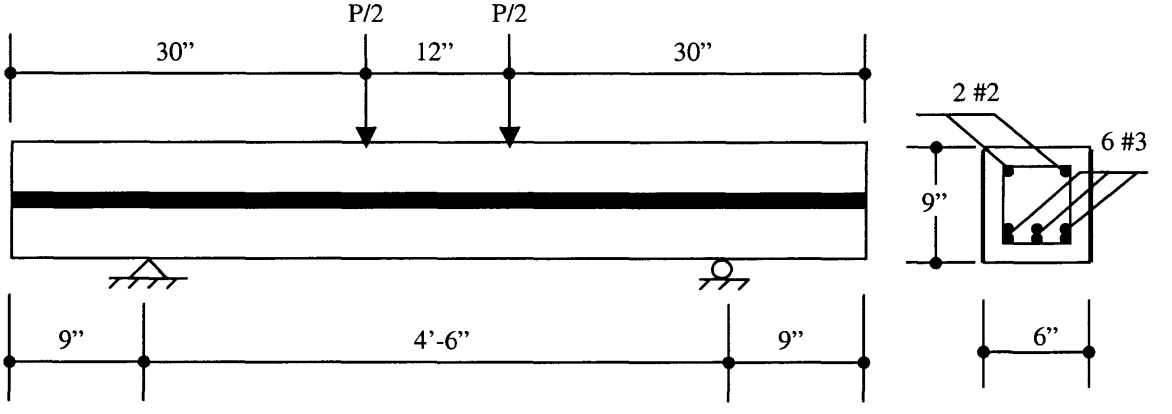

Figure 2.11 Beam Z6-Mid.

2.2 Instrumentation and Test Procedure

All 4-foot long beams and 6-foot long beams were tested on a 220-kip MTS testing system. Two steel rollers served as the supports were placed under both ends of the beam, respectively. There was a small piece of metal plate between the beam and the support at each end to prevent local failure of the concrete. Four pairs of mechanical strain gages (or called demec gages) were installed in the middle of one side of the beam before the test started. They were located 4" each side from the mid-span of the beam. The strain was measured at different loading steps during the entire test. The data was used to calculate

the strains and plot the Moment-Curvature curve. An automatic data acquisition system was used to monitor loading as well as midspan deflection. The load was applied by a hydraulic jack and measured by a load cell. Deflection control was used in all the tests. Deflection measurements were taken at the midspan of the beam. All beams were statically tested to failure in a single load cycle.

2.2.1 4-Foot Long Beams

Three point bending tests were performed on all 4-foot long beams.

a) Beam ZC4

The first beam tested was the 4-foot long control beam ZC4 (Figure 2.1). It was a typical shear failure. As the load went up to 20.5 kips, a sudden crack originating from the loading point developed at 45 degrees at left edge of the beam; there was no noticeable cracks at the other edge. Then the load dropped quickly and the test stopped at 10.9 kips (Figure 2.12).

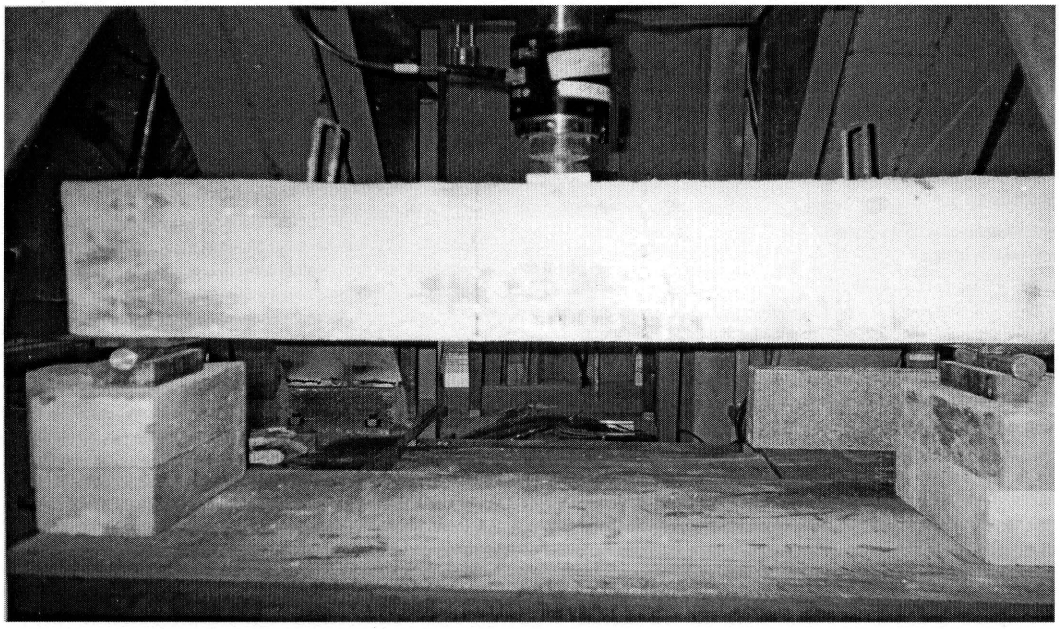

Figure 2.12 Failure of Beam ZC4.

b) Beam Z4-90

The next beam was Z4-90 (Figure 2.2). The initial cracks occurred at the tension side of the beam when the load reached 30.1 kips. Apparently, these were flexural cracks. As the load continued growing, more flexural cracks developed while there was no significant load increasing. Meanwhile, small shear cracks started to appear and there was no CFRP strips delamination. At about 32.3 kips, the load suddenly dropped down and final shear cracks formed, which caused a severe delamination along the third strip from the supports (Figure 2.13).

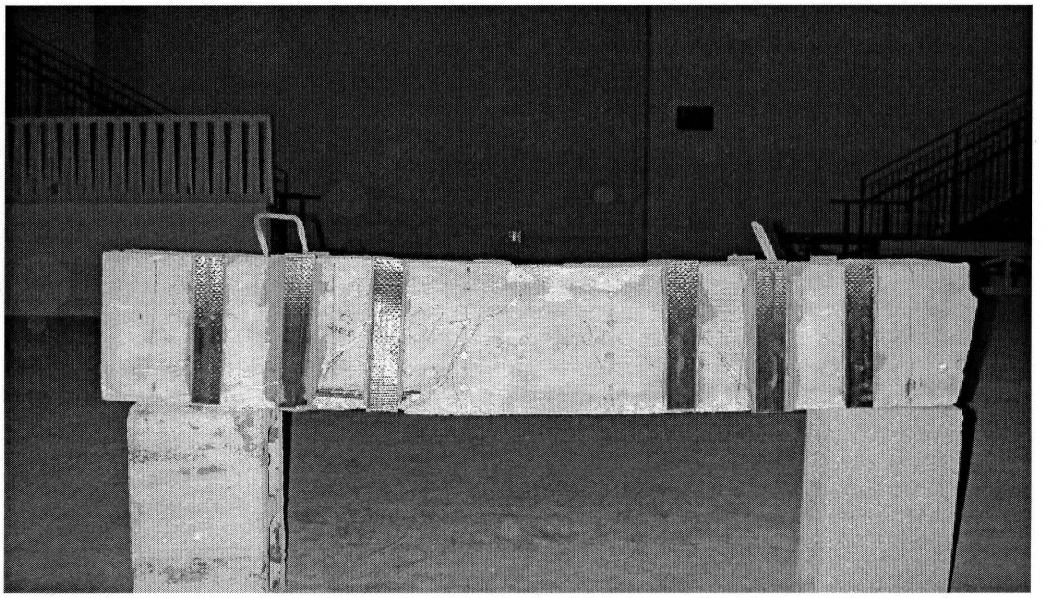

Figure 2.13 Failure of Beam Z4-90.

c.) Beam Z4-45

The third beam tested was Z4-45 (Figure 2.3). Z4-45 and Z4-90 have the same number of CFRP strips and the same spacing. The only difference between them is the strip orientation. When the load arrived at about 28.2 kips, it dropped slightly because of the concrete crushing under the load plate due to the imperfection of the

concrete surface. The load continued to increase and vertical flexural cracks began to form at about 31.8 kips, and it was followed by the small inclined flexure-shear cracks. Obviously, the load increase became much slower, and flexural cracks became wider. That meant that the flexural reinforcement started to take over the load. From the load-deflection curve, it can be observed that during this period the deflection increased about 1.2 inches, while the load only increased about 5 kips. At about 33.6 kips, the full shear cracks developed followed by the delamination along the 2nd and 3rd CFRP strips from the supports. The test stopped when the load dropped to 2.4 kips (Figure 2.14).

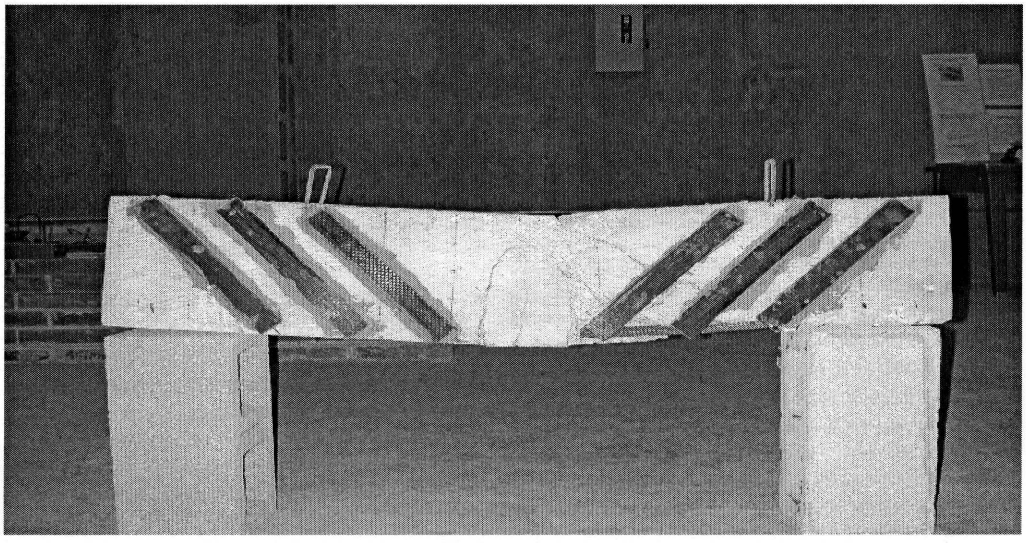

Figure 2.14 Failure of Beam Z4-45.

d.) Beam Z4-Mid

The fourth beam was Z4-Mid (Figure 2.5). The load dropped from 6.6 kips to 2.9 kips shortly after the test started due to the local concrete crush at one of the support. After that, the load-deflection curve remained linear until the load reached 27.8 kips. The beam failed in shear at the load of 27.8 kips and at the same time one end of the

CFRP strip suddenly detached from the concrete surface accompanied by a sharp sound. The load dropped to 8.2 kips and the test stopped. Due to the potential danger of getting hurt, it's recommended that observers stay at least five feet away from the test specimen, especially when the specimen is about to break (Figure 2.15).

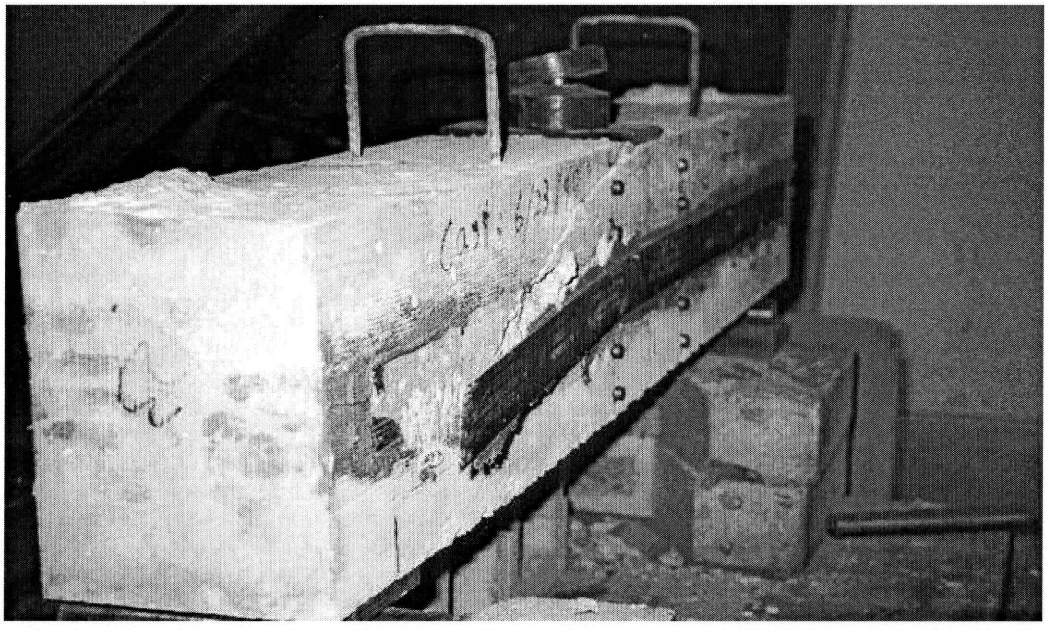

Figure 2.15 Failure of Beam Z4-Mid.

e.) Beam Z4-Fab

The last one tested for 4-foot long beams was Z4-Fab (Figure 2.4). The load increased smoothly after the test started. This can be observed from the load-deflection curve. The first shear crack appeared when the load reached 24.1 kips. It was accompanied by the fabric rupture at the center of the crack. It was noticed that only part of the fabric was torn apart. The load dropped to 17.2 kips and then began to increase. A second load drop was observed as soon as the increasing load approached the value of 19.8 kips. After that, the load dropped slowly to 5.4 kips until the test

was done. Meanwhile, more CFRP fabric was ruptured along the shear crack (Figure 2.16).

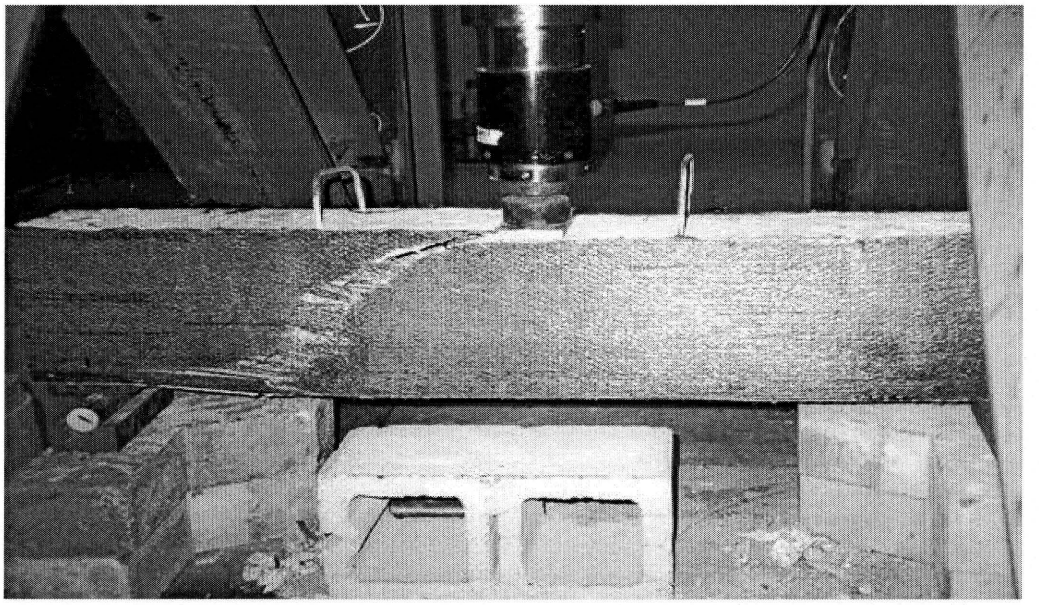

Figure 2.16 Failure of Beam Z4-Fab.

2.2.2 6-Foot Long Beams

a) Beam ZC6 and Beam ZC6(2)

The first 6-foot beam tested was ZC6 (Figure 2.6). 1-point loading was performed on this beam. Vertical flexural cracks were the first to form. It was followed by flexural-shear crack. Ductile behavior was observed in this test. The peak load for the whole test was 19.1 kips. It was a shear-flexural failure (Figure 2.17). To eliminate the shear-flexure failure of the beam, it was decided to test another control beam ZC6(2) (Figure 2.7), and 2-point loading was performed on this beam. Typical shear failure was observed for beam ZC6(2) (Figure 2.18), with a failure load at 19.3 kips.

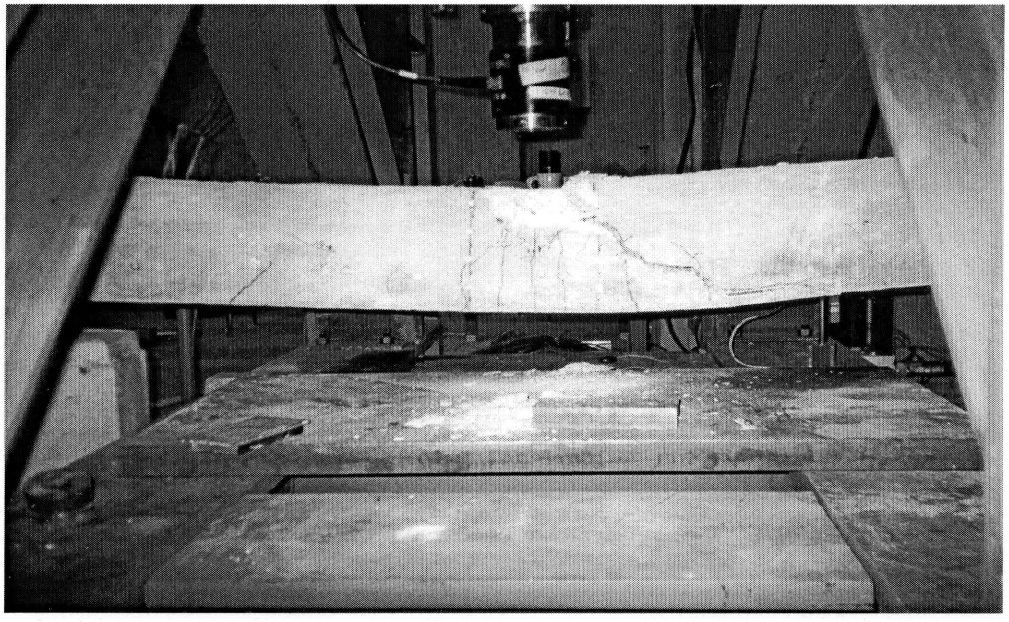

Figure 2.17 Failure of Beam ZC6.

Figure 2.18 Failure of Beam ZC6(2).

b) Beam Z6-45

Since the failure mode for the first beam is not a perfect shear failure, the clear span between the supports was changed from 5.5 feet to 4.5 feet to increase the bending moment capacity of the beam (Figure 2.9). Cracking in the beam started at midspan with vertical flexural cracks. As the load continued to increase, more flexural cracks developed. However, the load increase became very slow. At about 24.3 kips, the load changed back and forth slightly due to the development of cracks. Although there were some flexural-shear cracks, the beam failed in flexure eventually. Only one strip near the center of the beam delaminated at the lower end (Figure 2.19).

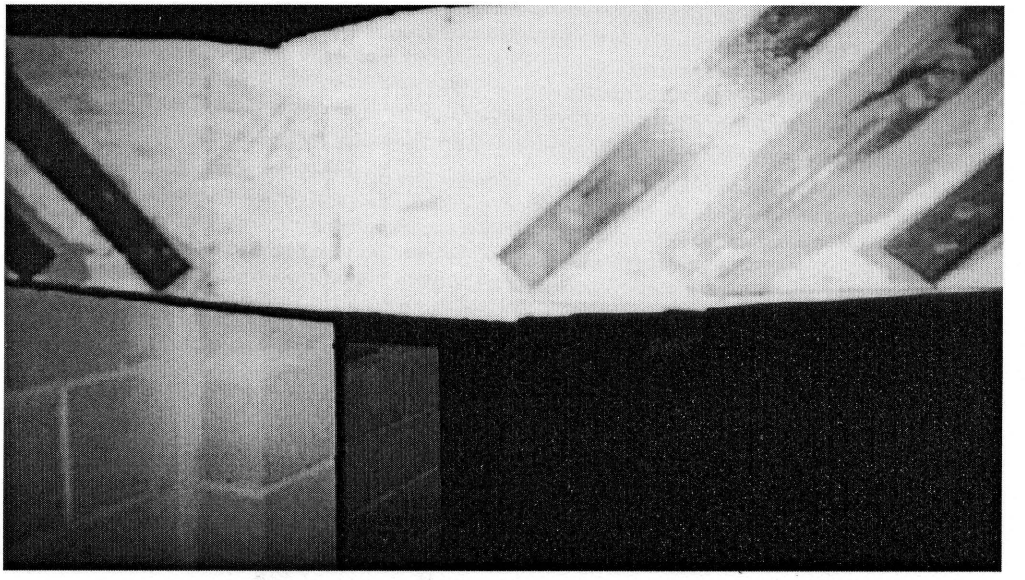

Figure 2.19 Failure of Beam Z6-45.

c) Z6-Mid

2-point loading was employed in the testing of this beam (Figure 2.11). The clear span between the supports was still 4.5 feet. The distance between the two loading points was one foot. The purpose of this setup was to increase bending moment

capacity. The load went straight to 26.8 kips without any sign of any kind of crack. Then one shear crack appeared and there was a quick drop of the load. The beam failed in shear, while the CFRP strip crossing the shear crack stretched to a large extent without rupture. The bonding between epoxy and concrete was perfect, but there was a slip between epoxy and CFRP strip in the vicinity of the crack (Figure 2.20).

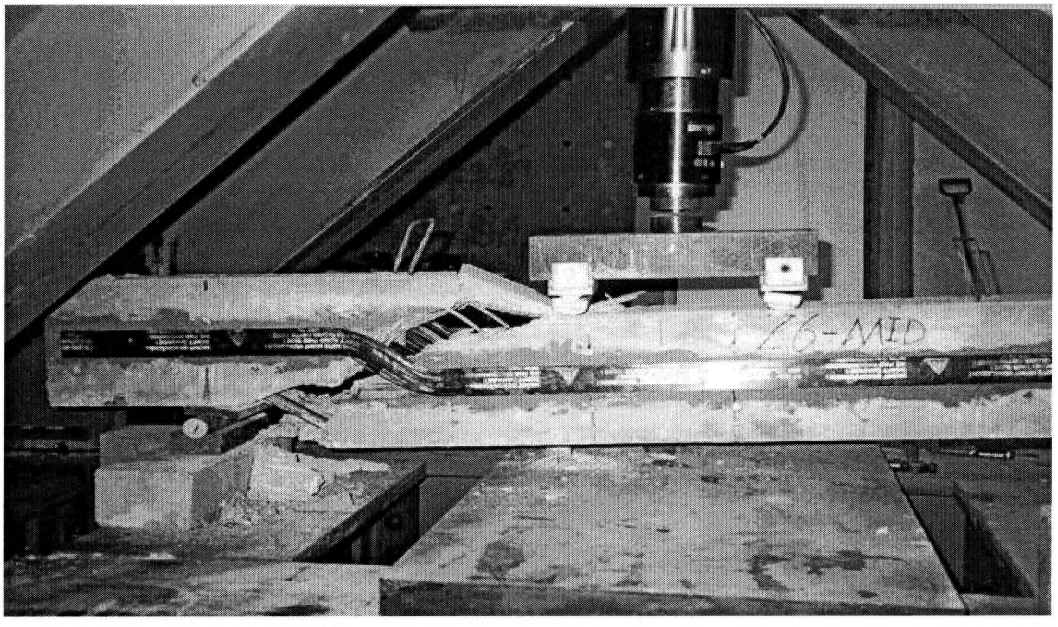

Figure 2.20 Failure of Beam Z6-Mid.

d) Beam Z6-Fab

The test set up for beam Z6-Fab was the same as that of beam Z4-Fab (Figure 2.10). The load-deflection curve generated by the computer began to develop as soon as the test started. It went all smooth without any interruption until the peak load occurred at 22.9 kips. Then it plunged to 9.1 kips. The failure was brittle by observing the load-deflection curve as well as the shear crack that occurred at one side of the beam. The

fiber at the crack was partially ruptured. The test finished when the deflection reached 0.58 in. (Figure 2.21)

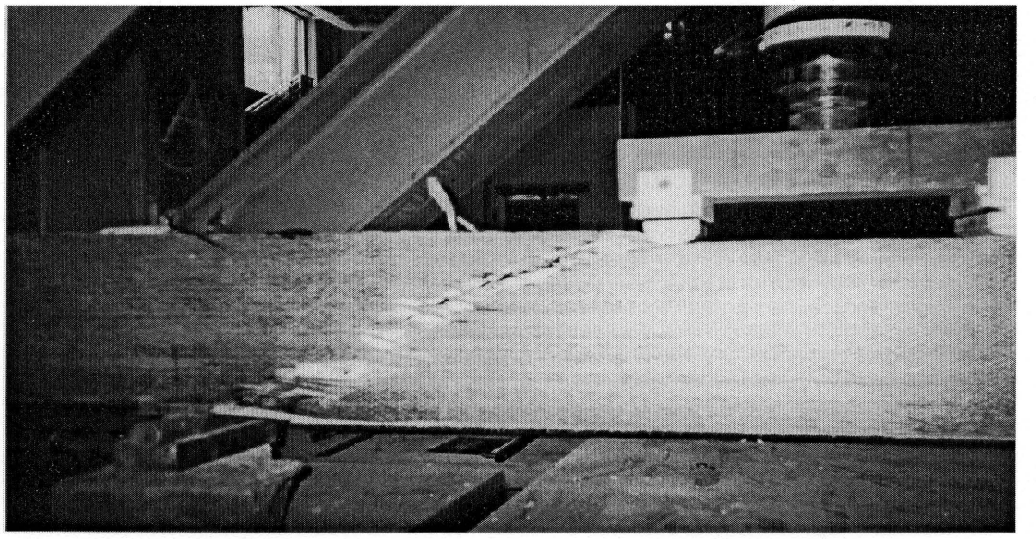

Figure 2.21 Failure of Beam Z6-Fab.

e) Beam Z6-90

The beam tested used the same 2-point loading setup (Figure 2.8). The load went up to 3.9 kips and suddenly dropped to 0.267 kips because of local failure at the support. Then the load went straight up again, as can be observed from the load-deflection curve. At about 26.9 kips, small flexural cracks located at mid-span of the beam started to grow. Meanwhile, the load continued to increase at a lower rate, which could be interpreted by the slope of the load-deflection curve. At about 28.7 kips, a big shear crack suddenly appeared and the load dropped to zero. The failure mode for this beam was CFRP strip delamination from the first strip near the mid-span to the third strip. No rupture was observed (Figure 2.22).

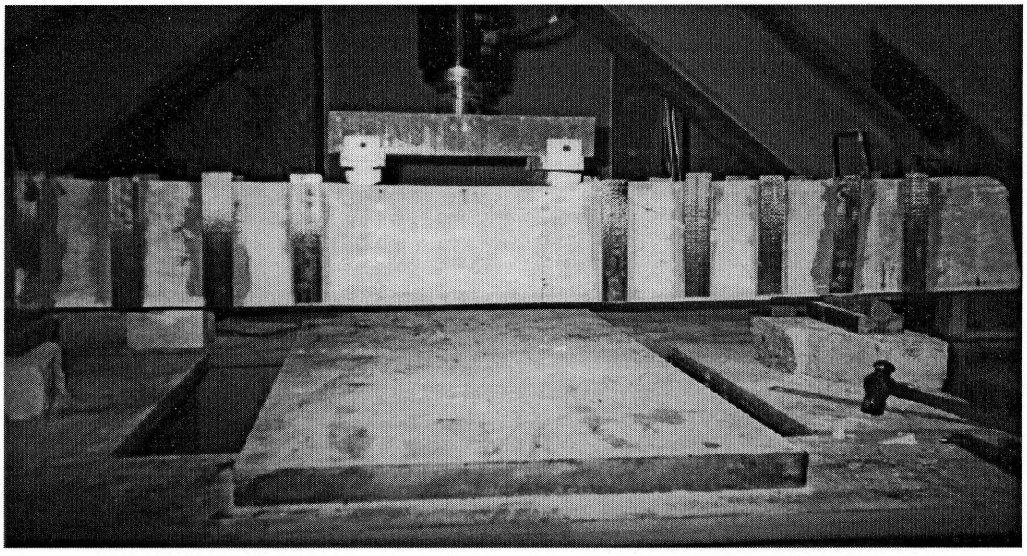

Figure 2.22 Failure of Beam Z6-90.

2.3 Test Results and Discussions

2.3.1 Results of 4-Foot Long Beams

a) Strength

From Table 2.4 and Figure 2.23, it can be concluded that CFRP strips and fabrics do help in shear strengthening of RC beams. However, due to different material and configurations, the contribution of CFRP in shear strengthening varies. Compared with the control beam ZC4, Z4-45 gives 16.5 Kips increase in shear capacity, which is the most efficient system among the five beams. Z4-90 increases 12.4 kips in shear capacity, which is less than Z4-45. It is noticed that the only difference between Z4-45 and Z4-90 is the strip orientation. Thus, 45-degree strip orientation is recommended. Z4-Mid has less shear contribution as compared with the above two, and Z4-Fab has the least shear contribution among the four CFRP shear strengthened beams.

b) Ductility

Table 2.4 and Figures 2.23 and 2.24 also show that Z4-45 and Z4-90 beams give large deflections at ultimate, which are 0.9381 in. and 0.5782 in., respectively, as compared to other beams. This means that CFRP strengthened beams give not only the increase in shear strength, but also the increase in ductility as well. This is a particularly important physical phenomenon because the CFRP strengthened beams can exhibit more ductility than the beams strengthened by the regular steel bars. From the moment-curvature curves in Figure 2.24, beams Z4-45, Z4-Mid and Z4-Fab show more ductility than that of control beam ZC4.

Table 2.4 Experimental Results of 4-foot Beam Series

Beam Designation	Load P at Ultimate (kips)	Deflection at Ultimate (inch)	CFRP Shear Capacity (Kips)	Failure Mode
ZC4(control)	20.7	0.1836	—	Shear Diagonal Cracking
Z4-45	37.2	0.9381	8.3	Strip Delamination
Z4-90	33.1	0.5782	6.2	Strip Delamination
Z4-Mid	27.5	0.2162	3.4	Strip Delamination
Z4-Fab	24.1	0.1790	1.7	Fiber Rupture

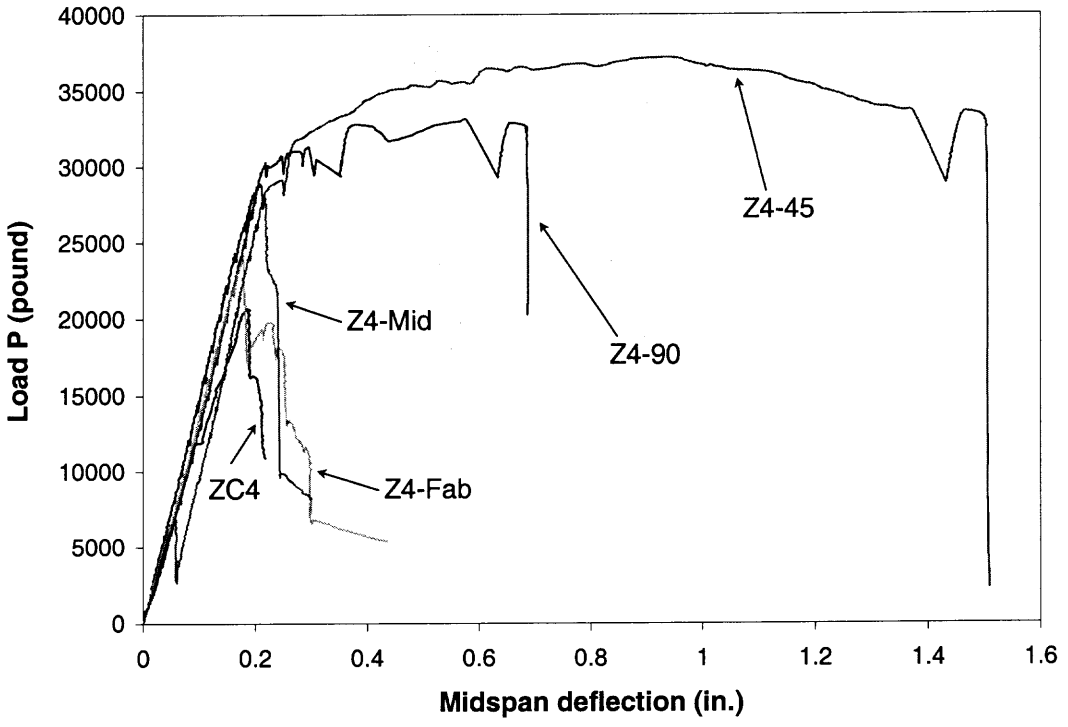

Figure 2.23 Comparison of load-deflection curves of 4-foot long beams.

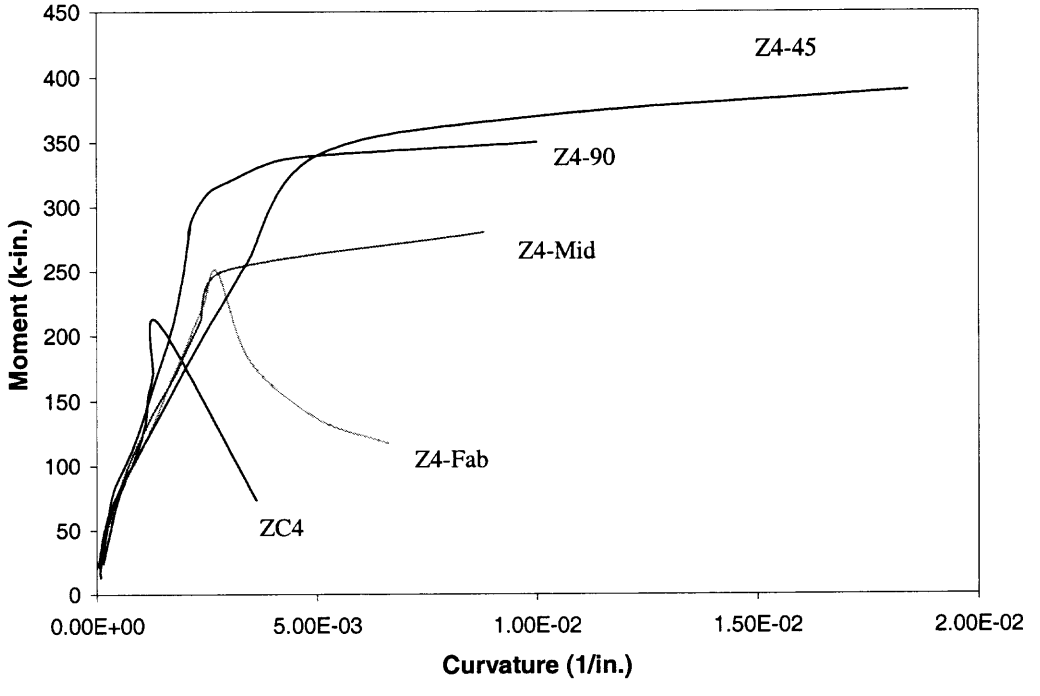

Figure 2.24 Comparison of moment-curvature curves of 4-foot long beams.

c) Failure Mechanism

Apparently, the control beam ZC4 failed in shear. From the load-deflection curve shown in Figure 2.23, it can be observed that the descending part of the curve is very steep, which means that there is a sudden drop of the load. Z4-90 failed in shear ultimately. But the first crack appeared was flexural crack located at the tension zone. Because of the existence of the CFRP strips, the shear capacity increased and therefore the ductility increased at the same time. Figure 2.23 shows that Z4-90 and Z4-45 have similar behavior, but Z4-45 has more ductility. The failure mode for both Z4-90 and Z4-45 was the delamination of the CFRP strips from the concrete surface. It should be noted that delamination here was the concrete rip-off underneath the epoxy. The bonding between the CFRP strips and the epoxy was good, except there were few spots where small piece of epoxy blocks were pulled off from the CFRP strip surface. The failure mode for Z4-Mid was also strip delamination. Since there was no anchorage at the end of the strip, the delamination was started from one end of the strip and developed approximately two feet in a very short time. Beam Z4-Fab failed in shear because of the fiber rupture of the CFRP sheets. The bonding between the sheets and the epoxy was perfect at the failure.

2.3.2 Results of 6-Foot Long Beams

The test set-ups involving in the 6-foot beams had to change as the experiments went along in order to make the beams fail in shear rather in bending. Both beam ZC6 and beam Z6-45 failed primarily in bending, while the other three beams failed in shear due to the change of the shear span. Since it was not feasible to compare the shear strength

and ductility of the other three beams with the original control beam ZC6, a second control beam ZC6(2) was thus cast exactly the same as the original control beam ZC6, but was tested under 2-point loading with a 4.5-foot clear span. Beam ZC6(2) eventually failed in shear with an ultimate load of 19.3 kips.

a) Strength

Unlike the 4-foot beams, The test results for 6-foot beams seemed a little bit unusual, yet they could be explained. Beam Z6-45 was not the strongest beam of the five tested beams. It was mainly because that 1-point loading system was used in the test setup for relatively longer span (4.5'), which caused the beam Z6-45 failed in bending rather than in shear. Compared with Beam ZC6, the failure load of beam Z6-45 was 5.9 kips higher.

Beam Z6-90 was the strongest beam among the beams under 2-point loading. The beam failed in shear at 28.7 kips, which was 9.4 kips higher than that of beam ZC6(2). Beam Z6-Mid followed that of Beam Z6-90 and failed at 27 kips. Beam Z6-Fab was the least effective one, which failed at 23.1 kips (Table 2.5, Figure 2.25).

b) Ductility

By observing the load-deflection curve at mid-span of the simply supported beam, one can get some idea about the ductility of the beam, however it can not give the whole picture. The ductility of the cross section of the beams is best described by the moment-curvature curves. From Figures 2.25 and 2.26, ZC6 and Z6-45 have more ductility than other beams have. However, the failure for the two beams was not completely shear failure. Flexural cracks also developed as well, which made the two beams looked more ductile. Beam Z6-90 also behaved ductile, which could be

observed by a prolonged portion of the peak moment-curvature curve. Beam Z6-Mid and Z6-Fab were more brittle. This was mainly caused by the force redistribution in the beams at the peak load, when the brittle shear failures occurred (Table 5, Figure 2.25, and Figure 2.26).

Table 2.5 Experimental Results of 6-foot Beam Series

Beam Designation	Load P at Ultimate (kips)	Deflection at Ultimate (in.)	CFRP Shear Capacity (Kips)	Loading System	Clear Span	Failure Mode
ZC6 (control)	19.1	1.1	—	1-point	5.5'	Shear & Flexure Cracking
Z6-45	25.0	0.9195	3.0	1-point	4.5'	Strip Delamination & Flexure Cracking
ZC6(2) (control)	19.3	0.1290	—	2-point	4.5'	Shear Cracking
Z6-90	28.7	0.3778	4.7	2-point	4.5'	Strip Delamination
Z6-Mid	27.1	0.2648	3.9	2-point	4.5'	Strip Delamination
Z6-Fab	23.0	0.2339	1.9	2-point	4.5'	Fiber Rupture & Delamination

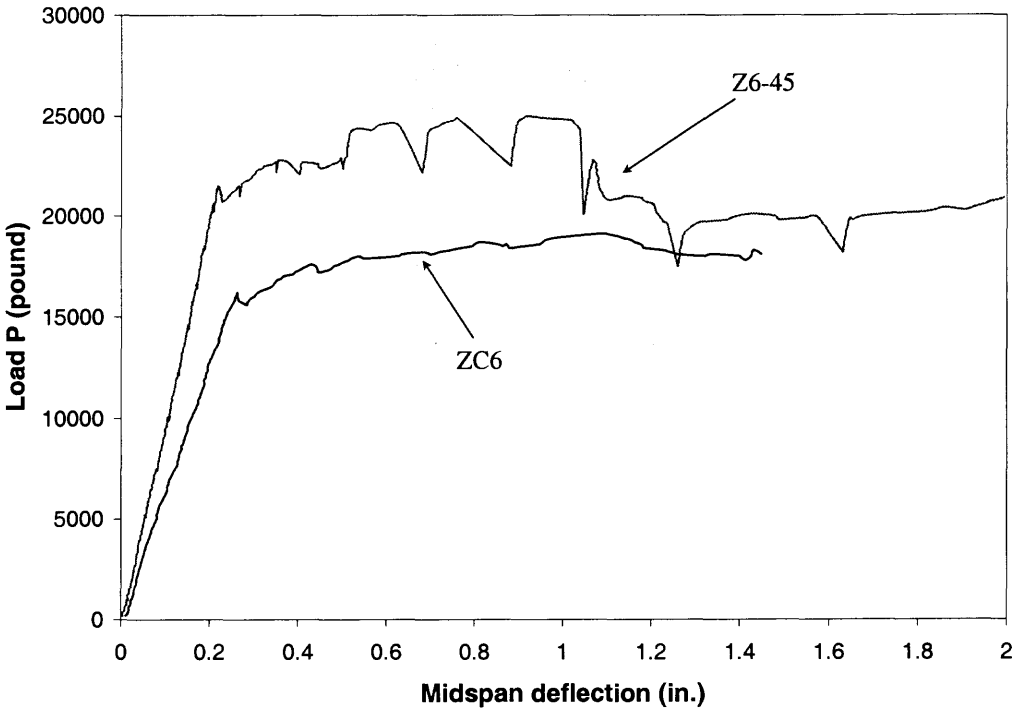

(a) Comparison of beams failed in bending.

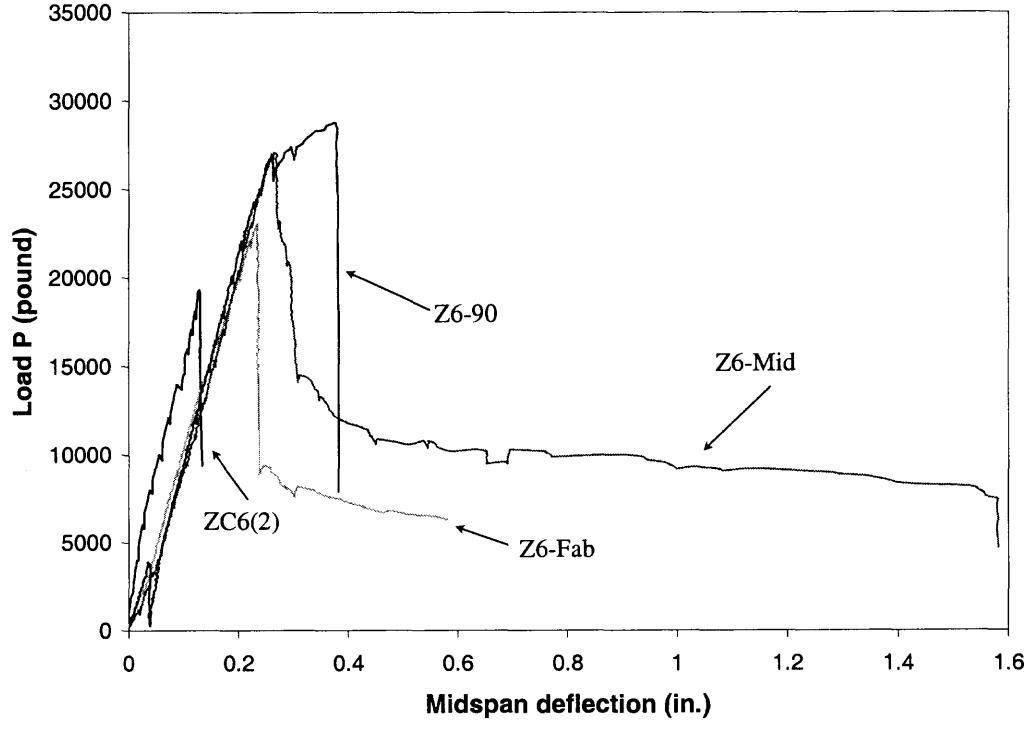

(b) Comparison of beams failed in shear.

Figure 2.25 Comparison of load-deflection curves of 6-foot long beams.

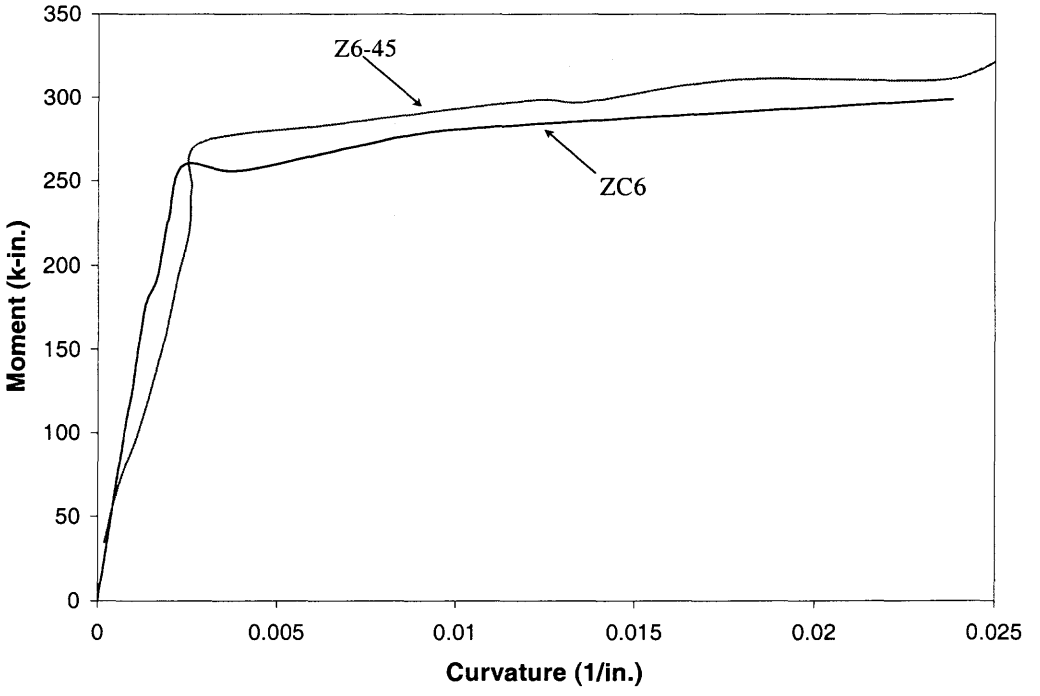

(a) Comparison of beams failed in bending

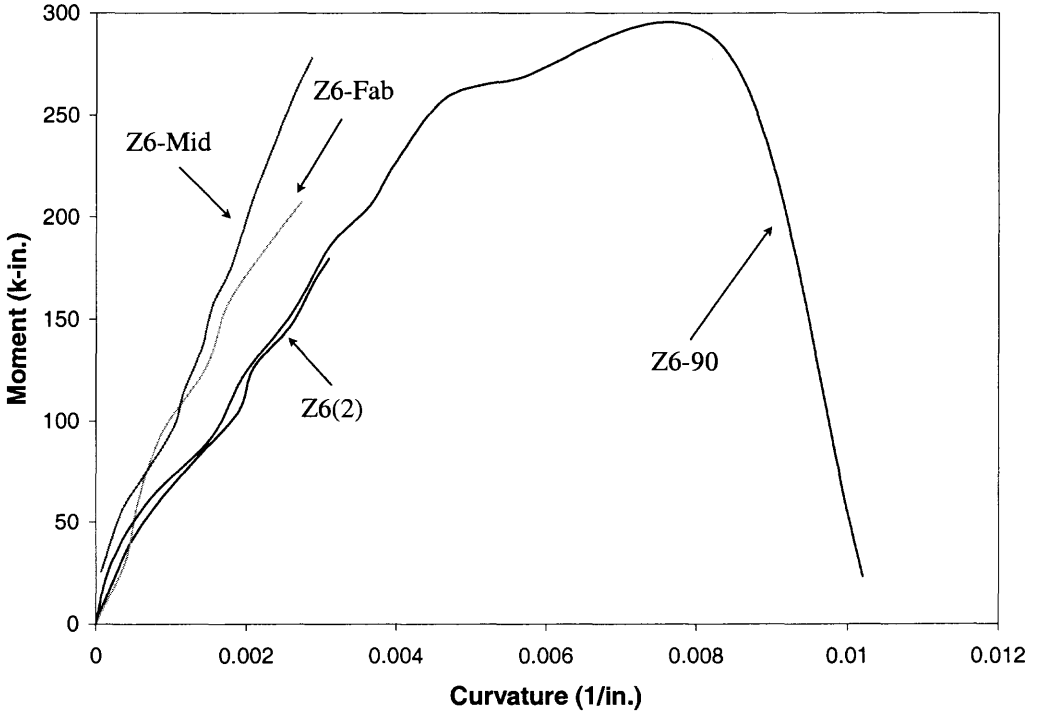

(b) Comparison of beams failed in shear

Figure 2.26 Comparison of moment-curvature curves of 6-foot long beams.

c) Failure Mechanism

Since different loading systems and different beam spans were adopted in the test of this beam series, the failure mechanism was more diverse than previous 4-foot beam series. The control beam ZC6 actually failed in combined shear and flexure. Beam Z6-45 failed in flexure because the CFRP shear reinforcement was so strong and the flexural reinforcement could not carry more loads. Another beam ZC6(2) failed in shear. Beam Z6-Mid also failed in shear ultimately, and the CFRP strip delaminated partially around the crack. Beam Z6-Fab failed in the same way as beam Z4-Fab did. It was the fiber rupture at the location of the crack. Beam Z6-90 and beam Z4-90 had the same failure mechanism, which was the CFRP delamination (Table 2.5, Figure 2.25).

CHAPTER 3

ANALYTICAL STUDY ON SHEAR STRENGTHENING OF REGULAR RC BEAMS USING CARBON FIBER REINFORCED POLYMER LAMINATES

3.1 Shear Design Philosophy and Current Design Approach

From the results of the tests, one can figure out the contribution of CFRP to the total shear resistance of the beams. It is also possible to theoretically estimate the CFRP contribution through the traditional truss analogy. The nominal shear strength of a regular RC beam may be computed by the basic design equation presented in ACI 318-99 (ACI Building Code; 1999) and is given as Equation 1.1.

In this equation, the nominal shear strength is the sum of the shear strength of the concrete (which for a cracked section is attributable to aggregate interlock, dowel action of longitudinal reinforcement, and diagonal tensile strength of the uncracked portion of concrete) and the strength of steel shear reinforcement.

If the beam is strengthened with the externally bonded CFRP sheets, the nominal shear strength may be computed by adding a third term to account for the contribution of CFRP laminates to the shear strength. Below is a given equation.

$$V_n = V_c + V_s + V_f \tag{3.1}$$

The design shear strength is obtained by multiplying the nominal shear strength using a strength reduction factor φ. The reduction factor of 0.85 given in ACI 318-99 is to be used for concrete and steel terms. However, the reduction factor for CFRP reinforcement will require an adjustment, too. It was suggested to be 0.70 by Khalifa et al. (1998). Equation 3.2 presents the design shear strength, thus,

$$\phi V_n = 0.85(V_c + V_s) + 0.7V_f \tag{3.2}$$

The equation to compute CFRP shear contribution is similar to what is used for steel shear reinforcement. The equation to compute V_f is given below.

$$V_f = \frac{A_f f_{fe} (\sin\alpha + \cos\alpha) d_f}{s_f} \tag{3.3}$$

In Equation 3.3, A_f is the area of CFRP shear reinforcement, which is the total thickness of the CFRP on both sides of the beam, $2t_f$, times the width of the CFRP strip w_f. α is the angle between the orientation of the principal fibers in the CFRP laminates and the longitudinal axis of the beam. d_f is the CFRP laminates effective depth. s_f is the CFRP strip spacing. f_{fe} is the effective tensile stress of CFRP laminates when the beam failed in shear.

Equation 3.3 can also be expressed as follows:

$$V_f = \frac{A_f E_f \varepsilon_{fe} (\sin\alpha + \cos\alpha) d_f}{s_f} \tag{3.4}$$

In Equation 3.4, E_f is the elastic modulus of CFRP laminates. ε_{fe} is the effective tensile strain of CFRP laminates.

As suggested by the experimental evidence, failure of the CFRP reinforcement may occur either by debonding through the concrete that is nearing the concrete-CFRP interface, or by tensile fracture of CFRP laminates at a stress which may be lower than tensile strength of the composite material due to stress concentrations (at rounded corners or at debonded areas, etc) (Traiantafillou, 1998). Thus, the effective tensile stress f_{fe} is used in Equation 3.4, instead of using the ultimate tensile stress f_{fu}.

To apply Equations 3.3 or 3.4, it is necessary to get the actual value of effective strain ε_{fe}. Since the ultimate tensile strain ε_{fu} of CFRP laminates can be obtained from the material properties provided by the manufacturer, a reduction factor R is needed to calculate the effective strain ε_{fe}.

$$\varepsilon_{fe} = R\varepsilon_{fu} \tag{3.5}$$

$$f_{fe} = Rf_{fu} \tag{3.6}$$

Khalifa et al. (1998) presented two equations to calculate R, one for CFRP rupture and another for delamination of CFRP from the concrete surface. The smaller R calculated from the two equations will be used in Equations 3.5 and 3.6. The two equations are listed below:

$$R = 0.5622(\rho_f E_f)^2 - 1.2188(\rho_f E_f) + 0.778 \tag{3.7}$$

Although Equation 3.7 is calibrated from the test results of both CFRP rupture and delamination, Khalifa et al. (1998) claimed it should only be used to calculate the reduction factor for rupture. In this equation, ρ_f is the CFRP shear reinforcement ratio, which is defined as $\frac{2t_f w_f}{b_w s_f}$. t_f is the CFRP thickness, w_f is the CFRP strip width, b_w is the cross section width of the RC beam, s_f is the CFRP strip spacing.

$$R = \frac{0.0042\left(f_c^{'}\right)^{2/3} w_{fe}}{\left(E_f t_f\right)^{0.58} \varepsilon_{fu} d_f} \tag{3.8}$$

Equation 3.8, which is derived from his analysis, has been used to calculate the reduction factor for CFRP delamination from the concrete surface, In this equation, w_{fe} is defined as the effective width of CFRP sheets.

3.2 Design Approach Based on Model Calibration

Triantafillou (1998) observed that the effective strain is a function of the axial rigidity of the CFRP sheet, which is $\rho_f E_f$. The implication of this argument is that as the CFRP laminates become stiffer and thicker, the effective CFRP strain decreases. Since V_f can be determined by most of the experiments available in the literature, it is fairly easy to attain the effective strain ε_{fe}. Based on the experimental results, the effective strain ε_{fe} can be calculated using Equation 3.9, which is the rearrangement of Equation 3.4.

$$\varepsilon_{fe} = \frac{V_f s_f}{A_f E_f (\sin\beta + \cos\beta) d_f} \tag{3.9}$$

Thus, the effective strain versus the axial rigidity is plotted and a relationship between effective strain and axial rigidity can be found by means of curve fitting.

Since the database used includes various kinds of CFRP sheets, for a certain kind of CFRP laminates the effective strain calculated using curve fitting would introduce some errors. To eliminate this effect, Khalifa et al. (1998) suggested that the ratio of effective strain to ultimate strain, $R = \varepsilon_{fe}/\varepsilon_{fu}$, be plotted versus axial rigidity, instead of using effective strain versus axial rigidity. A polynomial can be used as the best fit to the data in the case of $\rho_f E_f < 1.1GPa$. This polynomial is presented in Equation 3.7. Since more test results came up recently, Equation 3.7 is updated based on all current available test results, which is shown below as Equation 3.10. Figure 3.1 shows the comparison between Equation 3.10 and the experimental data.

$$R = 0.0387(\rho_f E_f)^2 - 0.5236(\rho_f E_f)^2 + 0.6393 \tag{3.10}$$

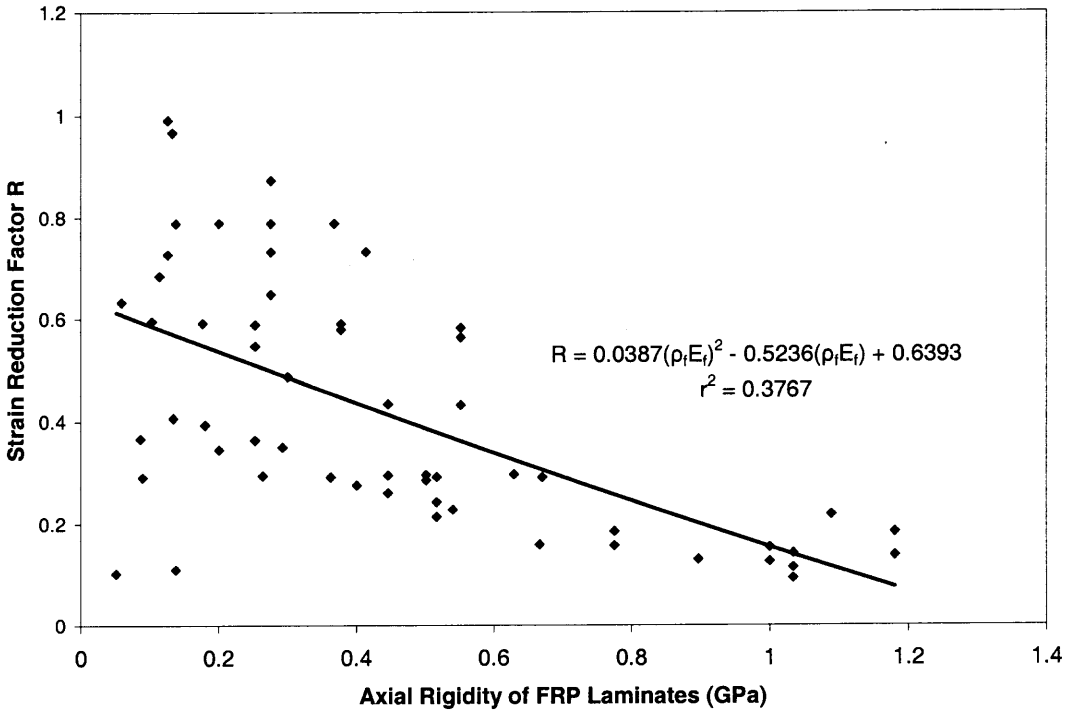

Figure 3.1 Strain reduction factor $R = \varepsilon_{fe}/\varepsilon_{fu}$ in terms of $\rho_f E_f$ (GPa), based on all available test results.

Equation 3.10 was derived from calibration of 60 test results including two modes of failure, of which 30 test results showed CFRP debonding failure mode and the other 30 test results showed CFRP rupture failure mode. Note that Equation 3.10, instead of Equation 3.7, can be used to calculate the reduction factor for both rupture and delamination.

In order to get more accurate analysis, it is necessary to divide the available test results into two categories based on CFRP rupture and CFRP debonding. All the test results of CFRP rupture are listed in Table 3.1; all the test results of CFRP debonding are listed in Table 3.2. The experimental data of CFRP rupture and debonding are shown in Figure 3.2 and Figure 3.3, respectively.

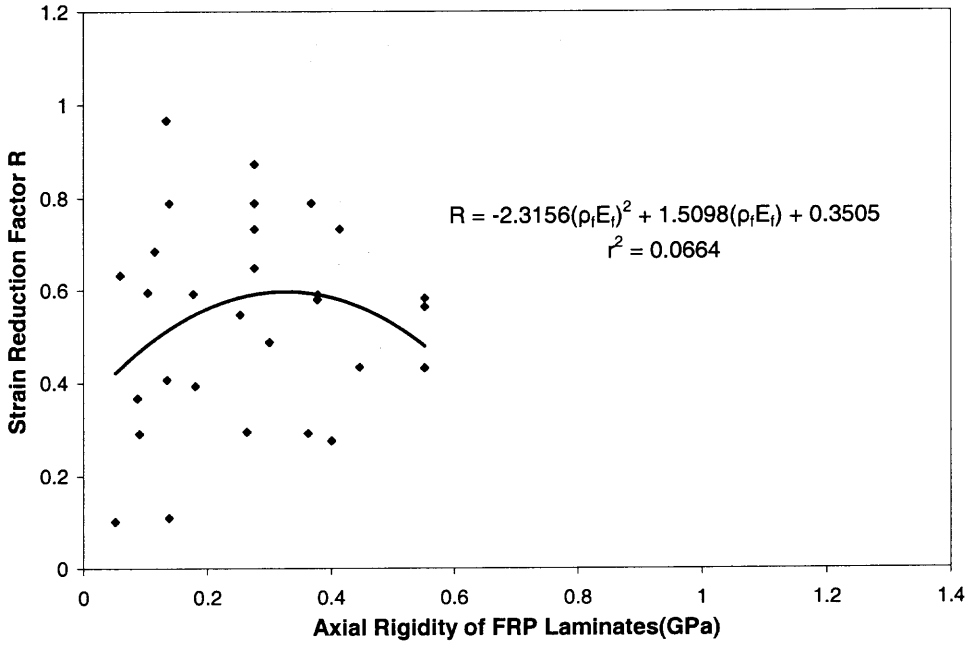

Figure 3.2 Strain reduction factor $R = \varepsilon_{fe}/\varepsilon_{fu}$ in terms of $\rho_f E_f$ (GPa), only based on test results of CFRP rupture.

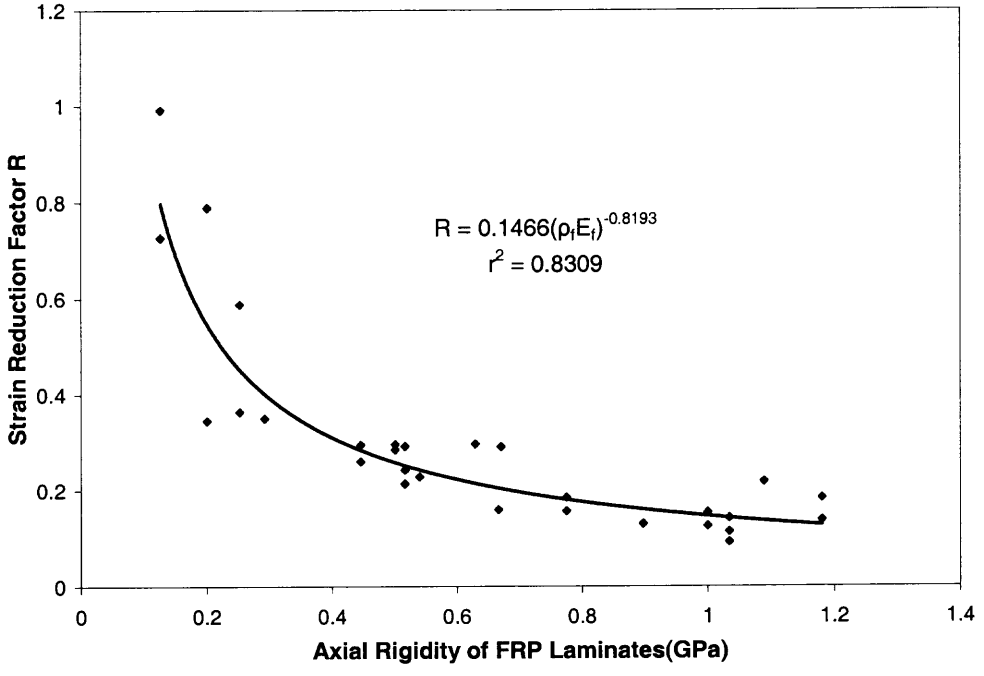

Figure 3.3 Strain reduction factor $R = \varepsilon_{fe}/\varepsilon_{fu}$ in terms of $\rho_f E_f$ (GPa), only based on test results of CFRP debonding.

From Figure 3.2, it can be observed that the data points are rather scattered. When $\rho_f E_f < 0.55GPa$, the rupture of CFRP laminates seems to occur randomly. The r-squared value of the trend line from these data is extremely low, which means this trend line does not give a reasonable estimation of the experimental data. In other words, the relation between the strain reduction factor and the axial rigidity can not be described using a simple equation based on the regression curve from the experiments. The fracture failure of CFRP laminates is far more complicated than what is expected. The effective strain of CFRP laminates can vary considerably because CFRP may fracture either exactly at the peak load or a little after due to excess stressing in the vicinity of the diagonal cracks.

On the other hand, the data points in Figure 3.3 are well distributed. Clearly, one can see that the strain reduction factor becomes smaller as the axial rigidity of CFRP laminates becomes larger. Instead of using a polynomial as a best fit to the data, a power regression line is adopted, since it gives the highest number of r-squared value, which means that this regression line gives the experimental data a more realistic equation to simulate the actual structural behavior. The equation for the power regression line is given below.

$$R = 0.1466\left(\rho_f E_f\right)^{-0.8193} \tag{3.11}$$

Table 3.1 Test Results Based on CFRP Rupture

Beam	bw(m)	d(m)	CFRP type	t(mm)	ρ_{CFRP}	E_{frp} (GPa)	E*t	f_{fu} (MPa)	Beta (deg)	Strain (ε_{fe})	E*ρ	R
U(3)	0.1	0.17	C, Wrap	0.097	0.00194	230	22.31	2650	90	0.005	0.4462	0.434
O(BS12)	0.18	0.36	C,Wrap	0.216	0.0012	230	49.68	2450	90	0.0084	0.276	0.789
O(BS24)	0.18	0.36	C,Wrap	0.432	0.0024	230	99.36	2450	90	0.0062	0.552	0.582
O(BM06)	0.18	0.36	C,Wrap	0.108	0.0006	230	24.84	2450	90	0.0012	0.138	0.11
O(BM12)	0.18	0.36	C,Wrap	0.216	0.0012	230	49.68	2450	90	0.0093	0.276	0.873
O(BM18)	0.18	0.36	C,Wrap	0.324	0.0018	230	74.52	2450	90	0.0078	0.414	0.732
O(BM24)	0.18	0.36	C,Wrap	0.432	0.0024	230	99.36	2450	90	0.006	0.552	0.563
O(BL06)	0.18	0.36	C,Wrap	0.108	0.0006	230	24.84	2450	90	0.0084	0.138	0.789
O(BL12)	0.18	0.36	C,Wrap	0.216	0.0012	230	49.68	2450	90	0.0078	0.276	0.732
O(BMW06)	0.18	0.36	C,Wrap	0.288	0.0016	230	66.24	2450	90	0.0084	0.368	0.789
O(BMW12)	0.18	0.36	C,Wrap	0.216	0.0012	230	49.68	2450	90	0.0069	0.276	0.648
O(BMW24)	0.18	0.36	C,Wrap	0.432	0.0024	230	99.36	2450	90	0.0046	0.552	0.432
O(2)	0.4	0.34	C,Wrap	0.0522	0.00029	230	12.006	2450	90	0.012	0.0667	1.127
O(3)	0.4	0.34	C,Wrap	0.1044	0.00058	230	24.012	2450	90	0.0103	0.1334	0.967
C(A)	0.064	0.153	A,s&b	1.04	0.033	11	11.44	185	90	0.0049	0.363	0.291
C(E)	0.064	0.153	A,s&b	0.4572	0.021	14.3	6.538	185	90	0.0063	0.3003	0.487
C(G)	0.064	0.153	A,s&b	0.58	0.018	21	12.18	185	90	0.0052	0.378	0.59
C(45G)	0.064	0.153	A,s&b	0.58	0.018	21	12.18	185	45	0.0051	0.378	0.579
F(S-2)	0.6	0.51	C,Wrap	0.167	0.00056	240	40.08	3834	90	0.0065	0.1344	0.407
F(S-3)	0.6	0.51	C,Wrap	0.334	0.0011	240	80.16	3834	90	0.0047	0.264	0.294
F(S-4)	0.6	0.51	C,Wrap	0.501	0.00167	240	120.24	3834	90	0.0044	0.4008	0.275
U(CS1)	0.6	0.257	C,Wrap	0.11	0.00074	244	26.84	4280	90	0.0069	0.1806	0.393
U(CS2)	0.3	0.257	C,Wrap	0.11	0.00037	244	26.84	4280	90	0.0051	0.0903	0.291
U(CS3)	0.3	0.272	C,Wrap	0.11	0.00047	244	26.84	4280	90	0.012	0.1147	0.684
A(CF045)	0.2	0.34	C,Wrap	0.11	0.00026	230	25.3	3480	90	0.0096	0.0594	0.632
A(CF064)	0.2	0.34	C,Wrap	0.11	0.00045	230	25.3	3480	90	0.009	0.1035	0.595
A(CF097)	0.2	0.34	C,Wrap	0.11	0.00077	230	25.3	3480	90	0.0089	0.1771	0.591
A(CF131)	0.2	0.34	C,Wrap	0.11	0.0011	230	25.3	3480	90	0.0083	0.253	0.546
A(AF060)	0.2	0.34	A,Wrap	0.144	0.00059	87	12.528	2450	90	0.0029	0.0513	0.102
A(AF090)	0.2	0.34	A,Wrap	0.144	0.001	87	12.528	2450	90	0.0103	0.087	0.367

Note 1: C=CFRP; A=AFRP; s&b=CFRP sheet bonded to beam sides and bottom only.

Note 2: The letters for the beam name = Reference; The letters in the parenthesis after the beam name = Beam designation

A = Araki (1997); C = Chajes et al. (1995); F = Funakawa et al. (1997); O = Ohuchi et al. (1994); U = Umezu et al. (1997).

Table 3.2 Test Results Based on CFRP Debonding

Beam	f_c'(MPa)	bw(m)	d(m)	CFRP type	ρ_{CFRP}	E_{frp} (GPa)	f_{fu} (MPa)	Beta (deg)	Strain(ε_{fe})	$E_f\rho_{CFRP}$	$\frac{E_f * \rho_{frp}}{f_c'}$	R
*B(3)	20	0.114	0.085	G, Sides(s)	0.011	16.8		45	0.0066	0.1848	9.24	
*B(4)	20	0.114	0.085	G,s	0.027	16.8		45	0.0056	0.4536	22.68	
U(5)	24	0.1	0.17	C,s	0.00194	230	2650	90	0.003	0.4462	18.59	0.2604
U(6)	27	0.1	0.17	C,s	0.00194	230	2650	56	0.0034	0.4462	16.53	0.2951
U(7)	27	0.1	0.17	C,s	0.0039	230	2650	90	0.0015	0.897	33.22	0.1302
*A(WO)	20	0.15	0.113	G,s	0.04	16		90	0.0008	0.64	32	
*A(SO)	20	0.15	0.113	G,s	0.016	16		90	0.0018	0.256	12.8	
S(S2)	45.2	0.2	0.26	C,s	0.00055	230	3480	90	0.011	0.1265	2.799	0.727
S(S3)	41.3	0.2	0.26	C,s&b	0.00055	230	3480	90	0.015	0.1265	3.063	0.9914
S(S4)	37.5	0.2	0.26	C,s	0.0011	230	3480	90	0.0055	0.253	6.747	0.3635
S(S5)	39.7	0.2	0.26	C,s&b	0.0011	230	3480	90	0.0089	0.253	6.373	0.5882
T(S1a)	30	0.07	0.1	C,s	0.0022	235	3300	90	0.0041	0.517	17.23	0.292
T(S1b)	30	0.07	0.1	C,s	0.0022	235	3300	90	0.0034	0.517	17.23	0.2421
T(S2a)	30	0.07	0.1	C,s	0.0023	235	3300	90	0.0032	0.5405	18.02	0.2279
T(S2b)	30	0.07	0.1	C,s	0.0033	235	3300	90	0.0026	0.7755	25.85	0.1852
T(S3a)	30	0.07	0.1	C,s	0.0044	235	3300	90	0.002	1.034	34.47	0.1424
T(S3b)	30	0.07	0.1	C,s	0.0044	235	3300	90	0.0016	1.034	34.47	0.1139
T(S1-45)	30	0.07	0.1	C,s	0.0022	235	3300	45	0.003	0.517	17.23	0.2136
T(S2-45)	30	0.07	0.1	C,s	0.0033	235	3300	45	0.0022	0.7755	25.85	0.1567
T(S3-45)	30	0.07	0.1	C,s	0.0044	235	3300	45	0.0013	1.034	34.47	0.0926
Z(Z4-90)	42.4	0.1524	0.2286	C,s	0.00496	238	2625	45	0.0015	1.1805	27.86	0.1379
Z(Z4-45)	42.4	0.1524	0.2286	C,s	0.00496	238	2625	90	0.002	1.1805	27.86	0.1834
CH(RS90-1)	35	0.15	0.25	C,s	0.00667	150	2400	90	0.002	1	28.57	0.1258
CH(RS90-2)	35	0.15	0.25	C,s	0.00667	150	2400	90	0.0025	1	28.57	0.1536
CH(RS135-1)	35	0.15	0.25	C,s	0.00444	150	2400	135	0.0025	0.6667	19.05	0.1591
CH(RS135-2)	35	0.15	0.25	C,s	0.00444	150	2400	135	0.0025	0.6667	19.05	0.1591
CZ(T2)	56	0.26	0.5	C,s,l	0.00123	238	2400	90	0.0035	0.2929	5.231	0.3504
K(BT2)	35	0.15	0.405	C,uw	0.0022	228	3790	90	0.0047	0.5016	14.33	0.2849
K(BT3)	35	0.15	0.405	C,uw	0.0022	228	3790	90	0.0049	0.5016	14.33	0.2959
K(BT4)	35	0.15	0.405	C,uw-strip	0.00088	228	3790	90	0.0131	0.2006	5.733	0.7891
K(BT5)	35	0.15	0.405	C,strip	0.00088	228	3790	90	0.0057	0.2006	5.733	0.3452
TA(S2)	65.2	0.18	0.5	C,side wrap	0.00667	101	1450	45	0.0042	0.6707	10.29	0.2908
TA(S3)	50.2	0.18	0.5	C,side wrap	0.02222	49	577	45	0.0026	1.0889	21.69	0.2179
TA(SR2)	52.7	0.18	0.5	C,side wrap	0.00889	70.8	860	45	0.0036	0.6293	11.94	0.2969

Note: C=CFRP; A=AFRP; s=CFRP sheets on both sides only; U=CFRP sheet in the form of a U jacket; G=GFRP

Note 2: The letters for the beam name = Reference; The letters in the parenthesis after the beam name = Beam designation

A = Araki (1997); B = Berset (1992); CH = Chaallal et al. (1998); CZ = Czaderski (1998); K = Khalifa et a. (1999); S = Sato et al. (1996); T = Triantafillou (1998); TA = Täljsten (1999); U = Umezu et al. (1997); Z = Present Study, Zhang.

Furthermore, by comparing Figure 3.2 and Figure 3.3, it can also be observed that the CFRP ruptures occurred when $0 < \rho_f E_f < 0.55Gpa$ and the CFRP debonds when $0 < \rho_f E_f < 1.2GPa$. So when the value of $\rho_f E_f$ is between 0 and 0.55GPa, both rupture and debonding can occur. However, when $\rho_f E_f$ is between 0.55 and 1.2GPa, only CFRP debonding exists. This behavior proves that as CFRP laminates become stiffer and thicker, the debonding dominates over the tensile fracture and thus the effective strain is reduced. When more test data become available, the actual number for the limits can be adjusted accordingly. It should be noted that the anchorage of the CFRP laminates was not taken into consideration when the data was analyzed.

There was a series of tests carried out at NJIT (Hsu, Bian and Jia, 1997) on the direct-shear behavior between CFRP laminates and the concrete. It has been found out that the maximum concrete compressive strength, $f_c^{'}$, plays a very important role on the direct-shear behavior using Sika's Carbodur System. As the concrete compressive strength becomes stronger, the bonding stress between the CFRP laminates and the concrete becomes higher at the same time. If the axial rigidity of the CFRP laminates is the same, higher compressive strength means higher bonding stress. If the failure is due to CFRP debonding, then higher effective tensile stress is expected. However, compressive strength is not a factor in Equation 3.11. In order to take concrete compressive strength into consideration, the data need to be modified. Instead of using axial rigidity $\rho_f E_f$, $\rho_f E_f / f_c^{'}$ is used as a dimensionless variable to plot the curve. Figure 3.4 is the modified chart. The r-squared value, which is called the multiple correlation coefficient, has a closer value to 1 than that of Figure 3.3. That means that

Equation 3.12 from curve fitting gives a better physical correlation to the experiments than Equation 3.11.

$$R = 1.8589 \cdot \left(\rho_f E_f / f_c'\right)^{-0.7488} \tag{3.12}$$

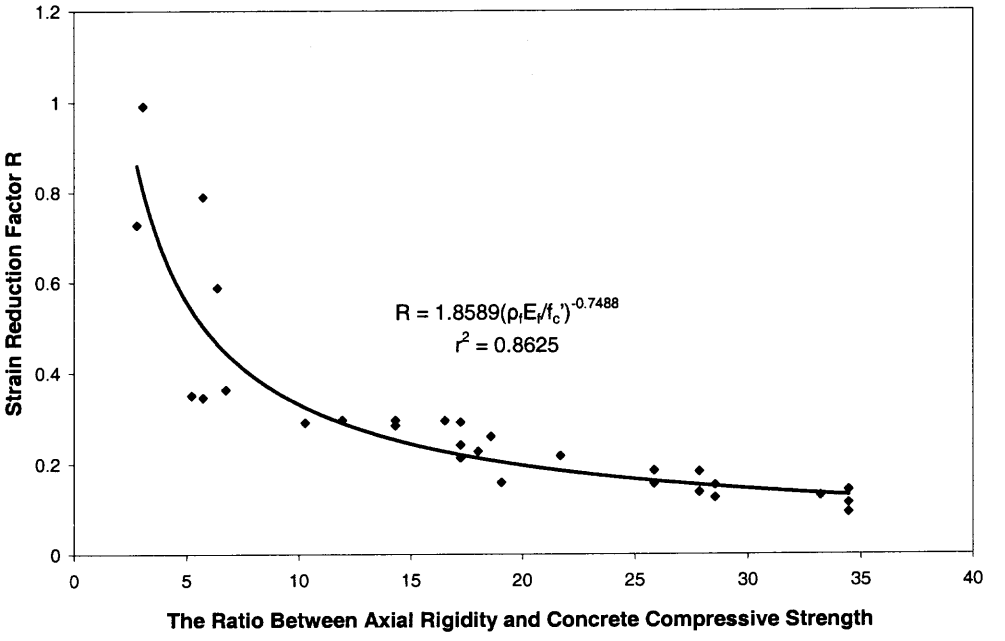

Figure 3.4 Strain reduction factor $R = \varepsilon_{fe} / \varepsilon_{fu}$ in terms of $\rho_f E_f / f_c'$, only based on test results of CFRP debonding.

Considering that Equation 3.12 proposed above is based on a regression line and the data points are not distributed right on it, a safety factor should be applied to the equation to account for the data points below the line. As can be seen in Figure 3.4, the curve for the modified equation is well below most of the data points. Equation 3.12 can then be transformed to Equation 3.13 after multiplying a safety factor 0.8.

$$R = 1.4871 \cdot \left(\rho_f E_f / f_c'\right)^{-0.7488} \tag{3.13}$$

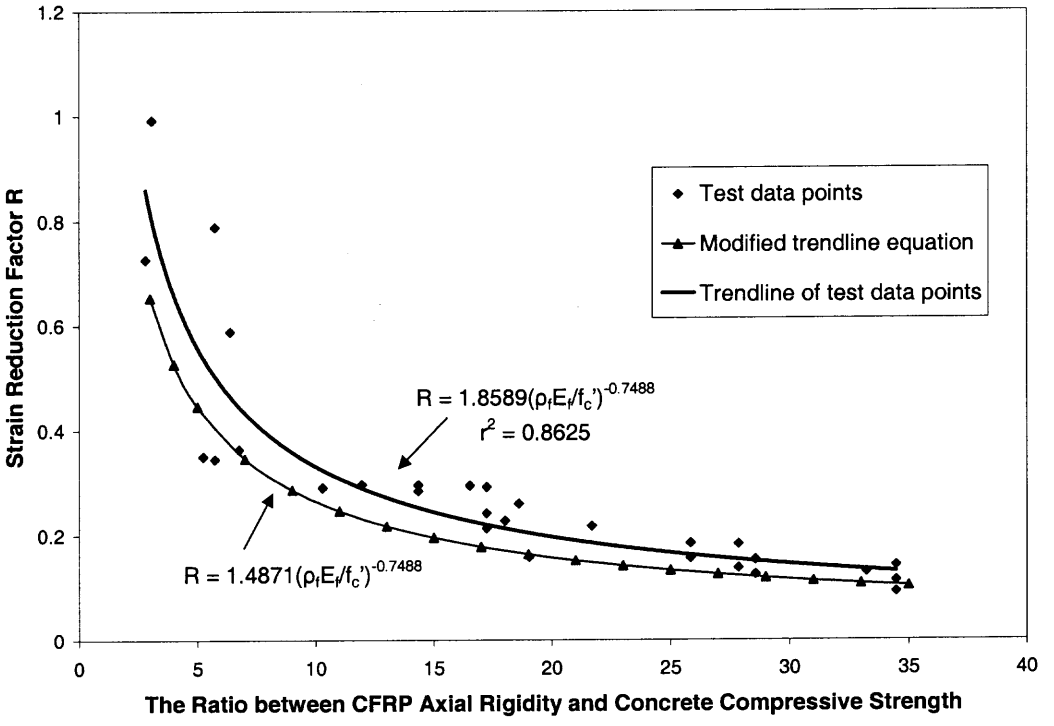

Figure 3.5 Comparison of the equations with and without the safety factor.

It is concluded that Equation 3.12, or the more conservative Equation 3.13 with a safety factor 0.8, can be used to calculate R for delamination of CFRP in RC beams. However, for CFRP rupture failure mode, no satisfactory equation for R can be obtained from calibration of the test results. Thus another method based on bond mechanism was introduced to calculate the reduction factor R, regardless the failure modes.

The value of reduction factor R, which will be used to Equations 3.5 and 3.6, should be the lower value from the results of both model calibration method (Equation 3.13) and bond mechanism method (Equation 3.32).

Furthermore, there are several other parameters, such as CFRP thickness, with or without anchorage and effective bond length, etc., will also affect the determination of this reduction factor besides the CFRP axial regidity and the concrete compressive

strength. The method based on bond mechanism, which is discussed in next section, will address these issues.

3.3 Design Approach Based on Bonding Mechanism

3.3.1 Effective Bonding Length

Maeda et al. (1997) studied the bond mechanism of carbon fiber sheet by tensioning of CFRP bonded to the surface of two concrete blocks. He observed that ultimate load increases as CFRP stiffness becomes stronger and is almost the same for different bonding lengths except for bond length of less than 100mm. The reason for this is that at early stage of loading, load is sustained in the vicinity of loading point. If delamination occurs in this vicinity due to fracture of concrete surface, the area of active bonding is shifted to a new area. This is repeated until the delamination propagates completely throughout the whole length of the CFRP. The length of CFRP that includes the active bonding area is called the effective bonding length.

He also concluded that the effective bonding length decreases as the stiffness of CFRP increases. That means the bonding stress increases as the stiffness of CFRP increases. However, a rather general agreement on the failure modes for debonding is that the bond strength of externally bonded plates depends mainly on the quality of the surface preparation and the quality of the concrete itself. The maximum shear stress of the concrete at debonding is mainly a function of concrete, rather than a function of the stiffness of the CFRP. The surface of bond strength of concrete is suggested to be $0.91\sqrt{f_c'}$, MPa ($11\sqrt{f_c'}$, psi) according to "Sika CarboDur® Engineering Guidelines for Design and Application". In the research for direct-shear using Sika's CarboDur System

in 1997, Hsu, Bian and Jia found out that the maximum concrete compressive strength, f_c', played a dominant role on the direct-shear behavior and they proposed an empirical direct-shear design equation based on that. It is shown as follows:

$$\tau = 5\times10^{-6}\times f_c'^2 - 2.73\times10^{-2}\times f_c' + 925.3 \qquad (3.14a)$$

where τ : direct shear strength (psi)

f_c': maximum concrete compressive strength (psi)

$$\tau = 7.64\times10^{-4}\times f_c'^2 - 2.73\times10^{-2}\times f_c' + 6.38 \qquad (3.14b)$$

where τ : direct shear strength (MPa)

f_c': maximum concrete compressive strength (MPa)

Based on analytical and experimental data from bond test, Miller (1999) showed that effective bond length increases as CFRP stiffness increases, which is exactly the opposite of the conclusion by Maeda et al.. He also suggested a conservative value for effective bond length equal to 75mm and it may be modified when more bond test data become available.

From the experiments by Bizindavyi et al. (1999) shown in Table 3.3, the measured transfer length of 0.33mm thick CFRP before the initial cracking load is about 50mm; the measured transfer length of 0.66mm thick CFRP before the initial cracking load is about 70mm. It also demonstrated that the effective bond length increases as CFRP stiffness increases. However, their experiments showed that as the initial transfer length develops, there is a point where the failure mode changed from debonding to rupture, which is different from what Maeda et al. (1997) has observed.

Table 3.3 CFRP-Concrete Bond Tests and Observed Modes of Failure (Bizindavyi et al., 1999)

Number of plies	Thickness (mm)	Bond length (mm)	Failure mode
1	0.33	50	C-S[a]
1	0.33	80	P-R[b]
1	0.33	135	P-R
1	0.33	145	P-R
1	0.33	160	P-R
2	0.66	100	C-S
2	0.66	120	C-S
2	0.66	160	C-S
2	0.66	220	C-S/P-R
2	0.66	240	P-R
2	0.66	260	P-R
2	0.66	320	P-R

[a]Concrete shearing beneath glue line
[b]CFRP laminates rupture after development of its full tensile capacity

Chajes, M. J. et al. (1996) also found out that, for concrete with strengths in the 24 MPa to 45 MPa (3500 psi to 6500 psi) range, the load transferred from the CFRP to the concrete increases with concrete strength and does not increase with bond lengths longer than approximately 100 mm (4 in.)

Based on the argument above, it can be seen that although there are quite a few researches done in the past, they do not agree with each other very well, sometimes even contradictory. However, most researchers agreed that there exists an effective bond length, beyond which little load increase can be achieved. The determination of the effective bond length involves with the stiffness of the CFRP, epoxy, and the concrete compressive strength. No practical equation is available so far. Generally speaking, 75 mm as effective bond length is a reasonable estimation for design purpose.

3.3.2 Requirement of Effective Bonding Surface

When shear failure occurs, diagonal shear cracks usually develop at a particular angle. Only the portion of CFRP extending past the shear cracks by the effective bond length will carry the shear force efficiently. If it is less than the effective length, premature debonding will occur and the shear strengthening capacity of the CFRP will be compromised. Therefore, for continuous CFRP fabric sheet, the width, w_f, is suggested to be replaced by effective width, w_{fe}; for CFRP strip, the effective width will not be changed, but the maximum spacing between strips needs to be adjusted so that there is at least one strip past the crack by the effective bonded length. The shear crack angle is assumed to be $45°$. The bonding surface configurations are shown in the following figures.

1. For CFRP continuous fiber sheet:

   1) CFRP continuous fiber sheet in the form of U-jacket (Figure 3.6):

      Equilibrium can be found as:

$$L_e \cdot \sin\alpha = \left(\frac{d - t_s}{\sin 45°} - \frac{w_{fe} \cdot \sin\alpha}{\sin 45° \cdot \cos\alpha + \cos 45° \cdot \sin\alpha} \right) \cdot \sin 45° \tag{3.15}$$

      Rearrange the above equation, the effective width of the CFRP is:

$$w_{fe} = (d - t_s - L_e \cdot \sin\alpha) \cdot (1 + \cot\alpha) \tag{3.16}$$

   2) CFRP continuous fiber sheet bonded on two sides of the beam only (Figure 3.7):

$$L_e \cdot \sin\alpha = 0.5 \cdot \left(\frac{d - t_s}{\sin 45°} - \frac{w_{fe} \cdot \sin\alpha}{\sin 45° \cdot \cos\alpha + \cos 45° \cdot \sin\alpha} \right) \cdot \sin 45° \tag{3.17}$$

      The effective width of the CFRP is:

$$w_{fe} = (d - t_s - 2L_e \cdot \sin\alpha) \cdot (1 + \cot\alpha) \tag{3.18}$$

3) CFRP continuous fiber sheet in the form of U-jacket with anchorage (Figure 3.8):

$$(d - t_s) \cdot (\cot 45^\circ + \cot \alpha) = w_{fe} \tag{3.19}$$

The effective width of the CFRP is:

$$w_{fe} = (d - t_s)\ (1 + \cot \alpha) \tag{3.20}$$

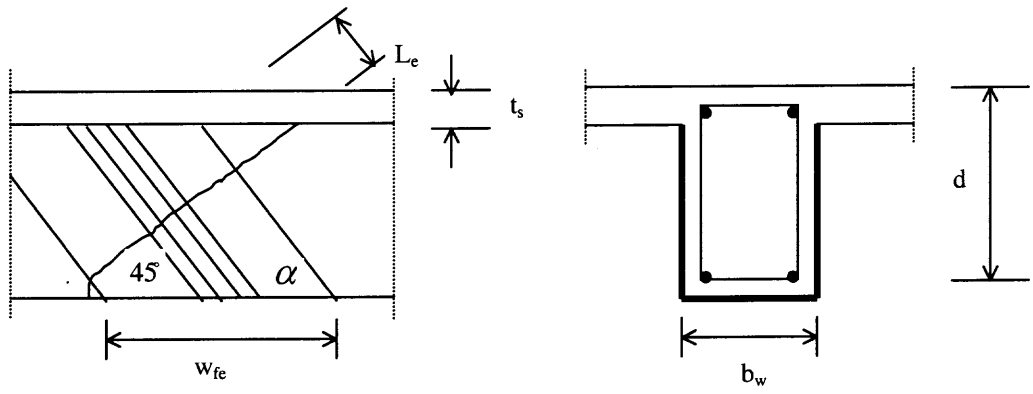

Figure 3.6 CFRP continuous fabric sheet in the form of U-jacket.

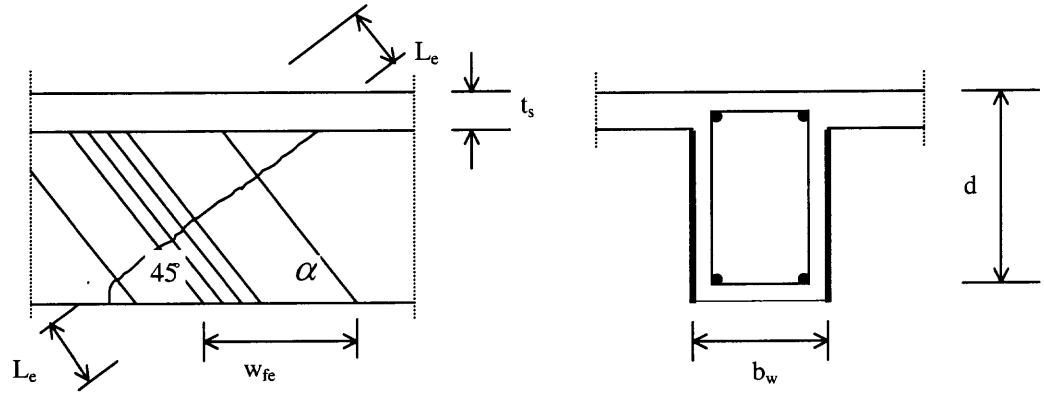

Figure 3.7 CFRP continuous fabric sheet bonded on two sides only.

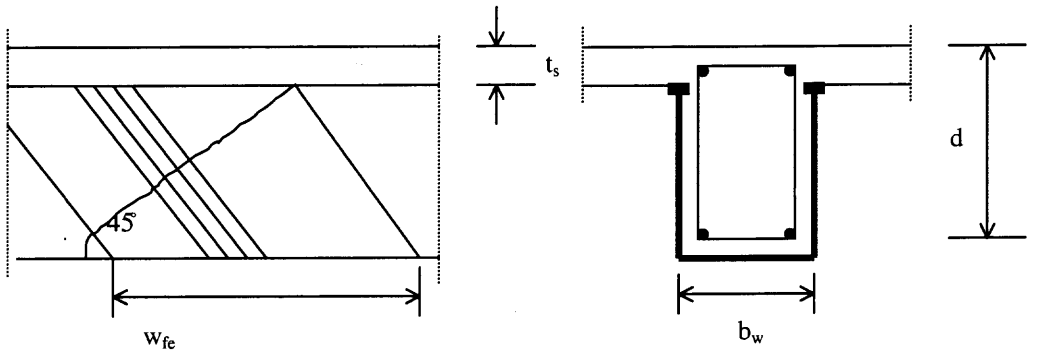

Figure 3.8 CFRP continuous fabric sheet in the form of U-jacket with anchorage.

1. For CFRP strips:

   1) U-jacket (Figure 3.9):

   Equilibrium can be found as:

$$L_e \cdot \sin\alpha = \left(\frac{d - t_s}{\sin 45^\circ} - \frac{s_{\max} \cdot \sin\alpha}{\sin 45^\circ \cdot \cos\alpha + \cos 45^\circ \cdot \sin\alpha} \right) \cdot \sin 45^\circ \tag{3.21}$$

   Maximum spacing $s_{\max} = (d - t_s - L_e \cdot \sin\alpha) \cdot (1 + \cot\alpha)$ (3.22)

   2) CFRP strips on two sides of the beam without anchorage (Figure 3.10):

$$L_e \cdot \sin\alpha = 0.5 \cdot \left(\frac{d - t_s}{\sin 45^\circ} - \frac{s_{\max} \cdot \sin\alpha}{\sin 45^\circ \cdot \cos\alpha + \cos 45^\circ \cdot \sin\alpha} \right) \cdot \sin 45^\circ \tag{3.23}$$

   Maximum spacing $s_{\max} = (d - t_s - 2 \cdot L_e \cdot \sin\alpha) \cdot (1 + \cot\alpha)$ (3.24)

   3) U-jacket with anchorage (Figure 3.11):

   Maximum spacing $s_{\max} = (d - t_s) \cdot (1 + \cot\alpha)$ (3.25)

   Effective width of CFRP for all three cases above is

$$w_{fe} = \frac{s_{\max}}{s} \cdot w_{fs} \tag{3.26}$$

The above configurations are based upon T-shaped cross section. For rectangular cross section, everything remains the same except t_s disappears from above equations.

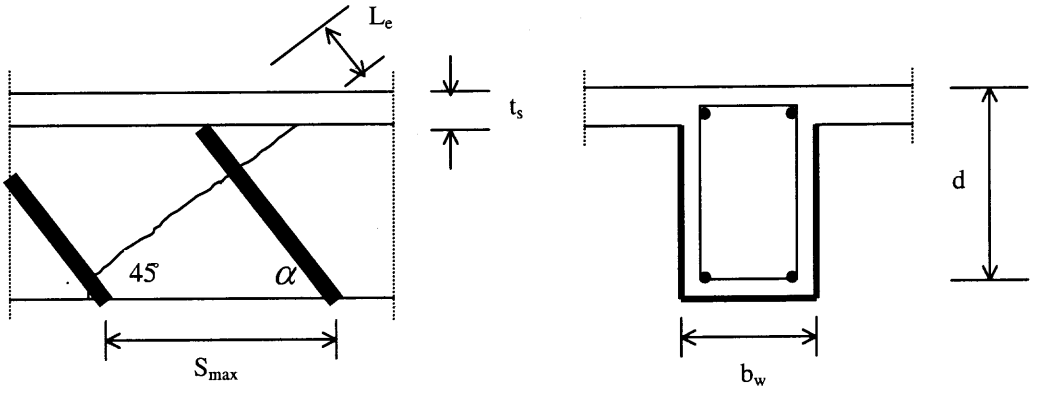

Figure 3.9 CFRP strip in the form of U-jacket.

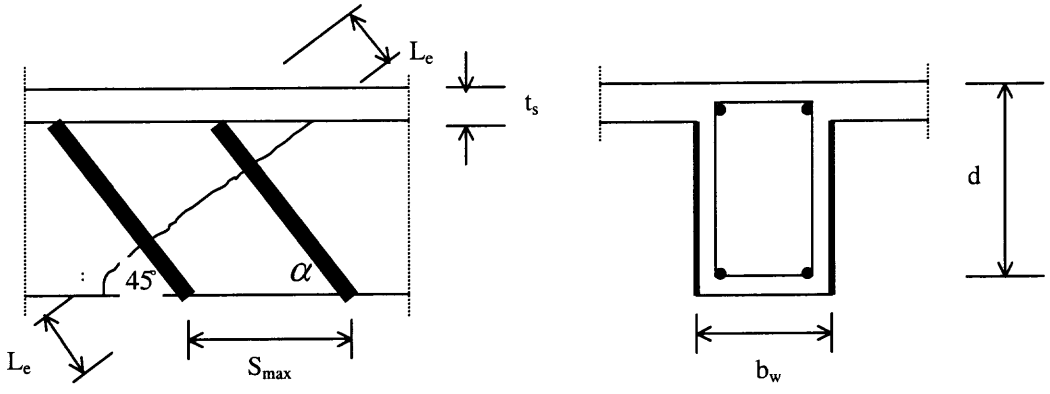

Figure 3.10 CFRP strip bonded on two sides of the beam.

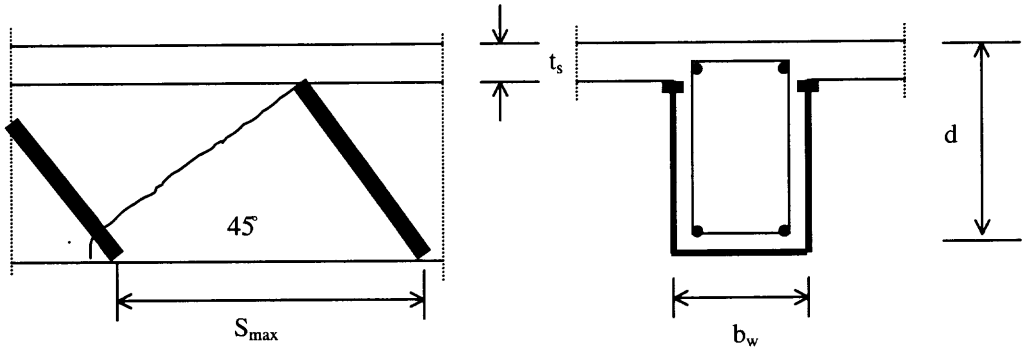

Figure 3.11 CFRP strip in the form of U-jacket with anchorage.

3.3.3 Design Equation

The direct shear design Equation 3.14a or Equation 3.14b presented earlier describes a relationship between shear stress and the compressive strength of the concrete. However, the stress given by this equation is the maximum direct shear stress in concrete at failure. In shear design of externally bonded CFRP, the beam is considered losing the shear capacity at the instant when the debonding occurs in the vicinity of the crack even through the debonding has not yet developed through the whole length. The shear stress distribution along the CFRP laminates is very complicated, as indicated earlier. However, for design purpose the stress distribution can be simplified as a triangle shape along the effective length, which is illustrated as below.

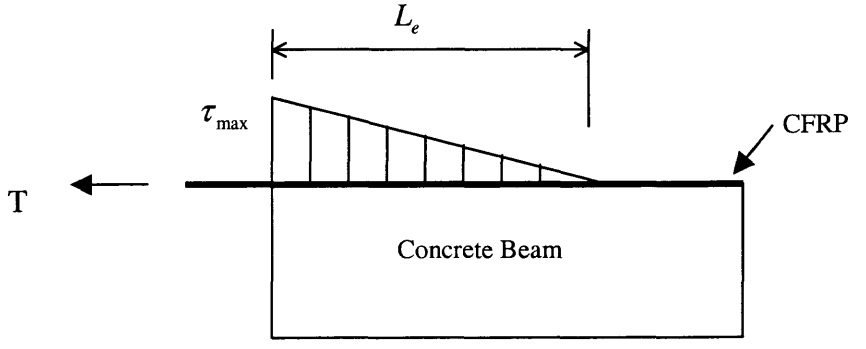

Figure 3.12 Concrete shear stress distribution beneath the epoxy.

The total force that can be developed on two sides of the beam is given

$$T = \frac{1}{2} \cdot \tau_{max} \cdot L_e \cdot (2w_{fe}) \tag{3.27}$$

Which can be simplified as

$$T = \tau_{max} \cdot L_e \cdot w_{fe} \tag{3.28}$$

Thus, a relationship between the force in CFRP and the shear force in the concrete at the instant of shear failure can be described as follows:

$$T = 2 \cdot w_{fe} \cdot t_f \cdot f_{fe} \tag{3.29}$$

With Equation 3.28, we obtain:

$$\tau_{\max} \cdot L_e \cdot w_{fe} = 2 \cdot w_{fe} \cdot t_f \cdot f_{fe} \tag{3.30}$$

Rearrange and introduce f_{fu} into the equation, we get:

$$\frac{\tau_{\max} \cdot L_e}{2 \cdot t_f \cdot f_{fu}} = \frac{f_{fe}}{f_{fu}} \tag{3.31}$$

Thus, the stress reduction factor R can be expressed as:

$$R = \frac{\tau_{\max} \cdot L_e}{2 \cdot f_{fu} \cdot t_f} \tag{3.32}$$

It should be noted that $\tau_{\max}$ is from Equation 3.14a or Equation 3.14b, L_e is 75mm(rough estimate, further research is needed), f_{fu} is the ultimate tensile stress of CFRP material and t_f is the thickness of the CFRP material.

3.4 Summary of the Proposed Design Approach

The shear design for externally bonded CFRP reinforcement is based on traditional truss analogy. In order to quantify the contribution of CFRP to the shear reinforcement, a reduction factor R is introduced to account for the effective stress and strain of CFRP at shear failure. There are several parameters that will affect the determination of this reduction factor, such as stiffness of the CFRP, compressive strength of concrete, CFRP orientation, CFRP thickness, with or without anchorage, effective bonding length, etc. It is very difficult to introduce all of the parameters in a single equation. Thus one equation

based on model calibration of available experiments and another equation based on bond mechanism between CFRP and concrete are established in this research.

In the method of model calibration, Equation 3.13 is based on curve fitting of current available experiments. Equation 3.13 mostly emphasizes an overall CFRP shear strengthening scheme with less parameters, which gives a simple design approach. CFRP stiffness and concrete compressive strength are considered as two main dominant parameters. However, there are so many uncertain variables in each experiment that can not be properly justified, and as more test data become available in the future, current equation needs to be adjusted to accommodate these changes. Equation 3.32, on the other hand, is based on the bonding mechanism, thus several important parameters such as effective bonding length are properly addressed. Since it has been found out previously that when $\rho_f E_f < 0.55GPa$, CFRP laminates tends to fail in rupture and no equation from model calibration gives reasonable explanation. This can also be compensated by using Equation 3.32.

Equation 3.13 and Equation 3.32 should be used together and the lower value of R from these two equations will be applied to Equations 3.5 and 3.6. It should also be noted that the maximum reduction factor is suggested to be 0.6 for Sika CarboDur and 0.45 for Sika Wrap, according to "Sika CarboDur® Engineering Guidelines for Design and Application". Since a variety of CFRP materials were used in the past, the maximum reduction factor is suggested to be 0.4 in this research.

The shear contribution of CFRP laminates may be calculated by the following equations:

For CFRP continuous fiber sheet:

$$V_f = w_{fe} \cdot t_f \cdot f_{fe} \cdot \sin^2 \alpha \leq \left(\frac{2\sqrt{f_c'} b_w d}{3} - V_s \right) \text{ (Metric)} \quad (3.33a)$$

$$V_f = w_{fe} \cdot t_f \cdot f_{fe} \cdot \sin^2 \alpha \leq \left(8\sqrt{f_c'} b_w d - V_s \right) \text{ (English)} \quad (3.33b)$$

For CFRP strips:

$$V_f = \frac{A_f f_{fe} (\sin \alpha + \cos \alpha) d_f}{s_f} \leq \left(\frac{2\sqrt{f_c'} b_w d}{3} - V_s \right) \quad \text{(Metric)} \quad (3.34a)$$

$$V_f = \frac{A_f f_{fe} (\sin \alpha + \cos \alpha) d_f}{s_f} \leq \left(8\sqrt{f_c'} b_w d - V_s \right) \quad \text{(English)} \quad (3.34b)$$

3.5 Validity of the Proposed Design Approach

The comparisons between the test results (from NJIT) and calculated shear strength using the proposed design approach are listed in Table 3.4.

Table 3.4 Comparison Between Test Results and Calculated Values

Beam Designation	Experimental Results		Design Approach			Failure Mode
	V_n (kN)	V_f (kN)	V_f (kN)	V_c (kN)	$\phi V_n=0.85V_c+0.7V_f$ (kN)	
ZC4 (control)	46.1 (10.4 kips)	-	-	34.1 (7.7 kips)	29.0 (6.5 kips)	Shear Diagonal Crack
Z4-90	73.7 (16.6 kips)	27.6 (6.2 kips)	21.8 (4.9 kips)	34.1 (7.7 kips)	44.3 (10.0 kips)	Strip delamination
Z4-45	82.8 (18.6 kips)	36.7 (8.2 kips)	30.7 (6.9 kips)	34.1 (7.7 kips)	50.5 (11.3 kips)	Strip delamination
Z4-Fab	53.6 (12.1 kips)	7.5 (1.7 kips)	0	34.1 (7.7 kips)	29.0 (6.5 kips)	Fiber Rupture
Z4-Mid	61.2 (13.8 kips)	15.1 (3.4 kips)	0	34.1 (7.7 kips)	29.0 (6.5 kips)	Strip delamination
ZC6(2) (control)	42.9 (9.7 kips)	-	-	34.1 (7.7 kips)	29.0 (6.5 kips)	Shear Diagonal Crack
Z6-90	63.9 (14.4 kips)	21.0 (4.7 kips)	21.8 (4.9 kips)	34.1 (7.7 kips)	44.3 (10.0 kips)	Strip delamination
Z6-Fab	51.2 (11.5 kips)	8.3 (1.8 kips)	0	34.1 (7.7 kips)	29.0 (6.5 kips)	Fiber Rupture
Z6-Mid	60.5 (13.6 kips)	17.6 (3.9 kips)	0	34.1 (7.7 kips)	29.0 (6.5 kips)	Strip delamination

Beam ZC6 and beam Z4-45 are excluded from Table 3.4 because both of them fail in bending rather in shear.

The beam with CFRP strips and the beam with CFRP fabrics have completely different failure mechanisms. The failure of the strips is resulted from the concrete delamination underneath the epoxy; while the failure of the fabrics is due to the fiber rupture. Consequently the CFRP strips increase more shear capacity than those of the CFRP fabrics.

From Table 3.4, it can also be observed that the calculated values of beam Z4-90, beam Z6-90 and beam Z4-45 conform with the test results very well. In beam Z4-Fab and beam Z6-Fab, the CFRP fiber orientations are horizontal with respect to the longitudinal axis of the beam, thus the calculated values are assumed to be zero. Also, since the effect of longitudinal shear reinforcement is not considered in the design equation, the calculated values of beam Z4-Mid and beam Z6-Mid are also assumed to be zero, while the experimental values are not. This also demonstrates the importance of the longitudinal shear reinforcement in RC beams with shorter shear spans. The in-depth research of this effect will be covered in the following chapters.

In summary, the calculated values of V_f in Table 3.4 show that the design equation at present study can be used only to predict the shear contribution of simply supported RC beams having 90° and 45° CFRP shear reinforcement. It is not applicable to RC beams having longitudinal CFRP shear reinforcement. Meanwhile, the strength reduction factor ϕ in Table 3.4 in conjunction with load factors as suggested by ACI Building Code 318-99 will usually provide the safety factors for design purposes.

CHAPTER 4

EXPERIMENTAL PROGRAM ON SHEAR STRENGTHENING OF DEEP BEAMS USING CARBON FIBER REINFORCED POLYMER LAMINATES

4.1 Design of Deep Beam Specimen

Similar to the design of regular beams in Chapter 2, the deep beam was designed as an under reinforced section in accordance with ACI code (ACI Building Code 318-99). Web reinforcement, including longitudinal and vertical reinforcements, was omitted from the design. In an actual design practice, however, the web reinforcement is a must inside the deep beam. It was decided to choose the span and cross-section of the deep beam for this study to be 3', 4" and 9", respectively.

The design of the deep beam consists of two parts: flexural reinforcement design and shear reinforcement design.

According to ACI Building Code 318-99, deep beam action must be considered when designing for flexure if the clear span to effective depth ratio l_n/d is less than 1.25 for simple spans. Excluding the 3" distance from the support to the edge of the beam, the clear span to effective depth ratio of the deep specimen l_n/d is 3.75, which is more than 1.25. Thus, deep beam action is not considered for flexural design and the assumption of Whitney's rectangular stress distribution can be used to determine the flexural strength. The flexural design calls for the use of four individual #4 re-bars as reinforcement, which represents a steel reinforcement ratio of 0.022. This value is within the ACI 75% of the steel reinforcement at the balanced condition, which is equal to 0.0283.

According to ACI, deep beam action must be considered when designing for shear if the clear span to depth ratio l_n/d is less than 5.0 for simple spans. With l_n/d

equal to 3.75, the beam specimens in this research obviously fit into this category. Special design procedures are required by ACI when designing a deep beam for shear. For a concentrated load, the critical distance for shear design is located at a distance 0.5 times the span length from the support. The use of a special multiplier is required when determining the shear capacity of the concrete. This is due to the fact that a tied-arch effect occurs as the beam is loaded, which gets the concrete shear capacity increased even after the shear cracks have formed. The ACI detailed method is used with the multiplier to calculate the shear capacity of the plain concrete in this experiment. As stated earlier, there are no shear reinforcement in the beam, however, two #2 stirrups at each support and one #2 stirrup under each loading point are placed in the beam to prevent local failure.

A deep beam is a special case where the loading condition creates a multi-axial state of stress in the beam. The shear stresses and strains generated within a deep beam are non-linear and have components in both the longitudinal and transverse directions. This state of multi-axial stress within deep beam places a large amount of stress on the anchorage zone and the main tension reinforcement. The development length for the tension reinforcement terminating in a standard hook was determined by using ACI 7.1 and 7.2. A value of 11 inches was determined for the development length of the deep beam specimens.

4.2 Fabrication of Re-bar Cage and Forms

Due to the small size of the specimen, the steel bars had to be bent to exact tolerances. An oxygen acetylene torch was used to heat the steel so that they could be bent into the exact shape as required.

After the individual components of the steel re-bars had been fabricated, they were combined together to form the cage. Two #2 re-bars were used as temperature control bars at the top of the beam and also served as location points to attach the stirrups under the load. Standard tie wire was used to secure the stirrups and flexural reinforcement together.

In order to maintain the half-inch of clear cover around the re-bar cage, a spot weld was used at the top of the stirrup to keep the re-bar cage from expanding.

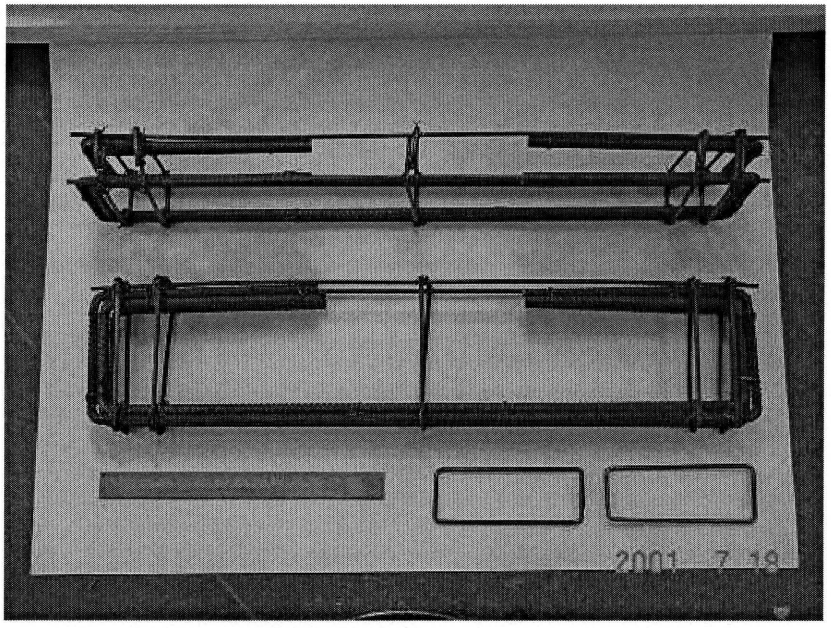

Figure 4.1 Re-bar cage.

The forms were constructed from grade A/A three-quarter inch pressure treated plywood to insure that the beams had a smooth surface on which to bond the CFRP

laminates. The surfaces of the forms were painted with several coats of paints to protect the wood from the concrete. The forms were designed so that four beams could be cast simultaneously to insure the consistency of the concrete quality.

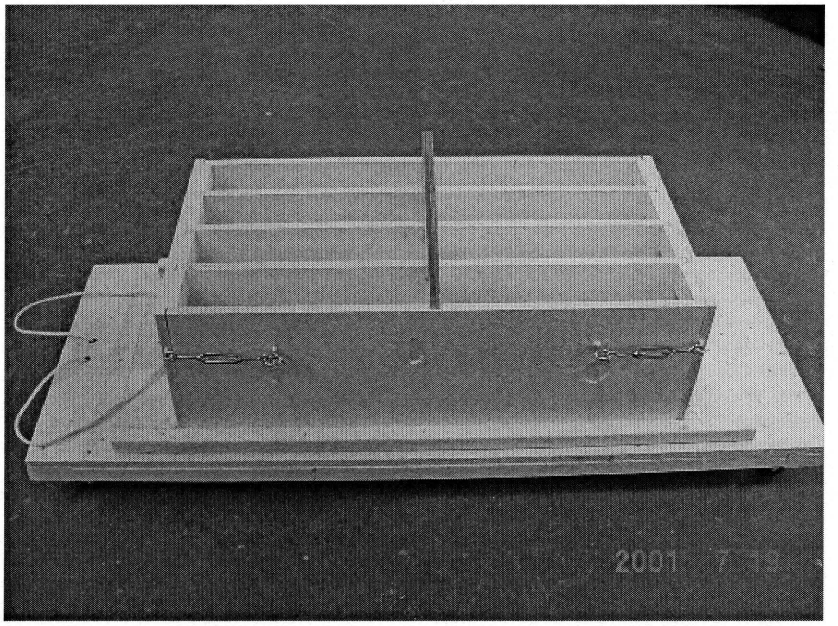

Figure 4.2 Wooden formwork.

4.3 Casting of Concrete Beams

The concrete mix was designed in accordance with ACI 211 "Standard Practice for Selecting Proportions for Normal, Heavyweight, and Mass Concrete". The target strength for the mix design was 5000 psi, with a water cement ratio 0.41 and a predicted slump and air content of three inches and 2%, respectively. Four deep beams were cast at one time using one batch of concrete mix. Four batches of concrete mix were used for 16 beams in total. Five concrete cylinders were cast using the same batch of concrete mix at the same time the beams were cast.

After the beams and the cylinders were cast, they were immediately transferred to the 100% humidity curing room and were kept there for two days. The forms then were removed and the beams as well as the cylinders stayed in the curing room for additional 26 days. The cylinders and the beams from the same batch of concrete mix were tested at the same time during experimental investigation.

Table 4.1 Test Results of Concrete Cylinders Compression

Concrete Batch	Ultimate Cylinder Compressive Strength f_c' (psi)					
	#1	#2	#3	#4	#5	Ave.
1	6526	6367	5570	5809	6446	6143.6
2	6446	6048	5660	6685	N.G.	6209.8
4	6605	5570	5332	6844	6286	6127.4
5	6207	5332	5729	6684	6844	6159.2

4.4 CFRP Strengthening Scheme

The shear span to depth ratio a/d has always been a major factor in deep beam shear behavior. Different shear span to depth ratio a/d can greatly affect the ultimate shear capacity. In a situation where CFRP laminates are applied to the deep beam surface for shear strengthening, the a/d ratio is assumed to have similar influence on shear behavior as those without CFRP shear reinforcement. For beams of the same dimensions, different a/d ratio conditions can be easily achieved by changing the shear span a. In this experiment, the changes of shear span by using different loading conditions. The shear span a is equal to 15" at 1-point loading condition and 10" at 2-point loading conditions with 10" distance between two loading points.

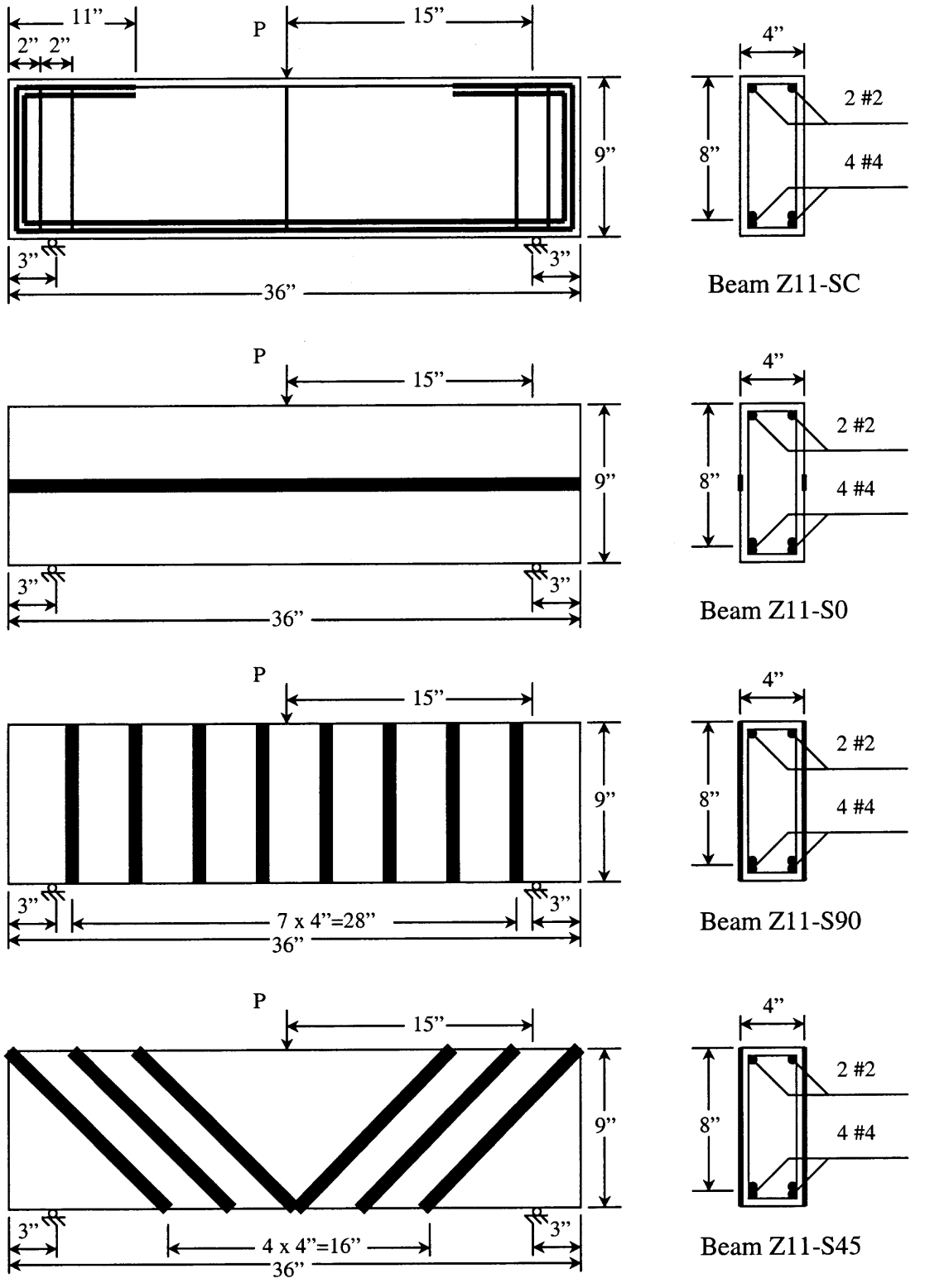

Figure 4.3 Configuration of CFRP strips under 1-point loading.

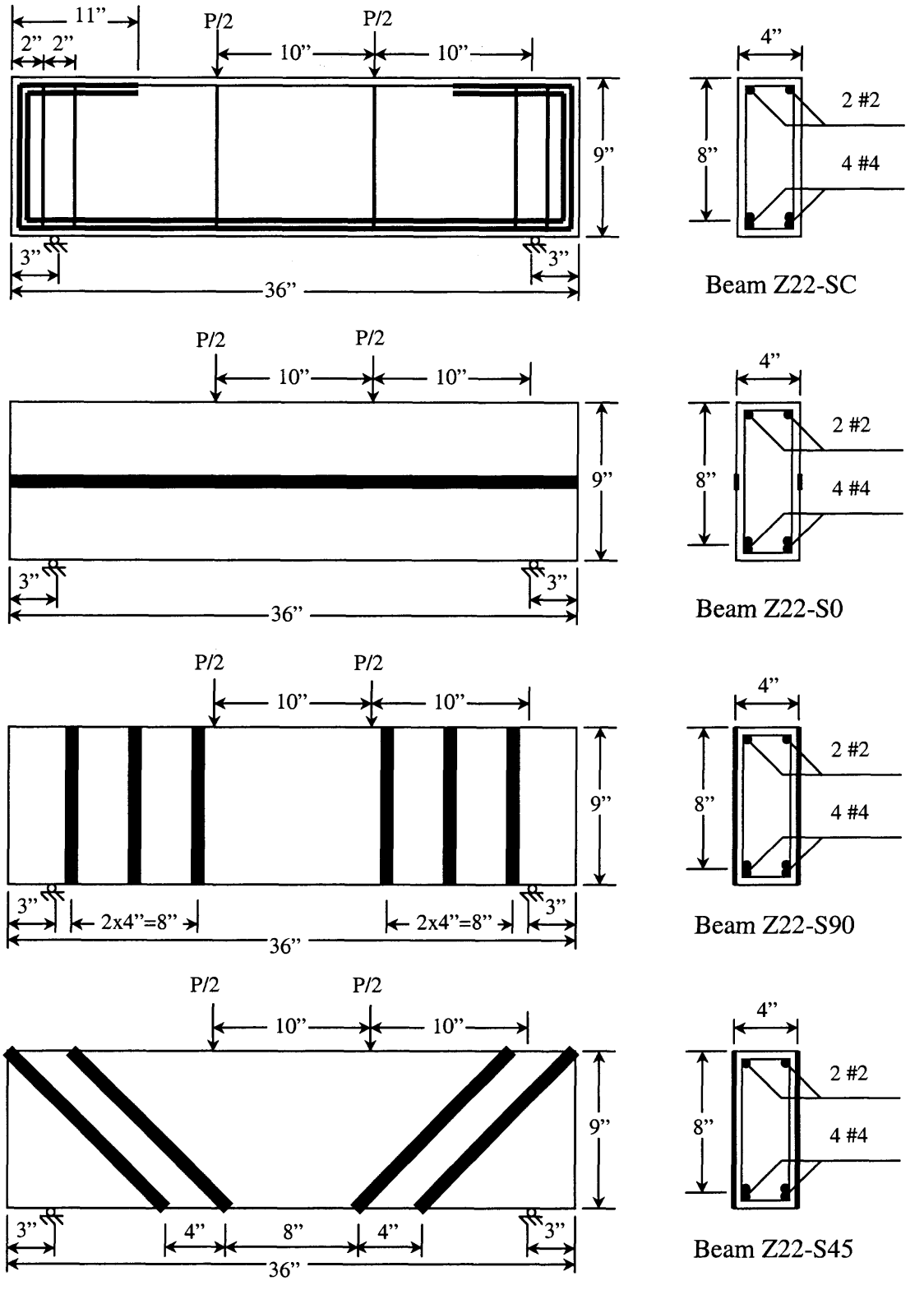

Figure 4.4 Configuration of CFRP strips under 2-point loading.

16 beams were tested in this research. They were divided into four groups. There were four beams in each group. One of them was a control beam, the rest of the beams in each group were strengthened by various types of CFRP shear reinforcement. Group 1 consisted of beams with CFRP strip shear reinforcement (Sika CarboDur Strip) of various orientations under 1-point loading condition; Group 2 had the same CFRP configurations as groups 1 but under 2-point loading condition; Group 3 contained beams with CFRP Fabrics shear reinforcement (SikaWrap Hex 230c) of various configuration under 1-point loading condition; Group 4 had the same CFRP configuration as group 3 but under 2-point loading condition.

The comprehensive experimental setups are illustrated in Figure 4.3 through Figure 4.6. The beams were named by the following rules:

1. All beam names start with capital letter "Z";
2. The number after the first letter indicates the group number;
3. The second number indicates the loading condition — "1" for 1-point loading condition, "2" for 2-point loading condition;
4. The first letter after the dash line indicates the type of CFRP — "S" for CFRP strip, "F" for CFRP fabrics;
5. The second letter after the dash line indicates the character of each individual beam — "C" for control beam, "0, 45, 90" for the angles between the CFRP orientation and longitudinal axis of the beam; "U" for U-shaped CFRP wrap; "D" for double-layered CFRP wrap.

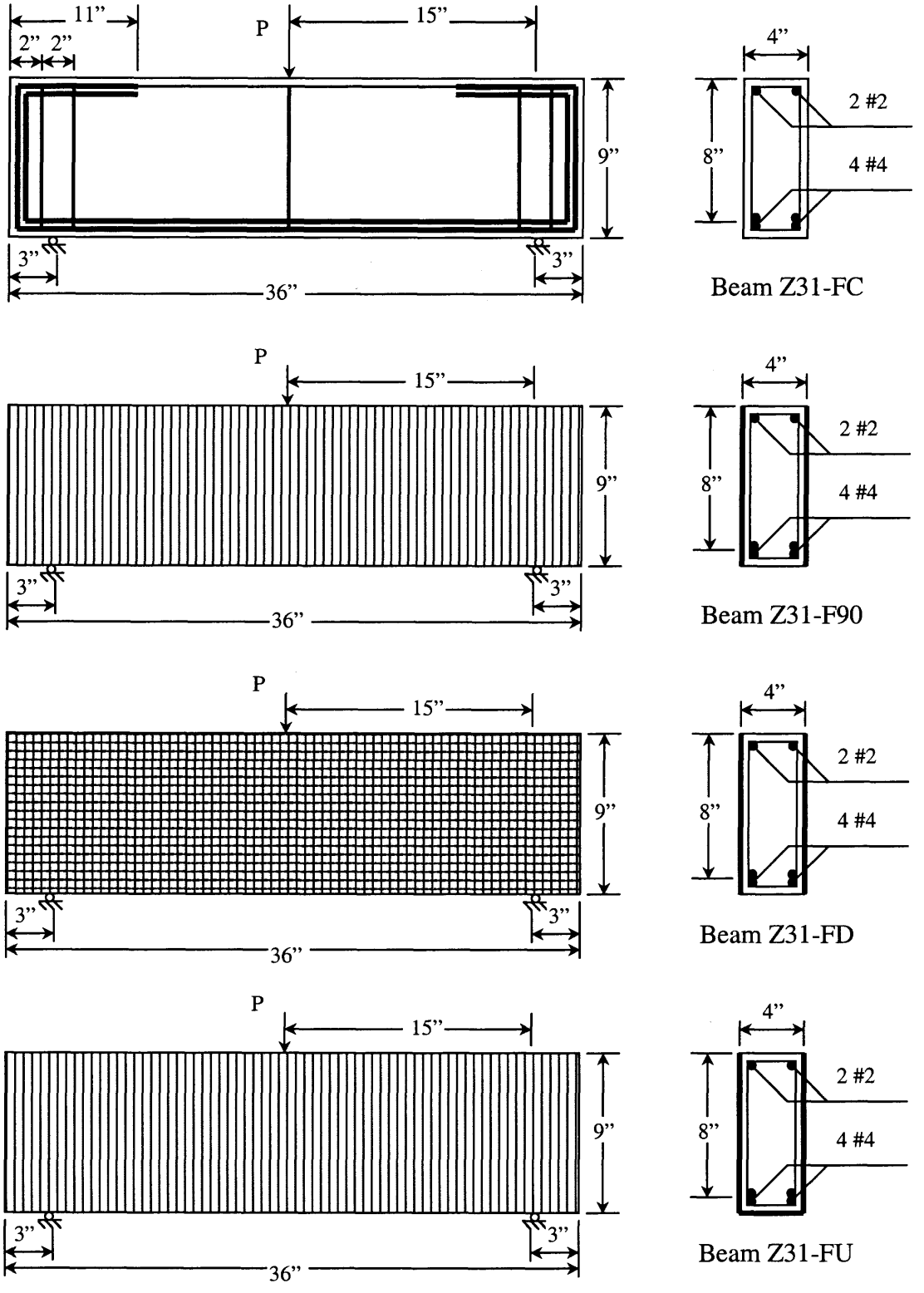

Figure 4.5 Configuration of CFRP fabrics under 1-point loading.

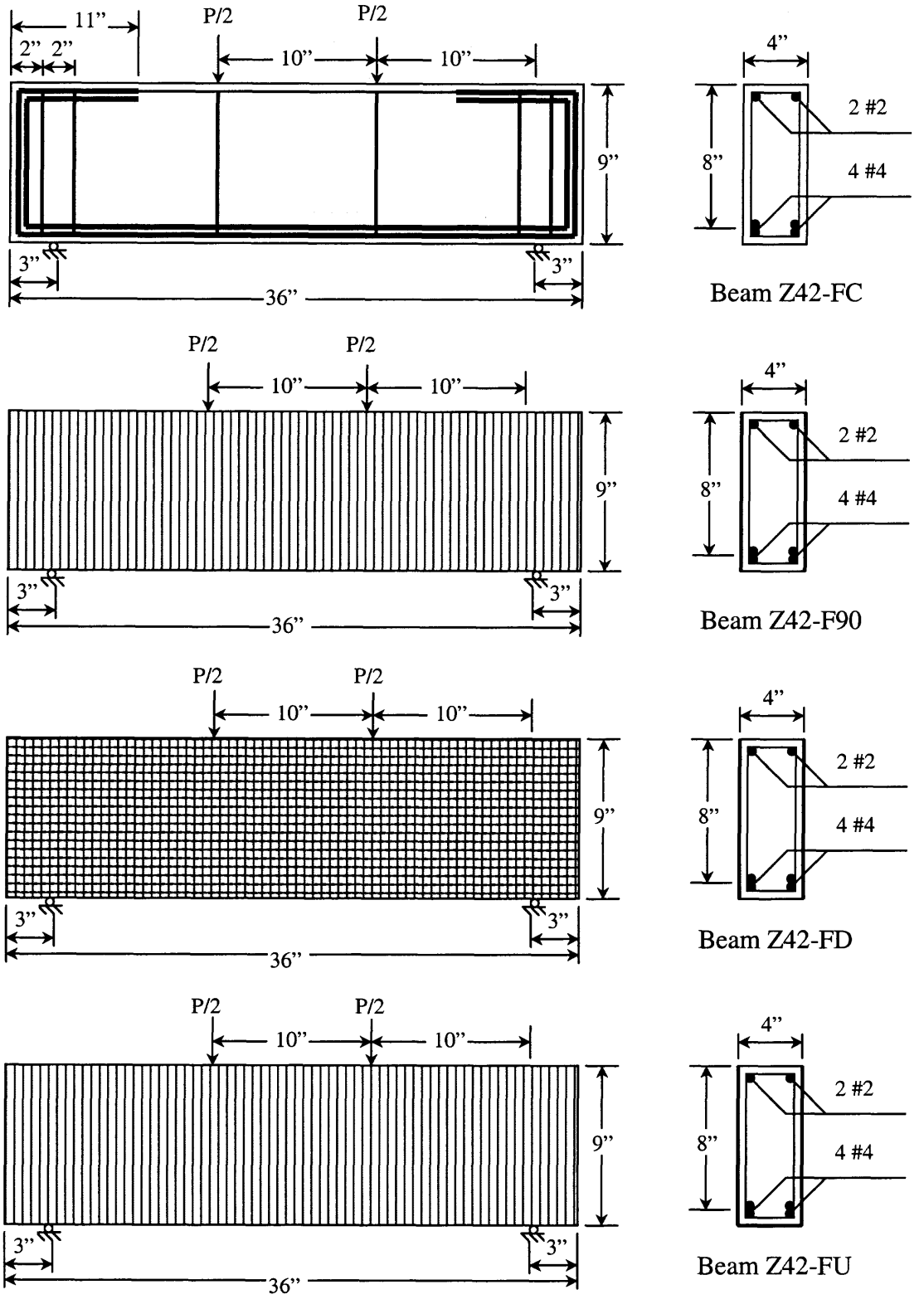

Figure 4.6 Configuration of CFRP fabrics under 2-point loading.

4.5 Instrumentation and Test Procedure

The testing equipment used in this experiment is the same as the one used in regular beam test: 220-kips capacity MTS testing system (Figure 4.7).

Each of the 3' long beams to be tested was simply supported by two 2" diameter steel rollers located 3" from each end of the beam. A steel plate was inserted between the concrete and the steel roller to ensure that the local failure did not occur at the support. It was necessary to place two 4" thick concrete blocks under each support to elevate the beam so that the stroke of the testing machine could reach the specimen. For 3-point loading condition, a 1" diameter steel ball bearing suspended between two steel plates was used to transfer the load evenly from the loading cell to the surface of the specimen. This same procedure was used under 4-point loading condition except that a thick steel block was used to separate the load into two equal components exactly 10" apart. Each loading point is located 5" from the center of the beam.

External LVDT (linear variable differential transducer) was placed under the beam right in the middle to measure the central defection. Although the deflection could be measured using an internal LVDT from the loading cell, a large amount of error would be introduced resulting from the deformation of the loading cell itself as well as the occasionally small local concrete crashes. Deflection control scheme was used during the loading process. The load applied on the beam was increased at a constant rate of 0.01 kips/sec and stopped when the beam failed or the deflection reached the maximum at 0.5", whichever came first. The load and deflection data were automatically recorded by the built-in data acquisition program. The load and deflection curves were shown on the monitor live for real time observation.

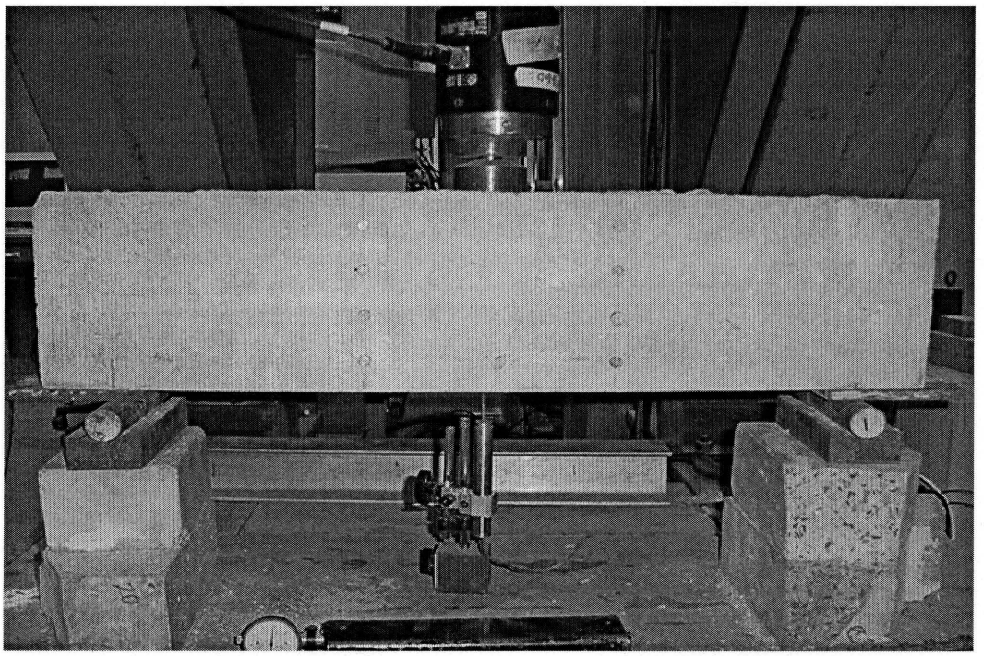

Figure 4.7 Typical test setup.

4.5.1 Beam Group 1

4.5.1.1 Beam Z11-SC. The first beam tested was a control beam Z11-SC, which was used to compare with the rest of the beams in this group in terms of shear capacity. As the beam was loaded at about 19 kips, a small crack developed directly under the load which was followed by flexural-shear cracks developing toward the left support. The load then dropped approximately 1.0 kip and continued to increase until another crack developed at the other side of the beam. The maximum load at failure was 21.3 kips. The flexural-shear cracks developed at approximately 45 degrees between the loading point and the support. The other three beams with various CFRP shear reinforcement were expected to have higher failure loads than 21.3 kips (Figure 4.8).

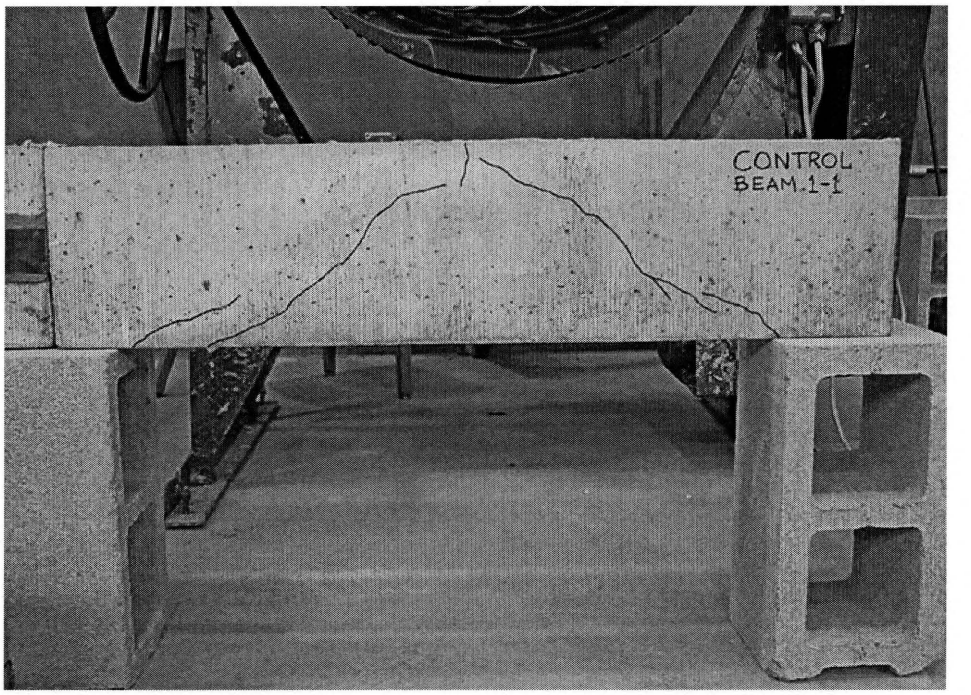

Figure 4.8 Failure of Beam ZC11-SC.

4.5.1.2 Beam Z11-S0. It is a known fact that longitudinal steel shear reinforcement is very important in shear strengthening of deep beam. This test is thus to investigate the effectiveness of longitudinal shear strengthening by an externally bonded CFRP strip.

When the load on the beam was increased to pass 17 kips, the first flexural – shear crack formed just below the CFRP laminates near the right support. As the load increased, the crack formed at a 45-degree angle with respect to the beam axis and extended all the way toward the loading point. At the ultimate load of 22.2 kips, the crack further developed and the beam failed suddenly with the load dropping to 17 kips. While the beam was continuously loaded, the load drop slowed down quite a bit. The beam still had about 11 kips capacity even when the test was stopped. It was observed that the cracks developed only at the right side of the beam. The left side of the beam remained

intact. The CFRP strip delaminated from underneath the concrete surface, but neither ends of the CFRP delaminated entirely from the concrete. The delamination extended approximately 2" across the cracks of both front and back sides of the beam (Figure 4.9).

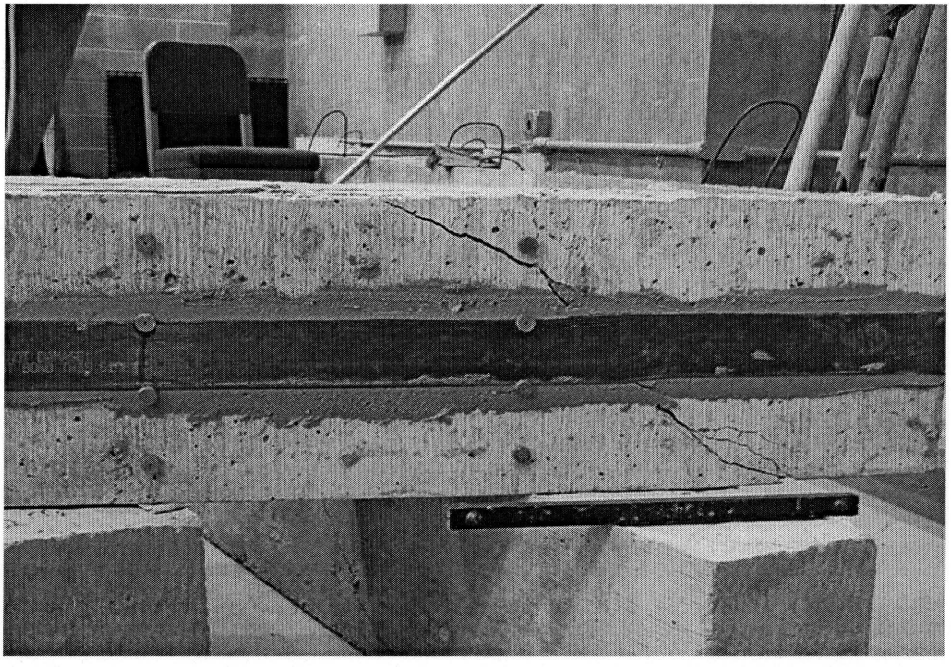

Figure 4.9 Failure of Beam Z11-S0.

4.5.1.3 Beam Z11-S90. Vertical stirrup is the most common type of reinforcement in shear strengthening of beams. The setup of this experiment is to investigate the effectiveness of vertical CFRP reinforcement in shear strengthening of a deep beam.

During testing, the first small flexural-shear crack appeared at 25 kips near the middle of the span on the tension side of the beam. As the load increased, more flexural cracks developed and small shear cracks started to develop at the supports between the CFRP laminates. As the load reached a maximum of 37.8 kips, the flexural cracks continued to grow and the deflection increased without any further load increase. At this point, there was a loud popping sound as the bond between the CFRP and the concrete

was broken. Then the load dropped dramatically from 37 kips to 6 kips, resulting in an explosive failure and causing large pieces of concrete peeled off from the beam. Two CFRP strips located 3rd and 4th from the left support became completely dislodged (Figure 4.10).

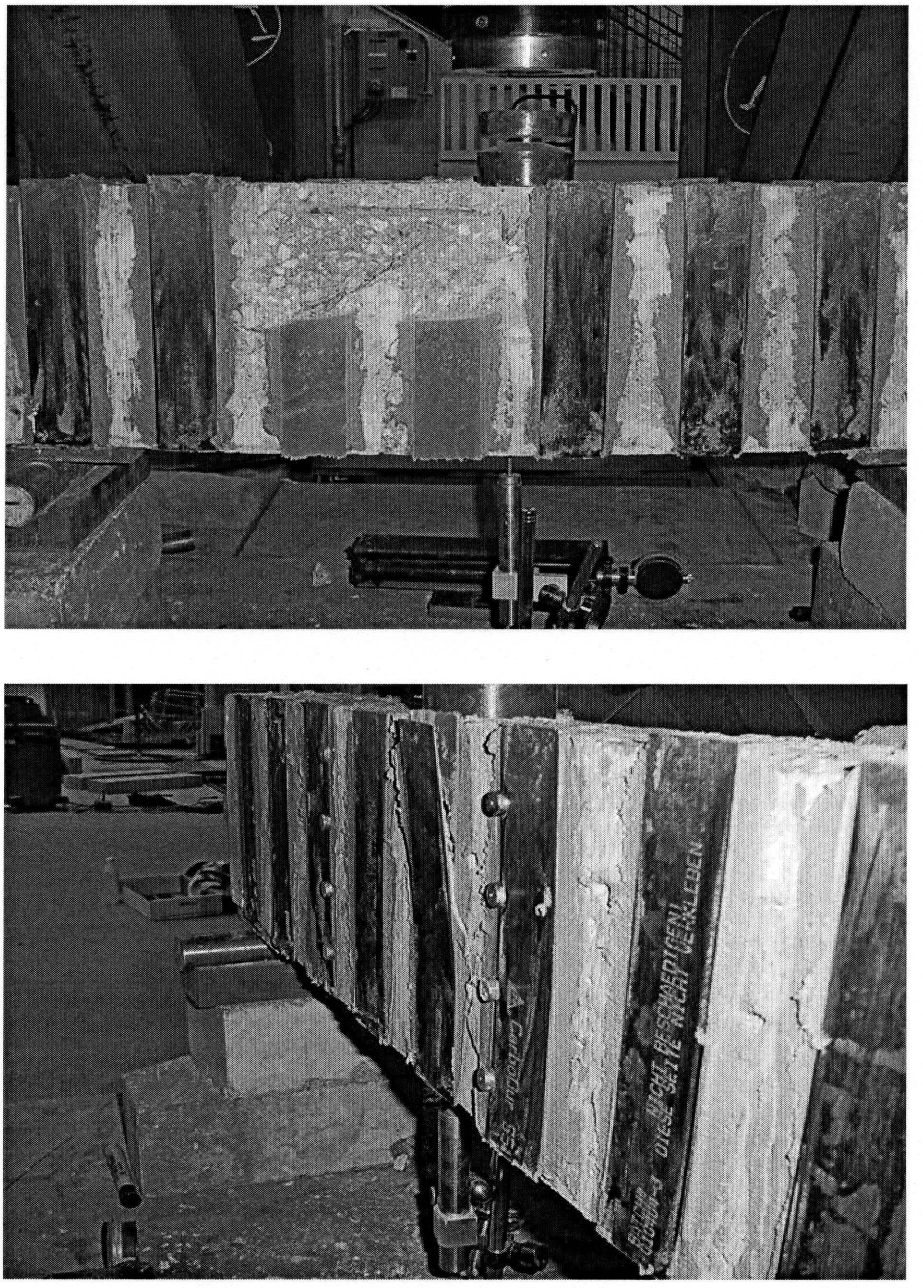

Figure 4.10 Failure of Beam Z11-S90.

4.5.1.4 Beam Z11-S45. The CFRP strip orientation of this test is supposed to be roughly perpendicular to the possible shear crack, provided the shear span is greater than the beam depth. It has been proven in the previous chapter that this configuration is the most effective in shear strengthening of a regular beam using CFRP. The load capacity of this specimen was expected to be higher than that of beam Z11-S90.

As the beam was loaded, local failure was observed directly under the load at about 20 kips with no other sign of crack until approximately 28 kips. At this point, flexural cracks began to form directly under the load on the tension side of the beam. As the load increased these cracks further extended into the compression zone of the beam. Meanwhile, shear cracks began to form perpendicularly to the CFRP strips as pictured in Figure 4.11. As the load increased to a maximum of 45.9 kips, the flexural cracks were approaching the neutral axis of the beam when the bonding between the CFRP and the concrete surface was broken. CFRP delamination accompanied by a loud popping sound was observed at the same time. The entire section located under the load fractured with large portions of concrete being dislodged and falling off.

Figure 4.11 Failure of Beam Z11-S45.

4.5.2 Beam Group 2

4.5.2.1 Beam Z22-SC. The test setup was similar to beam Z11-SC, except that the shear span was reduced from 15" to 10" due to the change in loading conditions. As the bam was loaded to reach 9 kips, a small crack appeared directly under the left loading point. At 18 kips, a small shear crack developed at the right support and continue to develop as the load increased. At about 24 kips a flexural shear crack developed at the left support, while the crack at the right support reached the neutral axis of the beam. There was no load drop observed as these small cracks developed. A major crack formed at the left side of the beam when the load reached the maximum value of 32.8 kips. Concrete crushing was also observed under the left loading point. The load gradually dropped to about 27 kips and then dropped quickly to about 20 kips before the test was stopped (Figure 4.12).

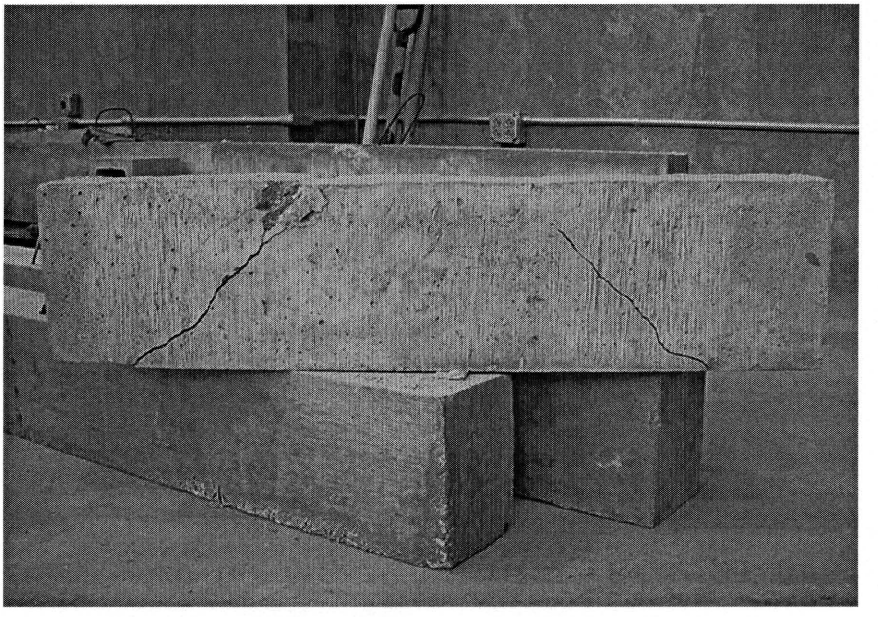

Figure 4.12 Failure of Beam Z22-SC.

4.5.2.2 Beam Z22-S0. This specimen was the same as beam Z11-S0, except that it was under 2-point loading conditions. As the load on beam Z22-S0 increased to pass 24 kips, the first flexural shear crack was observed below the CFRP laminate near the right support. The crack formed at 45-degree angle with respect to the beam axis. At an ultimate load of 46.7 kips, the crack further extended and shear failure occurred with the load dropping gradually to about 23 kips before the test was topped. The cracks developed only at the right side of the beam just like that of beam Z11-S0. The CFRP strip was delaminated from underneath the concrete surface and the delamination extended approximately 3" across the cracks of both front and back sides of the beam (Figure 4.13).

Figure 4.13 Failure of Beam Z22-S0.

4.5.2.3 Beam Z22-S90. This beam is basically the 2-point loading version of beam Z11-S90, excepted that the two CFRP strips in the middle were omitted. It will not affect the shear behavior of the beam since shear force does not exist between the two loading points. During the test, a small flexural crack developed first at 28 kips near the middle of the span on the tension side of the beam. As the load increased, more flexural cracks developed and shear cracks appeared at the supports and between the CFRP strips. At a result of CFRP strip delammination from the concrete, the beam finally failed at a maximum load of 47 kips, accompanied by a popping sound. It was observed that the delamination took place almost an inch below the concrete surface, more like a concrete block bonded by three CFRP strips being seperated from the beam. The load dropped instantly to about 31 kips and continued to drop to about 23 kips at a much slower pace. Pictured in Figure 4.14 are three CFRP strips that are debonded at failure.

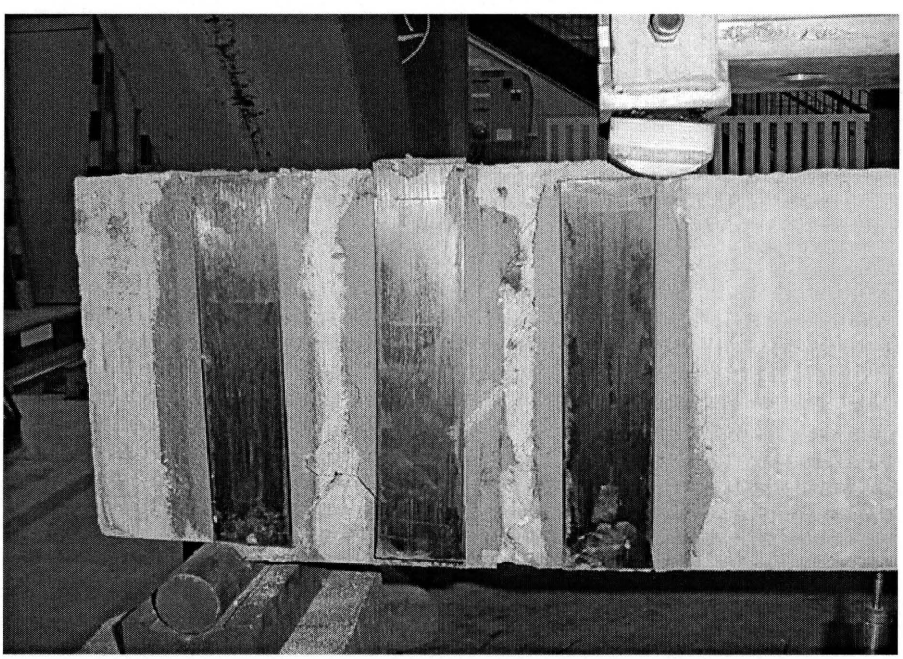

Figure 4.14 Failure of Beam Z22-S90.

4.5.2.4 Beam Z22-S45. Like beam Z22-S90, two CFRP strips were omitted from each side of the beam because of the shorter shear span under 2-point loading condition. Local failure was observed directly under both loading points. As the load reached 30 kips, flexural cracks began to develop under the loads on the tension side of the beam. The cracks propagated toward the direction of the loading points as the load increased. When the load increased to approximately 40 kips, shear cracks began to form perpendicularly to the CFRP strips as pictured in Figure 4.15. As the load increased to a maximum of 54.6 kips, the flexural cracks passed the neutral axis and connected with the shear cracks that had formed perpendicularly to the CFRP strips. At this point, the beam failed in CFRP delamination from the surface of the concrete. It was also observed that the entire concrete surface located from the support to the loading point fractured and separated from the beam.

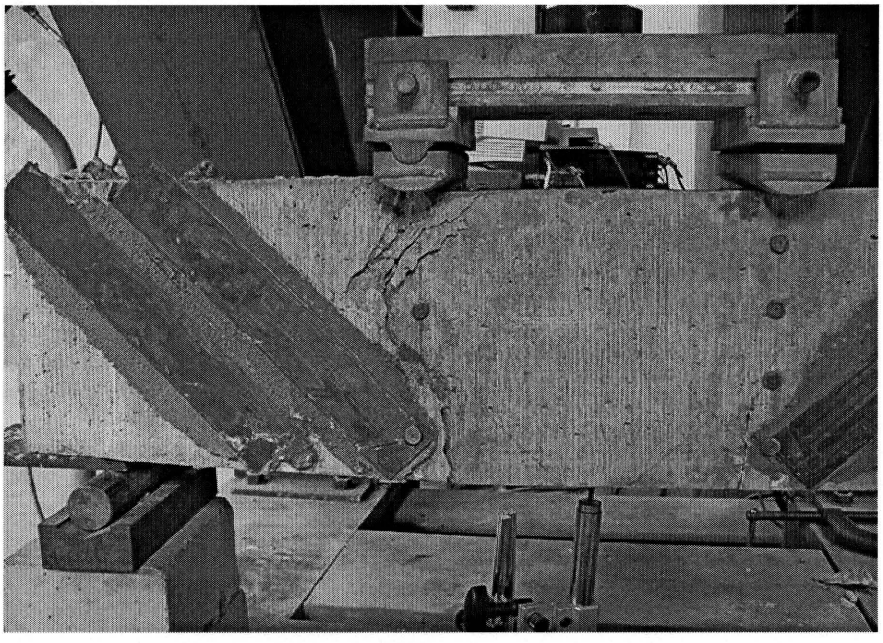

(a) Left Side

Figure 4.15 Failure of Beam Z22-S45.

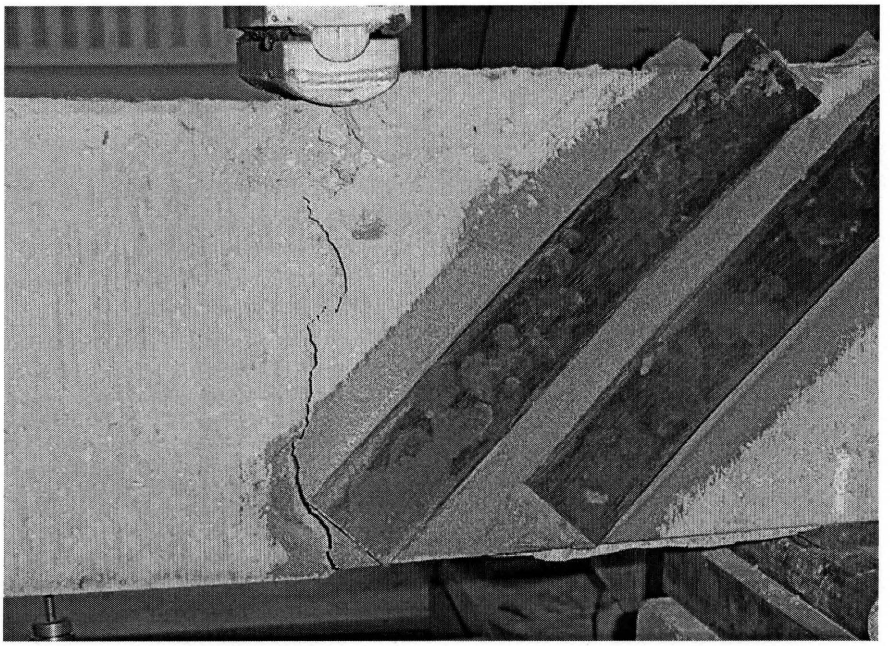

(b) Right Side

Figure 4.15 Failure of Beam Z22-S45 (Continued).

4.5.3 Beam Group 3

4.5.3.1 Beam Z31-FC. This test was identical to beam Z11-SC in almost every way, except this beam was cast from another batch of concrete. Small shear cracks originating from the left support was observed when the load arrived at 15 kips. The load continued to increase until it reached 18.8 kips. It dropped a little to 17 kips and then continued to increase slowly until it suddenly dropped to 12 kips. The beam failed along with a shear crack on the left side of the beam, while the other part of the beam remained intact. No flexural cracks were observed during the loading process (Figure 4.16).

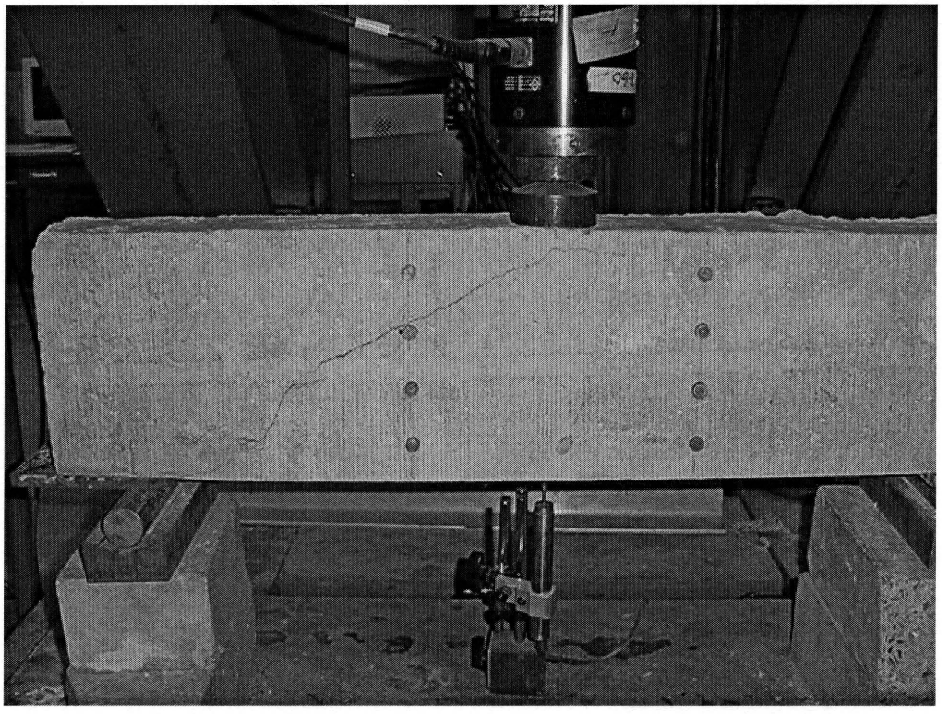

Figure 4.16 Failure of Beam Z31-FC.

4.5.3.2 Beam Z31-F90. This test was used to compare the behavior with beam Z11-S90. The continuous fabrics (SikaWrap Hex 230C) was used as laminates instead of CFRP strips (Sika CarnoDue Strip) in this test. The orientation of the CFRP fabrics was perpendicular to the beam longitudinal axis. During the loading process, almost inaudible popping sound was heard when the load increased beyond 20 kips. No delamination or rupture of the fabrics was observed. When the load approached 34 kips, the popping sounds became intense and the beam failed in a sudden manner at a maximum load of 34.7 kips with the CFRP fabrics delaminated from the concrete surface. It was also accompanied by a loud popping sound. A shear crack originating from the support to the loading point was unveiled from a close observation of the failed specimen. The pattern

of the delamination, which consisted of two triangles, was also unique to this specimen (Figure 4.17).

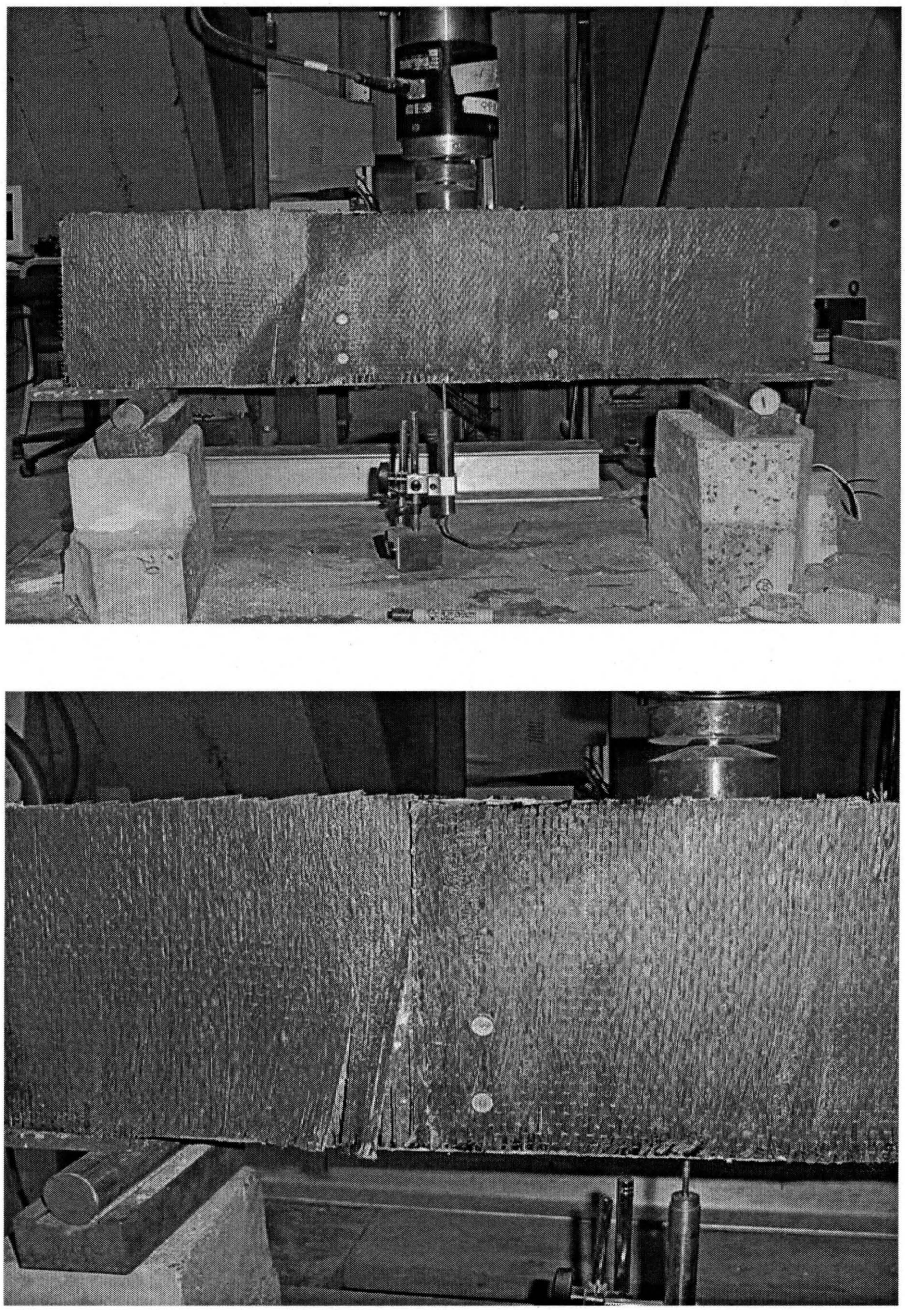

Figure 4.17 Failure of Beam Z31-F90.

4.5.3.3 Beam Z31-FD. This beam was strengthened by 2 layers of CFRP fabrics. The first layer was applied to the beam with the fiber orientation perpendicular to the longitudinal beam axis just like beam Z31-F90. The second layer was applied on top of the first layer with the same fiber orientation as the longitudinal beam axis. This strengthening scheme was trying to simulate the traditional web reinforcement in deep beam which included both horizontal and vertical steel bars. As the beam was loaded, weak scattered popping sounds were heard when the load passed beyond 25 kips. No delamination was observed, however. Local delamination was expected because of the popping sounds. The beam failed in a sudden manner at a maximum load of 39.5 kips. The load dropped to about 12 kips after the beam failed. Since the beam was heavily reinforced by double-layer CFRP fabrics, no apparent delamination or rupture was observed from both sides of the beam. However, a close observation from the top of the beam revealed that the shear crack had already formed in the beam and was covered by CFRP fabrics. The delamination across the crack was approximately 3" (Figure 4.18).

4.5.3.4 Beam Z31-FU. The beam was basically an "anchorage version" of beam Z31-F90. One CFRP sheet was used to wrap around both sides and bottom of the beam all together, which prevent the delamination of the CFRP sheets from both sides of the beam. This wrapping scheme was also called U-shaped wrapping.

Figure 4.18 Failure of Beam Z31-FD.

The beam Z31-FD behaved very similar to the beam Z31-F90 prior to the maximum load. It failed in shear at a maximum load of 43.2 kips. The delamination pattern appeared to be a upper triangle extending from the shear crack all the way to the top of the beam without any fiber rupture at the bottom of the beam. The anchorage function of the U-shaped wrapping seemed to work as intended. From Figure 4.19, it can be seen that the delamination is more like the concrete block attached by CFRP fabrics being dislodged under the heavy loading.

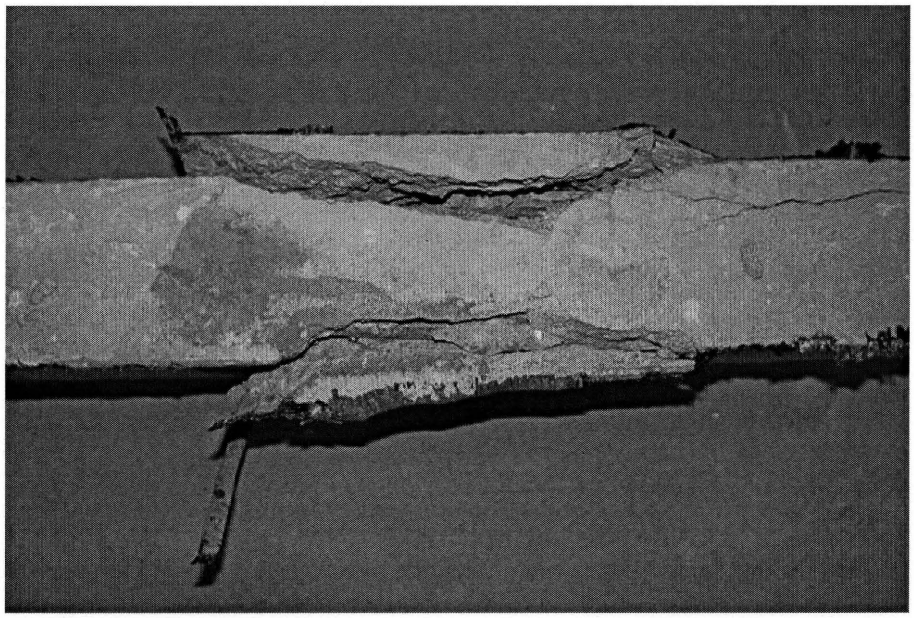

(a) Top View of the Failure Section

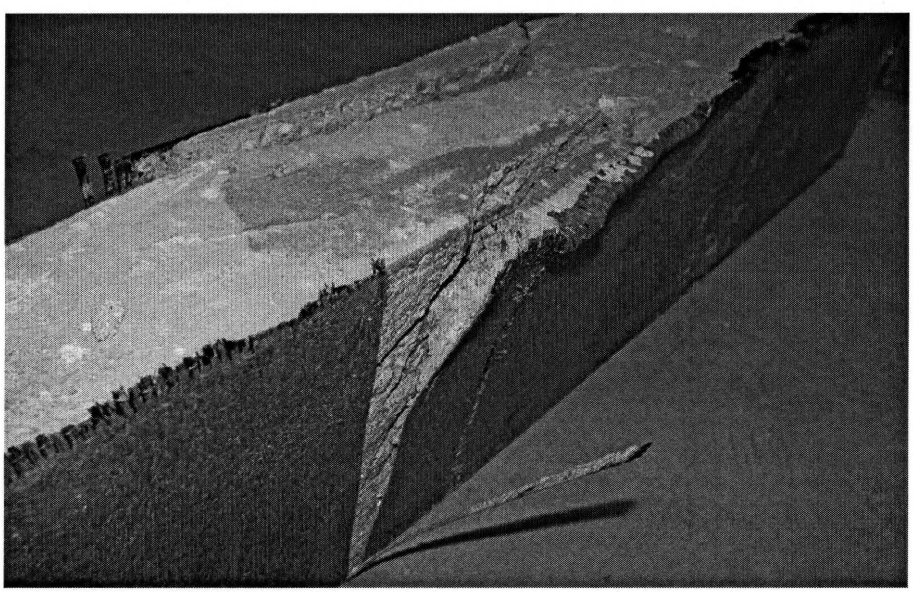

(b) Side View of the Failure Section

Figure 4.19 Failure of Beam Z31-FU.

4.5.4 Beam Group 4

4.5.4.1 Beam Z42-FC. This test was identical to beam Z22-SC in almost every way, except this beam was cast from another batch of concrete.

The first shear crack developed when the load reached 24 kips on the right side of the beam. As the load continued to increase, another shear crack was observed on the other side of the beam when the load passed 28 kips. The first crack continued to develop as higher load being applied on the beam, while the size of the second crack remained unchanged regardless of the load increase. The load started to drop gradually at a maximum of 39.4 kips. Even through the beam had already failed, it still showed a considerable ductility before the test was stopped (Figure 4.20).

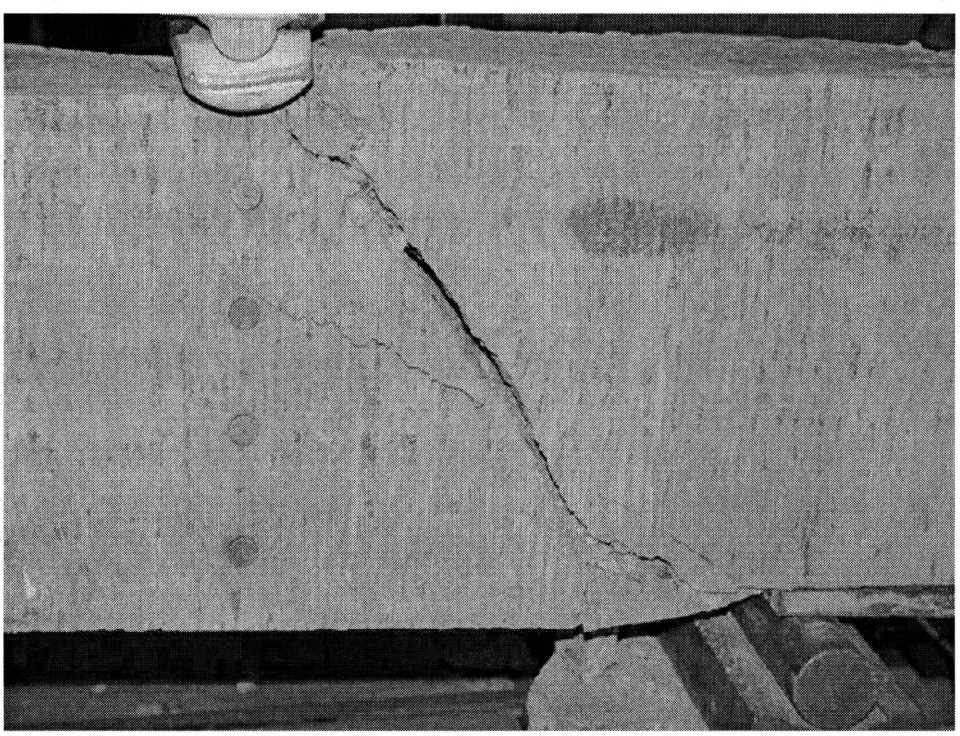

Figure 4.20 Failure of Beam Z42-FC.

4.5.4.2 Beam Z42-F90. The test setup was similar to beam Z31-F90, except the beam Z42-F90 had a shorter shear span because of the change in loading condition. As the load passed 10 kips, minor local failures occurred due to the uneven surface condition at the loading point. A weak cracking sound was heard when the load reached 26 kips. The shear cracks developed at a maximum load of 57.9 kips on the right side of the beam when the beam failed, which was in a sudden manner with a dramatic load dropping to about 36 kips. The delamination pattern of the beam could be comparable to that of beam Z31-F90. The delamination was originated from the shear crack and extended all the way to the top and bottom of the beam, forming a double-triangle pattern (Figure 4.21).

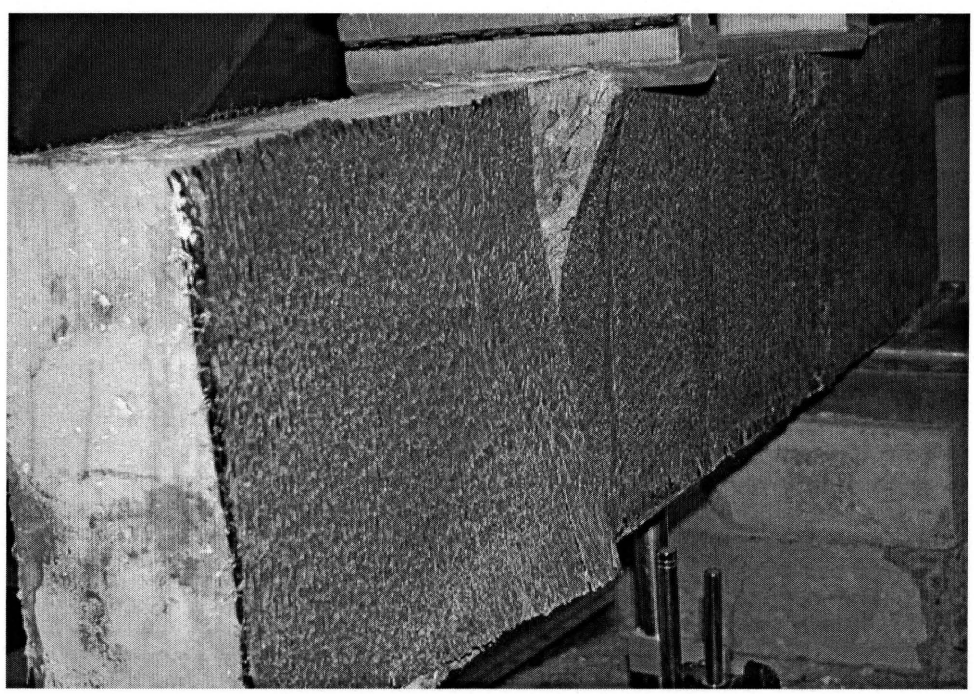

Figure 4.21 Failure of Beam Z42-F90.

4.5.4.3 Beam Z42-FD. This was the 2-point loading version of beam Z31-FD. The failure mechanism was almost identical with beam Z31-FD. The beam failed in shear at a maximum load of 60 kips. The length of delamination was approximately 3" across the shear crack. A close observation from the top of the failed beam showed that the delamination occurred beneath the concrete surface, with occasional bond failure between CFRP sheets and the epoxy. The load dropped to about 38 kips right after the peak load and continued to drop slowly until the test was stopped (Figure 4.22).

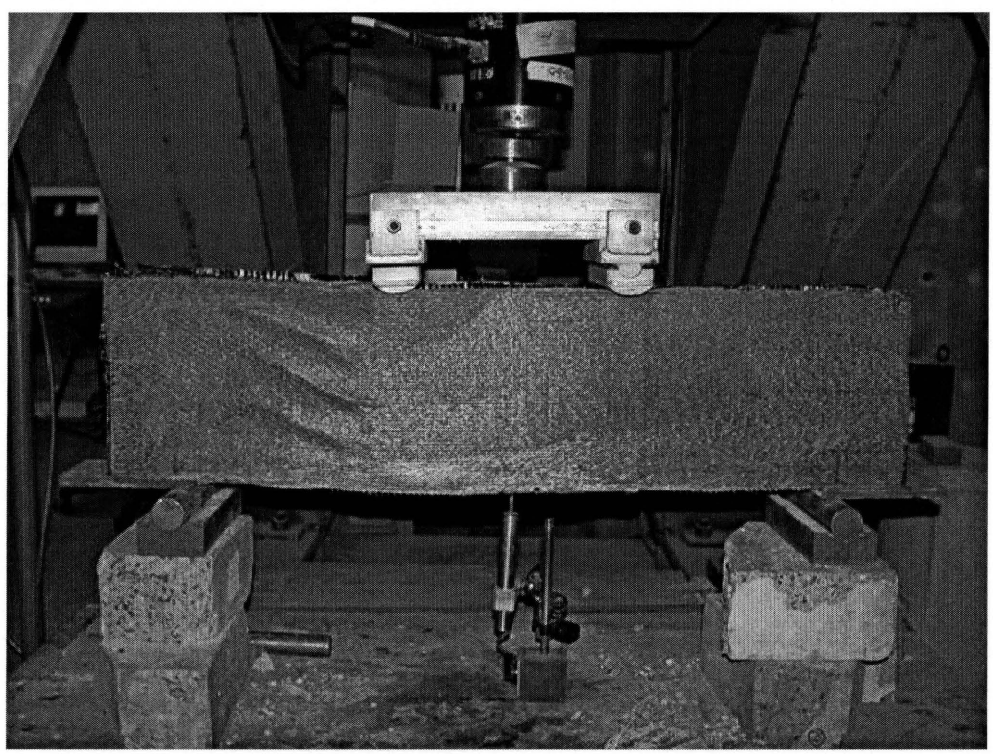

(a) Side View of the Beam at Failure

Figure 4.22 Failure of Beam Z42-FD.

(b) Top View of the Beam at Failure

Figure 4.22 Failure of Beam Z42-FD (Continued).

4.5.4.4 Beam Z42-FU. This setup of the beam was the same as that of beam Z31-FU, except that the shear span was shorter because of the change of the loading points. Neither flexural cracks nor shear cracks were observed prior to the failure of the beam. A little cracking sound was heard when the load reached beyond 24 kips. The beam failed in shear at a maximum load of 57.4 kips, and the load dropped to around 30 kips and continued to drop slowly until the test was stopped. Triangle-shaped delamination as well as a small part of fabrics rupture at the lower corner of the shear crack were observed from the specimen. The shear crack appeared on the right side of the beam, while no crack was observed on the left side of the beam (Figure 4.23).

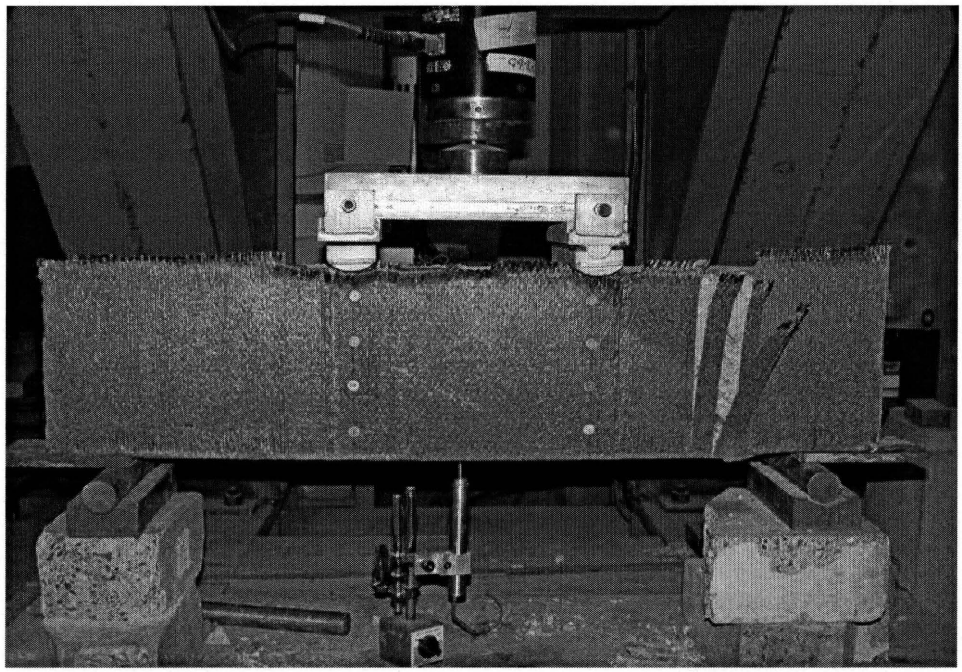

(a) Side View of the Beam at Failure

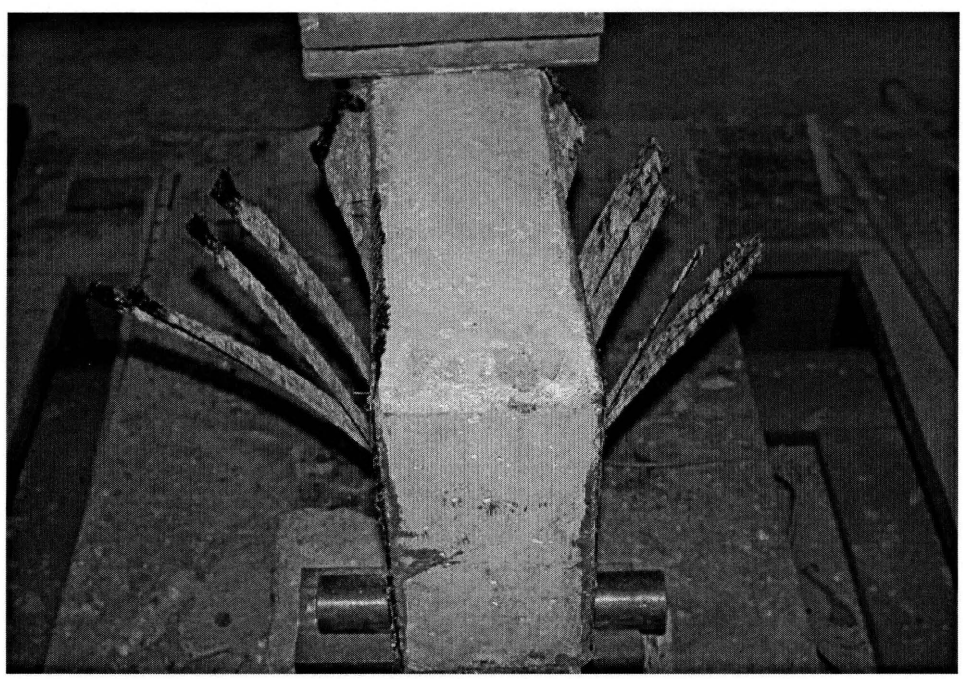

(b) Top View of the Beam at Failure

Figure 4.23 Failure of Beam Z42-FU.

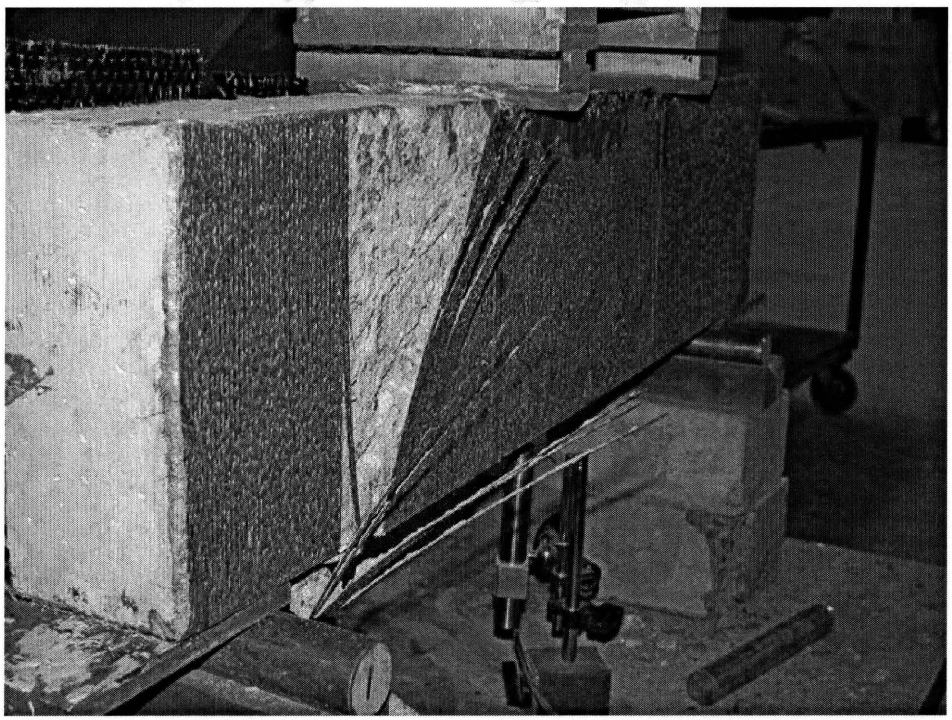

(c) Close-up View of the Beam at Failure

Figure 4.23 Failure of Beam Z42-FU (Continued).

4.6 Test Results and Discussions

4.6.1 Beam Group 1

A summary of the test results of four beams under 1-point loading was provided in Table 4.2. The load–deflection curves of four beams are plotted and placed together as shown in Figure 4.24.

4.6.1.1 Strength. From Table 4.2 and Figure 4.24, it can be observed that the beams with externally bonded CFRP strips increase the load carrying capacity of the tested beams in group 1. However, the contribution of CFRP strips in shear strengthening varies depending upon the CFRP configurations of the tested beams.

The above results are similar to those of the regular beams as discussed in Chapter 2. Beam Z11-S45, which is reinforced by 45-degree CFRP strips with respect to the beam axis, gets a 22.3 kips increase in load carrying capacity as compared with the control beam Z11-SC. It has been found out that beam Z11-S45 is the most efficient beam in shear strengthing in this group. The closest runner up is beam Z11-S90, which gets increased a 16.8 kips in load carrying capacity as compared with beam Z11-SC. Beam Z11-S0, which only increases merely 0.9 kips, is the least efficient beam in this group.

4.6.1.2 Ductility. Table 4.2 and Figure 4.24 also show that beam Z11-S45 and beam Z11-S90 give large deflections at ultimate, which are 0.1897 in. and 0.1132 in., respectively, as compared to other beams. This demonstrates that CFRP strengthened beams give not only an increase in shear strength, but also an increase in ductility as well. Despite the CFRP shear reinforcement, beams Z11-S0, Z11-S90 and Z11-S45 all had almost the same modulus of elasticity as beam Z11-SC prior to the formation of major

shear cracks. With the higher failure loads of the CFRP reinforced beams, the deflections also get increased accordingly. For beam Z11-S0, the deflection is almost the same as beam Z11-SC due to the small load increase.

Table 4.2 Experimental Results of Beams in Group 1

Beam Designation	Load P at Ultimate (kips)	Central Deflection at Ultimate (in.)	CFRP Shear Capacity (kips)	CFRP Failure Mode
Z11-SC	21.3	0.0709	N/A	Shear Diagonal Cracking
Z11-S0	22.2	0.0722	0.5	Strip Delamination
Z11-S90	38.1	0.1132	8.4	Strip Delamination
Z11-S45	43.6	0.1897	11.2	Strip Delamination

4.6.1.3 Failure Mechanism. Based on present test observations, delamination of the CFRP laminates from underneath the concrete surface is the dominant failure mode for all CFRP strengthened beams. As for crack patterns, no shear-tension failure is observed for all 4 beams due to the sufficient anchorage length of the flexural reinforcement. Inclined cracks are developed prior to the ultimate failure load in all 4 beams during the loading process. The failure of beam Z11-SC is due to the propagation of inclined crack through the compressive region, which is called "diagonal tension" failure. The failure of beam Z11-S0 is mainly due to the crushing of the concrete in the compressive region above the inclined crack, which is termed "shear compression"; the "diagonal tension" failure along the inclined crack and longitudinal reinforcement has been observed as well. The failure of beam Z11-S90 is found to be "diagonal tension"

failure along the inclined crack. The failure of Beam Z11-S45 is a combination of "shear compression" failure at the loading point and "diagonal tension" failure along the inclined crack.

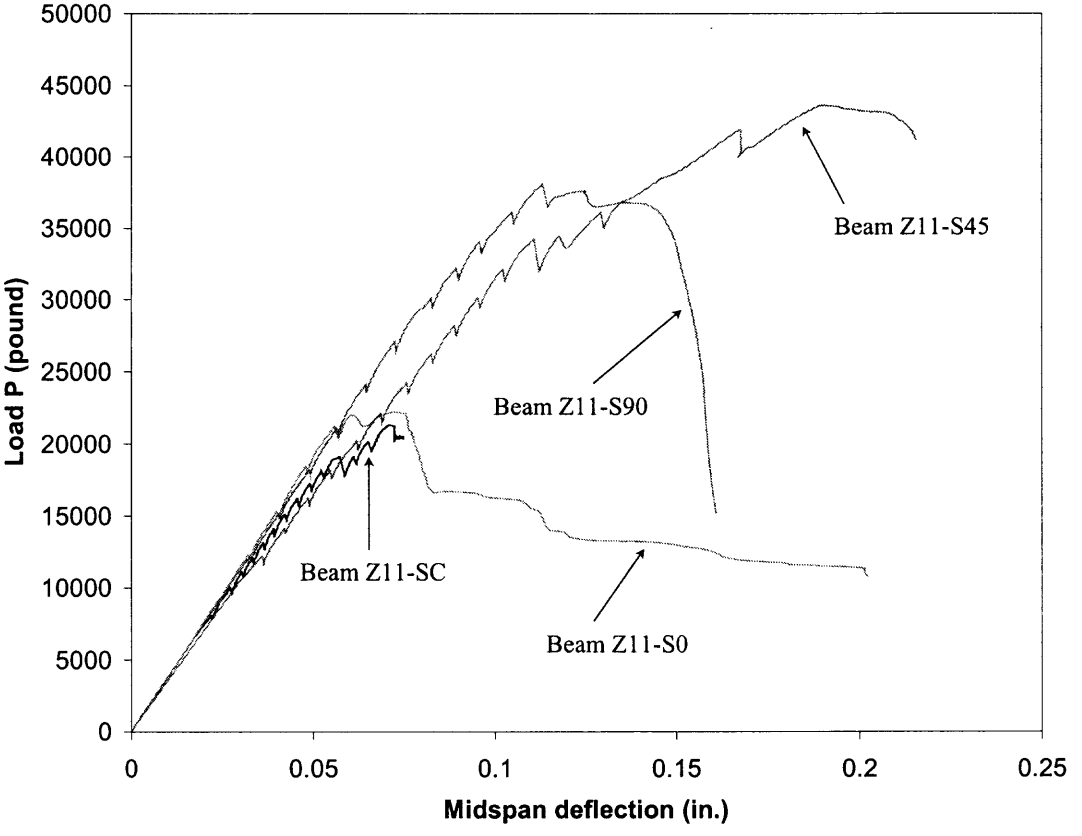

Figure 4.24 Load-deflection curves of beams in Group 1.

4.6.2 Beam Group 2

A summary of the test results of four beams under 2-point loading is shown in Table 4.3. The load–deflection curves of four beams are depicted in Figure 4.25.

4.6.2.1 Strength. As expected, the failure loads of the beams in this group are a lot higher than those of the corresponding beams in group 1 because of the shorter shear span. Beam Z22-S45 has the highest failure load of 54.6 kips, which gets a 21.8 kips increase in load carrying capacity as compared with the control beam Z22-SC. The load carrying capacity of beam Z22-S90 increases 14.2 kips. And the failure load of beam Z22-S0 increases 13.9 kips, which is almost identical.

4.6.2.2 Ductility. Table 4.3 and Figure 4.25 show that beams Z22-S90, Z22-S0 and Z22-S45 give largest deflections at ultimate, which are 0.1182 in., 0.1009 in. and 0.1005 in., respectively. From Figure 4.25, it can be observed that under 2-point loading condition, the load-deflection curve of beam Z22-S45 shows a slightly higher modulus of elasticity in the linear portion than the rest of the beams in this group. However, all CFRP strengthened beams give some improvement in ductility as compared to the control beam.

Table 4.3 Experimental Results of Beams in Group 2

Beam Designation	Load P at Ultimate (kips)	Central Deflection at Ultimate (in.)	CFRP Load Capacity (kips)	CFRP Failure Mode
Z22-SC	32.8	0.0696	N/A	Shear Diagonal Cracking
Z22-S0	46.7	0.1009	7.0	Strip Delamination
Z22-S90	47.0	0.1112	7.1	Strip Delamination
Z22-S45	54.6	0.1005	10.9	Strip Delamination

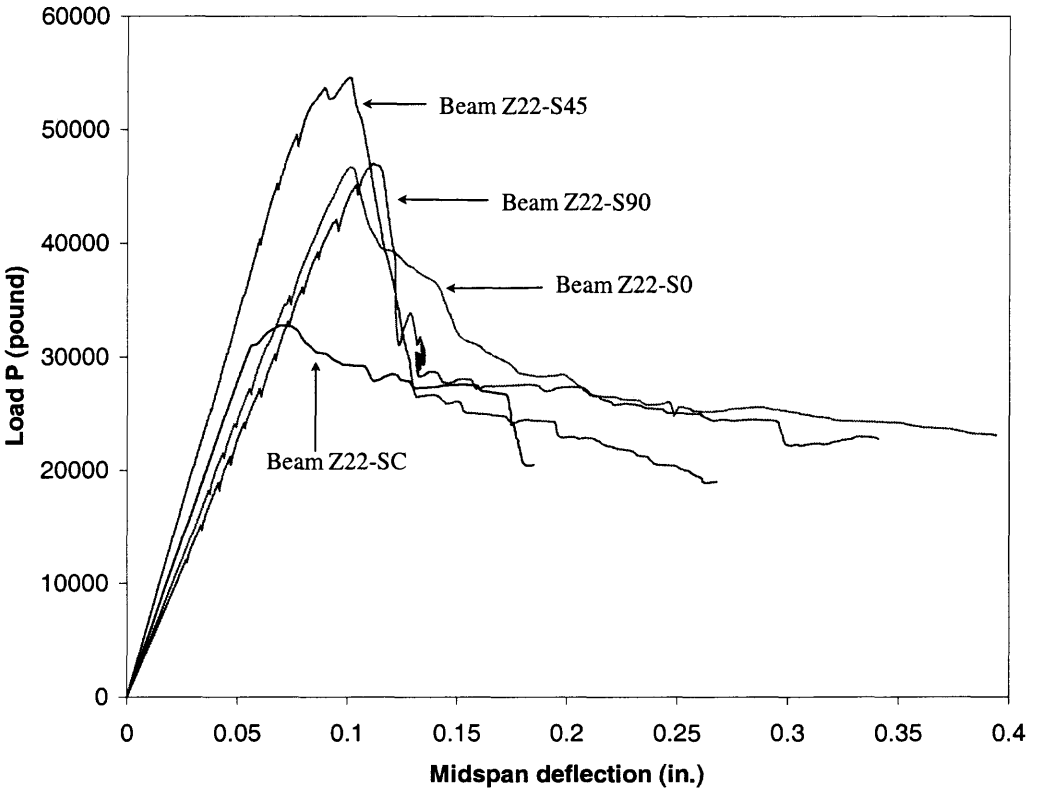

Figure 4.25 Load-deflection curves of beams in Group 2.

From Figure 4.25, it can also be observed that after the loads drop to a certain level, all of the beams still maintain a steady load reserve while the deflections continue to increase, which means that the beams still maintain a certain degree of ductility even after the beams have already failed in shear. The explanation for this can be drawn from the observation of the beams during the loading process. The load drop after the peak is resulted from the delamination of the CFRP strips. Since the bonding between the CFRP and the concrete has been destroyed, the load is mainly carried by the flexural reinforcement alone. This phenomenon is so-called dowel action in beam shear behavior.

4.6.2.3 Failure Mechanism. Delamination of the CFRP laminates from underneath the concrete surface has been found to be the dominant failure mode for CFRP strengthened beams in this group. There is no "shear tension" failure observed from all the beam tests in this group. The failure of Beam Z22-SC is due to concrete crushing at one of the loading points, which is called "shear compression" failure. "Diagonal tension" along the inclined crack through the compressive region in conjunction with partial CFRP strip delamination is the failure mode of beam Z22-S0. Beam Z22-S90 shows a similar failure mechanism with that of beam Z22-S0. The failure mode of beam Z22-45 includes a "shear tension" failure due to the concrete crushing in the compressive region, "diagonal tension" due to the propagation of the inclined crack through the compressive region and also the longitudinal reinforcement, and CFRP strip delamination across the inclined shear crack.

4.6.3 Beam Group 3

A summary of the test results of four beams under 1-point loading can be found in Table 4.4. The load–deflection curves of the four beams are illustrated in Figure 4.26.

4.6.3.1 Strength. It can be observed from Table 4.4 and Figure 4.26 that beam Z31-FU exhibits the highest loading capacity with a ultimate load of 43.2 kips, which is a 23.8 kips higher as compared with the 19.4 kips loading capacity of the control beam Z31-FC. Beam Z31-FD falls behind beam Z31-FU with an increase of 20.1 kips. Beam Z31-F90 is the least efficient beam in this group with an increase of 15.3 kips. The only difference between beam Z31-F90 and Z31-FU is to provide an anchorage in beam Z31-FU by means of U-shaped wrapping. A comparison of the results of the two beams shows that the anchorage provides an increase of 8.5 kips in load carrying capacity.

4.6.3.2 Ductility. Being the strongest beam in this group, beam Z31-FU also shows the highest ductility with a deflection of 0.1366 in.. The deflections of the rest of the beams in this group are distributed according to their ultimate loads. Higher loads mean larger deflections. Control beam Z31-FC shows some ductility during the peak load. While the CFRP reinforced beams show some improvement in ductility, however they become brittle after reaching their ultimate loads.

Table 4.4 Experimental Results of Beams in Group 3

Beam Designation	Load P at Ultimate (kips)	Central Deflection at Ultimate (in.)	CFRP Shear Capacity (kips)	CFRP Failure Mode
Z31-FC	19.4	0.0838	N/A	Shear Diagonal Cracking
Z31-F90	34.7	0.1045	7.7	Fabrics Delamination
Z31-FD	39.5	0.1288	10.1	Fabrics Delamination
Z31-FU	43.2	0.1366	11.9	Fabrics Delamination

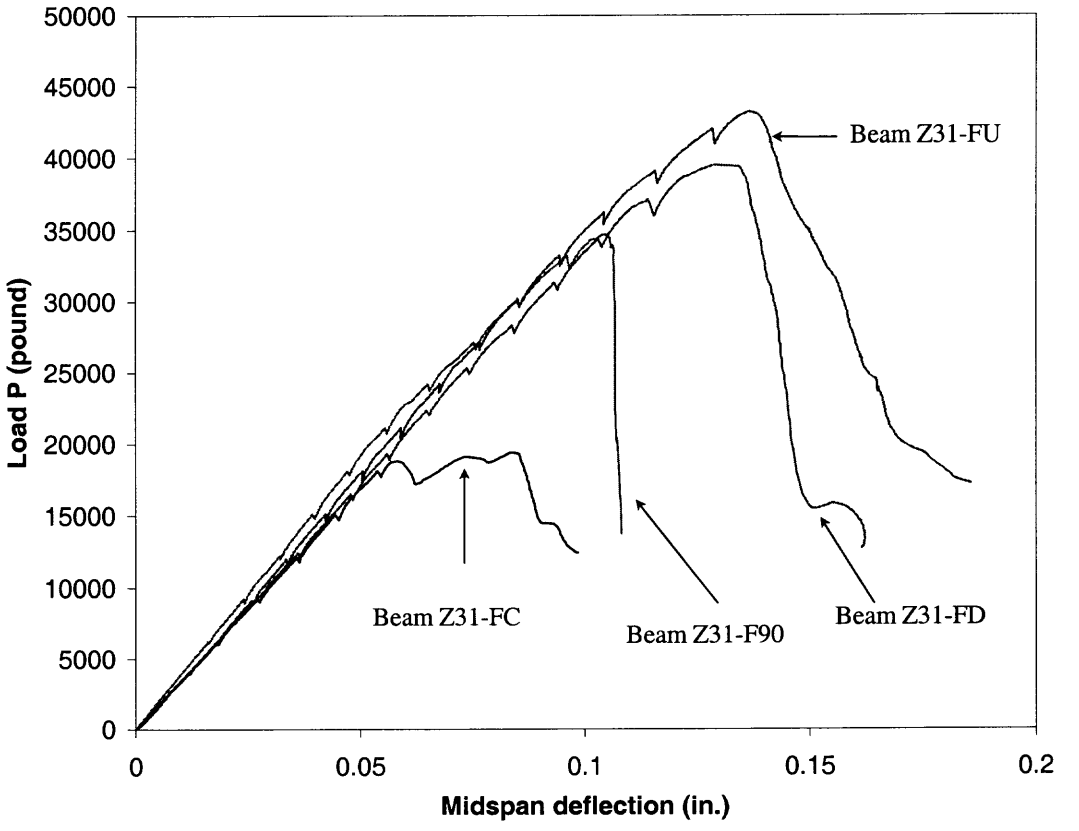

Figure 4.26 Load-deflection curves of beams in Group 3.

4.6.3.3 Failure Mechanism. No inclined shear cracks were observed in all CFRP strengthened beams due to the nature of strengthening scheme. The failure of control beam Z31-FC has been due to the propagation of the inclined shear crack. The failure mode of beam Z31-F90 is a combination of CFRP fabrics delamination in a double triangle shape and the propagation of the inclined shear crack. Beam Z31-FD fails in "shear compression" due to the crushing of the concrete in the compressive region above the inclined crack in conjunction with CFRP delamination. Beam Z31-FU fails at the same pattern as that of beam Z31-FD, except that the concrete crushing is more severe and the non-anchorage end of the CFRP has been delaminated completely in a triangle shape.

4.6.4 Beam Group 4

A summary of the test results of four beams under 2-point loading is indicated in Table 4.5. The load–deflection curves are shown and compared in Figure 4.27.

4.6.4.1 Strength. Beam Z42-FD has been found to exhibit the highest loading capacity with an ultimate load of 60.0 kips, which gets a 20.6 kips increase as compared with the 39.4 kips loading capacity of the control beam Z42-FC. Beam Z42-F90 and beam Z42-FU fall behind beam Z42-FD with an increase of 18.5 kips; and 18 kips, respectively. The overall increases of ultimate loads for all CFRP strengthened beams are very close to each other, despite their different configurations.

Table 4.5 Experimental Results of the Beams in Group 4

Beam Designation	Load P at Ultimate (kips)	Central Deflection at Ultimate (in.)	CFRP Shear Capacity (kips)	CFRP Failure Mode
Z42-FC	39.4	0.1182	—	Shear Diagonal Cracking
Z42-F90	57.9	0.1269	9.3	Fabrics Delamination
Z42-FD	60.0	0.1294	10.3	Fabrics Delamination
Z42-FU	57.4	0.1381	9.0	Fabrics Delamination

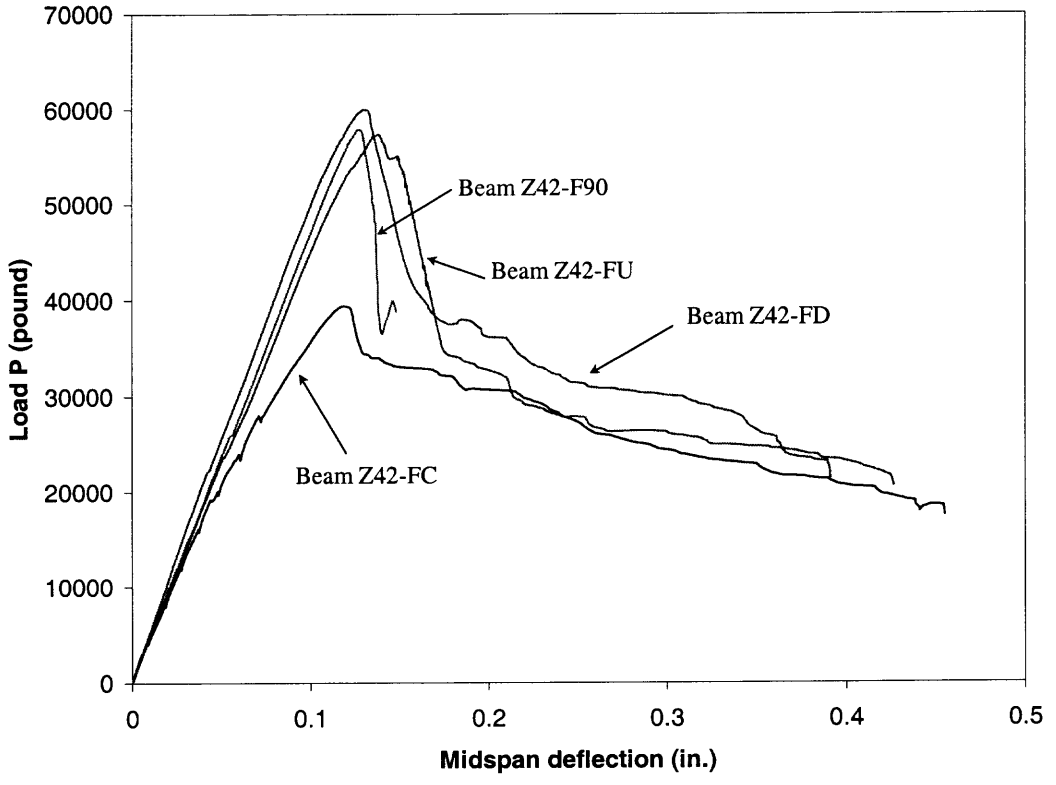

Figure 4.27 Load-deflection curves of beams in Group 4.

4.6.4.2 Ductility. Beams Z42-FU, Z42-FD and Z42-F90 show deflections at ultimate loads to be 0.1381in., 0.1294 in. and 0.1269in., respectively. All three CFRP reinforced beams have very close values of deflection at their ultimate loads.

From Figure 4.27, it can also be observed that for all beams in this group, the loads decrease at a much slower rate after a sudden drop at the peak, while the deflections continue to increase in the mean time. This is a similar phenomenon that is found for beams in group 2. In this group, the strengthened beam give only some improvement in ductility as compared to the control beam.

4.6.4.3 Failure Mechanism. The failure of beam Z42-FC is due to the propagation of the inclined shear crack and is also a "shear compression" failure as well. The failure mode for beam Z42-F90 has been a combination of propagation of inclined crack through the compressive region and delamination of CFRP fabrics in a double triangle pattern. The failure of beam Z42-FD is due to the "shear compression" failure and partial delamination of CFRP fabrics across the inclined crack. Beam Z42-FU has similar failure mode to beam Z42-FD, except that the concrete crushing is more severe and the non-anchorage end of the CFRP has been delaminated completely in a triangle shape. There is a very small percentage of CFRP rupture at the lower corner of the beam as well.

4.7 Parameter Study

The parameter study has been carried out herein to investigate the variation of shear strength with respect to several important factors involved in this experiment.

4.7.1 Shear Span to Effective Depth Ratio a/d

Since two types of CFRP material were used in this experiment, a/d ratio effect will be studied accordingly. A comparison has been made between the beams in group 1 and group 2. The same comparison has also been studied between the beams in group 3 and group 4.

4.7.1.1 a/d Effect on Deep Beams with CFRP Strips. The only difference between the beams in group 1 and group 2 is the loading condition. The four lines in Figure 4.28 show the variation of the shear strength with respect to the shear span to depth a/d ratio. Each line stands for different beam configuration. Line Z-SC means the variation of the shear strength of the control beam with respect to a/d ratio; line Z-S0 represents the variation of the shear strength of the beam with 0 degree CFRP strip reinforcement with respect to a/d ratio; line Z-S90 denotes the variation of the shear strength of the beam with 90 degree CFRP strip reinforcement with respect to a/d ratio; line Z-S45 shows the variation of the shear strength of the beam with 45 degree CFRP strip reinforcement with respect to a/d ratio.

All of the lines in Figure 4.28 indicate that as the a/d ratio gets lower, the shear strength of the deep beam gets higher at various rates. Line Z-S0 has the highest increase rate among the four lines in Figure 4.28 as a/d ratio decreases, which demonstrates the importance of the longitudinal shear reinforcement in deep beams, especially for those with short shear spans.

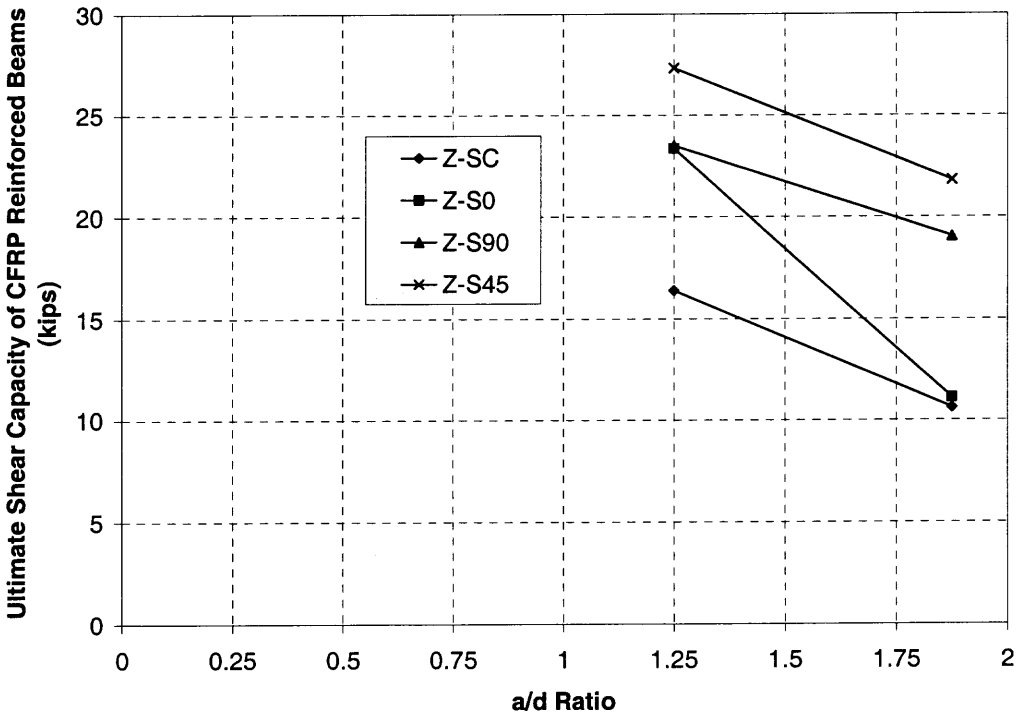

Figure 4.28 Variation of ultimate shear strength of CFRP strip reinforced beams with respect to a/d ratio.

Figure 4.29 shows the variation of the shear contribution of various CFRP reinforcement with respect to the a/d ratio. Line Z-S90 and Z-S45 show that the shear contributions of CFRP strip with 90-degree and 45-degree orientation increases while

a/d ratio increases. However, the shear contribution of CFRP strip with 0-degree (longitudinal) orientation decreases as a/d ratio increases. It can be concluded that in deep beams, the contribution of longitudinal and vertical CFRP strip shear reinforcement varies as the shear span changes. This behavior is very similar to the deep beams with regular steel shear reinforcement.

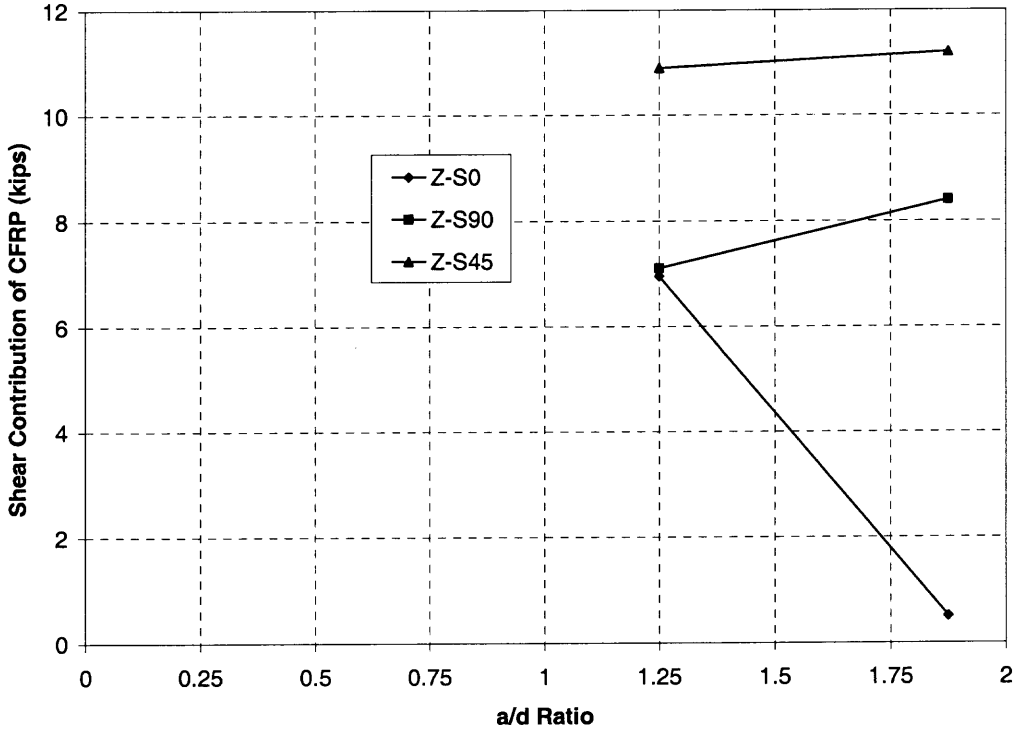

Figure 4.29 Variation of CFRP strip shear contribution with respect to a/d ratio.

4.7.1.2 a/d Effect on Deep Beams with CFRP Fabrics. The four lines in Figure 4.30 show the variation of the shear strength with respect to the shear span to depth a/d ratio. Each line is plotted for different beam configuration. Line Z-FC represents the variation of the shear strength of the control beam with respect to a/d

ratio; line Z-F90 means the variation of the shear strength of the beam with 90-degree CFRP fabrics reinforcement with respect to a/d ratio; line Z-FD denotes the variation of the shear strength of the beam with both 0-degree and 90-degree CFRP fabrics reinforcement with respect to a/d ratio; line Z-FU indicates the variation of the shear strength of the beam with U-shaped CFRP fabrics reinforcement with respect to a/d ratio.

Similar to beams with CFRP strip reinforcement, the shear strength of the deep beams with CFRP fabrics reinforcement also increases as the a/d ratio decreases. It is discovered that when $a/d = 1.875$, the beam with U-shaped CFRP wrap has the highest shear strength among the three CFRP fabrics shear strengthened beams, but its shear strength becomes lowest among the three when $a/d = 1.25$. Figure 4.31 shows the variation of the shear contribution of CFRP fabrics of various configurations with respect to the a/d ratio. Line Z-F90 and Z-FD shows that the shear contributions of one layer CFRP fabrics with 90-degree orientation and double layers with both 0-degree and 90-degree orientations decrease as a/d ratio increases. However, the shear contribution of CFRP fabrics with U-shaped wrapping scheme increases as a/d ratio increases. The double-layered CFRP strengthened beam is the most effective when $a/d = 1.25$, but is behind of beam with U-shaped wrap when $a/d = 1.875$. It can be concluded that in deep beams with CFRP fabrics as shear reinforcement, the anchorage from the CFRP U-shaped wrap becomes less effective as the shear span of the deep beam decreases. Meanwhile, the double-layered CFRP becomes more effective as the shear span of the deep beam decreased.

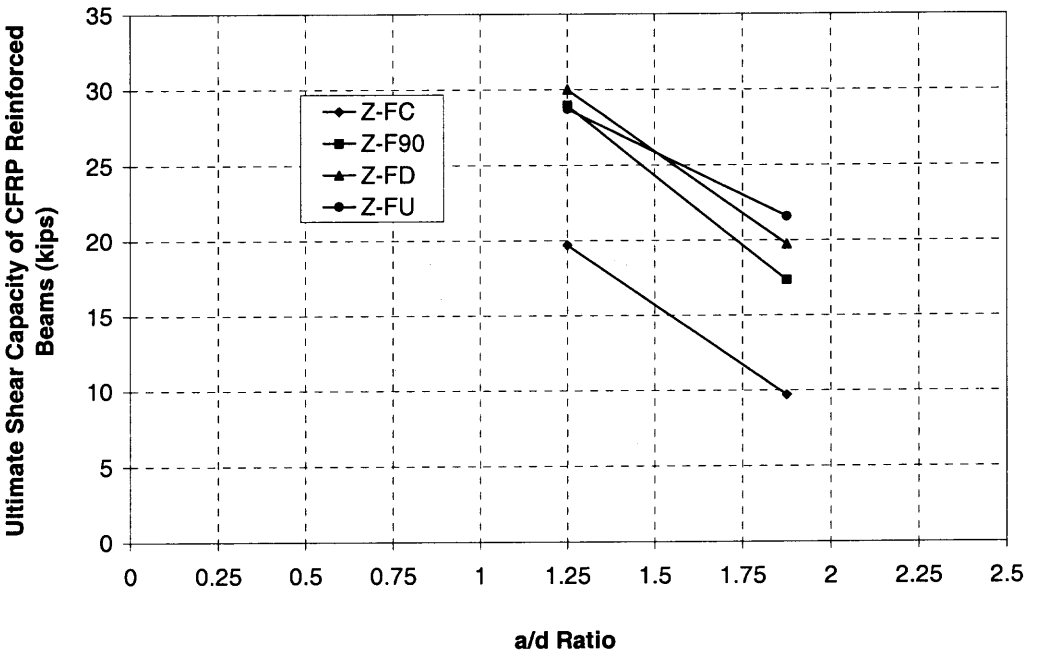

Figure 4.30 Variation of ultimate shear strength of CFRP fabrics reinforced beams with respect to a/d ratio.

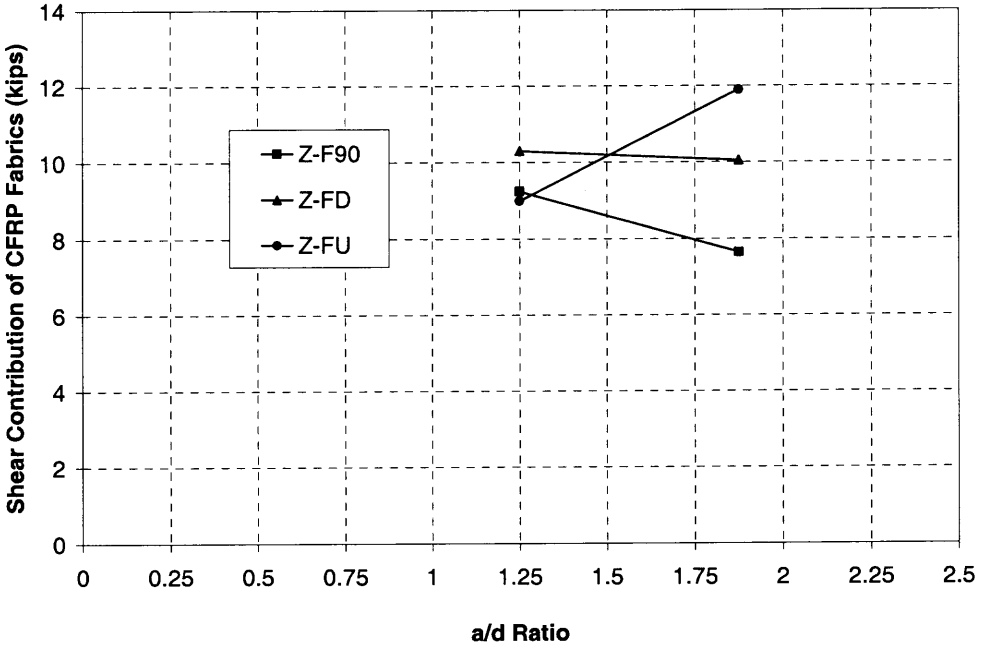

Figure 4.31 Variation of CFRP fabrics shear contribution with respect to a/d ratio.

Unlike regular beams with large shear span to effective depth ratio, deep beams with small shear span to effective depth ratio depend more on longitudinal reinforcement in shear strengthening. In this research, the shear strength of deep beams with CFRP strip shear reinforcement at 0, 45 and 90 degree orientations with respect to the longitudinal beam axis has been chosen for studying their effect.

4.7.2 CFRP Fiber Orientation

The shear contributions of CFRP strips with respect to the angle between the CFRP orientation and beam longitudinal axis are plotted in Figure 4.32. Polynomial regression line has been given for each data set at different shear span to effective depth ratio. It should be noted that the regression lines generated from three data points might not precisely describe the value of the CFRP shear contribution at various angles. However, these regression curves do give us a picture of the trend of the CFRP shear contribution. The maximum value of CFRP shear contribution occurs when the angle is between 0 and 90 degrees, depending on a/d ratio.

When $a/d = 1.875$, the shear contribution of CFRP strips reaches its maximum at an angle of approximately 58 degrees. CFRP strips at higher orientation angles are more effective in shear strengthening. CFRP longitudinal shear reinforcement in this case only provides some minor increase in shear capacity, whereas the vertical CFRP shear reinforcement provides a significant increase in shear strength.

When $a/d = 1.25$, the shear contribution of CFRP strips reaches its maximum at an angle of approximately 45 degrees, and gradually decreases when the angle is below

and above 45 degrees. The longitudinal and vertical CFRP shear reinforcements are equally effective in shear strengthening in this case.

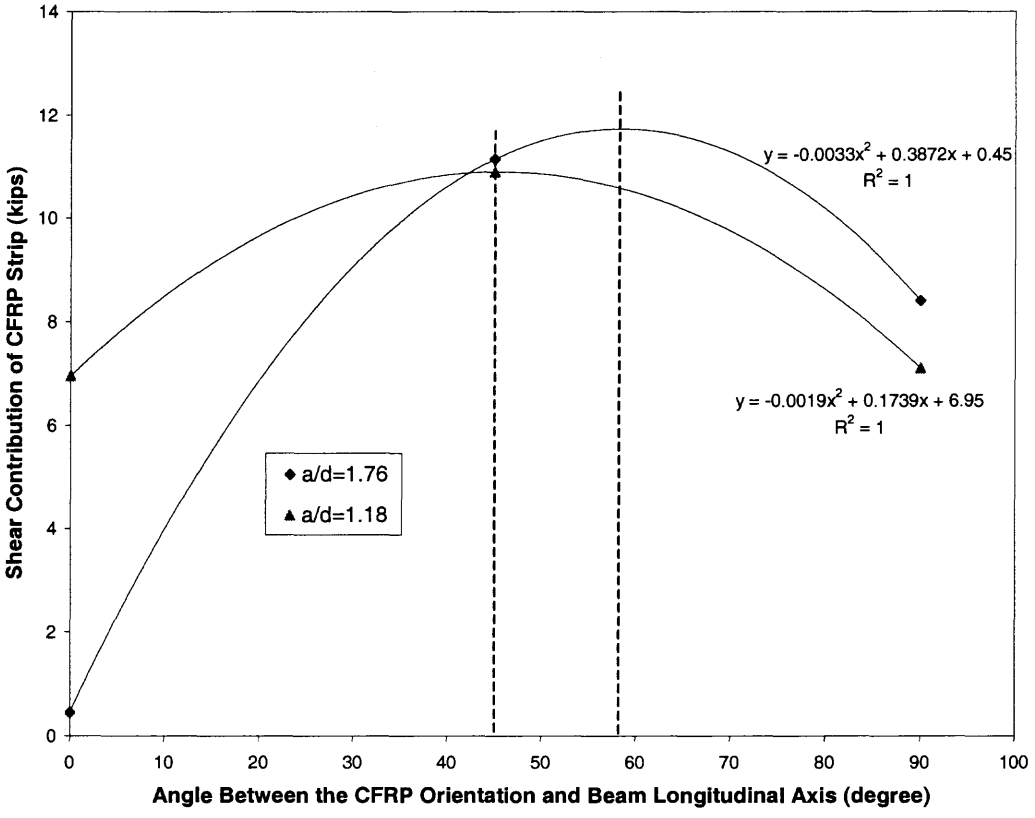

Figure 4.32 Variation of CFRP strip shear contribution with respect to angle between CFRP orientation and beam longitudinal axis.

The reason to explain the behavior as illustrated in Figure 4.32 can be derived from the shear failure mechanism of deep beam with externally bonded CFRP reinforcement. It is assumed that the principal shear crack is developed between the loading point and the left support at an angle α, which is equal to $\tan^{-1}(d/a)$, as shown in Figure 4.33. The principal tensile stress f_t in the diagonal direction, which is at an angle β with beam axis, is perpendicular to the principal shear crack. When the

orientation of the CFRP strips is in the same direction of the principal tensile stress, the tensile stress of the CFRP will reach the maximum value and the CFRP strip shear contribution will also reach the maximum as well.

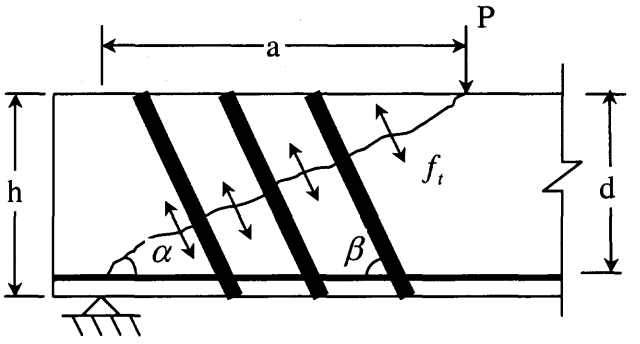

Figure 4.33 Direction of shear cracks and CFRP strips.

Theoretically, 45-degree CFRP strip configuration is most effective in shear strengthening when $a/d = 1$. In order to maximize the effectiveness of the CFRP shear strengthening, the CFRP orientation has to be perpendicular to the direction of the future shear crack, which is mainly determined by a/d ratio for deep beams.

CHAPTER 5

ANALYTICAL STUDY ON SHEAR STRENGTHENING OF DEEP BEAMS USING CARBON FIBER REINFORCED POLYMER LAMINATES

5.1 Introduction

Deep beam has always been a subject of considerable interest in structural engineering practice. A deep beam, generally speaking, is a beam having a depth comparable to the span length. Reinforced concrete deep beams have been used in tall buildings, offshore structures, and foundations, etc. Mostly, deep beams occur as transfer girders, which supports the load from one or more columns, transferring laterally to other columns. Deep beam action also occurs in some walls and in pile caps.

The transition from ordinary beam behavior to deep beam behavior is not precise. As for design purposes, ACI Sec. 10.7.1 (ACI 318-99) specifies "Flexural members with overall depth to clear span ratios greater than 0.4 for continuous spans, or 0.8 for simple spans, shall be designed as deep flexural members taking into account nonlinear distribution of strain and lateral buckling". In another word, deep beam action must be considered when designing for flexure if l_n/d is less than 2.5 for continuous spans or 1.25 for simple spans. ACI Sec. 11.8.1 also specifies that deep beam actions must be considered when designing for shear if l_n/d is less than 5.0 and the load is applied at the top or compression face. Obviously, deep beam action for shear design and flexure design has different requirements. Special shear requirements are needed if l_n/d is less than 5.0, but the beam can still be designed for flexure as a "shallow" or a regular beam even if l_n/d exceeds 1.25 or 2.5 for simple or continuously spans, respectively.

As for shear design of deep beams, ACI Sec. 11.8 applies to all beams having l_n/d less than 5.0, including simply supported and continuous beams, no matter how the load is applied. Since the provisions of ACI Sec. 11-8 are based on simply supported beams located at the top face and supported at the bottom face, it may seriously underestimated the strength of continuous beams. Since all loading conditions are included, a regular beam may exhibit deep beam behaviors. For example, a beam with l_n/d ratio of 5.5, under a single concentrated load at d from one of the support, is not a deep beam according to ACI Sec. 11.8.1. However, the short shear span acts as a deep beam and the other part of the beam should be considered as a regular beam. Preferably, the shear span a to the depth d (a/d) should be used to distinguish between a deep beam and an ordinary beam for shear.

The shear span to depth ratio a/d has shown experimentally to be a highly influential factor in establishing shear strength. When factors other than a/d are kept constant, the variation of shear capacity may be illustrated by Figure 5.1 (Edited from Wang and Salmon, 1992) using the results of rectangular beams.

From Figure 5.1, four general categories of failure may be established: (1) Deep beams for both flexure and shear with $a/d < 1$; (2) Deep beams for shear and regular beams for flexure, with a/d ratios from 1 to about 2.5, in which the shear strength exceeds the inclined cracking capacity; (3) Regular beams of intermediate length having a/d ratios from about 2.5 to 6.0, in which the shear strength equals the inclined cracking strength; and (4) Long beams with a/d ratios greater than 6.0, in which flexural strength is less than their shear strength.

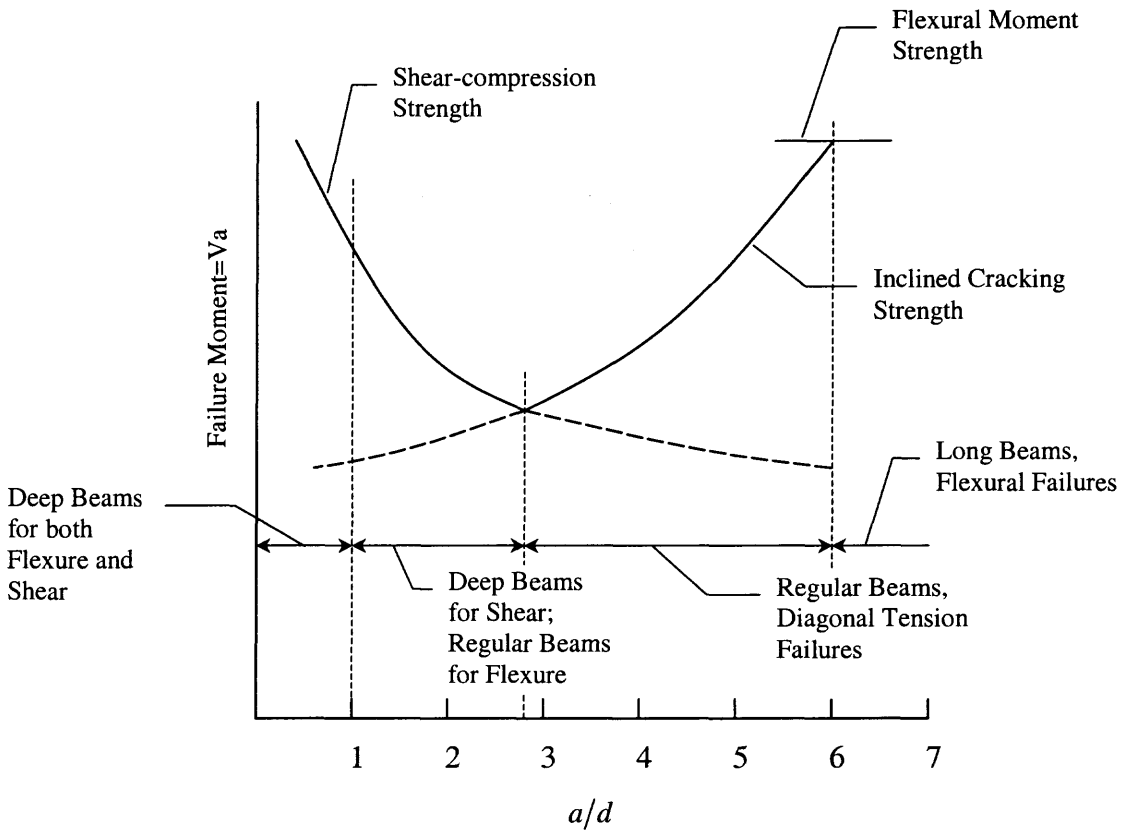

Figure 5.1 Variation in shear strength with a/d for rectangular beams (Edited from "Reinforced Concrete Design", Wang and Salmon, 1992).

5.2 Behavior of Deep Beam

Elastic analysis of deep beams is only meaningful prior to cracking. After cracks develop, major stress redistribution is necessary since there is no tension across the cracks. But the elastic analysis is still valuable because it shows the distribution of stresses that causes cracking and gives guidance to the direction of cracking and the flow of forces after cracking.

In the past, there were two basic approaches to analyze shear problems of reinforced concrete structures. One of them is mechanism method. Current shear

provisions of ACI Code (ACI 318-99) incorporated this method with test results. It actually became more of a semi-empirical approach. The other one is the well-known truss model method. It is generally agreed by the researchers that this method provides a clear concept of how a reinforced concrete beam resists shear after cracking.

The original truss model concept was first introduced to treat shear problems by Ritter (1899) and Morsch (1909) at the beginning of twentieth century. The theory has undergone major developments since it was first introduced. One of the most important breakthroughs was that the concept of the reduction of the compressive strength of the reinforced concrete elements subjected to shear stress was theoretically and experimentally confirmed. Batchelor et al. (1986) found out in order to make the test results of more than 100 deep beams reported in the literature conform with the truss model analysis, a reduction factor from 0.6 to 0.7 has to be applied to the compressive strength $f_c^{'}$ from the standard plain concrete cylinder compression test. This effect has been called the softening of concrete by Robinson and Demorieux (1968). Vecchio and Collins (1989) quantified this phenomenon by proposing a softened stress-strain curve, in which the softening effects depends on the ratio of the two principal strains. Combining equilibrium, compatibility and softened stress-strain relationships, a theory named softened truss model theory was developed which emphasized on the importance of the concrete softening phenomenon. This theory can predict with good accuracy with the test results of various types of reinforced concrete structures subjected to shear. Extensive researches on deep beam had been carried out by Mau and Hsu (1990) and a rigorous analysis and solution algorithm as well as an explicit formula for deep beam shear strength design had been proposed. A comparison of this theory and several other

empirical formulas found in the literature by Mau and Hsu (1987) showed that the explicit formula had the least coefficient of variation.

There are many researches done on shear strengthening of RC beams by externally applied CFRP material in the past, however, none of the researchers has done any experimental studies as well as design recommendations on shear strengthening of deep beams by externally bonded CFRP. Since Mau and Hsu's approach is based on a robust theory analysis and gives very good estimation of shear strength of RC deep beams, the analysis and design of shear strengthening of CFRP reinforced deep beam has been based on this model.

5.3 Modeling of Deep Beams with Externally Applied CFRP Laminates

Consider a simply supported deep beam of a rectangular cross section, with concentrated loads on top as shown in Figure 5.2. Within the shear span a, the beam can be divided into three elements. Each element is specified with a different function to resist part of the applied load. The top element, which includes longitudinal compression steel bars and the concrete above them, is to resist the longitudinal compression resulting from bending. The bottom element, which includes only the longitudinal tension reinforcement, is to resist longitudinal tension resulting from bending. The shear element, which consists of the web reinforcement, including longitudinal and vertical steel reinforcement and externally bonded CFRP reinforcement, both the top and bottom longitudinal steel reinforcement, and the concrete in between, is to resist the sectional shear. It should be noted that the top and the bottom longitudinal steel bars are used to resist the longitudinal

stress due to shear as well as the flexural stress due to bending, and the externally applied CFRP laminates on the left side of the beam are symmetrical to the ones on the right side.

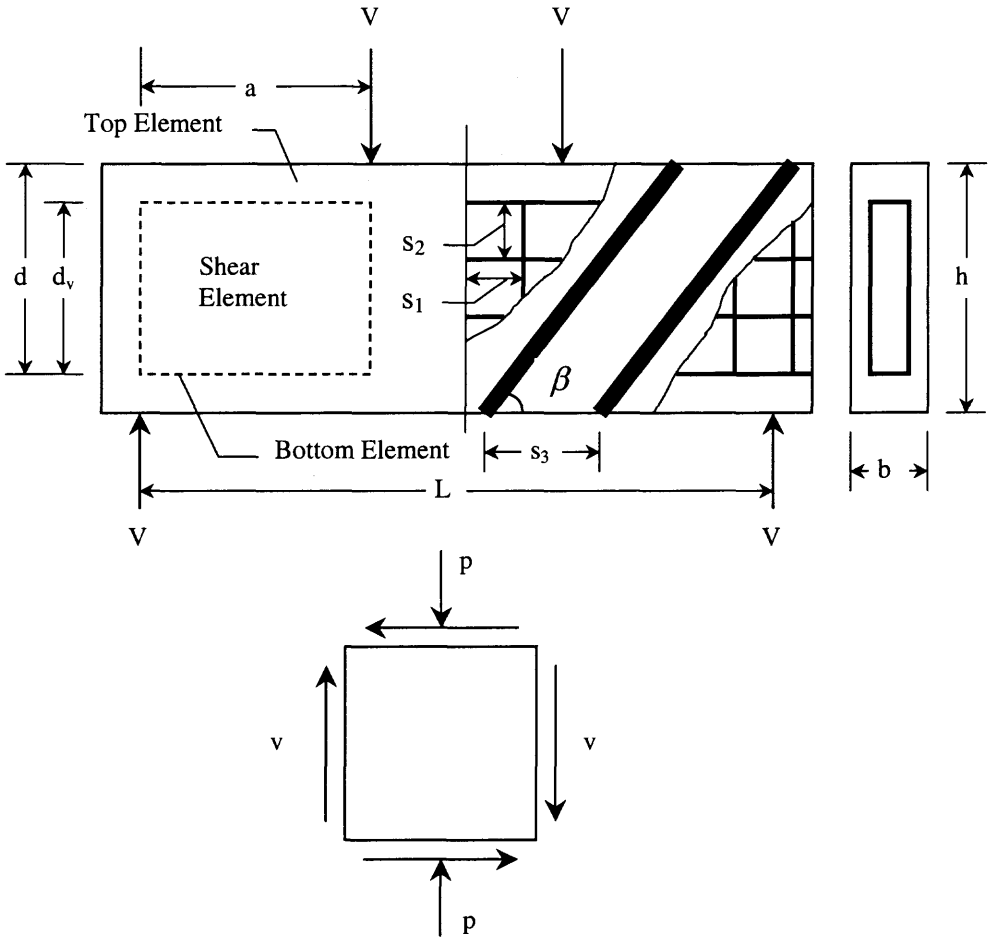

Figure 5.2 Deep beam modeling and stress condition in shear element.

For deep beam shear design, four most important factors must be considered. They are the concrete compressive strength, the amount of longitudinal reinforcement, the amount of transverse reinforcement and shear span to depth ratio a/d, respectively. In fact, it is the shear span to depth ratio a/d that sets apart the deep beam analysis from the regular beam analysis. In order to incorporate a/d ratio into theoretical study and address the special characteristic of deep beams, Mau and Hsu (1990) proposed the

concept of effective transverse compressive stress in the shear element, and gave an estimation of effective transverse compression in terms of a/d. Thus a model of shear element carrying an average shear stress and a transverse compressive stress is given and is illustrated in Figure 5.2. The concept has been thoroughly discussed by Mau and Hsu (1990). However, because of the importance of this concept in deep beam behavior, it will be discussed and given below.

5.4 Effective Transverse Compression

According to Mau and Hsu (1990), for a simply supported deep beam with concentrated load on top, the top load and the bottom support reaction create large compression stresses transverse to the horizontal axis of the beam. Together with the shear stresses, they formed a complicated stress field in the web. The transverse compression stresses are ignored in the case of slender beams because of the relatively long distance between the top and the bottom loading points. However, due to the short shear span of the deep beam (small a/d ratio), the effect of such a transverse compression stress on the shear strength of the web is quite significant and should not be ignored. In fact, such a transverse compression stress is the source of the arch action, which is unique to deep beams.

The distribution of the transverse compression stresses within the shear span is illustrated Figure 5.2. The distribution of transverse compression stresses at mid-height of the beam are sketched in Figure 5.3 for various a/d ratio:

(a) $a/d = 0$: transverse stress is maximum at the line of action and gradually decreases when moving away from it;

(b) $a/d = 0.25$: the maximum transverse stress is located at the center of the shear span, and the magnitude decreases;

(c) $a/d = 0.5$: same pattern as $a/d = 0.25$, except that the maximum transverse stress is located at a larger area and has less magnitude;

(d) $a/d = 1$: the transverse stress at the center of the shear span decreases, the maximum transverse stress occurs at two locations near the two lines of action;

(e) $a/d = 2$: the transverse stress is approaching zero at the center of the shear span and the maximum transverse stress is also decreasing.

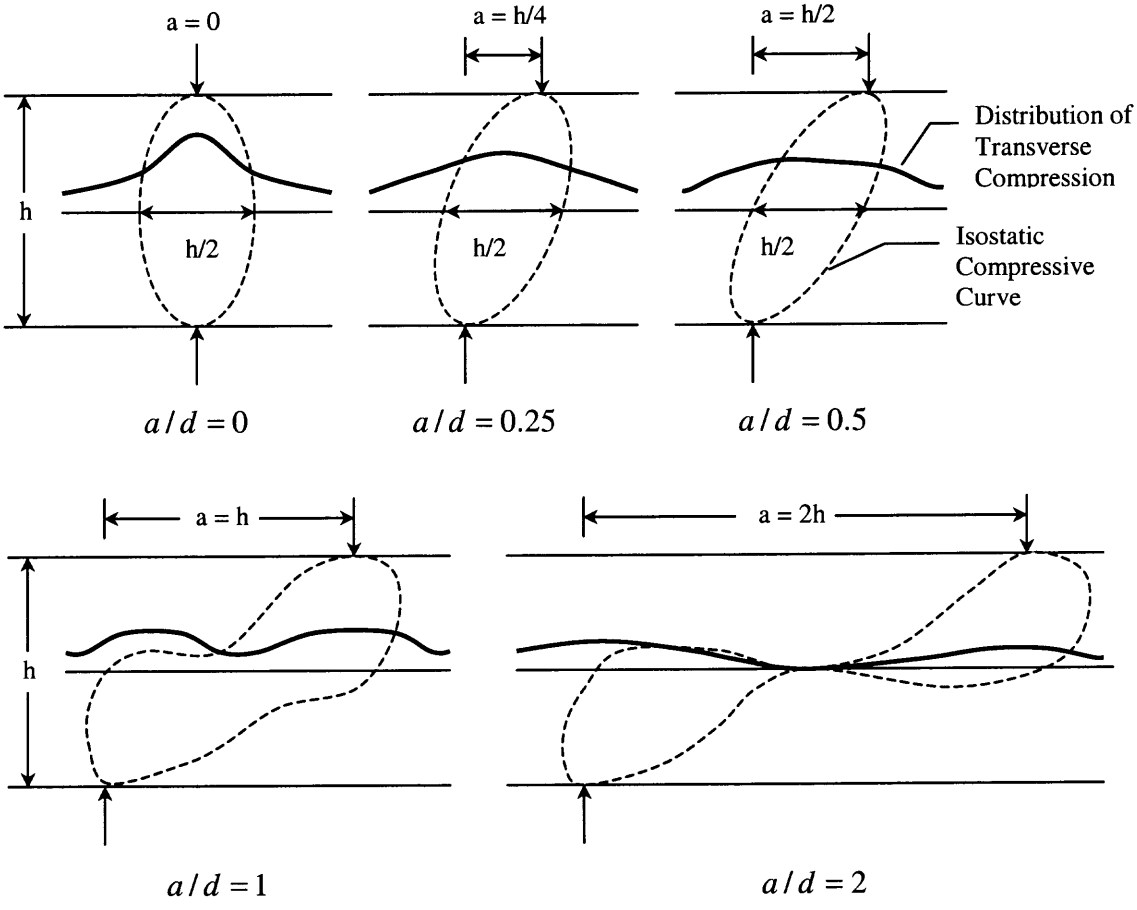

Figure 5.3 Distribution of transverse compressive stress for various shear span ratios (Mau 1990).

The effective transverse compressive stress can now be represented by p, acting evenly across the shear span. The magnitude of p is related not only to shear force V but also to the shear span ratio a/h as well. The equation proposed by Mau and Hsu (1990) is as follows:

$$p = \frac{2V}{bh} \qquad \text{when } 0 \le a/h < 0.5 \qquad (5.1a)$$

$$p = \frac{V}{bh}\left[\frac{4}{3}\left(\frac{h}{a} - \frac{1}{2}\right)\right] \qquad \text{when } 0.5 \le a/h \le 2 \qquad (5.1b)$$

Since the shear stress v can be expressed as:

$$v = \frac{V}{bd_v} \qquad (5.2)$$

The effective transverse stress p can be expressed as a function of v by introducing a constant K:

$$p = K \cdot v \qquad (5.3)$$

Where the parameter K is:

$$K = \frac{2d_v}{h} \qquad \text{when } 0 \le a/h < 0.5 \qquad (5.4a)$$

$$K = \frac{d_v}{h}\left[\frac{h}{a}\left(\frac{4}{3} - \frac{2}{3}\frac{a}{h}\right)\right] \qquad \text{when } 0.5 \le a/h \le 2 \qquad (5.4b)$$

$$K = 0 \qquad \text{when } a/h > 2 \qquad (5.4c)$$

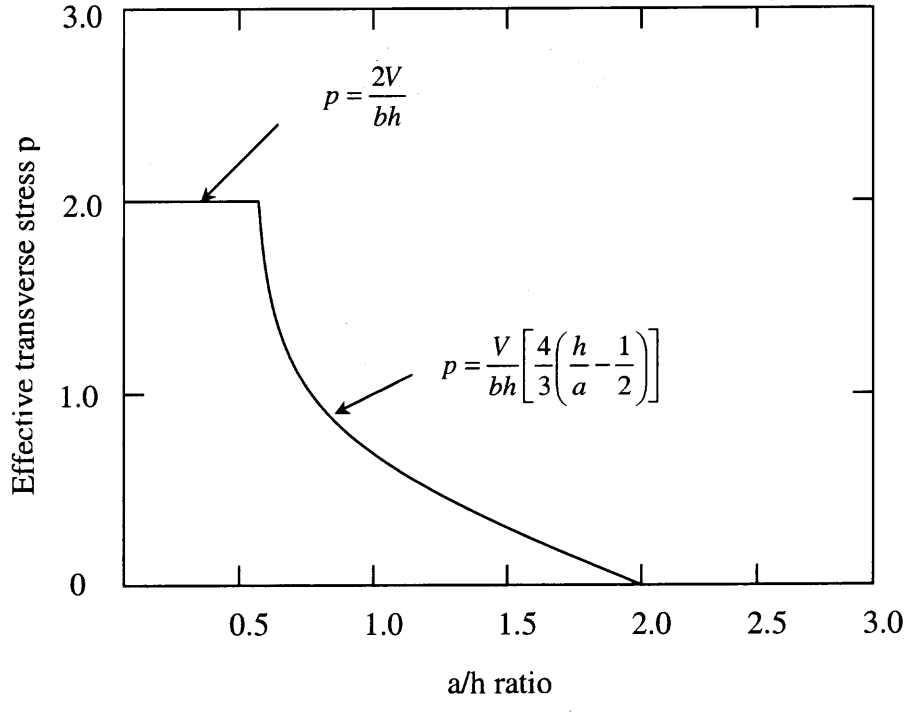

Figure 5.4 Estimation of effective transverse compressive stress (Mau and Hsu 1990).

5.5 Shear Element Modeling

The stress v and transverse compressive stress p of the shear element are jointly resisted by steel reinforcement, concrete and externally bonded CFRP reinforcement (Figure 5.2). Once the diagonal cracks are developed, the concrete struts are subjected mainly to compression and the steel bars and CFRP laminates act as tension links, thus forming a truss action. This is a lower bound solution.

The contribution of steel reinforcements is $\rho_v f_v$ and $\rho_h f_h$ in vertical and horizontal directions, respectively, where ρ_v and ρ_h stand for vertical and horizontal steel reinforcement ratio and f_v and f_h stand for the tensile strength of steel reinforcement. The concrete is assumed to be cracked. The stresses in cracked concrete

may be represented by a principal compressive stress σ_c and a principal tensile stress σ_t, which are perpendicular to each other as shown in Figure 5.5. It should be noted that the tensile stress σ_t carried by the concrete strut is very small. The contribution of CFRP reinforcement is $\rho_{frp} f_{frp}$, where ρ_{frp} stands for CFRP reinforcement ratio and f_{frp} represents the tensile stress of CFRP at failure. The effective tensile stress is used because the tensile strength of CFRP material is very high, and the failure mode of the CFRP strengthened beam will be more likely to be delamination rather than fiber rupture.

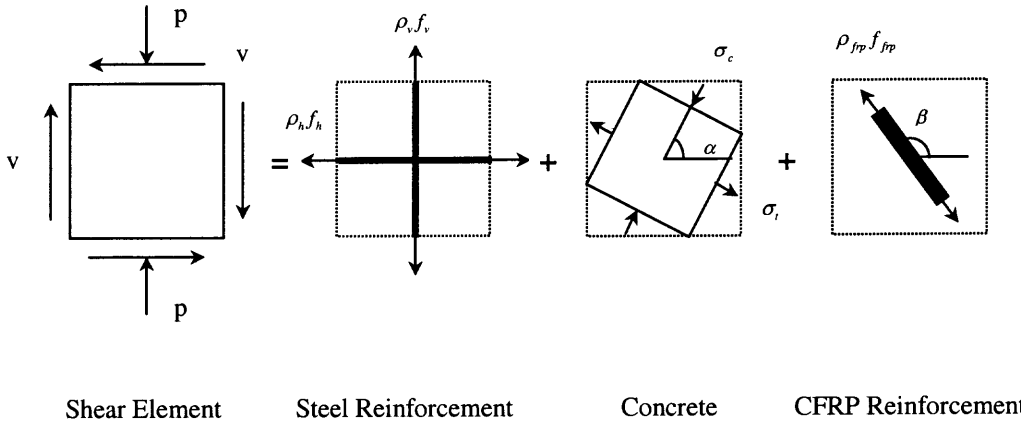

Figure 5.5 Stresses in shear element (Based on Mau and Hsu's (1990) Model).

The formulas for reinforcement ratio ρ_v, ρ_h and ρ_{frp} are:

$$\rho_v = \frac{A_v}{s_v b} \tag{5.5}$$

$$\rho_h = \frac{A_h}{s_h b} \tag{5.6}$$

$$\rho_{frp} = \frac{A_{frp}}{s_{frp} b} \sin\beta \tag{5.7}$$

Where A_v and A_h are the areas of vertical and horizontal steel reinforcements, and A_{frp} is the area of CFRP reinforcement; s_v and s_h are the spacing of vertical and horizontal steel reinforcement, and s_{frp} is the spacing of CFRP reinforcement in the direction of the beam axis; b is the width of the beam; β is the angle starting from the beam axis to the orientation of the CFRP laminates in a counterclockwise direction.

5.6 Design Approach

5.6.1 Development of Proposed Design Equation

Considering the equilibrium of the shear element, the following equations can be obtained by transforming the concrete principal stresses and CFRP tensile stress into horizontal and vertical coordinate system and superimposing them with the tensile stresses of the steel reinforcement.

$$\sigma_c \cos^2 \alpha + \sigma_t \sin^2 \alpha + \rho_h f_h + \rho_{frp} f_{frp} \cos^2 \beta = 0 \tag{5.8}$$

$$\sigma_c \sin^2 \alpha + \sigma_t \cos^2 \alpha + \rho_v f_v + \rho_{frp} f_{frp} \sin^2 \beta = -p \tag{5.9}$$

$$(\sigma_c - \sigma_t)\sin\alpha\cos\alpha + \rho_{frp} f_{frp} \sin\beta\cos\beta = -v \tag{5.10}$$

According to the softened truss model as proposed by Mau and Hsu (1990), the above equations only satisfy equilibrium conditions. In order to satisfy compatibility requirement, the strain transformation based on softened concrete material law and reinforcement material law has to be considered. The solution for the shear capacity of the shear element can be achieved through the numerical method and is rather complicated. However, in Mau and Hsu's (1990) studies on shear strength of deep beams without external CFRP reinforcement, the solution can be attained solely based on the

three equilibrium equations and the results are found to be just as good as the ones using the numerical method. Based on the above reason, only the equilibrium equations will be used at present study to develop the theoretical analysis of CFRP reinforced deep beams for practical design purposes. The concrete softening effect is not considered in the design approach.

Using $\sin^2\alpha+\cos^2\alpha=1$, Equation 5.8 can be changed to

$$(\sigma_c-\sigma_t)\cos^2\alpha=-\sigma_t-\rho_h f_h-\rho_{frp}f_{frp}\cos^2\beta \tag{5.11}$$

Together with Equation 5.3, Equation 5.9 can be rewritten as

$$(\sigma_c-\sigma_t)\sin^2\alpha=-\sigma_t-Kv-\rho_v f_v-\rho_{frp}f_{frp}\sin^2\beta \tag{5.12}$$

Multiplying Equation 5.11 by Equation 5.12, which gives

$$\begin{aligned}&(\sigma_c-\sigma_t)^2\sin^2\alpha\cos^2\alpha=\\&(\sigma_t+Kv+\rho_v f_v+\rho_{frp}f_{frp}\sin^2\beta)(\sigma_t+\rho_h f_h+\rho_{frp}f_{frp}\cos^2\beta)\end{aligned} \tag{5.13}$$

Equation 5.10 can then be rearranged and squared as

$$(\sigma_c-\sigma_t)^2\sin^2\alpha\cos^2\alpha=(\rho_{frp}f_{frp}\sin\beta\cos\beta+v)^2 \tag{5.14}$$

Thus the equilibrium equations can be established from Equation 5.13 and Equation 5.14 and is given below:

$$\begin{aligned}&(\rho_{frp}f_{frp}\sin\beta\cos\beta+v)^2=\\&(\sigma_t+Kv+\rho_v f_v+\rho_{frp}f_{frp}\sin^2\beta)(\sigma_t+\rho_h f_h+\rho_{frp}f_{frp}\cos^2\beta)\end{aligned} \tag{5.15}$$

Rewritten Equation 5.15 as

$$\begin{aligned}&v^2+[2\rho_{frp}f_{frp}\sin\beta\cos\beta-K(\sigma_t+\rho_h f_h+\rho_{frp}f_{frp}\cos^2\beta)]v+\\&\rho^2{}_{frp}f^2{}_{frp}\sin^2\beta\cos^2\beta-(\sigma_t+\rho_v f_v+\rho_{frp}f_{frp}\sin^2\beta)\\&(\sigma_t+\rho_h f_h+\rho_{frp}f_{frp}\cos^2\beta)=0\end{aligned} \tag{5.16}$$

This is a quadratic equation of v. A solution for v can be obtained as

$$v = \frac{1}{2}\left[K\left(\sigma_t + \rho_h f_h + \rho_{frp} f_{frp}\cos^2\beta\right) - 2\rho_{frp} f_{frp}\sin\beta\cos\beta\right] + \frac{1}{2}\sqrt{\left[K\left(\sigma_t + \rho_h f_h + \rho_{frp} f_{frp}\cos^2\beta\right) - 2\rho_{frp} f_{frp}\sin\beta\cos\beta\right]^2 + 4\left[\left(\sigma_t + \rho_v f_v + \rho_{frp} f_{frp}\sin^2\beta\right)\left(\sigma_t + \rho_h f_h + \rho_{frp} f_{frp}\cos^2\beta\right) - \rho^2{}_{frp} f^2{}_{frp}\sin^2\beta\cos^2\beta\right]} \quad (5.17)$$

Assuming the steel bars reach yielding limit and CFRP laminates reach the effective tensile stress, the variables $\rho_v f_v$, $\rho_h f_h$ and $\rho_{frp} f_{frp}$ in Equation 5.17 can be replaced by dimensionless reinforcement index ω as follows

$$\omega_h = \frac{\rho_h f_h}{f_c'} = \frac{\rho_h f_y}{f_c'} \quad (5.18)$$

$$\omega_v = \frac{\rho_v f_v}{f_c'} = \frac{\rho_v f_y}{f_c'} \quad (5.19)$$

$$\omega_{frp} = \frac{\rho_{frp} f_{frp}}{f_c'} = \frac{\rho_{frp} f_{frp\_e}}{f_c'} \quad (5.20)$$

Also $$C = \frac{\sigma_t}{f_c'} \quad (5.21)$$

Equation 5.17 thus becomes

$$\frac{v}{f_c'} = \frac{1}{2}\left[K\left(\omega_h + \omega_{frp}\cos^2\beta + C\right) - \omega_{frp}\sin 2\beta\right] + \frac{1}{2}\sqrt{\left[K\left(\omega_h + \omega_{frp}\cos^2\beta + C\right) - \omega_{frp}\sin 2\beta\right]^2 + 4\left[\left(\omega_v + \omega_{frp}\sin^2\beta + C\right)\left(\omega_{frp}\cos^2\beta + \omega_h + C\right) - \omega^2{}_{frp}\sin^2\beta\cos^2\beta\right]} \quad (5.22)$$

Since the principal tensile stress σ_t carried by the concrete strut is very small, the parameter C given by Equation 5.12 is even smaller. For practical design purposes, parameter C can be treated as zero and thus omitted from Equation 5.22. The updated equation can be expressed as:

$$\frac{v}{f_c'} = \frac{1}{2}\left[K\left(\omega_h + \omega_{frp}\cos^2\beta\right) - \omega_{frp}\sin 2\beta\right] + \frac{1}{2}\sqrt{\left[K\left(\omega_h + \omega_{frp}\cos^2\beta\right) - \omega_{frp}\sin 2\beta\right]^2 + 4\left[\left(\omega_v + \omega_{frp}\sin^2\beta\right)\left(\omega_{frp}\cos^2\beta + \omega_h\right) - \omega^2{}_{frp}\sin^2\beta\cos^2\beta\right]} \quad (5.23)$$

5.6.2 Effective Tensile Stress of CFRP Laminates

As discussed earlier in the regular beam design, a strain (stress) reduction factor R has to be applied to the ultimate tensile strain (stress) of the CFRP laminates. However, in the previous chapter, R is determined by either model calibration or bonding mechanism. For CFRP strengthened deep beams, R will be solely determined by the bonding mechanism between CFRP laminates and surface of the concrete since there are no available test results for calibration.

5.6.3 Validity of the Proposed Design Approach

At experimental study on shear behavior of deep beams with externally bonded CFRP, a total of 16 beams were tested, of which 8 beams were strengthened by CFRP strips (Sika CarboDur) and the other 8 beams were strengthened by continuous CFRP fabrics (SikaWrap Hex 230c). Results of the experimental study indicate that shear span to depth ratio a/d plays a very important role in shear behavior of deep beams strengthened by externally bonded CFRP laminates.

Due to the relatively small size of the beams in this research, the effective transfer length of CFRP laminates is assumed to be 2" (50mm) without anchorage, 3" (75mm) with anchorage. The stress reduction factor R can be obtained by Applying the effective transfer length to Equation 3.32, the effective tensile stress of the bonded CFRP

laminates can be obtained from Equation 3.6. The maximum allowable stress reduction factor R will be set as 0.3 without anchorage, 0.5 with anchorage. The bottoms of the beams wrapped by CFRP laminates are treated as anchorages in this experiment.

The theoretical shear strength of the CFRP strengthened deep beams can be calculated using the following equation

$$V_{theo} = vbd_v \tag{5.24}$$

It is particularly important that the flexural steel reinforcement is included when calculating the shear strength capacity of the longitudinal web reinforcement of the shear element. In a situation where there is no web reinforcement, however, this will likely overestimate the contribution of the flexural reinforcement, especially when there are heavy flexural steel bars present in the deep beam. Thus a factor of 0.5 is applied to the longitudinal reinforcement ratio if there is no web reinforcement. The effective depth of the shear element d_v is the distance from the center of the compression steel reinforcement to the center of the flexural steel reinforcement. The distance between the top of the beam and the top of the shear element is taken as $0.1d$ when no compression steel reinforcement is provided, as suggested by Mau and Hsu (1990).

The theoretical values of the shear strength are calculated based on the proposed formula. The computed results as well as the experimental results are listed in Table 5.1 and Table 5.2. The ratio of the theoretical value to the experimental value is also calculated. It can be seen that the results from the proposed design approach agree with the test results quite well. Most of the values in the table are more than 1, which means that the design approach is on the conservative side. The comparison of the theoretical and experimental results is presented in Figure 5.6. A linear regression line is plotted and

an equation is established between the experimental and theoretical results. A reference line is also given for comparison purposes. It is observed that the reference line is well below the regression line, which means that the design equation gives good yet conservative results. The slope of the regression line, which is 1.0419 from the equation in Figure 5.6, is only a little more than 1. This means that the calculated value of the shear strength tends to get more conservative as the shear strength of the deep beams with CFRP shear reinforcements gets higher.

5.6.4 General Design Equation

In Equation 5.19, steel reinforcement and CFRP reinforcement are the only two types of reinforcement used. Other types of reinforcement may also be used in the retrofitting of deep beams. For web steel reinforcement, the orientation of steel bars is normally horizontal and vertical to the beam axis. However, there is a possibility that the web steel bars may have a certain angel with respect to the beam axis. Thus, a generalized equation is proposed:

$$\frac{v}{f_c'} = \frac{1}{2}\left(K\sum\omega_i\cos^2\beta_i - \sum\omega_i\sin 2\beta_i\right) + \frac{1}{2}\sqrt{\left(K\sum\omega_i\cos^2\beta_i - \sum\omega_i\sin 2\beta_i\right)^2 + 4\left[\left(\sum\omega_i\sin^2\beta_i\right)\left(\sum\omega_i\cos^2\beta_i\right) - \left(\sum\omega_i\sin\beta_i\cos\beta_i\right)^2\right]} \tag{5.25}$$

The orientation of the all reinforcement now is denoted by angle β_i, which starts from the beam longitudinal axis to reinforcement longitudinal axis in a counterclockwise direction. The reinforcement index for various types of reinforcement is denoted by ω_i

$$\omega_i = \frac{\rho_i f_i}{f_c'} \tag{5.26}$$

Table 5.1 Experimental and Computed Results

	Beam Designation	Loading Condition	Shear Span (in.)	f_c' (psi)	b (in.)	h (in.)	d (in.)	d_v (in.)
Group 1	Z11-SC	1 point	15	6173	4	9	8	7.2
	Z11-S0	1 point	15	6173	4	9	8	7.2
	Z11-S45	1 point	15	6173	4	9	8	7.2
	Z11-S90	1 point	15	6173	4	9	8	7.2
Group 2	Z22-SC	2-point	10	6173	4	9	8	7.2
	Z22-S0	2-point	10	6173	4	9	8	7.2
	Z22-S45	2-point	10	6173	4	9	8	7.2
	Z22-S90	2-point	10	6173	4	9	8	7.2
Group 3	Z31-SC	1 point	15	6176	4	9	8	7.2
	Z31-S90	1 point	15	6176	4	9	8	7.2
	Z31-SD	1 point	15	6176	4	9	8	7.2
	Z31-SU	1 point	15	6176	4	9	8	7.2
Group 4	Z42-SC	2-point	10	6176	4	9	8	7.2
	Z42-S90	2-point	10	6176	4	9	8	7.2
	Z42-SD	2-point	10	6176	4	9	8	7.2
	Z42-SU	2-point	10	6176	4	9	8	7.2

Table 5.2 Experimental and Computed Results

Beam Designation	R	K	ω_h	ω_v	ω_{frp}	β (degree)	V_{theo} (kips)	V_{exp} (kips)	$\frac{V_{exp}}{V_{theo}}$
Z11-SC	N/A	0.107	0.148	0.016	0	0	9.6	10.5	1.09
Z11-S0	0.0492	0.107	0.148	0.016	0.0170	0	10.4	11.1	1.07
Z11-S45	0.0492	0.107	0.148	0.016	0.0537	135	21.5	21.8	1.01
Z11-S90	0.0492	0.107	0.148	0.016	0.038	90	16.4	19	1.16
Z22-SC	N/A	0.427	0.148	0.024	0	0	16.4	16.3	0.99
Z22-S0	0.0492	0.427	0.148	0.024	0.017	0	18.0	23.2	1.29
Z22-S45	0.0492	0.427	0.148	0.024	0.0537	135	29.5	27.3	0.93
Z22-S90	0.0492	0.427	0.148	0.024	0.038	90	22	23.5	1.07
Z31-FC	N/A	0.107	0.148	0.016	0	0	9.6	9.7	1.01
Z31-F90	0.3	0.107	0.148	0.016	0.044	90	17.3	17.2	0.99
Z31-FD	0.3	0.107	0.148	0.016	0.044	90, 0	20.1	19.7	0.98
Z31-FU	0.3	0.107	0.148	0.016	0.073	90	20.7	21.6	1.04
Z42-FC	N/A	0.427	0.148	0.024	0	0	16.4	19.7	1.20
Z42-F90	0.3	0.427	0.148	0.024	0.044	90	22.8	28.9	1.27
Z42-FD	0.3	0.427	0.148	0.024	0.044	90, 0	27.4	30	1.09
Z42-FU	0.3	0.427	0.148	0.024	0.073	90	26.0	28.5	1.10

Where i denote each type of reinforcement at a certain orientation with respect to the beam axis. ρ_i is defined as

$$\rho_i = \frac{A_i}{s_i b} \sin \beta_i \tag{5.27}$$

Thus, as long as the effective stresses of all types of reinforcement at failure are identified, the shear stress of the deep beam can be determined by Equation 5.25.

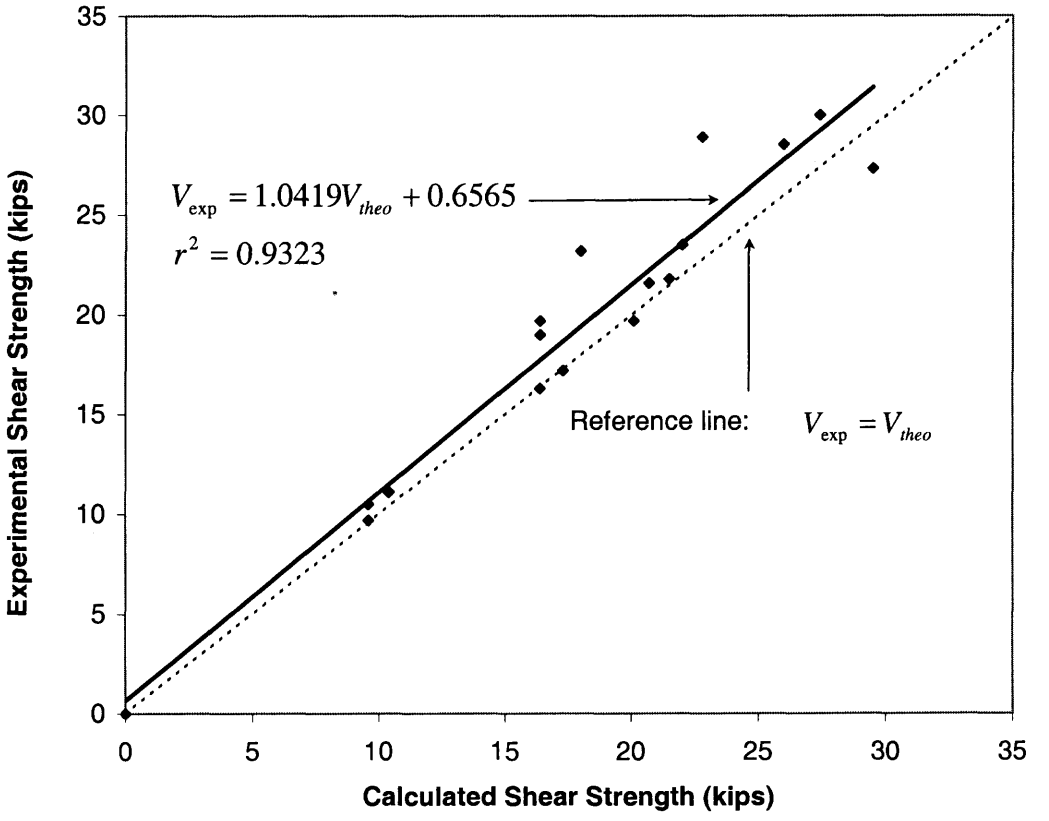

Figure 5.6 Comparison of experimental and calculated shear strength.

CHAPTER 6

BEHAVIOR OF REPAIRED SHEAR-DAMAGED BEAM USING CARBON FIBER REINFOECED POLYMER LAMINATES

6.1 Introduction

The research described from Chapter 2 to Chapter 5 mainly deals with CFRP shear strengthening of beams with shear deficiency but without shear cracks prior to the application of the CFRP laminates. The results of the loading tests show that the beams with CFRP shear strengthening have greatly improved the shear behavior in general. In engineering field where retrofitting of structural members is heavily practiced, the beams that need to be repaired may or may not have shear cracks developed prior to the repair, depending the actual loading conditions. If shear cracks have already developed, special treatment has to be employed before attaching CFRP laminates to the concrete beams.

This chapter is therefore studying the behavior of repaired shear-damaged RC beams using CFRP. Four beams, which include one regular beam and three deep beams, are used here for studying CFRP shear repairing. Control Beam ZC4 in chapter 2, control beams Z11-SC, Z22-SC and Z31-FC in chapter 3 all have previously developed shear cracks, which makes them ideal specimens for shear repairing. Beam Z42-FC in chapter 4 has not been used for this study due to the fact that the beam has been severely damaged during the load test and the repair technique used in this research is not suitable for this beam.

The CFRP configuration for each beam is to design the same configuration of the most effective CFRP strengthened beam in that group. For example, the repaired control beam ZC4, named as Z4-R45, has the same CFRP configuration as beam Z4-45, which is

the strongest beam in the 4-foot regular beam category. The other three repaired beams, named as Z11-SR45, Z22-SR45 and Z31-FRU follow the same configurations as beam Z11-S45, Z22-S45 and Z31-FU, respectively. A comparison has been made for the repaired beam, the control beam and the beam with same CFRP configuration but no shear crack. The effectiveness of the shear repair will be evaluated and a conclusion will be made based on the test results and their comparisons.

6.2 Experimental Program

6.2.1 Materials

The only different material used in the repair was SikaDur 35 Hi-Mod LV, which was used to fill up the shear cracks before bonding CFRP laminates to the beam surface. SikaDur 35 Hi-Mod LV is a two-component, solvent free, moisture-insensitive, low-viscosity, high-strength, multipurpose epoxy resin adhesive, according to Sika Corp. It consists of two components, which will be mixed at a 2:1 ratio by volume before use. It has a pot life of 25 min. after mixing. Mix only that quantity that can be used within its pot life. SikaDur 35 Hi-Mod LV is not applicable for cracks greater than 6mm.

The tensile strength of and the modulus of elasticity of SikaDur 35 Hi-Mod LV after 14 days are 58 MPa and 2.8 GPa, respectively.

The properties of the CFRP laminates and epoxy used for the bonding are described in Chapter 2.

6.2.2 Repair Procedure

The dust and laitance on the surface of the concrete were cleaned to provide an open roughened texture. The beams were laid on one side so gravity feed could be used to fill up the cracks. Proportion 1 part component B to 2 parts component A by volume were mixed thoroughly for approximately three minutes until they were uniformly blended. The mixed epoxy was poured into the crack until it was completely filled. The underside of the beams was sealed to prevent the epoxy from running through.

The actual bonding of CFRP to the beam was the same as the regular beam described earlier in Chapter 2.

6.2.3 Test Procedure

The procedure for testing the repaired beams is the same as the regular beams and deep beams reported in Chapters 2 and 4.

6.2.3.1 Beam ZC4-R45. As the beam was loaded, no flexural or shear cracks were observed until the load reached 20 kips. The epoxy-filled shear crack as well as the CFRP strip across the crack was still intact when a small shear crack was observed on the other side of the beam where there was no previously developed flexural and shear cracks before the loading. The shear crack continued to grow until the load reached 26.9 kips. Popping sound and CFRP delamination were observed as the beam started to fail. The epoxy-filled shear crack was still the same as it was before the loading. The CFRP strip across the epoxy-filled shear crack did not experience any delamination either.

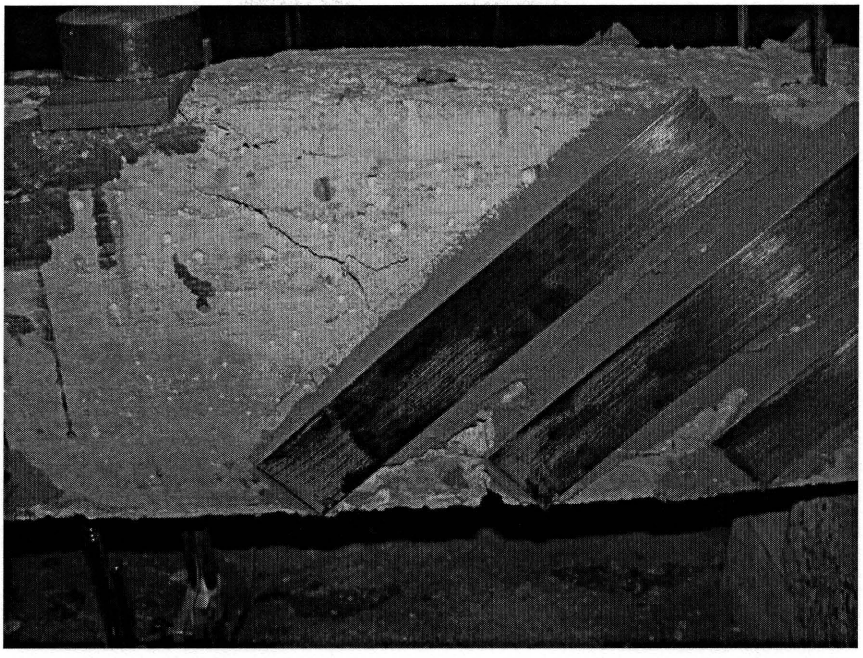

Figure 6.1 Failure of Beam ZC4-R45.

6.2.3.2 Beam Z11-SCR45. This beam had previously developed shear cracks on both left and right sides of the beam. Although these cracks extended all the way from the bottom to the top, they were very tiny in width and almost invisible. Epoxy was not used to inject into the cracks due to small size of the cracks.

No more cracks or flexural cracks were observed during the initial loading process. When the load approached 30 kips, the shear cracks on right side of the beam developed wider cracks, while the cracks on the other side of the beam seemed to remain unchanged. When the load approached 35 kips, the beam suddenly dropped to 32.5 kips due to its crack propagation and delamination of one of the CFRP strips. Then it picked up the load a little bit and continued to increase until the beam failed at the maximum load of 37.2 kips. The shear cracks and the CFRP delamination resulting from the failure only occurred on right side of the beam.

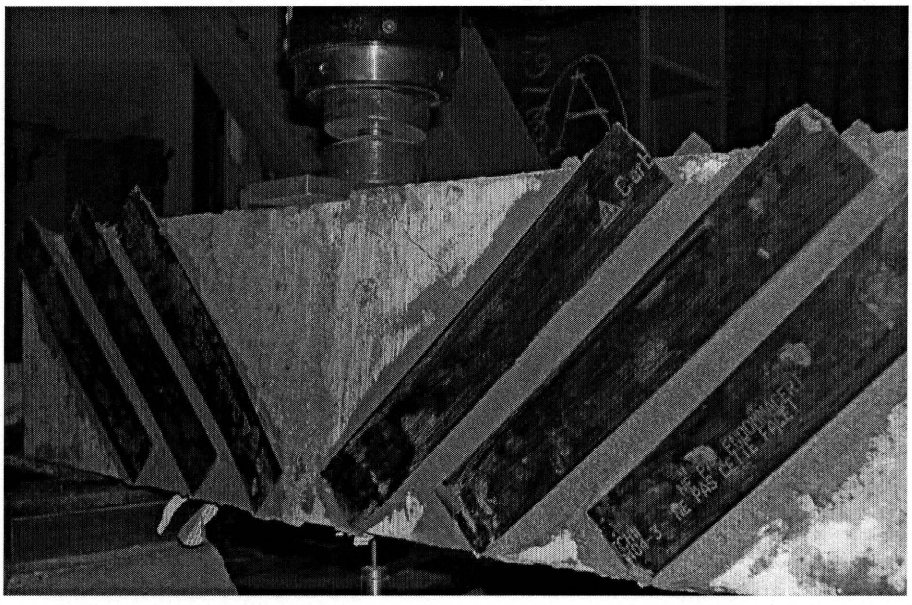

Figure 6.2 Failure of Beam Z11-SCR45.

6.2.3.3 Beam Z22-SCR45. The previous shear crack, which was located only at the left side of the beam, was the largest among the four beams, but its width was still less than 6 mm, which was the largest width allowed for the epoxy injection method to be used in this research.

The first shear crack was observed when the load reached about 42 kips. Another crack developed when the beam was loaded to about 50 kips. The beam failed at a maximum load of 60 kips, resulting from the shear crack propagation and the delamination of the CFRP strips. The delamination underneath the concrete surface was more like the concrete block attached by CFRP being dislodged from the beam. Similar to beam ZC4-R45, beam Z11-SCR45 failed in shear from the newly developed crack, rather than the previously-developed-then-repaired shear cracks.

Figure 6.3 Failure of Beam Z22-SCR45.

6.2.3.4 Beam Z31-FCRU. The previously developed shear crack, which was located at the right side of the beam, was covered by the U-shaped CFRP wraps.

Since both sides of the beams were covered by CFRP fabrics, neither shear cracks nor flexural cracks were observed during the loading process prior to the failure of the beam. However, fainted cracking sound was heard as the load approached 35 kips, which indicated that a small fraction of delamination might be developed under the cover of the CFRP fabrics. The beam failed at an ultimate load of 48.2 kips, resulting from the shear crack propagation and the CFRP fabrics delamination underneath the concrete surface. Partial fiber rupture was also observed at the lower corner of the beam. The shear crack

and the delamination were located at the left side of the beam, the opposite of where the previously developed shear crack was.

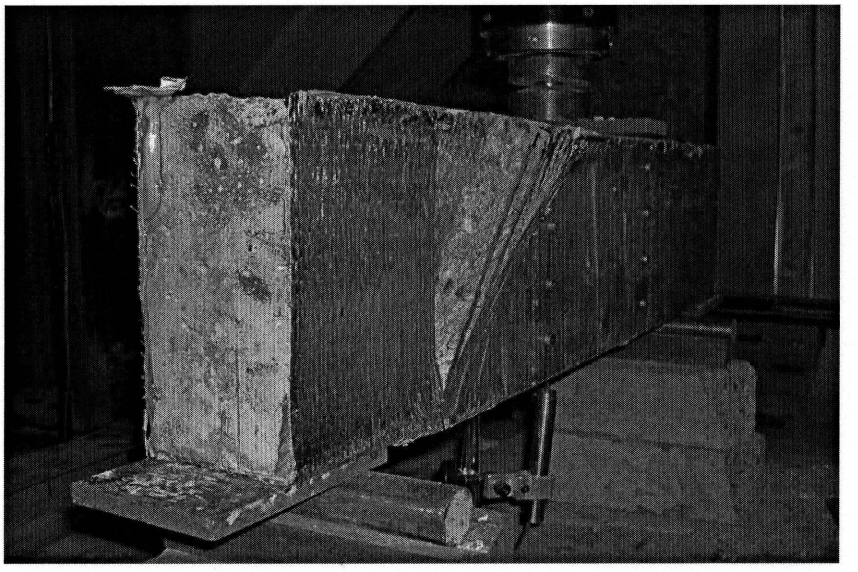

(a) Side view of the failure section

(b) Close-up view of the failure section

Figure 6.4 Failure of Beam Z31-FCRU.

6.2.4 Analysis of Test Results

6.2.4.1 Beam ZC4-R45. The experimental result of beam ZC4-R45 and its comparison with the results of beam ZC4 and ZC4-45 are summarized in Table 6.1 and Figure 6.5. Although it is not as strong as beam Z4-45, beam ZC4-R45 does show some increase in shear strength. There is a 6.2 kips increase in failure load, or 3.1 kips increase in shear capacity, which is a 30% increase as compared with beam ZC4. Beam Z4-45 offers an 80% increase in shear capacity as compared with beam ZC4. The central deflection of beam ZC4-R45 at the ultimate load is even less than the deflection of control beam ZC4. Beam Z4-45, the original beam with 45 degrees CFRP configuration, still posseses the highest shear strength and the largest central deflection at failure.

Table 6.1 Test Result of Beam ZC4-R45 and Comparison with Other Beams

Beam Designation	Load P at Ultimate (kips)	Central Deflection at Ultimate (in.)	CFRP Shear Capacity (kips)	CFRP Failure Mode
ZC4	20.7	0.1877	N/A	Shear Diagonal Cracking
Z4-45	37.2	0.9381	8.3	Strip delamination
ZC4-R45	26.9	0.1644	3.1	Strip delamination

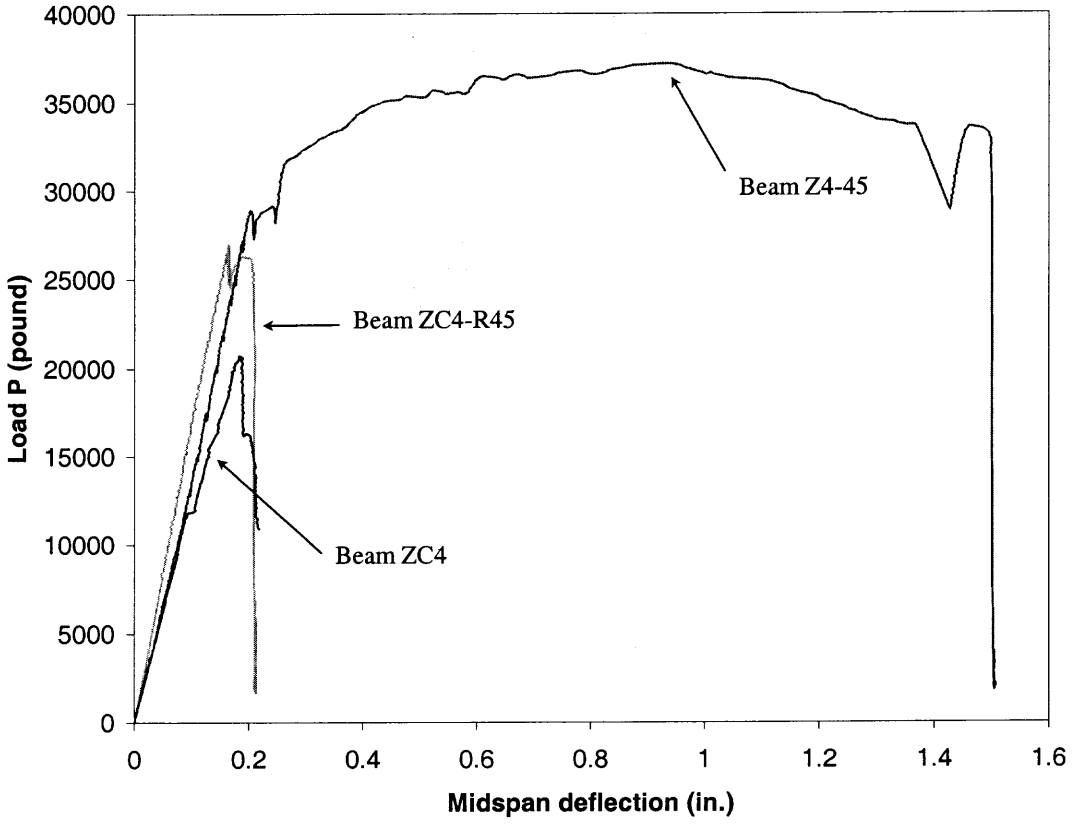

Figure 6.5 Load-deflection curve of beam ZC4-R45 and comparison with other beams.

6.2.4.2 Beam Z11-SCR45. The experimental result of beam Z11-SCR45 and its comparison with the results of beam Z11-SC and Z11-S45 are summarized in Table 6.2 and Figure 6.6. As described earlier, there is no SikaDur 35 filled in the shear crack for beam Z11-SCR45 before bonding of the CFRP strips. The failure load of beam Z11-SCR45 is 37.2 kips, which is 75% increase in load carrying capacity as compared with the control beam Z11-SC. Beam Z11-S45 increases 22.3 kips, which is 105% more that the control beam Z11-SC. As compared with the 168% increase by beam Z11-S45, the central deflection of beam Z11-SR45 gets increased only 69%. The repair however still

improves the performance of the beam in terms of strength and ductility. However, it is still not as good as the original beam with CFRP reinforcement.

Table 6.2 Test Result of Beam Z11-SCR45 and Comparison with Other Beams

Beam Designation	Load P at Ultimate (kips)	Central Deflection at Ultimate (in.)	CFRP Shear Capacity (kips)	CFRP Failure Mode
Z11-SC	21.3	0.0709	N/A	Shear Diagonal Cracking
Z11-S45	43.6	0.1897	11.2	Strip delamination
Z11-SCR45	37.2	0.1198	8.0	Strip delamination

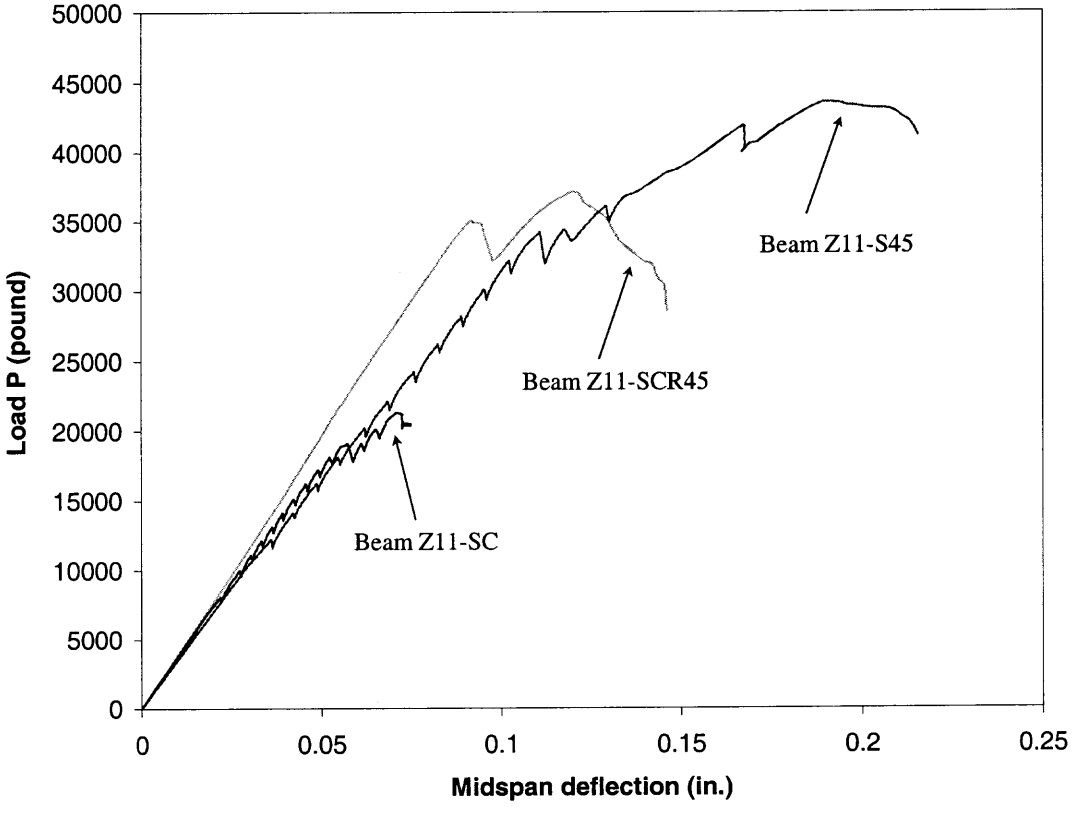

Figure 6.6 Test result of Beam Z11-SCR45 and comparison with other beams.

6.2.4.3 Beam Z22-SCR45. The experimental result of beam Z22-SCR45 and its comparison with the results of beam Z22-SC and Z22-S45 are summarized in Table 6.3 and Figure 6.7.

The repaired beam Z22-SCR45 develops a failure load of 60 kips, which is the largest failure load among the three beams. The increase in load carrying capacity is 83% as compared with the control beam Z22-SC. Beam Z22-SCR45, the original beam with CFRP reinforcement, has an increase of 66% in failure load. The deflection of beam Z22-SCR45 at the ultimate load is also the highest among the three beams. Due to the limitation of the data acquisition used in the experiment, the data was unable to be collected when the load suddenly dropped to 50 kips. However, the beam did not fail immediately right after the load drop. Very good ductility has been observed after the peak load, although there was no data to support this observation. In conclusion, the repaired beam Z22-SCR45 shows a significant increase in strength and ductility.

Table 6.3 Test Result of Beam Z22-SCR45 and Comparison with Other Beams

Beam Designation	Load P at Ultimate (kips)	Central Deflection at Ultimate (in.)	CFRP Shear Capacity (kips)	CFRP Failure Mode
Z22-SC	32.8	0.0696	N/A	Shear Diagonal Cracking
Z22-S45	54.6	0.1005	10.9	Strip delamination
Z22-SCR45	60.0	0.1222	13.6	Strip delamination

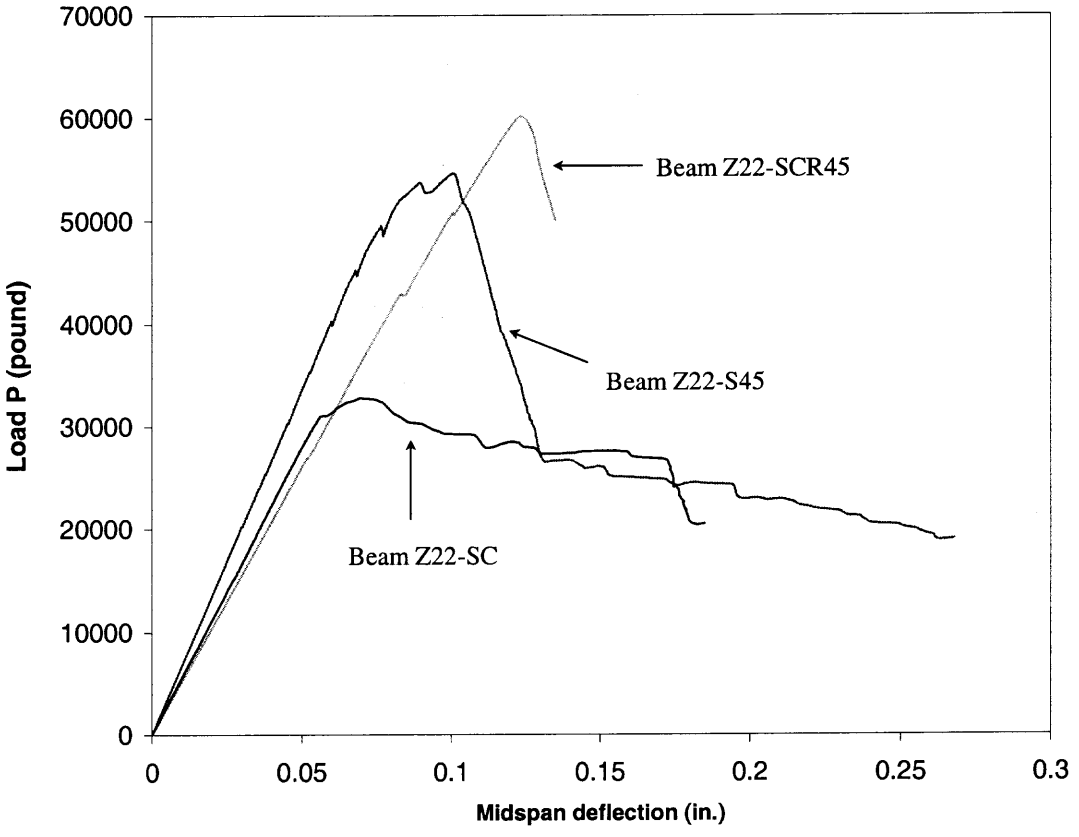

Figure 6.7 Test result of beam Z22-SCR45 and the comparison with other beams.

6.2.4.4 Beam Z31-FCRU. The experimental result of beam Z31-FCRU and its comparison with the results of beam Z31-FC and Z31-FU are summarized in Table 6.4 and Figure 6.8.

The repaired beam Z31-FCRU has a failure load of 48.3 kips, which is the largest failure load among the three beams. The increase in load carrying capacity is 149% as compared with the control beam Z31-FC. Beam Z31-FU, the original beam with CFRP U-shaped wrapping reinforcement, follows beam Z31-FCRU with an increase of 123% in failure load. The central deflection of beam Z31-FCRU at the ultimate load is also the highest among the three beams. The data was not collected when the load dropped to 45

kips due to the reason described earlier. Very good ductility was observed after the peak load, through there was no data to support this observation. The repaired beam Z31-FCRU shows a significant increase in strength and ductility.

Table 6.4 Test Result of Beam Z31-FCRU and Comparison with Other Beams

Beam Designation	Load P at Ultimate (kips)	Central Deflection at Ultimate (in.)	CFRP Shear Capacity (kips)	CFRP Failure Mode
Z31-FC	19.4	0.0838	N/A	Shear Diagonal Cracking
Z31-FU	43.2	0.1366	11.9	Fiber delamination
Z31-FCRU	48.3	0.1390	14.5	Fiber delamination & Rupture

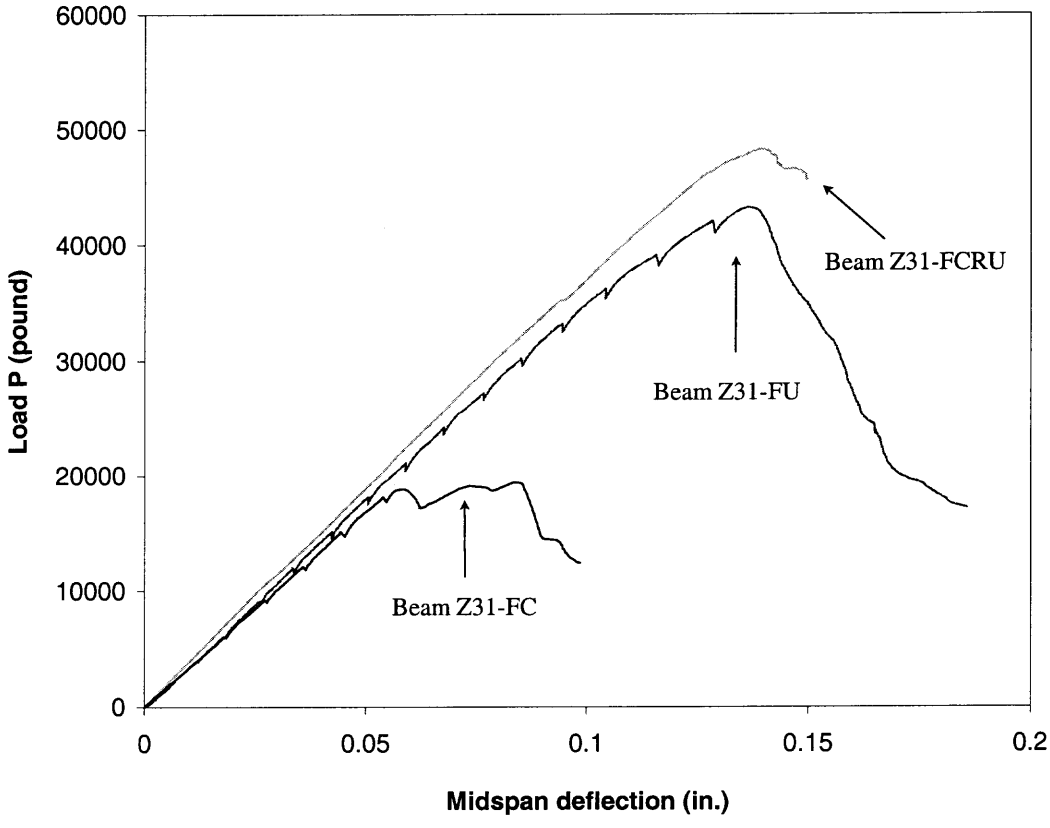

Figure 6.8 Test result of Beam Z31-FCRU and comparison with other beams.

CHAPTER 7

SUMMARY AND CONCLUSIONS

The experimental and the analytical study of the shear strengthening in RC beams using Carbon Fiber Reinforced Polymer (CFRP) laminates are carried out in this research. The beams studied are ranged from regular beams to deep beams with various configurations of CFRP laminates. The present research also includes studying the repair of shear damaged beams using CFRP laminates. Based on the results obtained, the following conclusions can be drawn:

1. Results of test performed in the present study demonstrate the feasibility of using externally applied, epoxy-bonded CFRP system to restore or increase the load-carrying capacity in shear of RC beams. The CFRP system can significantly increase the serviceability, ductility, and ultimate shear strength of a concrete beam if proper configuration is chosen. Restoring beam shear strength using CFRP is a highly effective technique.
2. The angle between the CFRP fiber orientation and the beam longitudinal axis has been found to be a major influential factor in determining the shear capacity of the beam with CFRP shear reinforcement. The shear crack angle is determined by the shear span to depth ratio a/d. Assuming the crack is developed from the loading point to the support at an angle of $\tan^{-1}(d/a)$, the most effective angle between the CFRP fiber orientation and the beam longitudinal axis will be $\tan^{-1}(a/d)$. From the test results in Chapter 2, the 4-foot long beam with 45-degree CFRP strip orientation outperforms the similar beams with other CFRP configurations in terms of ultimate shear strength and the ductility at peak load. Theoretically, $\tan^{-1}(a/d)$, which is

equal to 69 degrees in this case, should be the optimum angle of the CFRP. As the shear span to depth ratio continues to increase, the angle will gradually approaches 90 degrees, which is also the angle of the steel stirrups commonly used in engineering practice. Based on the test results of Beam group 2 in Chapter 4, the 3-foot long beam with 45-degree CFRP strip orientation has the highest shear strength in that group. Theoretically, $\tan^{-1}(a/d)$, which is equal to 50 degrees in this case, should be an optimum angle of the CFRP. As the shear span to depth ratio continues to decrease, the angle will gradually approach to 0 degree. That explains why the horizontal shear reinforcement becomes more active in carryying the shear load in deep beams.

3. The actual failure mechanism of the CFRP strengthened beam depends on the beam size and reinforcement ratio, etc. From the observation of the test results, it has been found out that the CFRP delamination, which occurs mostly underneath the concrete surface where the CFRP has been bonded, is the dominant failure mode for CFRP strips strengthened beams. CFRP fabrics strengthened beams which exhibit fiber rupture failure for 4-foot long regular beams while fiber delamination develops for most 3-foot long deep beams.
4. The use of anchorage by means of U-shaped CFRP wrapping scheme can greatly increase the shear capacity of beams with CFRP shear reinforcement. But as the shear span to depth ratio decreases, the anchorage in vertical direction does not seem to help the shear strength at all. When $a/d = 1.875$, the beam Z31-FU with anchorage increases 104% in shear strength as compared with the control beam Z31-FC; while beam Z31-F90 without anchorage increases only 79%. When $a/d = 1.25$, the beam

Z42-FU with anchorage increased 46% in shear strength as compared with the control beam Z42-FC; while beam Z42-F90 without anchorage increases 47%, which is more than that of beam with anchorage. It can be concluded that in a regular beam situation when the shear span to effective depth ratio has larger value, the anchorage for vertical CFRP shear reinforcement will greatly improve the shear strength. When the shear span to effective depth ratio becomes smaller value, or when the beam behaves like a deep beam, the anchorage for vertical CFRP shear reinforcement will not likely to improve the shear strength as much as in a regular beam case.

5. The effective stress of the CFRP laminates at beam failure will be less than the ultimate tensile stress of the CFRP laminates. Thus, a stress reduction factor R has to apply to reduce the ultimate tensile stress of the CFRP laminates when calculating the shear strength of the beam. It has been found out through calibration that when the shear failure is controlled by CFRP delamination, R is a function of the axial rigidity, which is a production of the CFRP shear reinforcement ratio and the modulus of elasticity of the CFRP, and the compressive strength of the concrete.
6. In shear strengthening of deep beams using CFRP laminates, when shear span to effective depth ratio a/d decreases, the shear strength of the beam has been found to increase. However, the shear contribution of CFRP laminates varies depending on the CFRP configuration. For deep beams with CFRP strips, as the shear span to depth ratio decreases, the shear contribution of vertical CFRP reinforcement also decreases, while the contribution of the contribution of horizontal and 45-degree CFRP reinforcement increases. For deep beams with CFRP fabrics, as the shear span to depth ratio decreases, the contribution of the U-shaped vertical CFRP laminates also

decreases, while the shear contribution of the double-layered CFRP laminates increases, which includes one layer of vertical CFRP laminates and one layer of longitudinal CFRP laminates. The importance of the longitudinal CFRP reinforcement has once again been verified.

7. Very good deflection ductility has observed at peak load for regular beams with 90-degree or 45-degree CFRP shear reinforcement. The CFRP shear strengthened deep beams, however, display virtually no much deflection ductility at peak load when beams fail. For regular beams with shear reinforcement, as long as the flexural steel bars are not over-reinforced, the bending failure is most likely to take place before the shear capacity of the beam is reached because the relatively large shear span creates higher bending moment at mid-span. In this research, with 90-degree or 45-degree CFRP shear reinforcement applied to the beam, the weak shear resistance due to the lack of steel stirrups has been compensated to a certain level where the failure is controlled by bending failure or a combination of bending and shear failures. This is why a good deflection ductility has been found for regular beams with CFRP shear reinforcement. For deep beams, however, shear failure usually controls due to the very short shear span, even with the CFRP shear reinforcement. Since the CFRP debonding or rupture at peak load is very brittle, the shear capacity is lost almost instantly. This explains why there is not much deflection ductility being observed for deep beams in this research.
8. The proposed design approaches shown in Equations 3.33, 3.34 and 5.24 for shear strengthening of both regular beams and deep beams using CFRP laminates give very

good estimates for the shear strength as compared with the present experimental results.

9. The shear cracks from the failure of all repaired beams, except those from beam Z11-SCR45, are all newly developed cracks. The previously developed shear cracks, which are repaired by means of the injection of SikaDur 35 Hi-Mod LV, all remain unchanged throughout the whole tests. Based on these observations, It is recommended that the shear repair of the beam should be carried out prior to the development of cracks whenever it is applicable.

10. Epoxy injection in the cracks is strongly recommended for shear repair. If the shear cracks are already developed prior to the repair, the shear force upon the beam will be carried by existing shear reinforcement, the dowel action by flexural reinforcement and the aggregate interlock force. If the shear cracks are too wide, the aggregate interlock may not exist at all. Part of the bonding between the steel reinforcement and the concrete at the crack interface may be lost due to the shear failure impact and the friction force afterwards. The meaning of the epoxy injection has two fold:

    i). To rebuild the bonding between the concrete blocks and the steel reinforcement at the shear crack interface, thus to create a similar state it used to be before the cracking.

    ii). To change the loading path after the beam is repaired by the epoxy injection as well as the CFRP reinforcement. As can be observed in the tests, the failure of the repaired beam usually occurs on one side of the beam where there are no previously developed cracks, whereas the other side of the beam where epoxy injection has been provided gives stronger resistance to the applied load.

APPENDIX A

LOAD DEFLECTION CURVES OF REGULAR BEAMS

Load deflection curves of 11 regular beams covered in Chapter 2, including 4-foot long and 6-foot long beams, are listed in this Appendix.

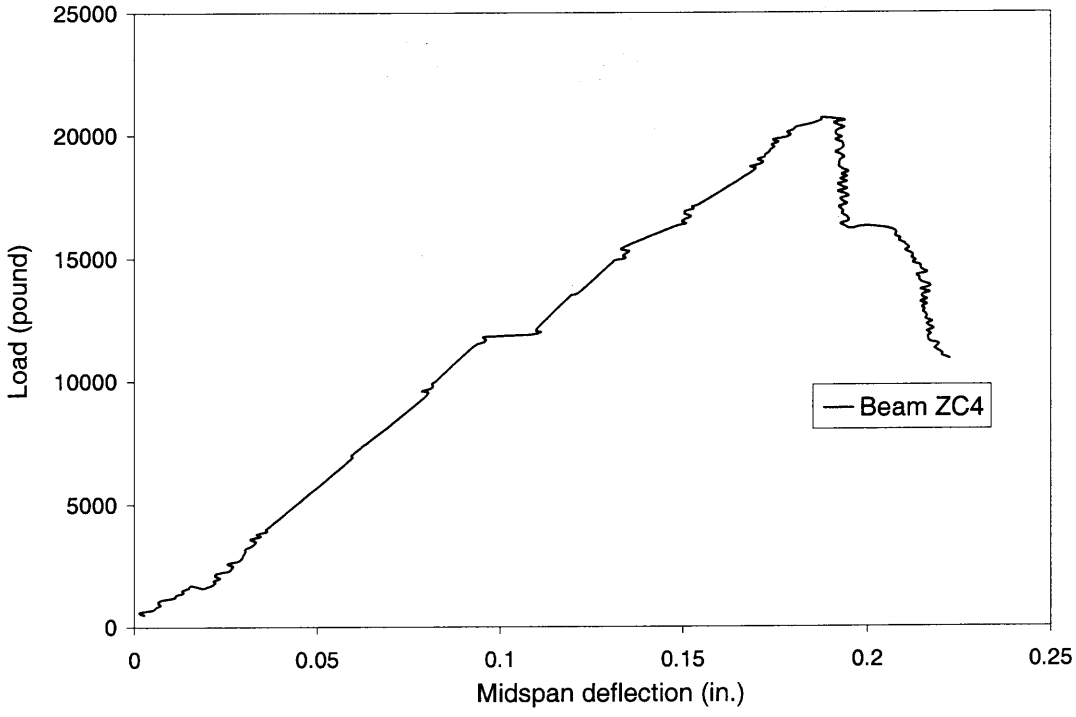

Figure A.1 Load deflection curve of Beam ZC4.

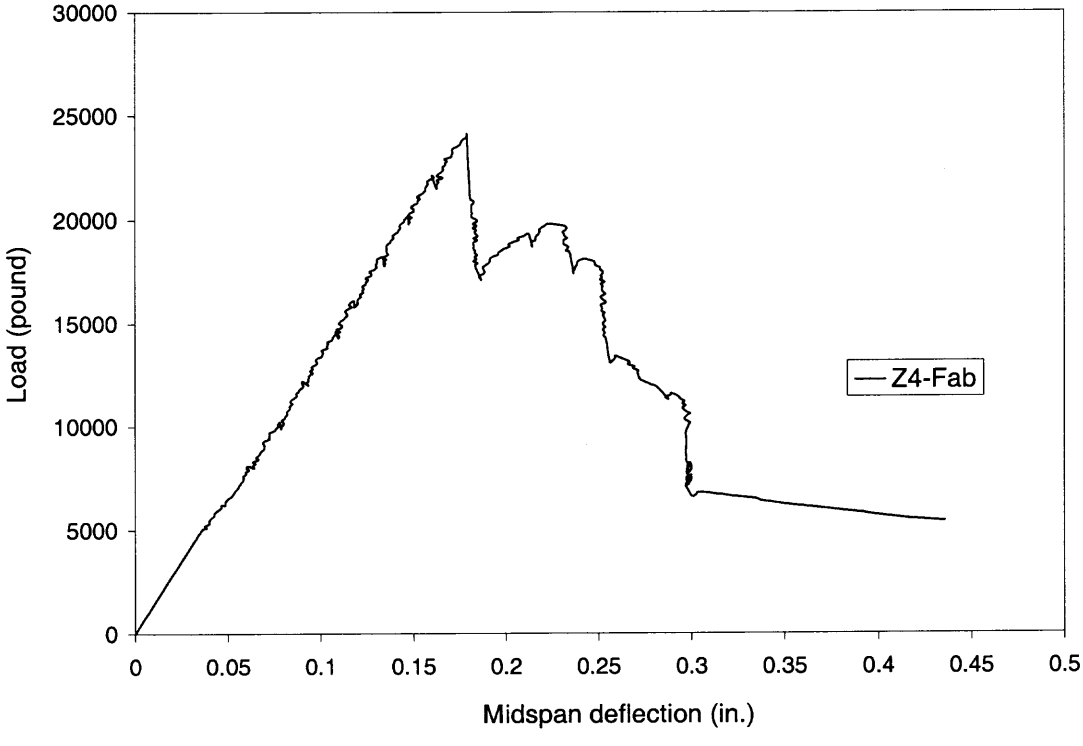

Figure A.2 Load deflection curve of Beam Z4-Fab.

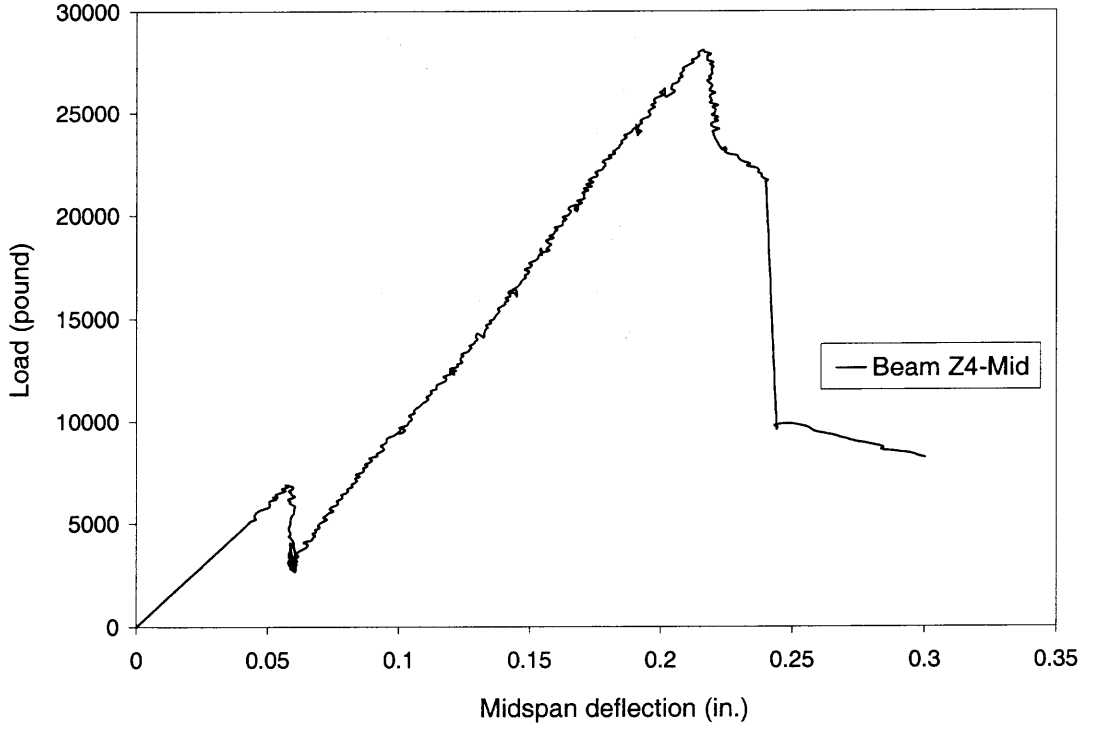

Figure A.3 Load deflection curve of Beam Z4-Mid.

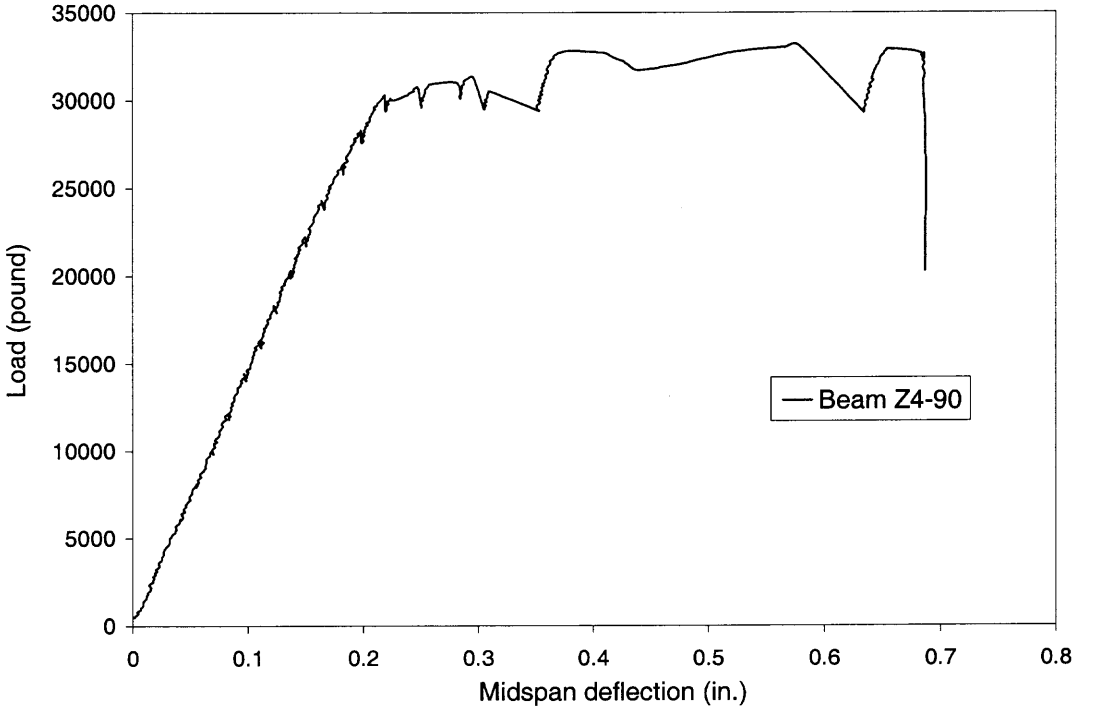

Figure A.4 Load deflection curve of Beam Z4-90.

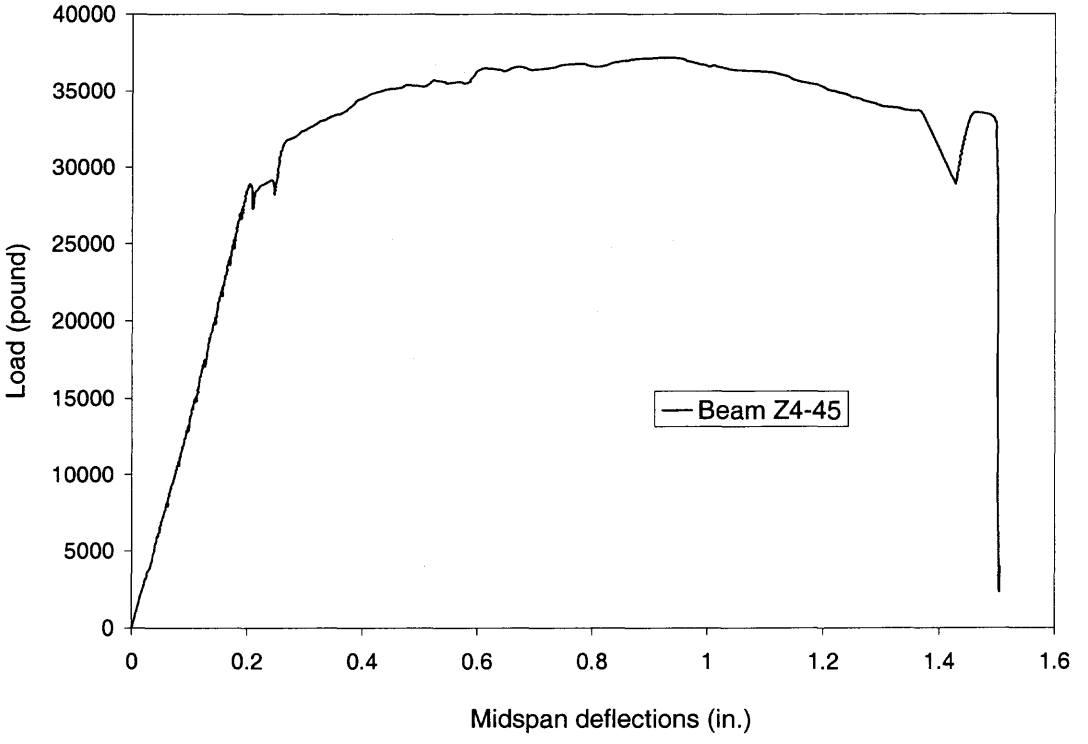

Figure A.5 Load deflection curve of Beam Z4-45.

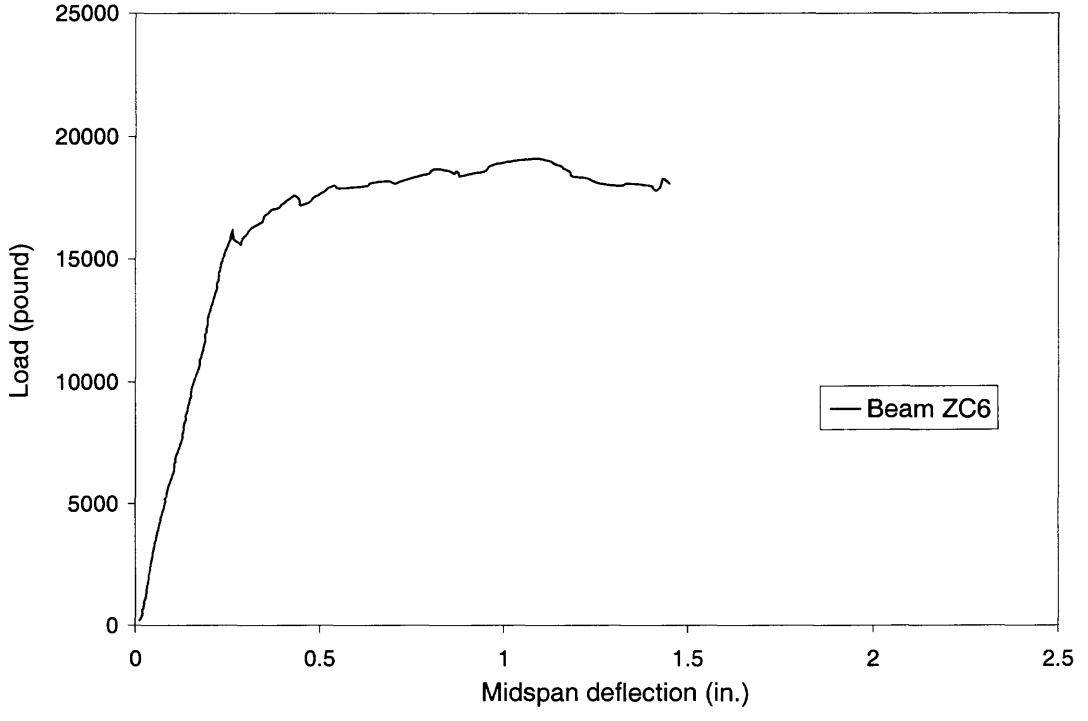

Figure A.6 Load deflection curve of Beam ZC6.

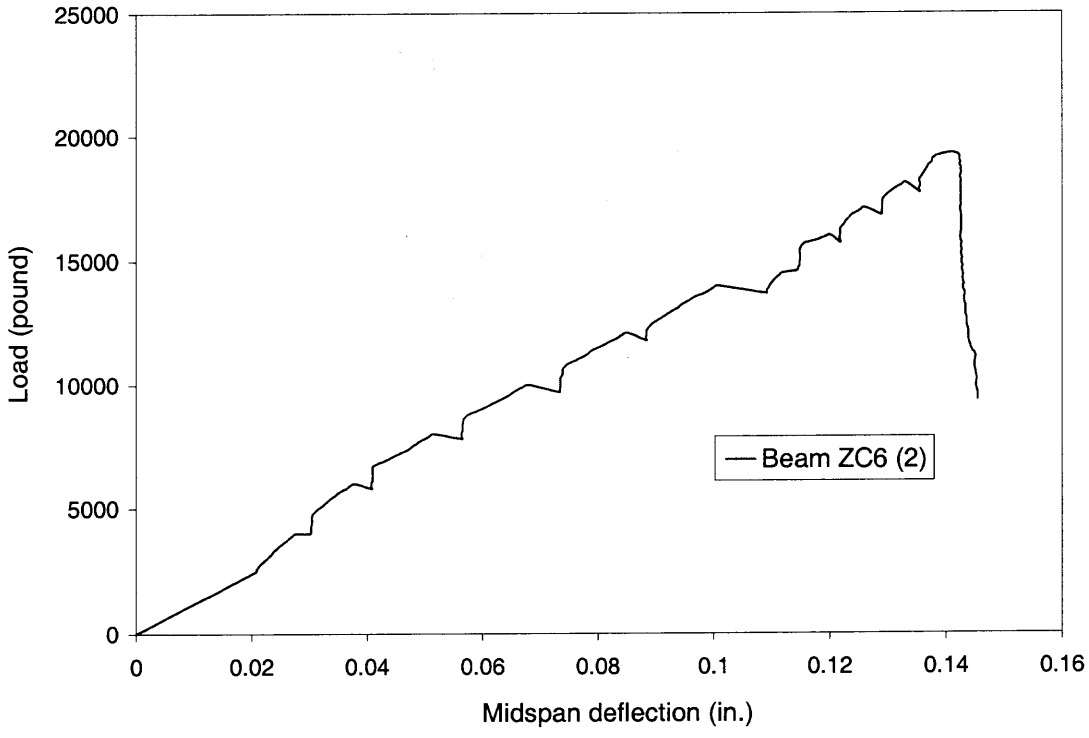

Figure A.7 Load deflection curve of Beam ZC6(2).

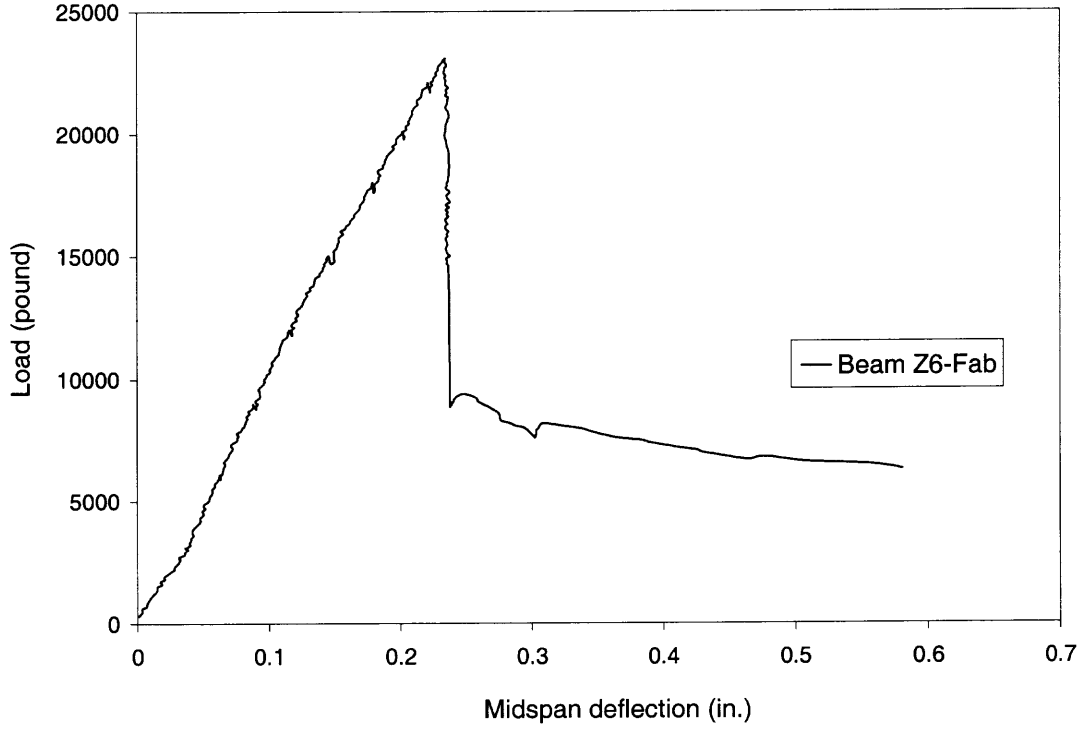

Figure A.8 Load deflection curve of Beam Z6-Fab.

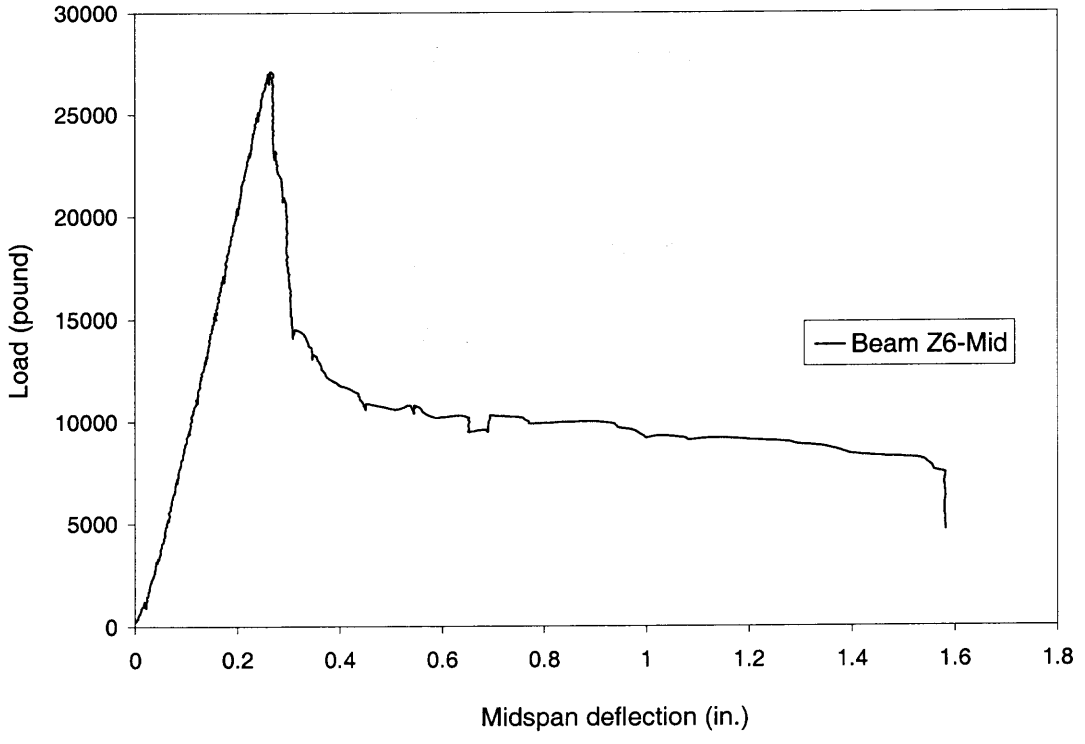

Figure A.9 Load deflection curve of Beam Z6-Mid.

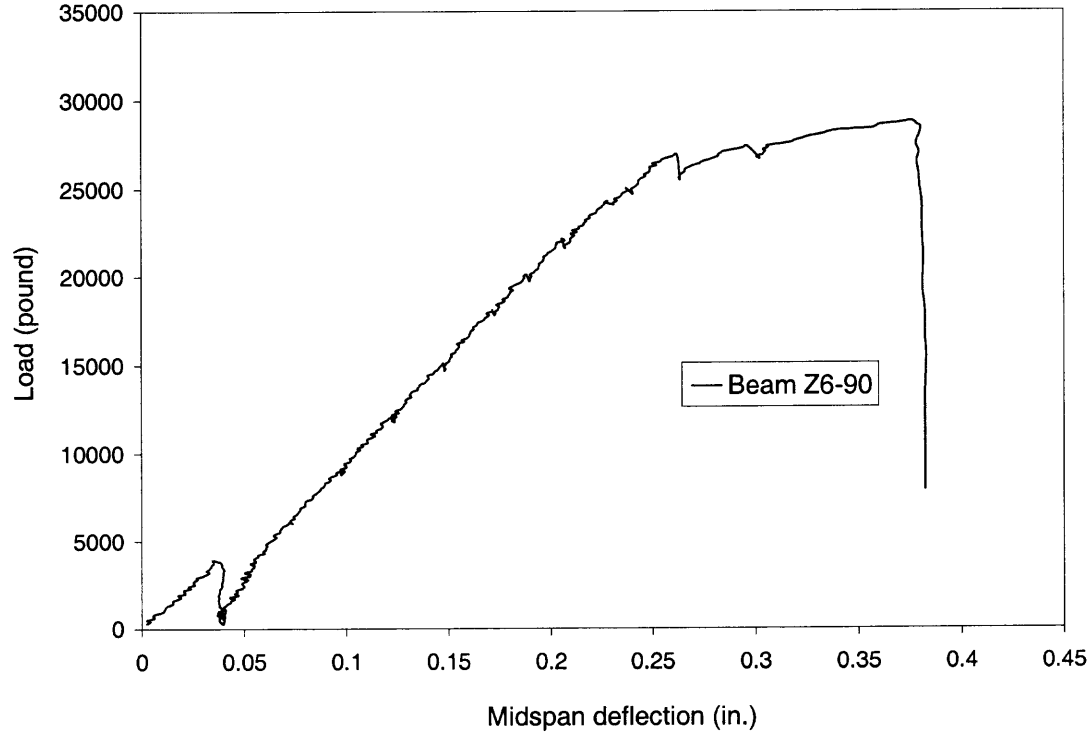

Figure A.10 Load deflection curve of Beam Z6-90.

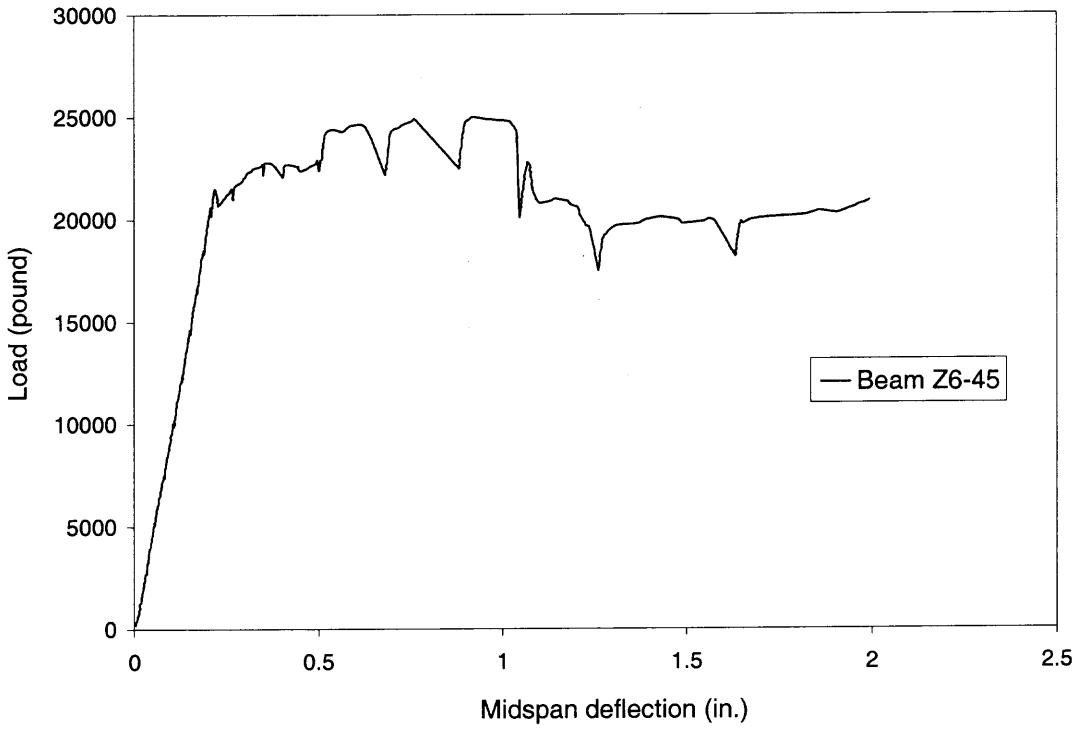

Figure A.11 Load deflection curve of Beam Z6-45.

APPENDIX B

LOAD DEFLECTION CURVES OF DEEP BEAMS

Load deflection curves of 16 deep beams covered in Chapter 4 are shown separately in this Appendix.

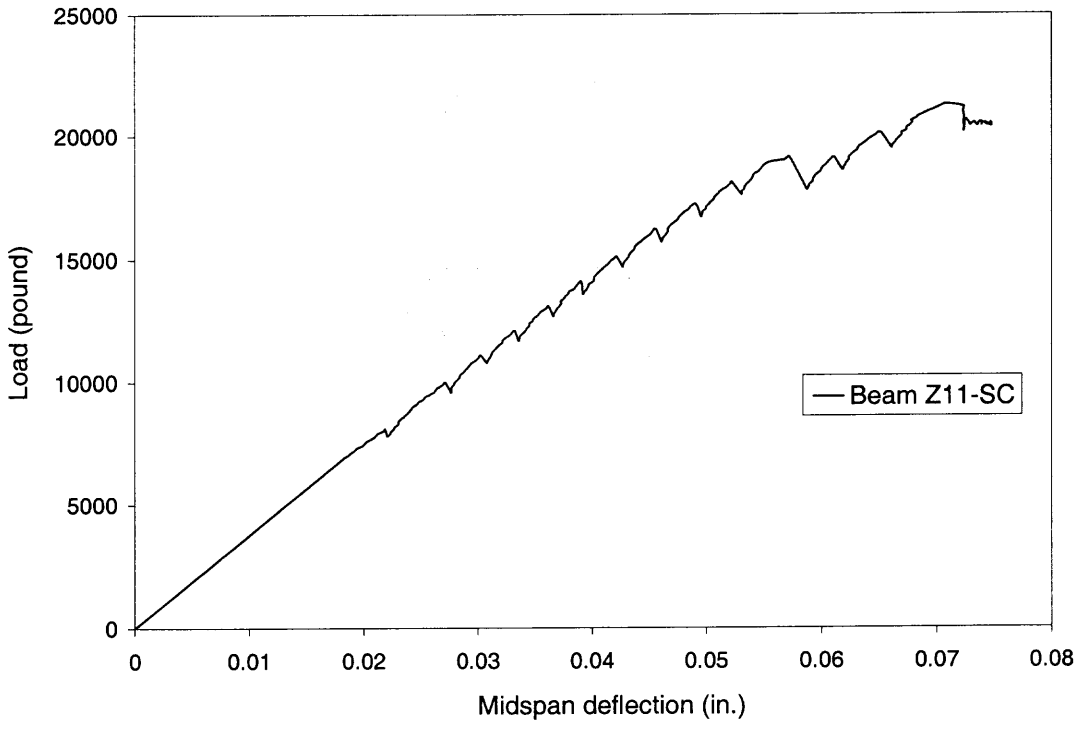

Figure B.1 Load deflection curve of Beam Z11-SC.

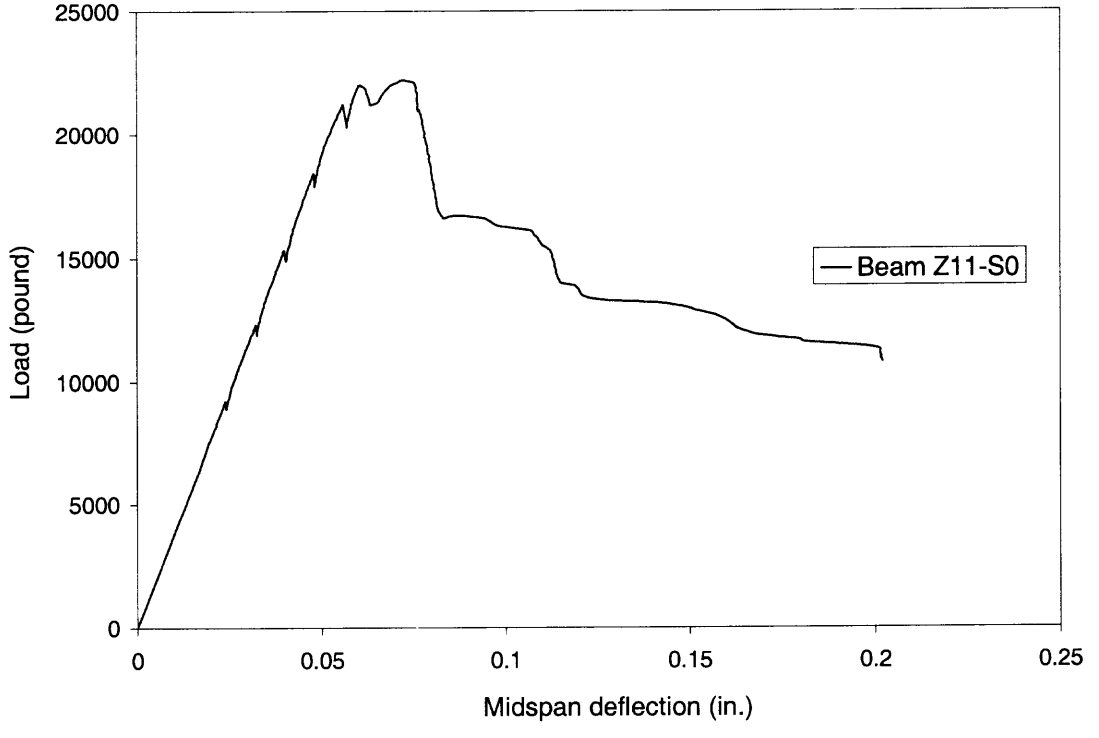

Figure B.2 Load deflection curve of Beam Z11-S0.

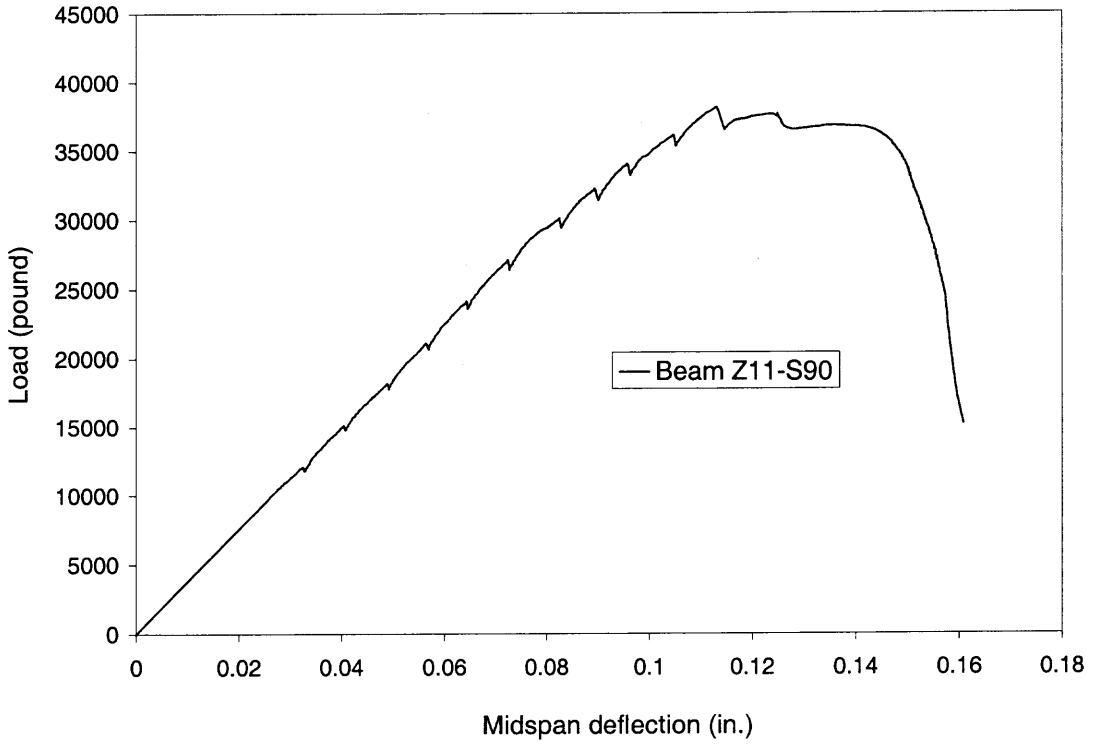

Figure B.3 Load deflection curve of Beam Z11-S90.

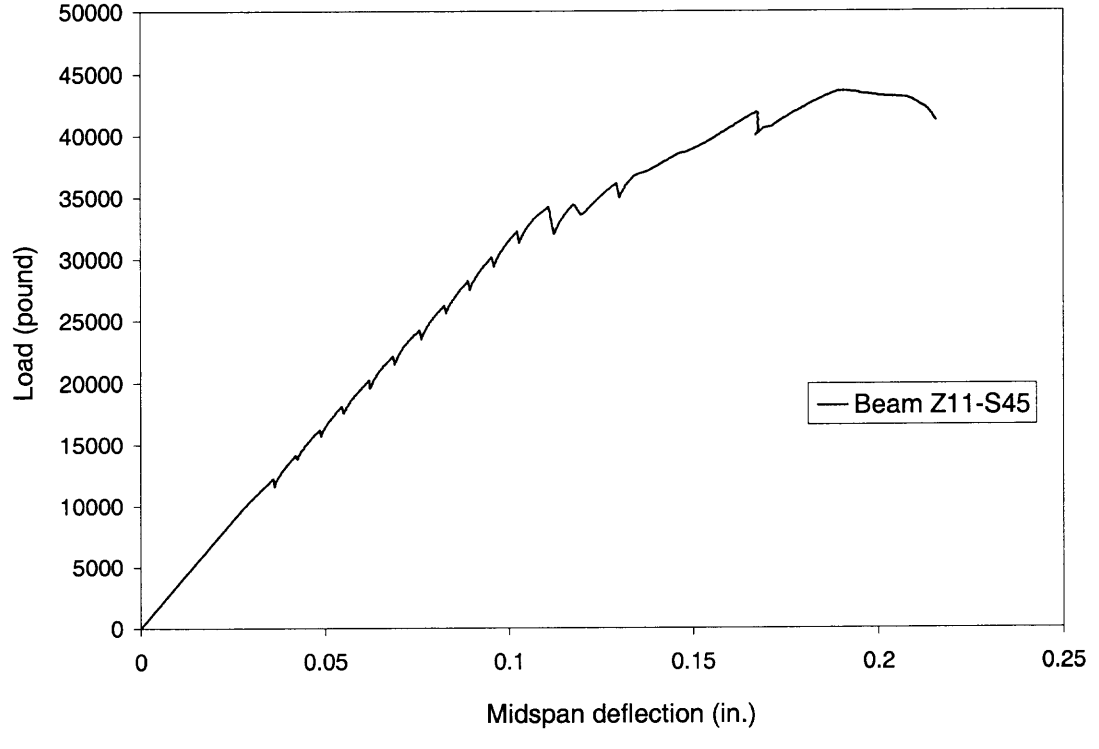

Figure B.4 Load deflection curve of Beam Z11-S45.

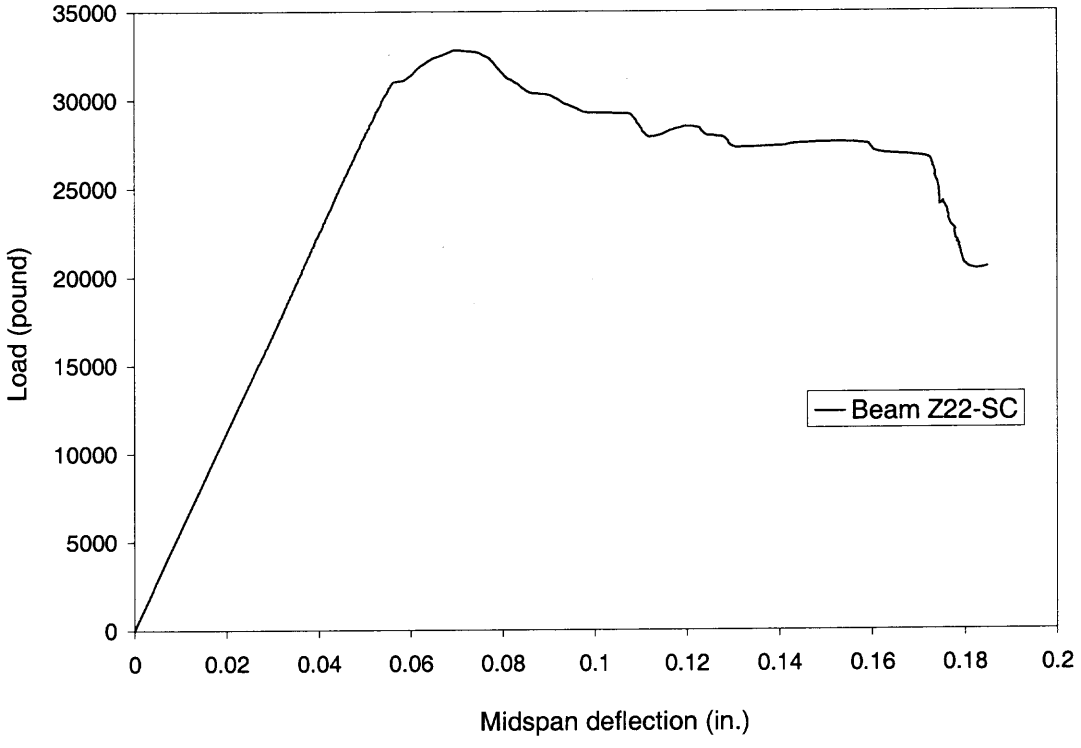

Figure B.5 Load deflection curve of Beam Z22-SC.

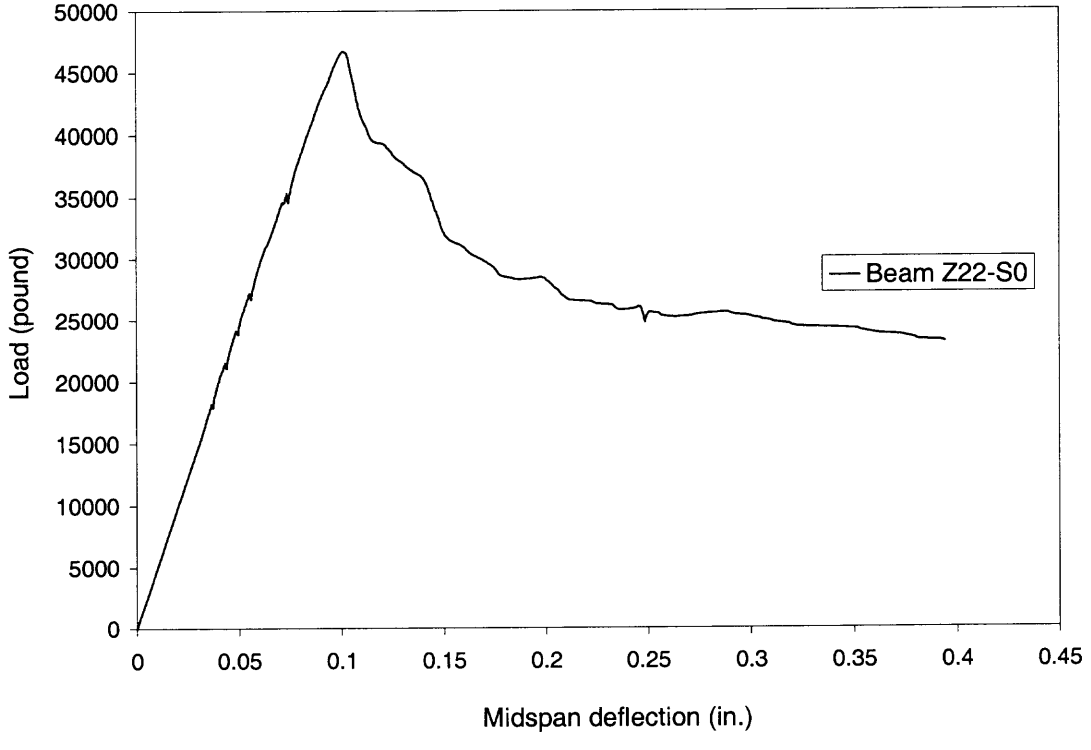

Figure B.6 Load deflection curve of Beam Z22-S0.

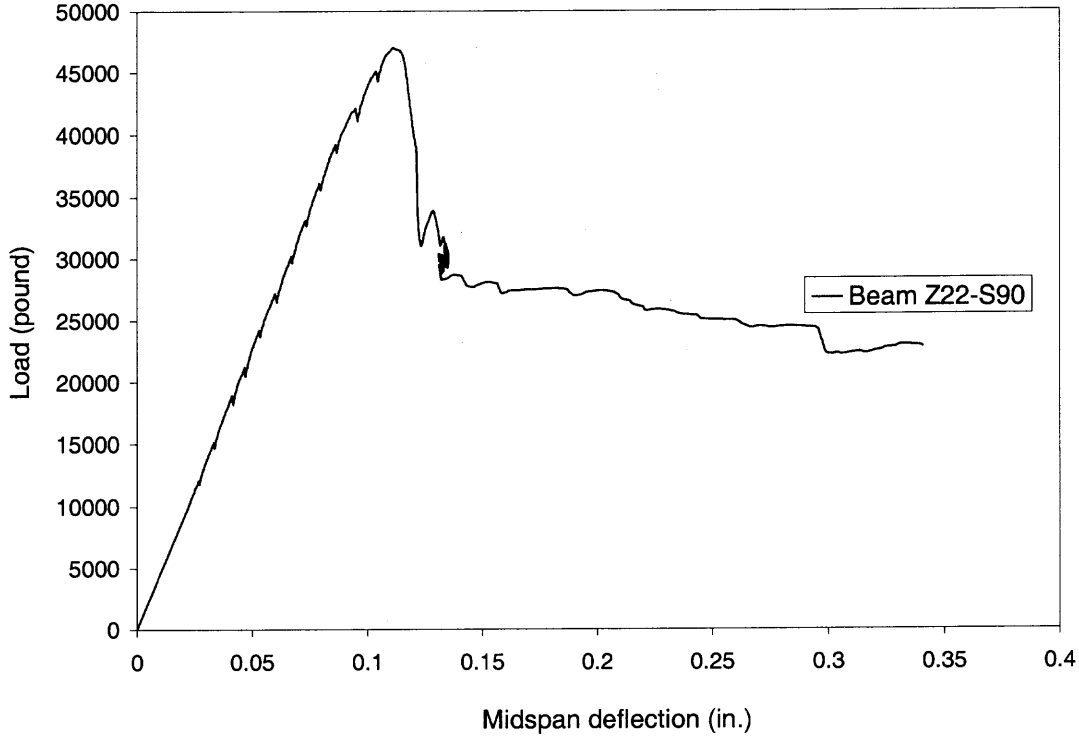

Figure B.7 Load deflection curve of Beam Z22-S90.

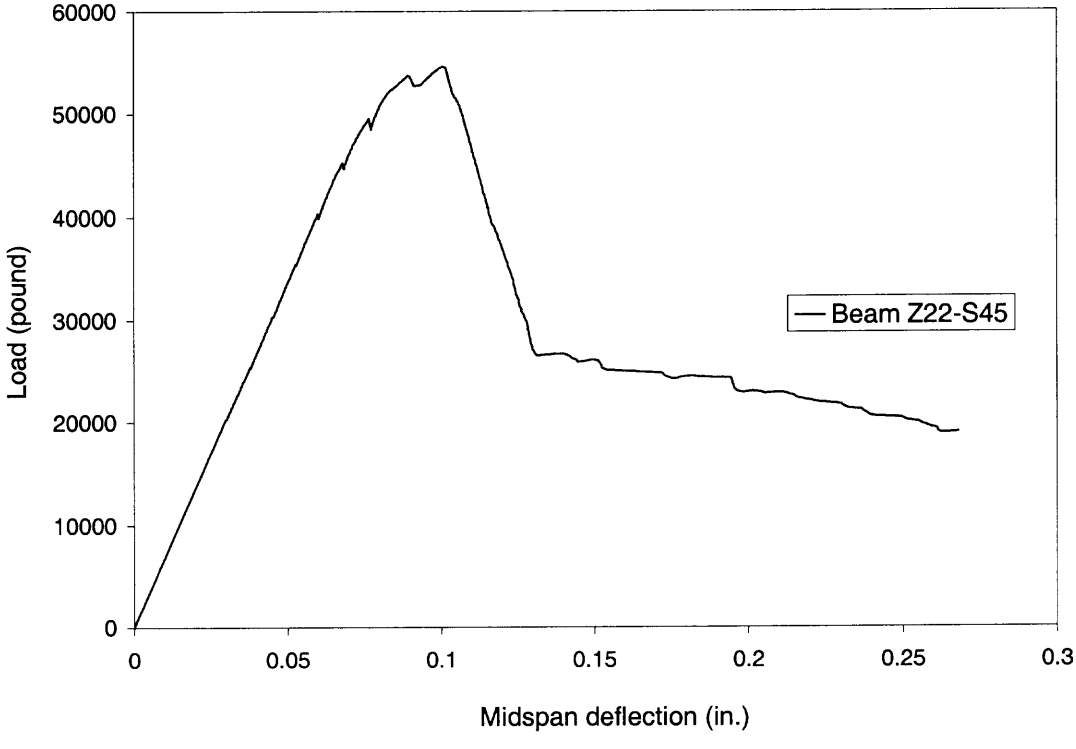

Figure B.8 Load deflection curve of Beam Z22-S45.

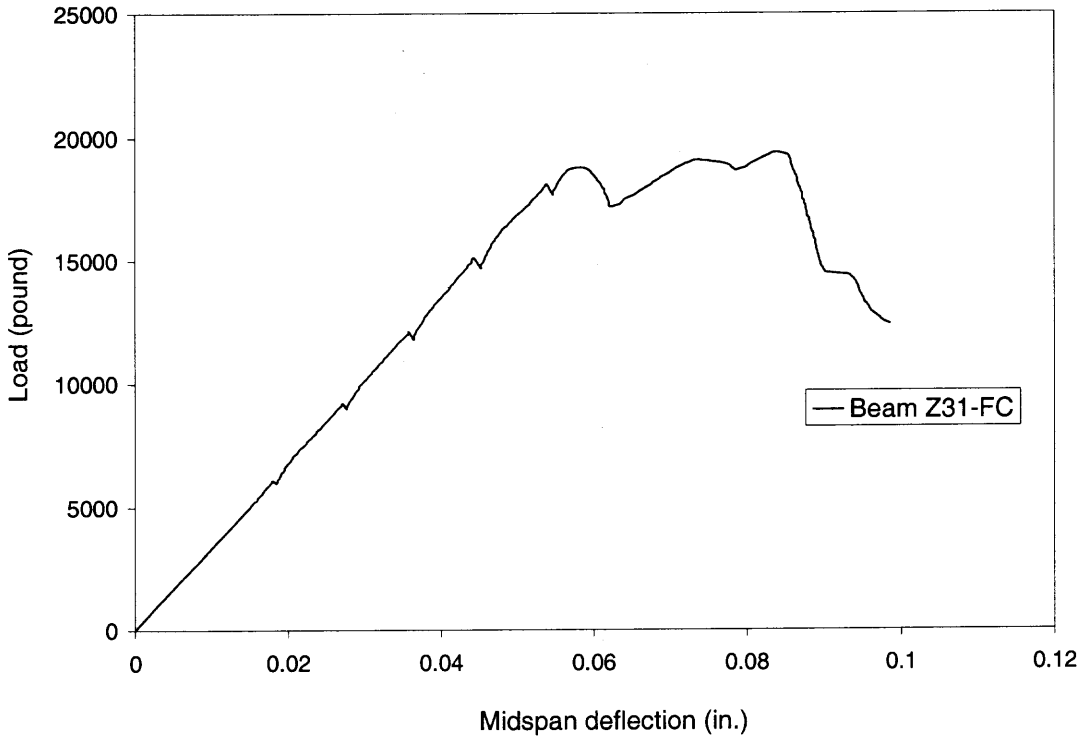

Figure B.9 Load deflection curve of Beam Z31-FC.

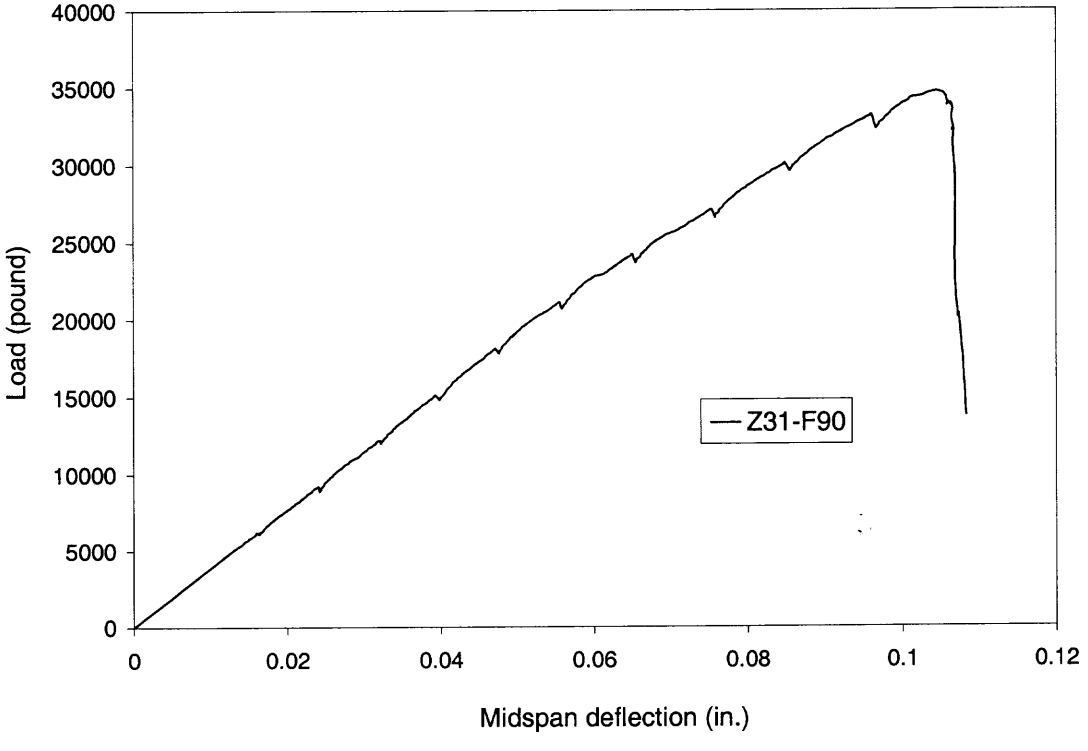

Figure B.10 Load deflection curve of Beam Z31-F90.

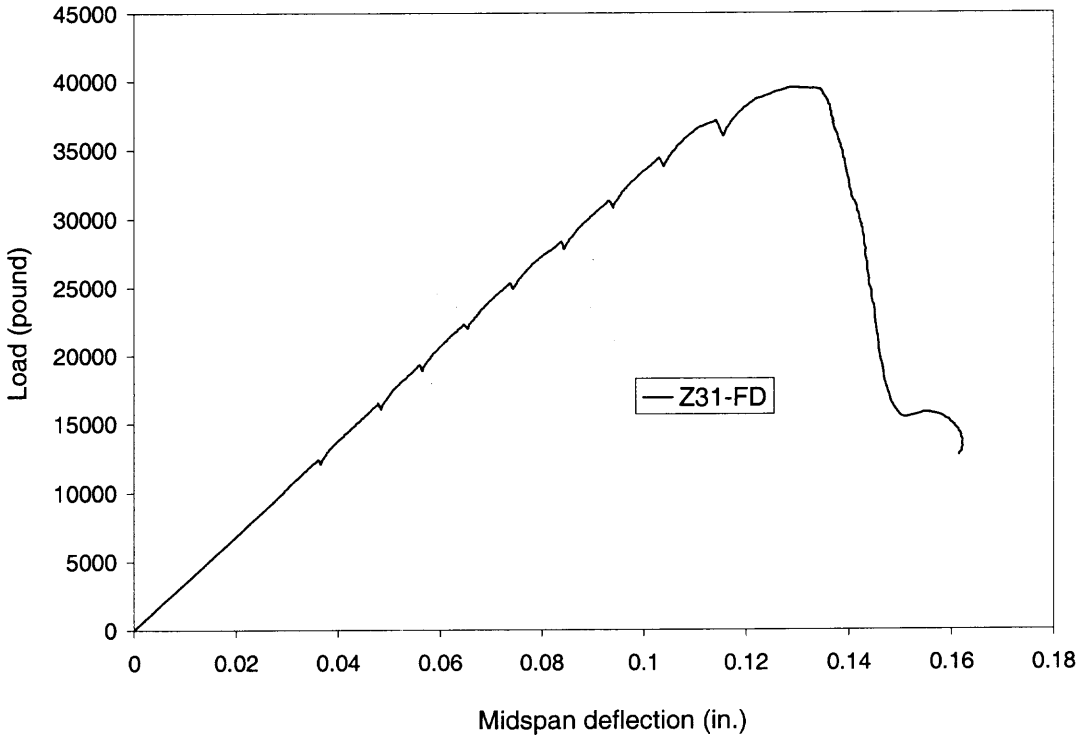

Figure B.11 Load deflection curve of Beam Z31-FD.

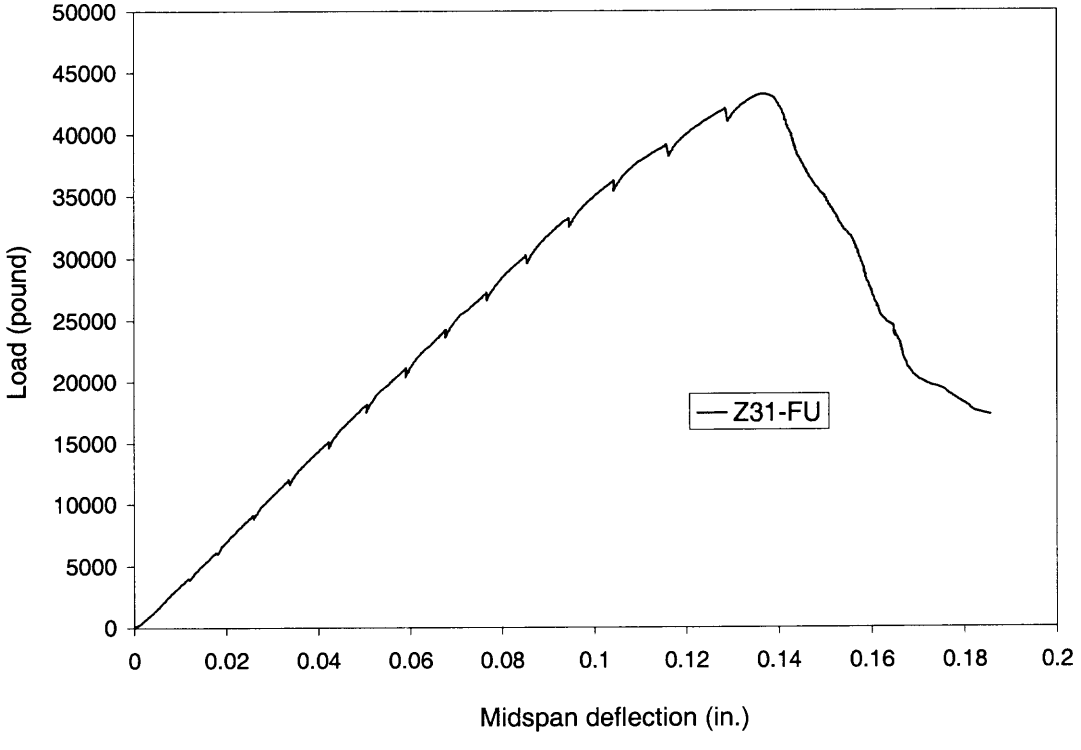

Figure B.12 Load deflection curve of Beam Z31-FU.

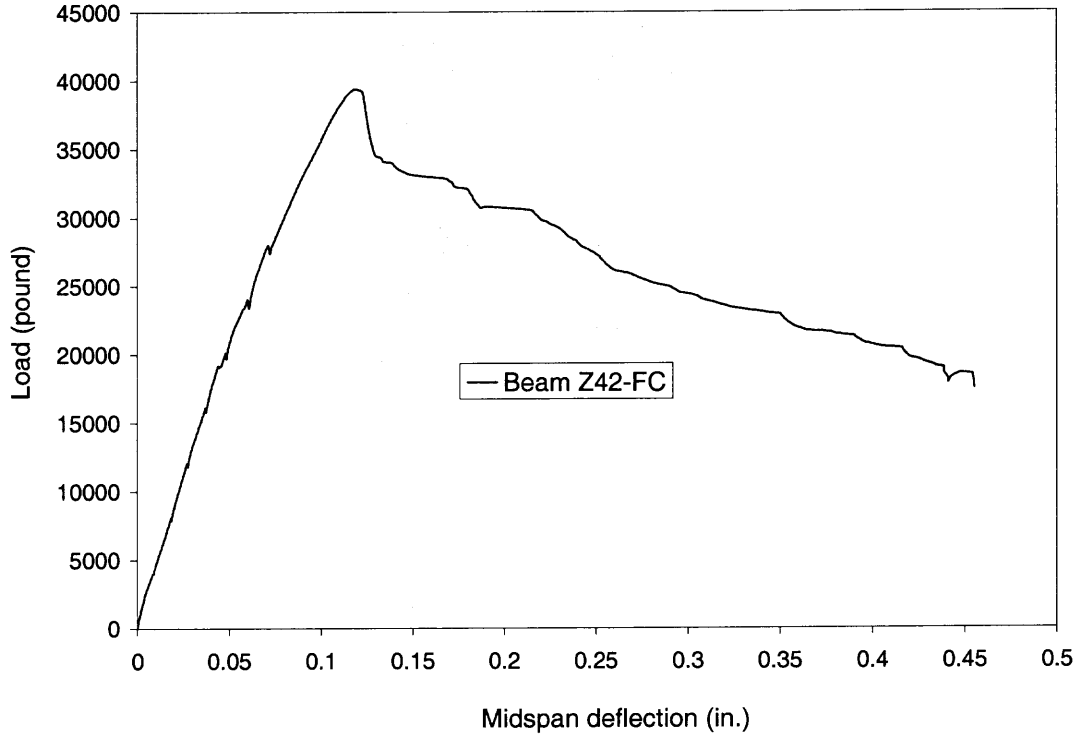

Figure B.13 Load deflection curve of Beam Z42-FC.

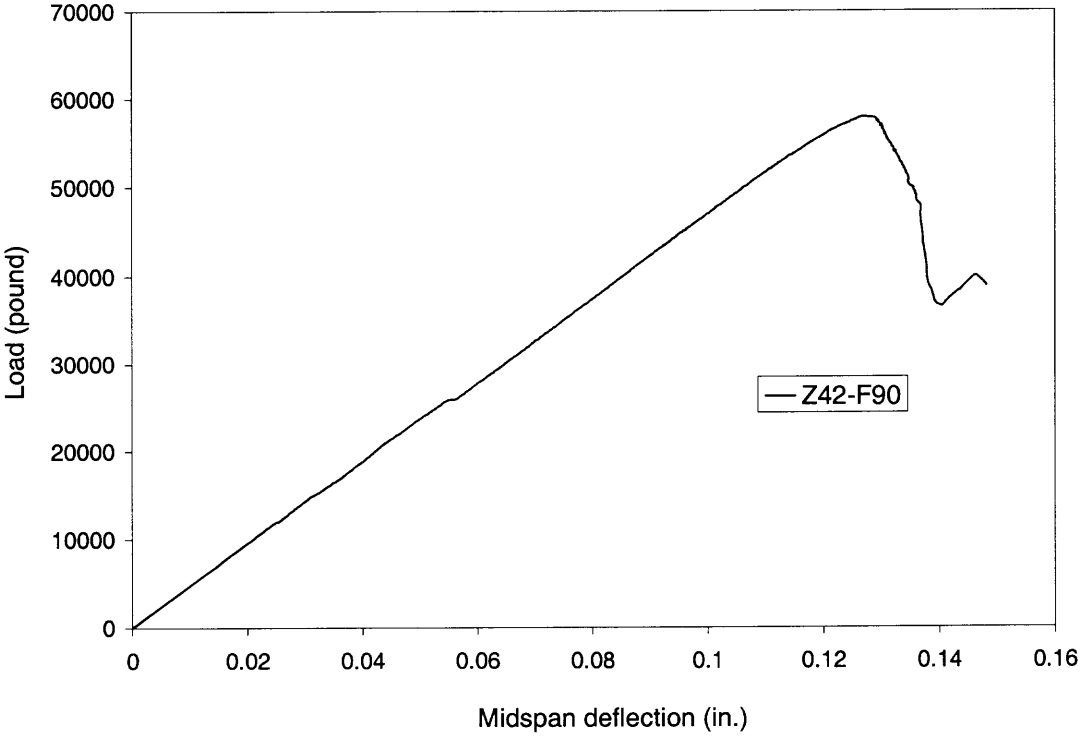

Figure B.14 Load deflection curve of Beam Z42-F90.

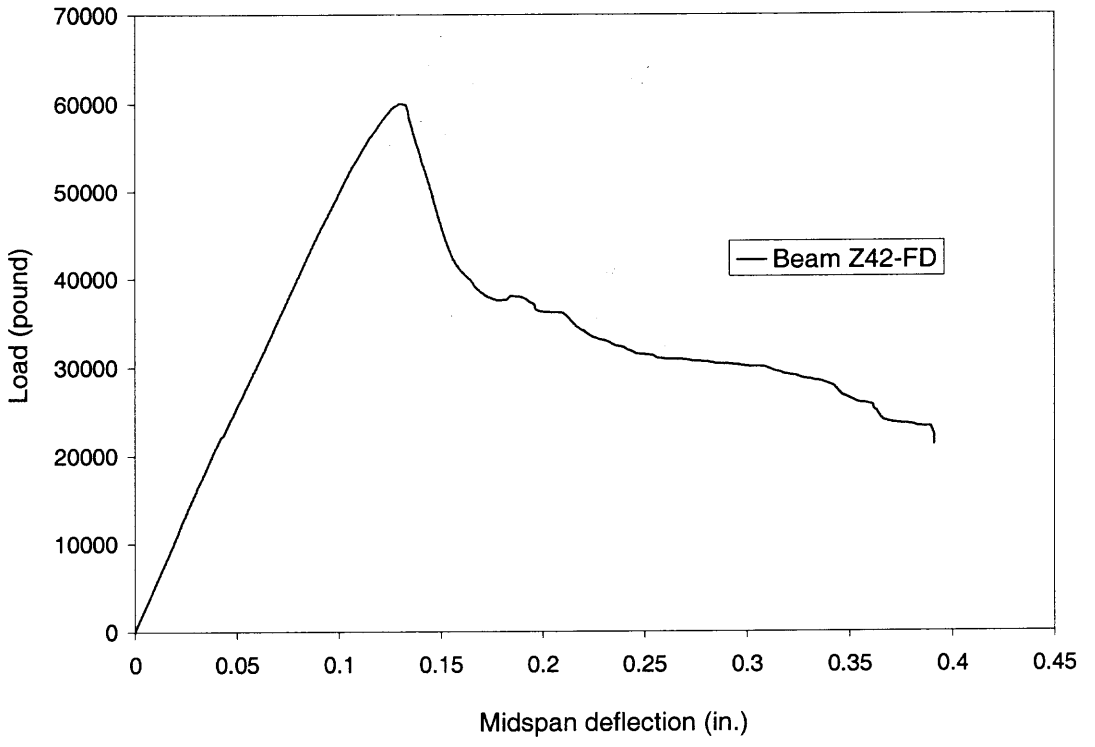

Figure B.15 Load deflection curve of Beam Z42-FD.

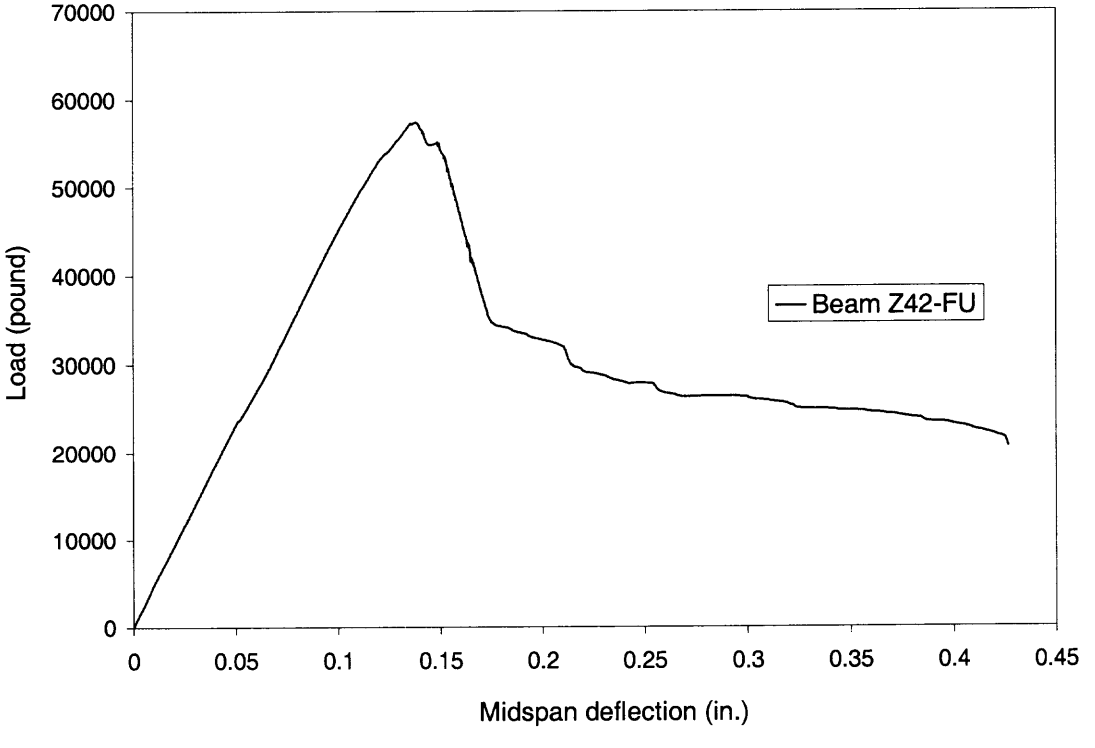

Figure B.16 Load deflection curve of Beam Z42-FU.

APPENDIX C

LOAD DEFLECTION CURVES OF REPAIRED SHEAR-DAMAGED BEAMS

Load deflection curves of four repaired shear-damaged beams covered in Chapter 6 are illustrated in this Appendix.

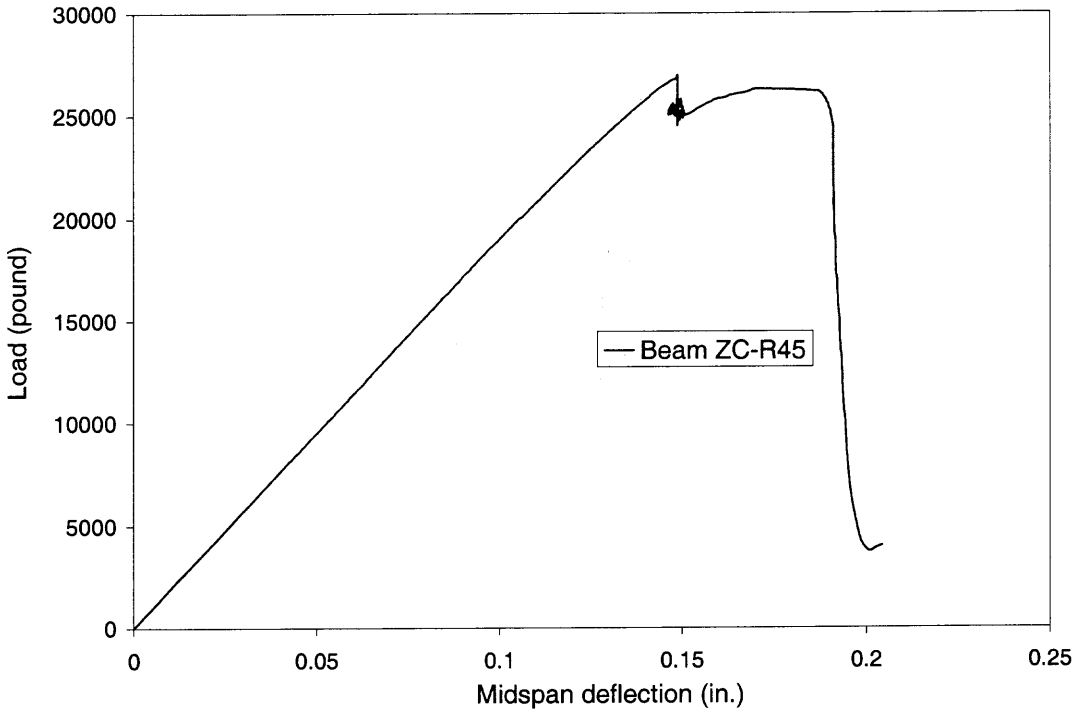

Figure C.1 Load deflection curve of Beam ZC-R45.

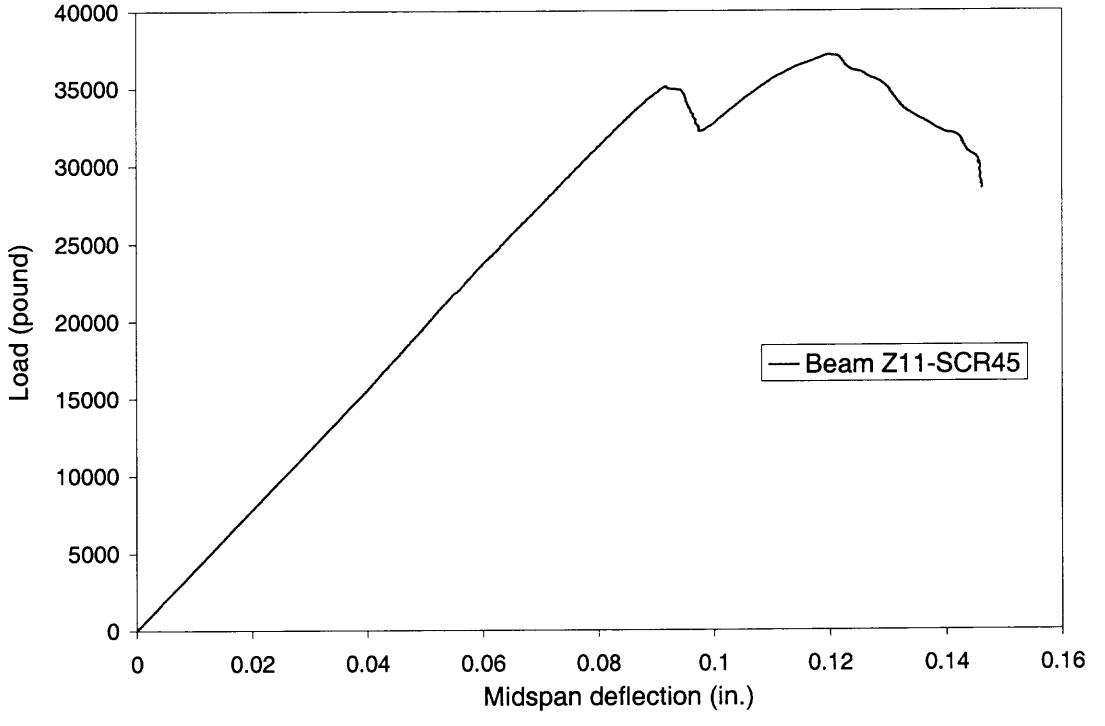

Figure C.2 Load deflection curve of Beam Z11-SCR45.

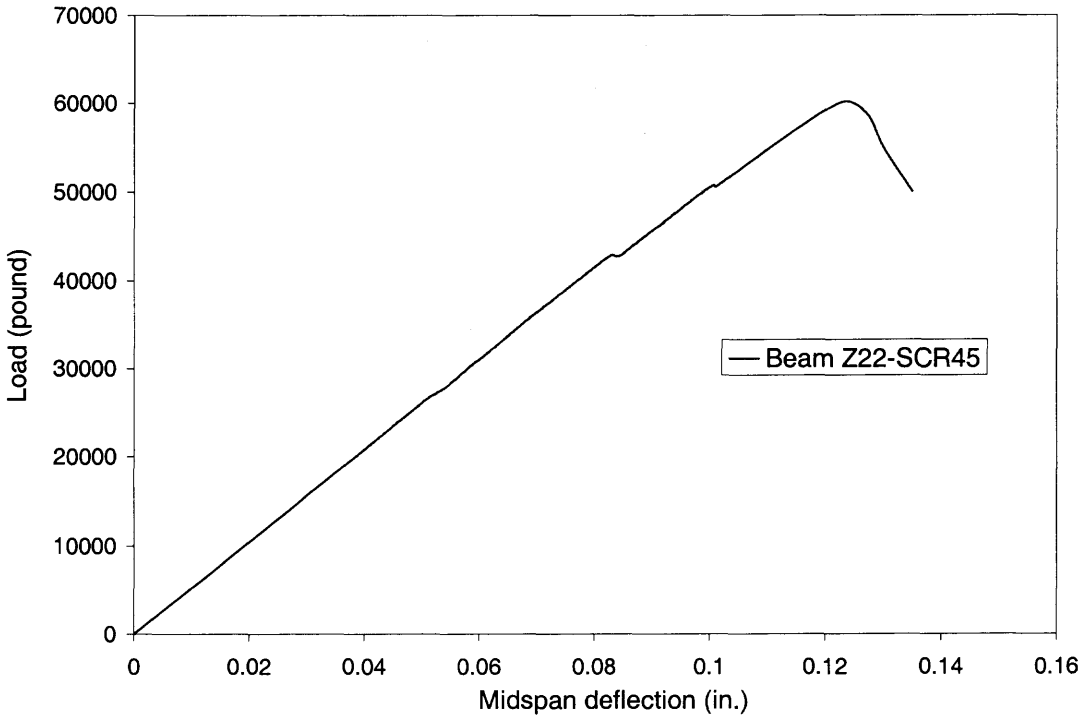

Figure C.3 Load deflection curve of Beam Z22-SCR45.

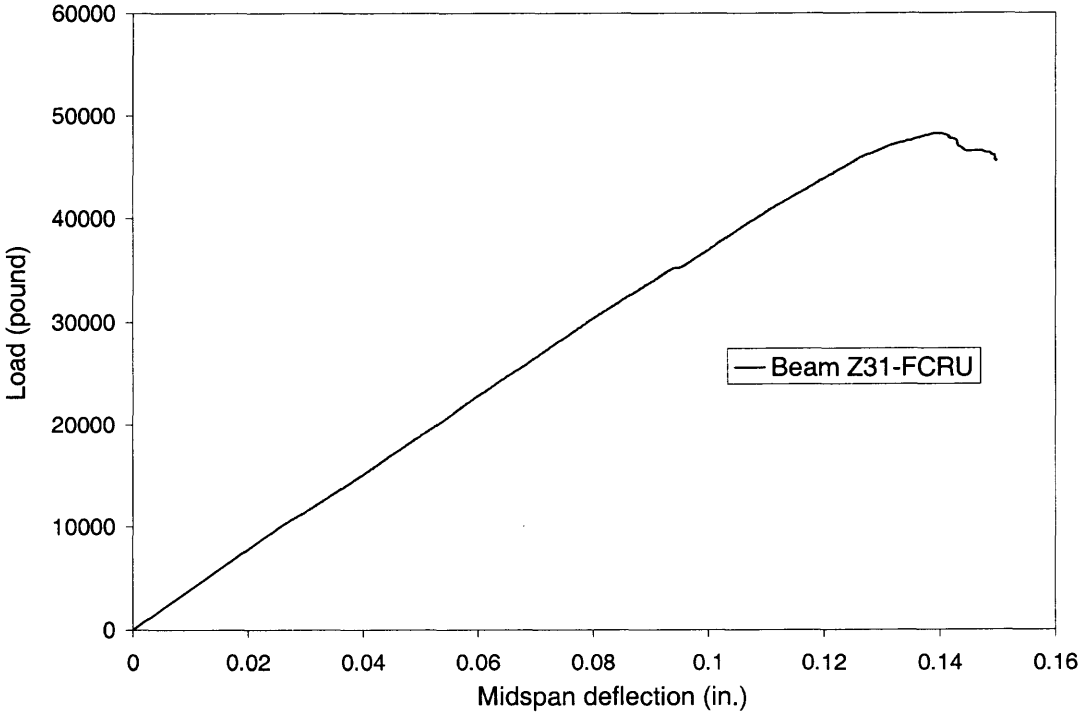

Figure C.4 Load deflection curve of Beam Z31-FCRU.

REFERENCES

ACI-ASCE Committee 326. "Shear and Diagonal Tension", *ACI Journal Proceedings*, 59, January, February, and March 1962, pp. 352-396.

Arduini, Marco; Tommaso, Angelo Di; and Nanni, Antonio. "Brittle Failure on FRP Plate and Sheet Bonded Beams", *ACI Structural Journal*, Vol. 94, No. 4, July-August 1997, pp. 363-370.

ASCE-ACI Task Committee 426 on Shear and Diagonal Tension of the Committee on Masonry and Reinforced Concrete of the Structural Division, "The Shear Strength of Reinforced Concrete Members", *Journal of the Structural Division, Proceedings of the American Society of Civil Engineers*, Vol. 99, No. ST6, June 1973, pp. 9791-1187.

Al-Sulaimani, G. J.; Sharif, A.; Basunbul, I. A.; Baluch, M. H.; and Ghaleb, B. N.. "Shear Repair for Reinforced Concrete by Fiberglass Plate Bonding", *ACI Structural Journal*, V.91, No.3, July-Aug. 1994, pp. 458-464.

Berset, J.-D. "Strengthening of Reinforced Concrete Beams for Shear Using FRP Composites", *MS thesis*, Department of Civil and Environmental Engineering, Massachusetts Institute of Technology, Jan. 1992.

Bian, H. T.; Hsu, C. T. T.; and Wang, W., "Rehabilitation of Concrete Structures Using the Sika's CFRP System", *A final research report to Sika Corporation*, New Jersey, New Jersey Institute of Technology, August 29, 1997.

Bizindavyi, L.; and Neale, K. W.. "Transfer Lengths and Bond Strengths for Composites Bonded to Concrete", *Journal of Composites for Construction*, Vol. 3, No. 4, Nov. 1999, pp. 153-160.

"Building Code Requirements for Reinforced Concrete (ACI 318-99)", *ACI Manual of Concrete Practice*, American Concrete Institute, Detroit, Michigan, 1999.

Chaallal, O.; Nollet, M. –J.; and Perraton, D.. "Shear Strengthening of RC Beams by Externally Bonded Side CFRP Strips", *Journal of Composites for Construction*, Vol. 2, No. 2, May 1998, pp. 111-113.

Chajes, M. J.; Januska, T. F.; Mertz, D. R.; Thomson, T. A., Jr.; and Finch, W. W., Jr.. "Shear Strengthening of Reinforced Concrete Beams using Externally Applied Composite Fabrics", *ACI Structural Journal*, V. 92, No. 3, May-June 1995, pp. 295-303.

Czaderski, Christoph. "Shear Strengthening of Reinforced Concrete with CFRP", *45th International SAMPE Symposium*, May 21-25, 2000, pp. 880-894.

Czaderski, Christoph. "Shear Strengthening with CFRP L-Shaped Plates", *Schweizer Ingenieur und Architekt SI + A*, No. 43/1998.

Dolan, C. W.; Rider, W.; Chajes, M. J.; and DeAscanis, M.. "Prestressed Concrete Beams Using Non-Metallic Tendons and External Shear Reinforcement", *Fiber-Reinforced Plastic Reinforcement for Concrete Structures*, SP-138, American Concrete Institute, Detroit, 1992, pp. 475-495.

Fanning P. J.; and Kelly, Oliver. "Ultimate Response of RC Beams Strengthened with CFRP Plates", *Journal of Composites for Construction*, Vol. 5, No. 2, May 2001, pp. 122-127.

Hsu, C. T. T.; Bian, H. T.; Jia, Y. X., "Research for Bond-Slip Using Sika's Carbodur System", *A report to Sika Corporation*, New Jersey, New Jersey Institute of Technology, November 14, 1997.

Khalifa, Ahmed; and Nanni, Antonio. "Improving Shear Capacity of Existing RC T-Section beams using CFRP Composites", *Cement & Concrete Composites*, Vol. 22, 2000, pp. 165-174.

Khalifa, Ahmed; Gold, William J.; Nanni, Antonio; and Aziz, Abdel M.I.. "Contribution of Externally Bonded FRP to Shear Capacity of RC Flexural Members", *Journal of Composites for Construction*, Vol. 2, No. 4, Nov. 1998, pp. 195-202.

Maeda Toshiya; ASANO, Yasuyuki; SATO, Yasuhiko; UEDA, Tamon; and KAKUTA, Yoshio. "A Study on Bond Mechanism of Carbon Fiber Sheet", *Non-Metallic (FRP) Reinforcement for Concrete Structures, Proceedings of the Third International Symposium*, Vol. 1, Oct. 1997, pp. 279-286.

Malver, L. J.; Warren, G. E.; and Inaba, C.. "Rehabilitation of Navy Pier Beams with Composites Sheets", *Non-Metallic (FRP) Reinforcement for Concrete Structures*, E & FN Spon, London, 1995, pp. 534-540.

Mau, S. T.; and Hsu, T. T. C.. "Shear Strength Prediction — Softened Truss Model", *Reinforced Concrete Deep Beams,* edited by Kong, F. K., 1990, pp. 157-181.

Mau, S. T.; and Hsu, T. T. C.. "Shear Strength Prediction for Deep Beams with Web Reinforcement", *ACI Structural Journal*, Vol. 84, No.6, Nov.-Dec. 1987, pp. 513-523.

MacGregor, J. G.. "Shear Friction, Deep Beams, Corbels, Discontinuity Regions, and Joints", *Reinforced Concrete Mechanics and Design*, 1988 pp. 679-730.

MacGregor, James G.; and Hawkins, N. M.. "Suggested Revisions to ACI Building Code Clauses Dealing with Shear Friction and Shear in Deep Beams and Corbels", *ACI Journal, Proceedings*, Vol. 74, Nov. 1977, pp. 537-545.

Mukhopadhyaya, phalguni; and Swamy, Narayan. "Interface Shear Stress: A new Design Criterion for Plate Debonding", *Journal of Composites for Construction*, Vol. 5, No. 1, Feb. 2001, pp. 35-43.

Norris, Tom; Saadatmanesh, Hamid; and Ehsani, M. R.. "Shear and Flexural Strengthening of R/C Beams with Carbon Fiber Sheets", *Journal of Structural Engineering*, Vol. 123, No. 7, July 1997, pp. 903-911.

Ohuchi, H.; Ohno, S.; Katasumata, H.; Kobatake, Y.; Meta, T.; Yamagata, K.; Inokuma, Y.; and Ogata, N.. "Seismic Strengthening Design Technique for Existing Bridge Columns with CFRP", *Seismic Design and Retrofitting of Reinforced Concrete Bridges*, edited by R. Park, 1994, pp. 495-514.

Rawdon de Paiva, H. A.; and Siess, Chester P.. "Strength and Behavior of Deep Beams in Shear", *Journal of the Structural Division, Proceedings of American Society of Civil Engineers*, Vol. 91, ST5, Oct. 1965, pp. 19-42.

Rogowsky, D. M.; and MacGregor, J. G.. "Design of Reinforced Deep Beams", *Concrete International*, Vol. 8, August 1986, pp. 49-58.

Rogowsky, D. M.; and MacGregor, J. G; and Ong., See Y.. "Tests of Reinforced Concrete Deep Beams", *ACI Journal, Proceedings,* Vol. 83, July-August 1986, pp. 614-623.

Sato, Y.; Ueda, T.; Kakuta, Y.; and Tanaka, T.. "Shear Reinforcing Effect of Carbon Fiber Sheet Attached to Side of Reinforced Concrete Beams", *Advanced Composite Materials in Bridges and Structures*, edited by M. M. El-Badry, 1996, pp. 621-627.

Smith, K. N.; and Fereig, S. M.. "Effects of Loading and Supporting Conditions on the Shear Strength of Deep Beams", *Shear in Reinforced Concrete*, Vol.2, SP-42, American Concrete Institute, 1974, pp. 441-460.

Smith, K. N.; and Vantsiotis, A. S.. "Shear Strength of Deep Beams", *ACI Journal, Proceedings*, Vol.79, May-June, 1982, pp. 201-213.

Täljsten, B.; Elfgren, L.. "Strengthening Concrete Beams for Shear Using CFRP-Materials: Evaluation of Different Application Methods", *Composites, Part B: Engineering*, 2000, pp. 87-96.

Triantafillou, T. C.. "Shear Strengthening of Reinforced Concrete Beams using Epoxy-Bonded FRP Composites", *ACI Structural Journal*, V. 95, No. 2, March-April 1998, pp. 107-115.

Triantafillow, T. C.; and Antonopoulos, C. P.. "Design of Concrete Flexural Members Strengthened in Shear with FRP", *Journal of Composites for Constructions*, Vol.

4, No. 4, Nov. 2000, pp. 198-205.

Tripi, J. M.; Bakis, C. E.; Boothby, T. E.; and Nanni, Antonio. "Deformation in Concrete with External CFRP Sheet Reinforcement", *Journal of Composites for Construction*, Vol. 4, No. 2, May 2000, pp. 85-94.

Uji, K.. "Improving Shear Capacity of Existing Reinforced Concrete Members by Applying Carbon Fibers Sheets", *Transactions of Japan Concrete Institute*, 1992, V.14, pp. 253-266.

Vielhaber, J.; and Limberger, E.. "Upgrading of Concrete Beams with a Local Lack of Shear Reinforcement", *Federal Institute for Materials and Research and Testing (BAM), Unpublished Report*, Berlin, Germany, 1995.

Wang, Chu-Kia; Salmon, Charles G.. "Reinforced Concrete Design", *Fifth edition,* HarperCollins Publishers Inc., 1992.

Wang, Wei; Jiang, Da-Hua; and Hsu, C. T. T.. "Shear Strength of reinforced Concrete Deep Beams", *Journal of Structural Engineering*, Vol. 119, No.8, August, 1993, pp. 2294-2312.

Wu, Hwai-Chung. "Mechanical Interaction Between Concrete and FRP Sheet", *Journal of Composites for Constructions*, Vol. 4, No. 2, May 2000, pp. 96-98.